

52688

CENTRAL LIBRARY	
TEZPUR UNIVERSITY	
Accession No.	52688
Date	3/10/12

CENTRAL LIBRARY, T. U
ACC. NO. 52688

VEGETABLE OIL BASED EPOXY NANOCOMPOSITES AND THEIR APPLICATIONS

**A THESIS SUBMITTED IN PARTIAL FULFILLMENT
OF THE REQUIREMENTS FOR THE DEGREE OF
Doctor of Philosophy**

**By
Gautam Das**

Registration Number 017 of 2011



**School of Science & Technology
Department of Chemical Sciences
Tezpur University**

*Dedicated to my
Dearest Parents*

ABSTRACT

Background

Polymer nanocomposite is a novel class of material that possesses a set of desired and improved properties. Consequently within a short span of time it has gained wide interest within the scientific and industrial fraternities. This is due to the remarkable enhancements of many desirable properties such as mechanical, chemical, barrier, thermal, biodegradability in case of a biodegradable polymer, interesting optical properties etc. by judicious incorporation of a low amount of nanofillers in the polymer system. Remarkably, these enhancements of properties are achieved without much affecting the fascinating properties of the virgin polymer such as lightweight characteristic, flexibility, impact resistance etc. However, despite of considerable progress in this field, researchers are still in search for the answers of some of the fundamental questions that are yet to decipher.

Again, epoxy resin is one the most fascinating materials which occupy a unique place of its own in the domain of polymeric materials. Epoxy resins are versatile as they can be tailored to obtain products with diverse properties without much affecting the cost to performance ratio. Most of the cured epoxy thermosets provide excellent mechanical strength, outstanding chemical resistance, thermal, adhesive, and electrical properties and dimensional stability. These unique combinations of properties are generally not found in any other polymeric material. The superior performance characteristics, coupled with outstanding formulating versatility and reasonable costs, have gained epoxy resins wide acceptance as materials of choice for a multitude of bonding, structural, and protective coatings applications.

However, lately much of the research interest has been devoted to the development of biobased polymeric material. This is due to the continuous depletion of petroleum feedstock, fluctuating petroleum prices and the global increase in environmental concerns. These have forced the global communities to look for alternative resources. Consequently, the utilization of renewable resources in energy and material applications has reached new heights. In this regard vegetable oil, a renewable resource, is worth to be mentioned here. Vegetables oil offer many advantages apart from their renewability. Their world-wide availability and relatively low price make them industrially attractive and feasible. Furthermore, diverse chemistry can be applied on them to obtain a large variety of monomers and polymers. A variety of oil bearing

seeds have been found in the forest resources and farm lands of India. Linseed, castor, soybean, sunflower, safflower, tung, coconut etc. are a few seed oils that are used traditionally for the preparation of polymeric materials. Non-traditional rubber seed oil, neem oil, jatropha seed oil, karanja oil, apricot oil, *Annona squamosa*, *Pongamia glabra*, African mahogany seed oil etc. are a few to mention. *Mesua ferrea* L. is a plant available abundantly in the countries such as India, Srilanka, Bangladesh, Nepal, Indochina (Southeast Asia), Malay Peninsula etc. This is non-drying oil and the fatty acid composition (52.3% oleic and 22.3% linoleic acids as unsaturated fatty acids and 15.9% palmitic and 9.5% stearic acids as saturated fatty acids) insisted to utilize it as a raw material for different industrial polymers.

The Thesis

Chapter one deals with the general introduction of vegetable oil based epoxy nanocomposites. A brief review on epoxy nanocomposites, the importance of such nanocomposites, history, general techniques for preparation, characterization, properties and applications are described in this chapter. This chapter also focuses the scopes and objectives along with the plans of the present investigation.

Chapter two reports the synthesis, characterization and properties evaluation of four different epoxy resins of monoglyceride of *Mesua ferrea* L. seed oil with or without BPA (bisphenol-A), a combination of BPA and BPS (bisphenol-S) and a combination of BPA and TBPA (tetrabromobisphenol-A) and epoxidized oil. The synthesized epoxidized oil and the resins were characterized by the measurements of physical properties like epoxy value, hydroxyl value, viscosity and specific gravity, and by employing other characterization techniques such as FTIR, ¹HNMR, XRD and SEM analyses. The performance characteristics such as hardness, flexibility, gloss, adhesion, impact resistance and chemical resistance in different media of the epoxy resins were determined. The sulfonated epoxy resin as well as brominated epoxy resin exhibited acceptable performance characteristics and hence both were used for further investigation. The chapter concludes that *Mesua ferrea* L. seed oil based epoxy resins can be utilized as thermosetting materials for various applications in the fields of surface coatings and paints, flame retardant materials, adhesives etc.

Chapter three reports the formation of nanocomposites of ENO (epoxidized *Mesua ferrea* L. seed oil) with OMMT (octadecyl ammonium ion modified montmorillonite). *Mesua ferrea* L. seed oil based epoxy resins viz. TBPAE (tetrabromobisphenol-A based epoxy) with OMMT, BPSE (bisphenol-S based epoxy) with OMMT, and MBPSE (modified BPSE, high viscosity) with OMMT, OMMT modified by fatty amido-amine of the oil, OMMT modified by hyperbranched polyurea, bentonite modified by fatty amido-amine of the oil (mMMT) and bentonite (MMT) nanocomposites were also prepared through *ex-situ* technique. The prepared nanocomposites were characterized by FTIR, XRD, SEM and TEM analyses. The thermal and rheological properties of the nanocomposites were also studied. The mechanical properties such as tensile strength, impact resistance, scratch hardness etc. were improved noticeably compared to the pristine system in each case. The study showed the high potentiality of the nanocomposites as surface coatings and paints, flame retardant, adhesives etc. materials.

Chapter four describes the modification of MBPSE by hyperbranched polyurethane and the preparation of nanocomposites of the modified system using organically modified montmorillonite (OMMT). The characterizations and properties of these modified epoxy systems and their nanocomposites are also discussed in this chapter. The various performance characteristics like tensile strength, impact resistance, hardness, thermal stability and chemical resistance in different media were improved through this modification, though these enhancements were much significant after the formation of nanocomposite.

Chapter five demonstrates the suitability of the MBPSE (modified BPSE) as the matrix for copper nanoparticles decorated OMMT nanoparticles. The formation and distribution of the copper nanoparticles-OMMT systems were examined by FTIR, XRD, SEM and TEM analyses. The mechanical properties such as tensile strength and impact resistance were found to be improved without much affecting the flexibility and elongation at break value of the pristine system. Excellent improvements in thermal properties were observed in the prepared nanocomposites. The nanocomposite also exhibited remarkable antimicrobial activity against Gram negative bacteria, *Klebsiella pneumoniae* and Gram positive bacteria, *Staphylococcus aureus*. Thus this chapter showed the high potentiality of the epoxy resin/Cu-OMMT nanocomposites as antimicrobial surface coating materials.

Chapter six includes the modification and the effect of insertion of modified MWCNTs in the MBPSE matrix on mechanical properties, thermal properties, biodegradation and cytocompatibility behaviors. Further the adhesive strength of the nanocomposites was also determined. The homogeneous distribution of the MWCNTs in the matrix was confirmed by FTIR, XRD, SEM and TEM analyses. The performance characteristics were enhanced with respect to the pristine system. The adhesive strength shows enhancement after nanocomposites formations. The biocompatibility nature in terms of non-toxicity at the cellular level and biodegradability of the nanocomposites indicate their high potentiality in biomedical applications.

Chapter seven describes the use of epoxidized *Mesua ferrea* L. as a plasticizer for commercially available unplasticized PVC. The nanocomposites of epoxidized *Mesua ferrea* L. seed oil plasticized PVC with OMMT was also investigated. This chapter also deals with the study of biodegradation of these nanocomposites for a period of 180 days by using *Pseudomonas aeruginosa* and *Achromobacter* sp. bacterial strains. Further the effect of biodegradation on the performance characteristics including thermal properties of the nanocomposites was also evaluated. The modified systems as


well the nanocomposites were characterized by FTIR spectroscopic technique, XRD, SEM and TEM studies. The biodegradability of the nanocomposites as studied by FTIR, SEM, thermal stability and measurement of mechanical properties showed significant biodegradation after 180 days of inoculations. The system exhibited high potentiality to be used as biodegradable plasticized PVC for various applications.

Chapter eight, the last chapter of the thesis includes the concluding remarks, highlights of the findings and future scopes of the present investigation.

DECLARATION

I do hereby declare that the thesis entitled "*Vegetable oil based Epoxy Nanocomposites and Their Applications*", submitted to the Department of Chemical Sciences, Tezpur University, is a record of original research work carried out by me. All sources of assistance have been assigned due acknowledgment. I also declare that neither this work as a whole nor a part of it has been submitted to any other University or Institute for any other degree, diploma or award.

Place: Tezpur University, Tezpur


(Gautam Das)

Date:



TEZPUR UNIVERSITY

Ph: 03712-267004

(A Central University established by an Act of Parliament) 03712-267005

NAPAAM, TEZPUR-784028

Fax:03712-267006

DISTRICT: SONITPUR:: ASSAM:: INDIA

03712-267005

E-mail: nkarak@tezu.ernet.in

CERTIFICATE

This is to certify that the thesis entitled "*Vegetable oil based Epoxy Nanocomposites and Their Applications*" submitted to the Tezpur University in the Department of Chemical Sciences under the School of Science & Technology, in partial fulfillment for the award of the Degree of Doctor of Philosophy in Science, is a record of research work carried out by Gautam Das under my personal supervision and guidance.

All helps received by him from various sources have been duly acknowledged.

No part of this thesis has been reproduced elsewhere for award of any other degree.

Place: Tezpur University

Date:

(Dr. Niranjana Karak)

Professor & Head

Department of Chemical Sciences

School of Science & Technology



TEZPUR UNIVERSITY

Ph: 03712-267004

(A Central University established by an Act of Parliament) 03712-267005

NAPAAM, TEZPUR-784028

Fax: 03712-267006

DISTRICT: SONITPUR:: ASSAM :: INDIA

03712-267005

CERTIFICATE

This is to certify that the thesis entitled "*Vegetable oil based Epoxy Nanocomposites and Their Applications*" submitted to the Tezpur University in the Department of Chemical Sciences under the School of Science and Technology, in partial fulfillment for the award of the Degree of Doctor of Philosophy in Science, has been examined by us on and found to be satisfactory.

The committee recommends for the award of the degree of Doctor of Philosophy.

Principal Supervisor

External Examiner

Date:

Date:


PREFACE

The designing of a polymer such as epoxy with desirable properties for their multifaceted applications is a real challenge to the synthetic polymer chemists. The formation of appropriate nanocomposites of such polymers has opened up a new avenue for advanced polymeric materials and leads to the genesis of a new era in material science. Further, the replacement of petroleum based raw materials by the renewable resource based feed stocks in the production of such polymers has attracted tremendous attention worldwide as sustainable material development is the ultimate motto for today's society. *Mesua ferrea* L. seed oil with exceptionally high oil content is one of such renewable resources with colossal potential to design various types of industrial polymers.

Thus the main objective of this thesis is to prepare epoxidized oil and epoxy resins by utilizing this vegetable oil and to develop their different nanocomposites to meet the service requirements of advanced epoxy based materials. The thesis describes the synthesis, characterization, property and application of *Mesua ferrea* L. seed oil based epoxy resins along with the epoxidized oil. Attempt has also been made to modify one of these epoxy resins by hyperbranched polyurethane of the same oil to improve its performance characteristics. The properties of the pristine epoxy resins and epoxidized oil and the modified system were further enhanced by formation of appropriate nanocomposites by using different types of nanomaterials such as organically modified clay, fatty amido-amine modified organoclay, functionalized MWCNTs and Cu nanoparticles. The epoxidized oil/clay system is also used to modify unplasticized PVC to obtain biodegradable thermostable advanced PVC material. The prepared nanocomposites exhibited high potential to be applicable in a spectrum of applications such as advanced thin film materials, highly thermo-stable and flame retardant materials, antimicrobial surface coating materials and biodegradable materials.

Date:

Place: Napam, Tezpur



(Gautam Das)

CONTENTS

<i>Content</i>	<i>Page No.</i>
Abstract	i
Declaration	vi
Certificate of Supervisor	vii
Certificate of Examiners	viii
Preface	ix
Contents	x
List of Abbreviations and Symbols	xviii
List of Tables	xxi
List of Figures	xxiv
List of Schemes	xxix
Acknowledgement	xxx

CHAPTER 1

General Introduction

1.1. Introduction	1
1.2. Background	2
1.3. Polymer Nanocomposites	4
1.4. Materials and Methods	5
1.4.1. Materials	5
1.4.1.1 Epoxy	6
1.4.1.2 Nanomaterials	12
1.4.2. Methods	18
1.4.2.1. Epoxy Matrix	18
1.4.2.2. Nanocomposites	21
1.5. Characterization	26
1.5.1. Epoxy Matrix	26
1.5.2. Nanocomposites	27
1.6. Properties	30
1.6.1. Mechanical	31
1.6.2. Dynamic Mechanical	31
1.6.3. Barrier	32

1.6.4. Thermal	32
1.6.5. Rheological	33
1.6.6. Flame Retardancy	33
1.6.7. Optical	34
1.6.8. Electrical	34
1.6.9. Magnetic	34
1.6.10. Catalytic Activity	34
1.6.11. Biodegradation	35
1.7. Applications	35
1.8. Short Review on Vegetable Oil Based Epoxy Nanocomposites	40
1.9. Scope and Objectives of the Present Investigation	57
1.10. Plans of Work	58
References	

CHAPTER 2

Synthesis and Characterization of *Mesua ferrea* L. seed oil based Epoxy resin and Epoxidized oil

2.1. Introduction	76
2.2. Experimental	78
2.2.1. Materials	78
2.2.2. Instruments and Methods	83
2.2.2.1. Synthesis of Epoxidized oil and Epoxy Resin	84
2.2.2.2. Curing of the Resins	86
2.3. Results and Discussion	86
2.3.1 Epoxidation	86
2.3.2. Resinification of Monoglyceride based Epoxy Resin	87
2.3.3. Characterization of the Epoxy Resins	90
2.3.3.1. Physical Properties	90
2.3.3.2. FTIR and ¹ H NMR Spectroscopic Studies	91
2.3.4. Rheological Behaviors	96
2.3.5. Curing Study for the Epoxy Resins	97
2.3.6. Performance Characteristics	98
2.3.7. Chemical Resistance	99
2.3.8. Flame Retardancy	100

2.3.9. Thermal Study	101
2.4. Conclusions	102
References	

CHAPTER 3

Epoxy/Clay Nanocomposites

3.1. Introduction	106
3.2. Experimental	109
3.2.1. Materials	109
3.2.2. Instruments and Methods	111
3.2.2.1. Preparation of Sodium Methoxide	111
3.2.2.2. Preparation of Methyl Ester of <i>Mesua ferrea</i> L. seed Oil	112
3.2.2.3. Preparation of <i>Mesua ferrea</i> L. seed Oil based Fatty Amido-Amine (AMNO)	112
3.2.2.4. Modification of Organo-MMT (OMMT) by Fatty Amido-Amine	113
3.2.2.5. Modification of Hydrophilic Bentonite (MMT) by Fatty Amido-Amine	113
3.2.2.6. Modification of Organo-MMT (OMMT) by Hyperbranched Polyurea	113
3.2.2.7. Preparation of Nanocomposites of Epoxidized Oil Modified Araldite LY 250 by OMMT	113
3.2.2.8. Preparation of nanocomposites of TBPAE and BPSE by OMMT	114
3.2.2.9. Preparation of Nanocomposites of MBPSE by OMMT, mOMMT, m-bentonite (mMMT), bentonite (MMT) and Hyperbranched Polyurea modified OMMT	114
3.2.2.10. Curing of the Resins and Nanocomposites	115
3.3. Results and Discussion	115
3.3.1. Modification of Nanoclay	115
3.3.2. Formation of Nanocomposites	116
3.3.3. Characterization of Modified Nanoclay	118
3.3.1.1. FTIR Analysis	118
3.3.1.2. XRD Analysis	120

3.3.4. Characterization of Nanocomposites	121
3.3.4.1. FTIR Analysis	121
3.3.4.2. XRD Analysis	125
3.3.5. Curing Study	127
3.3.6. SEM Study	130
3.3.7. TEM Study	133
3.3.8. Rheological Behaviors	136
3.3.9. Performance Characteristics	140
3.3.10. Thermal Study	147
3.3.11. Flame Retardancy	151
3.3.12. Chemical Resistance	153
3.4. Conclusions	155
References	

CHAPTER 4

Modified Epoxy and Clay Nanocomposites

4.1. Introduction	162
4.2. Experimental	163
4.2.1. Materials	163
4.2.2. Instruments and Methods	164
4.2.2.1. Synthesis of Hyperbranched Polyurethane (HBPU)	165
4.2.2.2. Modification of Epoxy Resin by HBPU	165
4.2.2.3. Preparation of Nanocomposites	165
4.2.2.4. Curing of the Hyperbranched Polyurethane Modified Epoxy and Nanocomposites	166
4.2.2.5. Water Vapor Permeability Measurement	166
4.2.2.6. Biodegradation by Broth Culture Technique	166
4.2.2.7. Microbe Selection	167
4.2.2.8. RBC Haemolysis Protection Assay	167
4.3. Results and Discussion	168
4.3.1. Modification of Epoxy Resin	168
4.3.2. Nanocomposites Preparation	168
4.3.3. Characterization	168
4.3.3.1. FTIR Studies of Hyperbranched Polyurethane Modified	169

MBPSE	
4.3.3.2. FTIR Studies of Nanocomposites	170
4.3.3.3. XRD Analysis of Hyperbranched Polyurethane Modified MBPSE	172
4.3.3.4. XRD Analysis of Nanocomposites	172
4.3.4. SEM Study	173
4.3.5. TEM Study	174
4.3.6. Curing Studies	174
4.3.7. Water Vapor Barrier Study	175
4.3.8. Performance Characteristics	176
4.3.9. Thermal Study	177
4.3.10. Biodegradation Study	178
4.3.11. RBC Haemolysis Protection Assay for Cytocompatibility	180
4.4. Conclusions	181
References	

CHAPTER 5

Epoxy/Nanoclay Copper Nanocomposites

5.1. Introduction	185
5.2. Experimental	186
5.2.1. Materials	186
5.2.2. Instruments and Methods	187
5.2.2.1. Preparation of Copper Nanoparticles	188
5.2.2.2. Fabrication of Nanocomposites	188
5.2.2.3. Curing of the Resin and Nanocomposites	188
5.2.2.4. Antibacterial Study	188
5.2.2.5. RBC Haemolysis Protection Assay	189
5.3. Results and Discussion	189
5.3.1. Formation of MBPSE/OMMT-Copper Nanocomposites	189
5.3.2. Characterization of the OMMT-Cu Systems and Nanocomposites	190
5.3.2.1. UV-Visible Spectroscopy	190
5.3.2.2. XRD Analysis	191
5.3.2.3. FTIR Analysis	193
5.3.2.4. SEM Study	194

5.3.2.5. TEM Study	195
5.3.3. Thermal Study	197
5.3.4. Performance Characteristics	198
5.3.5. Antibacterial Study	199
5.3.6. RBC Haemolysis Protection Assay for Cytocompatibility	200
5.4. Conclusions	201
References	

CHAPTER 6

Epoxy/Multi-Walled Carbon Nanotube Nanocomposites

6.1. Introduction	206
6.2. Experimental	208
6.2.1. Materials	208
6.2.2. Instruments and Methods	208
6.2.2.1. Modification of Pristine MWCNTs	209
6.2.2.2. Preparation of Diglycidyl Ether Bisphenol-S Epoxy Resin (MBPSE)	209
6.2.2.3. Fabrication of Nanocomposites	209
6.2.2.4. Curing of the Resin and Nanocomposites	210
6.2.2.5. Biodegradation by Broth Culture Technique	210
6.2.2.6. RBC Haemolysis Protection Assay	210
6.3. Results and Discussion	211
6.3.1. Functionalization of MWCNTs	211
6.3.2. Characterization of Modified MWCNTs and Nanocomposites	212
6.3.2.1. FTIR Analysis	212
6.3.2.2. Dispersion of MWCNTs	214
6.3.2.3. XRD Analysis	215
6.3.2.4. SEM & TEM Studies	215
6.3.3. Curing Studies	217
6.3.4. Thermal Study	217
6.3.5. Performance Characteristics	218
6.3.6. Adhesive Strength	219
6.3.7. Biodegradation Study	220
6.3.8. RBC Haemolysis Protection Assay for Cytocompatibility	222

6.4. Conclusions	223
References	

CHAPTER 7

Biodegradation of Epoxidized oil/Poly(vinyl chloride)/Clay Nanocomposites

7.1. Introduction	228
7.2. Experimental	230
7.2.1. Materials	230
7.2.2. Instruments and Methods	230
7.2.2.1. Plasticization of PVC by ENO and Nanocomposites Formation	231
7.2.2.2. Microbial Growth in Presence of Pristine PVC and PVC/ENO Nanocomposite	232
7.2.2.3. Biodegradation of PVC/ENO75 in Culture Medium	232
7.3. Results and Discussion	232
7.3.1. Plasticization and Biodegradation of PVC	232
7.3.2. Bacterial Culture in the Presence of Pristine PVC and PVC/ENO Nanocomposites Utilizing Bacteria	233
7.3.3. Biodegradation of PVC/ENO Nanocomposites in Culture	233
7.3.4. FTIR Analysis	236
7.3.4.1. FTIR Analysis of ENO and ENO Plasticized PVC/OMMT Nanocomposites	236
7.3.4.2. FTIR Analysis of PVC/ENO75 post Biodegradation	237
7.3.5. XRD Analysis of PVC and ENO Plasticized PVC/OMMT Nanocomposites	238
7.3.6. Morphological Characterization	239
7.3.6.1. SEM Study of PVC and ENO Plasticized PVC/OMMT Nanocomposites	239
7.3.6.2. TEM Study of Nanocomposite	240
7.3.6.3. SEM Study of PVC/ENO75 post Biodegradation	240
7.3.7. Brookfield Viscosity and Melt Flow Rate (MFR) of PVC and ENO Plasticized PVC/OMMT Nanocomposites	242
7.3.8. Performance Characteristics	243
7.3.8.1. Performance Characteristics of PVC, ENO	243

Plasticized PVC/OMMT Nanocomposites	
7.3.8.2. Performance Characteristics of PVCENC75 post Biodegradation	246
7.3.9. Thermal Study	247
7.3.9.1. Thermal Study of PVC and ENO Plasticized PVC/OMMT Nanocomposites	247
7.3.9.2. Thermal Study of PVCENC75 post Biodegradation	249
7.3.10. Isothermal Gravimetric Test	250
7.3.11. Flame Retardancy	252
7.3.12. Heat aging and Chemical Aging	253
7.4. Conclusions	255
References	

CHAPTER 8

Conclusions and Future Directions

8.1. Conclusions	260
8.2. Future Directions	261
List of Publications	262

LIST OF ABBREVIATIONS AND SYMBOLS

@	at the rate
Al	aluminum
A _w	atomic weight
b.p.	boiling point
C	carbon
Cl	chlorine
cm ³	cubic centimeter
cm	centimeter(s)
CNTs	carbon nanotubes
cps	centipoise
°C	degree centigrade
DSC	differential scanning calorimetry
DEHP	bis(2-ethylhexyl phthalate)
DOP	dioctyl phthalate
FTIR	Fourier transform infrared
F _w	Formula weight
g	gram(s)
h	hour(s)
K	Kelvin
kN	kilo-Newton
kV	kilo-volt
L	liter(s)
LOI	limiting oxygen index
lb	pound(s)
m	meter(s)
mA	mili ampere
MFR	melt flow rate
min	minute(s)
mL	mili liter(s)
mm	mili meter(s)
mol	mole
m.p.	melting point

MPa	Megapascal
M_n	number average molecular weight
M_w	weight average molecular weight
MWCNTs	multi walled carbon nanotubes
N	Newton
NMR	nuclear magnetic resonance
nm	nano meter(s)
Nm^{-1}	Newton per meter
OD	optical density
OMMT	organically modified montmorillonite
Pa	Pascal
Pas	Pascal second
phr	parts per hundred
ppm	parts per million
PBS	phosphate buffer saline
PVC	poly(vinyl chloride)
RBC	red blood cell
rpm	rotation per minute
RT	room temperature
s	second(s)
S.D.	standard deviation
SEM	scanning electron microscope
Si	silicone
sp.	species
SWCNTs	single walled carbon nanotubes
TEM	transmission electron microscopy
T_f	endset of thermal degradation temperature
T_g	glass transition temperature
T_{max}	peak temperature
T_{on}	onset of thermal degradation temperature
TGA	thermogravimetric analysis
TMS	tetramethyl silane
TPa	terapascal
UL 94	underwriters laboratories (estd. 1894), plastic flammability standard

UTM	universal testing machine
UV	ultraviolet
v	volume
wt	weight
XRD	X-ray diffraction
μg	micro gram(s)
μm	micro meter(s)
μM	micro molar(s)
μL	micro liter(s)
%	percentage
η_{inh}	inherent viscosity
λ_{max}	wavelength maximum
θ	scattering angle

LIST OF TABLES

- Table 1.1: Different aromatic diols with their structures and a few physical properties
- Table 1.2: Different curing agent with their physical properties
- Table 1.3: Different quaternary ammonium and phosphonium ions used for modification of hydrophilic clay
- Table 1.4: Chemical structure and physical properties of a few fatty acids of vegetable oils
- Table 1.5: A few important vegetable oils used to prepare epoxy resin with their physical properties and major fatty acids contents
- Table 2.1: Technical specifications of epoxy resin and hardener
- Table 2.2: Physical property of oil and ENO
- Table 2.3: Physical property of epoxy resins
- Table 2.4: Drying time and viscosity of epoxy resins
- Table 2.5: Performance characteristics of the epoxy resins
- Table 2.6: Chemical resistance of the epoxy films
- Table 2.7: Flame retardancy of epoxy resins
- Table 3.1: Composition of ENO modified Araldite LY 250 and OMMT nanocomposites
- Table 3.2: Drying time of ENO modified Araldite LY 250/OMMT nanocomposites
- Table 3.3: Drying time of TBP AE and nanocomposites
- Table 3.4: Drying time of BPSE and nanocomposites
- Table 3.5: Drying time of MBPSE and nanocomposites
- Table 3.6: Performance characteristics of ENO modified Araldite LY 250 nanocomposites
- Table 3.7: Performance characteristics of TBP AE and its OMMT nanocomposites
- Table 3.8: Performance characteristics of BPSE and its OMMT nanocomposites
- Table 3.9: Performance characteristics of MBPSE and its mOMMT, OMMT, mMMT and MMT nanocomposites
- Table 3.10: Performance characteristics of MBPSE and hyperbranched polyurea modified OMMT nanocomposites
- Table 3.11: LOI values and UL 94 ratings of TBP AE/OMMT nanocomposites
- Table 3.12: LOI values and UL 94 ratings of BPSE/OMMT nanocomposites

- Table 3.13: LOI values and UL 94 ratings of MBPSE and mOMMT, OMMT, mMMT and MMT nanocomposites
- Table 3.14: LOI values and UL 94 ratings of MBPSE and hyperbranched polyurea modified OMMT nanocomposites
- Table 3.15: Chemical resistance of ENO, ENO modified Araldite LY 250 and nanocomposites
- Table 3.16: Chemical resistance of TBP AE and nanocomposites in different media
- Table 3.17: Chemical resistance of BPSE and nanocomposites in different media
- Table 3.18: Chemical resistance of MBPSE and nanocomposites in different media
- Table 3.19: Chemical resistance for MBPSE and hyperbranched polyurea modified OMMT in different media
- Table 4.1: Compositions of HBPU modified MBPSE and its nanocomposites
- Table 4.2: Drying time of HBPU modified MBPSE and its nanocomposites
- Table 4.3: Performance characteristics of HBPU modified MBPSE and its nanocomposites
- Table 5.1: EDX data of OMMT-Cu and OMMT-Cu/MBPSE nanocomposites
- Table 5.2: Performance characteristics of MBPSE and its OMMT-Cu nanocomposites
- Table 5.3: Antimicrobial activity of OMMT-Cu systems
- Table 5.4: Antimicrobial activity of MBPSE/OMMT-Cu nanocomposites
- Table 6.1: Drying time of MBPSE and its MWCNTs nanocomposites
- Table 6.2: Performance characteristics of MBPSE and its MWCNTs nanocomposites
- Table 7.1: Compositions of pristine as well plasticized PVC nanocomposites
- Table 7.2: Yield of bacterial dry biomass and protein content after 96 h of culture
- Table 7.3: Viscosity and MFR value for PVC, PVCNC and PVC/ENO nanocomposites
- Table 7.4: Performance characteristics for PVC, PVCNC, PVCENO50 and PVC/ENO nanocomposites
- Table 7.5: Performance characteristics for PVCENC75 after biodegradation
- Table 7.6: Thermal degradation parameters for PVC, PVCNC, PVCENO50 and PVC/ENO nanocomposites
- Table 7.7: Thermal degradation parameters for PVCENC75 post biodegradation for 180 days
- Table 7.8: Weight losses of the systems as measured by isothermal test at three different temperatures
- Table 7.9: Limiting Oxygen Index (LOI) and UL94 ratings for PVC, PVCNC, PVCENO50 and PVC/ENO nanocomposites

LIST OF FIGURES

- Fig. 1.1: Different states of polymer/clay nanocomposites
- Fig. 1.2: Different types of nanomaterials
- Fig. 1.3: Structure of clay (2:1 phyllosilicates)
- Fig. 1.4: Structures of (a) SWCNTs, (b) MWCNTs and (c) cellulose chain
- Fig. 1.5: Different fields of applications of polymer nanocomposites
- Fig. 1.6: Structure of triglyceride of fatty acid
- Fig. 2.1: Structure of glycerol
- Fig. 2.2: Structure of bisphenol-A
- Fig. 2.3: Structure of tetrabromobisphenol-A
- Fig. 2.4: Structure of bisphenol-S
- Fig. 2.5: Structure of epichlorohydrin
- Fig. 2.6: FTIR spectrum of ENO
- Fig. 2.7: FTIR spectrum of TBPAE
- Fig. 2.8: FTIR spectrum of BPAE
- Fig. 2.9: FTIR spectrum of MGE
- Fig. 2.10: FTIR spectrum of BPSE
- Fig. 2.11: FTIR spectrum of MBPSE
- Fig. 2.12: ¹HNMR spectrum of TBPAE
- Fig. 2.13: ¹HNMR spectrum of BPAE
- Fig. 2.14: ¹HNMR spectrum of MGE
- Fig. 2.15: ¹HNMR spectrum of BPSE
- Fig. 2.16: Variation of viscosity against (a) time, (b) shear stress and (c) temperature for MGE, TBPAE and BPAE
- Fig. 2.17: Variation of viscosity against (a) time, (b) shear stress and (c) temperature for BPSE and MBPSE
- Fig. 2.18: TGA thermograms for epoxy resins
- Fig. 3.1: Structure of cyanuric chloride
- Fig. 3.2: Structure of urea
- Fig. 3.3: Structure of diisopropylethylamine
- Fig. 3.4: FTIR spectra of (a) AMNO, (b) OMMT, (c) mOMMT, (d) MMT and (e) mMMT
- Fig. 3.5: XRD patterns of (a) MMT, (b) mMMT, (c) OMMT, (d) mOMMT and (e)

hyperbranched polyurea modified OMMT

- Fig. 3.6: FTIR spectra of (a) ENO50 and (b) ECN2.5
- Fig. 3.7: FTIR spectra of (a) TBPAE and (b) TBPAEN5
- Fig. 3.8: FTIR spectra of (a) BPSE and (b) BPSEN2.5
- Fig. 3.9: FTIR spectra of (a) MBPSE, (b) ENMC1, (c) ENMC2, (d) ENMC3 and (e) ENC
- Fig. 3.10: FTIR spectra of (a) MBPSE, (b) HBPA1, (c) HBPA3 and (d) HBPA5
- Fig. 3.11: XRD patterns for epoxidized oil modified Araldite LY 250 OMMT nanocomposites (a) OMMT, (b) ECN1, (b) ECN2.5 and (d) ECN5
- Fig. 3.12: XRD patterns for (a) OMMT (b) TBPAEN5, (c) TBPAEN2.5, (d) TBPAEN1 and (e) TBPAE
- Fig. 3.13: XRD patterns for (a) OMMT, (b) BPSE, (c) BPSEN1, (d) BPSEN3 and (e) BPSEN5
- Fig. 3.14: XRD patterns for (a) ENMC1, (b) ENMC2, (c) ENMC3 and (d) ENC
- Fig. 3.15: XRD patterns for (a) MBPSE, (b) HBPA1, (c) HBPA3 and (d) HBPA5
- Fig. 3.16: SEM micrographs for (a) ENO50, (b) ECN1, (c) ECN2.5 and (d) ECN5
- Fig. 3.17: SEM micrographs for (a) TBPAE, (b) TBPAEN1, (c) TBPAEN2.5 and (b) TBPAEN5
- Fig. 3.18: SEM micrographs for (a) BPSE, (b) BPSEN1, (c) BPSEN2.5 and (d) BPSEN5
- Fig. 3.19: SEM micrographs for (a) MBPSE, (b) ENMC1, (c) ENMC2, (d) ENMC3 and (e) ENC
- Fig. 3.20: SEM micrographs for (a) MBPSE and (b) HBPA3
- Fig. 3.21: TEM micrograph for ECN2.5
- Fig. 3.22: TEM micrograph for TBPAEN2.5
- Fig. 3.23: TEM micrograph for BPSEN2.5
- Fig. 3.24: TEM micrographs for (a) ENMC1 and (b) ENMC3
- Fig. 3.25: TEM micrographs for HBPA3 at (a) 100 nm and (b) 10 nm scale
- Fig. 3.26: Rheological characteristics of ENO modified Araldite LY 250 nanocomposites (a) ENO100, (b) ENO50 and (c) ECN2.5
- Fig. 3.27: Rheological characteristics of (a) TBPAE, (b) TBPAEN1, (c) TBPAEN2.5, and (d) TBPAEN5
- Fig. 3.28: Rheological characteristics of (a) BPSE, (b) BPSEN1, (c) BPSEN2.5 and (d) BPSEN5
- Fig. 3.29: Rheological characteristics of (a) MBPSE, (b) ENMC1, (c) ENMC2, (d) ENMC3 and (e) ENC

- Fig. 3.30: Rheological characteristics of (a) MBPSE, (b) HBPA1, (c) HBPA3 and (d) HBPA5
- Fig. 3.31: TGA thermograms for (a) ENO50, (b) Araldite LY 250 and (c) ENCE2.5
- Fig. 3.32: TGA thermograms for (a) TBPAE, (b) TBPAEN1, (c) TBPAEN2.5 and (d) TBPAEN5
- Fig. 3.33: TGA thermograms for (a) BPSE, (b) BPSN1, (c) BPSN2.5 and (d) BPSN5
- Fig. 3.34: TGA thermograms for (a) MBPSE, (b) ENMC2, (c) ENMC3 and (d) ENMC1
- Fig. 3.35: TGA thermograms for (a) MBPSE, (b) HBPA1, (c) HBPA3 and (d) HBPA5
- Fig. 4.1: Structure of poly(ϵ -caprolactone) diol
- Fig. 4.2: Structure of toluene diisocyanate
- Fig. 4.3: FTIR spectra of (a) MBPSE, (b) EHBPU10, (c) EHBPU20 and (d) EHBPU30 before curing
- Fig. 4.4: FTIR spectra of (a) EHBPU10, (b) EHBPU20 and (c) EHBPU30 after curing
- Fig. 4.5: FTIR spectra of (a) EHPN1, (b) EHPN3 and (c) EHPN5 before curing
- Fig. 4.6: FTIR spectra of (a) EHPN1, (b) EHPN3 and (c) EHPN5 after curing
- Fig. 4.7: XRD patterns of (a) MBPSE, (b) EHBPU10, (c) EHBPU20 and (d) EHBPU3
- Fig. 4.8: XRD patterns of (a) EHPN1, (b) EHPN3 and (c) EHPN5
- Fig. 4.9: SEM micrographs for (a) EHBPU30 and (c) EHPN3
- Fig. 4.10: TEM micrograph for EHPN3
- Fig. 4.11: TGA thermograms for MBPSE, EHBPU30 and EHPN5
- Fig. 4.12: Growth of *P. aeruginosa* bacterial strain, MTCC 424 on (a) HBPU modified epoxy and (b) nanocomposites
- Fig. 4.13: SEM micrographs for films after six weeks of bacterial exposure (a) untreated MBPSE, (b) inoculated MBPSE, (c) EHBPU30 and (d) EHPN5
- Fig. 4.14: RBC protection assay of (a) HBPU modified MBPSE and (b) nanocomposites
- Fig. 5.1: UV-visible spectra of (a) OMMT-Cu systems and (b) nanocomposites
- Fig. 5.2: XRD patterns of OMMT-Cu systems, (a) N0.25, (b) N0.5 and (c) N1 (* = Cu, \circ = CuO and \bullet = OMMT)
- Fig. 5.3: XRD patterns of nanocomposites, (a) ECuN0.25, (b) ECuN0.5 and (c) ECuN1 (* = Cu, \circ = CuO and \bullet = OMMT)
- Fig. 5.4: FTIR spectra of (a) OMMT and (b) OMMT-Cu (N0.5)
- Fig. 5.5: FTIR spectra of (a) MBPSE, (b) ECuN0.25, (c) ECuN0.5 and (d) ECuN1
- Fig. 5.6: SEM micrographs for (a) N1 and (b) ECuN1
- Fig. 5.7: EDX spectra of (a) N1 and (b) ECuN1

- Fig. 5.8: HRTEM micrographs for N1
- Fig. 5.9: HRTEM micrographs for ECuN1
- Fig. 5.10: TGA thermograms of OMMT, OMMT-Cu and nanocomposites
- Fig. 5.11: RBC haemolysis protection assay for pristine polymer and OMMT-Cu nanocomposites
- Fig. 6.1: FTIR spectra of (a) unmodified MWCNTs and (b) modified MWCNTs
- Fig. 6.2: FTIR spectra of MWCNTs/MBPSE nanocomposites viz., (a) ECTN1, (b) ECTN2 and (c) ECTN3
- Fig. 6.3: Dispersion stability of (a) unmodified MWCNTs, (b) modified MWCNTs in DMF and (c) modified MWCNTs in DMAc
- Fig. 6.4: XRD patterns of (a) modified MWCNTs, (b) ECTN1, (b) ECTN2 and (c) ECTN3
- Fig. 6.5: SEM micrographs for (a) MBPSE, (b) ECTN1, (c) ECTN2 and (d) ECTN3
- Fig. 6.6: TEM micrograph for ECTN3
- Fig. 6.7: TGA thermograms of (a) MBPSE, (b) ECTN1, (c) ECTN2 and (d) ECTN3
- Fig. 6.8: Lap shear adhesive strength of MBPSE and MWCNT nanocomposites on different substrates (wood/aluminum/polypropylene)
- Fig. 6.9: Statistics of growth of *bacillus subtilis* in MBPSE and nanocomposites post 6 weeks of inoculations
- Fig. 6.10: SEM micrographs of (a) untreated MBPSE and MWCNTs/MBPSE nanocomposites post 6 weeks of inoculations (b) ECTN1, (c) ECTN2 and (d) ECTN3
- Fig. 6.11: RBC protection assay of MBPSE and nanocomposites
- Fig. 7.1: (a) Biodegradation of PVC/ENO systems in culture medium by individual bacterial isolates post 90 days of incubation and (b) Biodegradation of PVCENC75 by individual bacterial isolates post 180 days of incubation
- Fig. 7.2: (i) FTIR spectra of (a) OMMT, (b) ENO, (c) PVC and (d) PVCENO50 and (ii) FTIR spectra of (a) PVCNC, (b) PVCENC25, (c) PVCENC50 and (d) PVCENC75
- Fig. 7.3: FTIR spectra of PVCENC75 (a) control, (b) 30 days of post inoculation, (c) 60 days post treatment and (d) 180 days post treatment by *Pseudomonas aeruginosa* respectively
- Fig. 7.4: XRD patterns for (a) OMMT, (b) PVC, (c) PVCNC, (d) PVCENC25, (e) PVCENC50 and (f) PVCENC75

Fig. 7.5: Representative SEM micrographs for (a) PVC, (b) PVCENO50, (c) PVCNC and (d) PVCENC50

Fig. 7.6: TEM micrograph for PVCENC50

Fig. 7.7: SEM micrographs for PVCENC75 after 30 days of inoculations with (a) untreated PVCENC75, (b) control, (c) *Pseudomonas* sp. and (d) *Achromobacter* sp.

Fig. 7.8: SEM micrographs for PVCENC75 after 60 days of inoculations with (a) *Pseudomonas* sp., (b) *Achromobacter* sp. and (c) control

Fig. 7.9: SEM micrographs for PVCENC75 after 180 days of inoculations with (a) *Pseudomonas* sp., (b) *Achromobacter* sp. and (c) control

Fig. 7.10: Decrease in tensile strength with time of PVCENC75 post biodegradation with *Pseudomonas* sp. and *Achromobacter* sp.

Fig. 7.11: (i) TGA thermograms of (a) PVC, (b) PVCNC and (c) PVCENO50 and (ii) TGA thermograms of (a) PVCENC25, (b) PVCENC50 and (c) PVCENC75

Fig. 7.12: TGA thermograms of PVCENC75 (a) control, (b) after 180 days, inoculated with *Pseudomonas* sp. and (c) after 180 days inoculated with *Achromobacter* sp.

Fig. 7.13: (i) FTIR spectra of isothermally heated samples at 100 °C, (ii) FTIR spectra of isothermally heated samples at 150 °C and (iii) FTIR spectra of isothermally heated samples at 200 °C for (a) PVCENC25, (b) PVCENC50, (c) PVCENC75 and (d) PVCNC, respectively

LIST OF SCHEMES

- Scheme 1.1: Formation of epoxy resin
- Scheme 1.2: Synthesis of epoxy resin by taffy process
- Scheme 1.3: Synthesis of high molecular weight epoxy resin
- Scheme 1.4: Schematic diagram for the preparation of polymer nanocomposites by *in-situ* polymerization technique
- Scheme 1.5: Schematic diagram for the preparation of polymer nanocomposites by solution method
- Scheme 1.6: Schematic diagram for preparation of nanocomposites by the melt mixing technique
- Scheme 2.1: Epoxidation of *Mesua ferrea* L. seed oil (ENO)
- Scheme 2.2: Synthesis of MGE resin
- Scheme 2.3: Synthesis of BPAAE resin
- Scheme 2.4: Synthesis of TBPAAE resin
- Scheme 2.5: Synthesis of sulfone epoxy resin (BPSE)
- Scheme 3.1: Synthesis of fatty amido-amine
- Scheme 3.2: Probable interactions in epoxy nanocomposites
- Scheme 6.1: Probable interactions of MWCNTs with MBPSE matrix

ACKNOWLEDGMENT

It is my greatest pleasure to express my gratitude to large numbers of people who have directly or indirectly influenced and encouraged me over the course of my studies and my life in general.

First of all, I would like to express my deep sense of gratitude and indebtedness to my research guide Dr. Niranjan Karak, Professor and Head, Department of Chemical Sciences, Tezpur University for his invaluable guidance, support, advice and a wonderful accompany throughout my Ph.D. work. His dedication towards research and indomitable spirit would ever remain as a source of inspiration for me.

Words fall short as I extend my gratitude to Dr. A.K. Mukherjee Professor and Dr. A. K. Buragohain, Professor, Department of Molecular Biology and Biotechnology, Tezpur University for their cooperation during the course of my bio-related laboratory work.

It is my pleasant duty to acknowledge with thanks the cooperation and support extended to me by the authority of Tezpur University and entire community of the Department of Chemical Sciences, for allowing me to use the administrative and technical facilities required for my research work.

It is my greatest pleasure to acknowledge the present and former Heads of the Department, Prof. N. Karak, Prof. R.K. Dutta, Prof. N. S. Islam (Dean, Research and Development), Prof. T. K. Maji for giving me the opportunity to work on my topic and valuable advises throughout my stay at Tezpur University.

I would also like to express my sincere gratitude and humble respect to my doctoral research committee members Prof. S. K. Dolui and Dr. A.J. Thakur, Associate Professor for their timely help and advises.

I am immensely grateful to Prof. K. C. Majumdar, Prof. R.C. Deka, Dr. A.K. Phukan, Dr. R. Bora, Dr. P. Puzari, Dr. G.V. Karunakar, Dr. P. Bharali, Dr. N. M. Gogoi and Mr. K.K. Bania faculty members of Department of Chemical Sciences, Tezpur University for valuable suggestions and advices.

My heartfelt thanks go to my senior lab-mates Dr. Sibdas Singha Mahapatra, Dr. Suvangshu Dutta, Dr. Harekrishna Deka, Dr. Uday Konwar and Buddhadeb Roy for their manifold help and active co-operation over all these years. I would also like to thank my junior group members Rocktotpal Konwarh, Sujata Pramanik, Shaswat

Barua, Suman Thakur, Hemjyoti Kalita, Bibekananda De and Beauty Das for their constant inspiration and help during my Ph.D. work.

I would like to offer my sincere thanks to Dr. Biren Gohain, Dr. Binoy Saikia, Mr. Nipu Dutta, Mr. Raju K. Borah, Mr. Sankur Phukan, Mr. Rajen Borah, Mr. Biraj Borah, Mr. Arup Chakrabarty, Mr. Manaranjan Sarma, Mr. Jyotisankar Borah, Mr. Madhurjya Deka, Dr. Kishor K. Baruah, Mr. Ratan Baruah, Mr. Ankur Gogoi and Mr. Jayanta Bora for instrumental and experimental helps. IIT Guahati, NEIST Jorhat, IIT Kharagpur, NEHU Shillong and other institutions are highly acknowledged for their help in analyzing and testing works.

I would like to thank also the office staffs of Department of Chemical Sciences, Tezpur University, Mr. Prafulla Nath, Ms Babita Das and Mr. Hemanta Gogoi for their kind help during my Ph.D. work.

I also thank Dr. Naba Kumar Bordoloi, Mr. Ranjan Duttan Kalita and Mr. Jitendra Kumar Roy, Department of Molecular Biology and Biotechnology, Tezpur University for their cooperation and help in carrying out bio-related work for my study.

I wish to thank all my friends (research scholar) for their help and support during the course of my work.

I am also grateful to DRDO as well as UGC, RGNF, New Delhi for financial support to me as JRF and SRF.

I take this opportunity to express my sincere gratitude to Mrs. Susmita Karak for her great affection, which I continue to enjoy during my stay at Tezpur University.

Finally, I owe heartfelt gratitude to my parents and all my family members for their blessings, support and constantly inspiring me to carry out my research work to completion. I am thankful to all my relatives and well-wisher for their encouragement. The endless love of them will always be in my heart that will inspire me in every step of my future life.

Place : Tezpur University, Tezpur

(Gautam Das)

Date :

CHAPTER 1

General Introduction

1.1. Introduction

During the past decade, nanocomposites become a novel class of materials that circumvent the performance of classic composite material by accessing set of desired improved properties and exploiting unique synergism between materials. Among the different types of nanocomposites polymeric nanocomposites have engraved a unique position in the field of advanced materials. Various physico-chemical modifications of polymers are requisite in terms of their desired properties. Traditionally, polymeric materials have been filled with synthetic or natural substances in order to improve their properties, or simply to reduce cost. However, although conventionally filled or reinforced polymeric materials are widely used in various fields, it is often reported that the addition of these fillers impart drawbacks to the resulting materials. Thus both the filled systems and the conventional composites may not be an ideal case as the resultant materials lost the light weight characteristic with disproportionate increase in property. In recent years the incorporation of low concentrations of nanometer-sized fillers has become an important strategy to improve and diversify polymeric materials. This advent of nanoscience and nanotechnology has opened up a new avenue for structure-property tailoring in the domain of polymers for their multifaceted advanced applications.¹⁻³ The nanoscale materials are providing opportunities for outstanding property enhancement to the polymers with a low volume of reinforcing agents. This explains the genesis of polymer nanocomposites.

Further, among the different types of industrial polymers and resins, epoxy resin represents one of the most fascinating materials which share a unique place of its own in this realm. Epoxy resins are versatile as they can be tailored to obtain products with diverse properties without much affecting the cost to performance ratio.

Again, the utilization of renewable resources in energy and material applications is receiving more attentions in both industrial and academic settings, due to concerns regarding environmental sustainability. There is a continuous declination of the use of petroleum based feedstock in the manufacturing of different industrial products including polymers. With the continuous depletion of fossil oils, dramatic fluctuations in the price of oil and environmental concerns compels the scientific and the industrial

communities to develop polymeric materials from renewable resources.^{4,5} In this context, vegetable oils offer many advantages apart from their renewability. Their world-wide availability and relatively low price make them industrially attractive and feasible raw material. Furthermore, diverse chemistry can be applied on them to obtain a large variety of monomers and polymers. Vegetable oils have been used in the production of different polymeric materials such as epoxy, alkyd, poly(ester amide), polyurethane etc.⁶⁻¹⁵ There are also reports on utilization of such oils in different industrial applications like surface coatings including paints, varnishes, printing inks, lubricants, emulsifiers, plasticizers, multipurpose additives etc.¹⁰⁻¹⁸ The unique advantages of vegetable oils include physical and chemical stability, aptitude to facile chemical modification, reduced toxicity, reduced risk for handling and transport, possibility of recycling, renewable and biodegradable, and at the same time available in large quantities in low and stable prices, and are susceptible to agricultural diversification and environmentally benign in nature.⁷⁻⁹

A variety of oil bearing seeds have been found in the forest resources and farm lands of India and so far about 350 oil bearing crops are identified. Linseed, castor, soybean, sunflower, safflower, tung, coconut etc. are a few seed oils that are used traditionally for the preparation of polymeric materials. Non-traditional rubber seed oil,¹⁹ *Albizia benth* seed oil,²⁰ jatropha seed oil,²¹ karanja oil,²² *Prunus persica*,²³ apricot oil,²⁴ *Annona squamosa*,²⁵ melon seed oil,²⁶ *Pongamia glabra*,²⁷ African locust bean seed oil,²⁸ African mahogany seed oil,²⁹ etc. are also used for the same reason. Therefore, investigation of vegetable oil based epoxy resins and their nanocomposites may open up a new avenue in the field of polymer science and technology.

1.2. Background

The term nanocomposite has been universally accepted as describing a very large family of materials involving structure in the nanometer size range (e.g. 1–100 nm), where the properties are of interest due to the size of the structures and are typically different from those of the bulk materials.^{1,30-33} The incorporation of layered silicates into polymer matrices has been known for over 50 years.³⁴ In fact, one of the earliest systematic studies of the interaction between clay and a macromolecules dates back to 1949, when Bower³⁵ described the absorption of DNA by montmorillonite. In 1970 the term “nanocomposite” was first proposed by Theng.³⁶ One of the earliest reports described by Hess and Parker in 1966 was the stable dispersion of metallic cobalt

particles of uniform size of 1-100 nm range in the polymer solutions.³⁷ However it was Toyota's research works in 1988^{38,39} that instigated the popularity of polymer nanocomposites in the field of material science with colossal application oriented utilities. Though, commercially the interest has been mostly focused on nanocomposites based on thermoplastic polymers and thermoset nanocomposites are investigated still less. This exponential growth of interest in the field of polymer nanocomposites is due to the remarkable improvement in properties like moduli, mechanical strength, thermal, gas barrier, flame retardant, biodegradability etc. of pristine polymers.⁴⁰⁻⁴³ However the sparkling research thrust to unravel the mechanism of improvements is still in mist. Although it is thought that the altered properties of nanocomposites are associated with the changes in polymer molecular dynamics and crystallinity on addition of nano-dimensional reinforcing agents.⁴⁴ The geometrical shape and size of nanomaterials also play important roles in tuning the interactions and hence the properties of such systems.

Epoxy polymers have gained tremendous attention recently in the domain of polymer nanocomposites. The word epoxy is derived from the Greek prefix "ep" which means over and between, and "oxy" means combining form of oxygen. By strict definition epoxy resins refers to uncrosslinked monomers or oligomers containing at least two epoxy groups in each molecule. The epoxy resins are thermosetting polymers, which before curing, have more than one active epoxide or oxirane group(s) in each molecule. The vast majority of industrially important epoxy resins are bi or multifunctional epoxides. The monofunctional epoxides are primarily used as reactive diluents, viscosity modifiers, or adhesion promoters. Most cured epoxy thermosets provide excellent mechanical strength and toughness; outstanding chemical, moisture, and corrosion resistance; good thermal, adhesive, and electrical properties; no volatiles emission and low shrinkage upon curing; and dimensional stability. These unique combinations of properties are generally not found in any other polymeric material. These superior performance characteristics, coupled with outstanding formulating versatility and reasonable costs, have gained epoxy resins wide acceptance as materials of choice for a multitude of bonding, structural, and protective coatings applications.⁴⁵⁻

47

Commercial epoxy resins contain aliphatic, cycloaliphatic, or aromatic backbones and are available in a wide range of molecular weights from several hundreds to tens of thousands.⁴⁷ The most widely used epoxies are the glycidyl ether derivatives of

bisphenol A (>75% of resin sales volume).⁴⁷ The capability of the highly strained epoxy ring to react with a wide variety of curing agents under diverse conditions and temperatures imparts additional versatility to the epoxies. The major industrial utility of epoxy resins is in thermosetting applications. Treatment with curing agents gives insoluble and intractable thermoset polymers.^{46,47} In order to facilitate processing and to modify cured resin properties, other constituents like: fillers, solvents, diluents, plasticizers, catalysts, accelerators and tougheners are included in the compositions.

1.3. Polymer Nanocomposites

The term “nanotechnology” encompasses an emerging family of heterogeneous technologies including “nanosciences” and “nanotechnologies” enabling the manipulation of matter at the nanodimensional level. Polymer nanocomposites are defined as an interacting mixture of two phases—a polymer matrix and a solid phase (organic or inorganic) of nanometer size range (1-100 nm) in at least one dimension.⁴⁸ Conceptually, nanotechnology refers to the ability to control the composition of molecules and atoms, within the range of 1 to 100 nm, potentially enabling scientists to create specific molecular structures and devices. Polymer nanocomposite can broadly be divided into three categories depending on the dimension of the nanofillers. The first category is the iso-dimensional nanofillers (all dimensions within 100 nm) present in the polymeric matrix. The spherical silica, silica or titania oxides, metal nanoparticles etc. fall in this category.

The second class comprises of nanofillers having two of its dimensions in nanometer range while the third one is in micrometer. Such nanofillers possess elongated structure. Nanotube, nanofibers, cellulose whiskers reinforced polymer matrices are the examples of this category.

Third type of nanocomposites corresponds to the case where the nanofillers have only one dimension in nanometer range. The extensively studied polymer/clay and polymer/layer double hydroxide (LDH) nanocomposites represent this group.

Any physical mixture of a polymer and silicate (or inorganic material in general) does not necessarily form a nanocomposite. The situation is analogous to polymer blends. In most cases, separation into discrete phases normally takes place. In immiscible systems, the poor physical attraction between the organic and the inorganic components leads to relatively poor mechanical properties. Furthermore, particle agglomeration tends to reduce strength and produces weaker materials. Thus, when the

polymer is unable to intercalate between the silicate sheets, a phase-separated composite is obtained, whose properties are in the same range as for traditional microcomposites.^{49,50}

Depending on the nature of the components (layered silicate, organic cation and polymer matrix), preparative method and extent of interactions between nanofillers, two types of nanocomposites can be obtained (Fig. 1.1). These are as follows:

(a) *Intercalated*: In this nanocomposites, extended polymer chains are inserted between the silicate layers/bundles of nanotubes. This occurs in a crystallographically regular fashion, with a few nanometers repeat distance, irrespective of the ratio of polymer to layered/tube structure. This results in a well ordered multilayer/tube bundle structure of alternating polymeric and layers/tubes, such type of structure is called intercalated nanocomposites.

(b) *Exfoliated*: In this type of nanocomposites separation of the individual layers in the polymer matrix occurs with average distances between the layers depends only on the loading of nanomaterial. Exfoliated nanocomposites result in high storage modulus, improved tensile and flexural properties, high heat distortion temperature, decrease in gas permeability, along with improved flame retardancy and biodegradability compared to the pristine matrix or conventional micro and macro-composites.

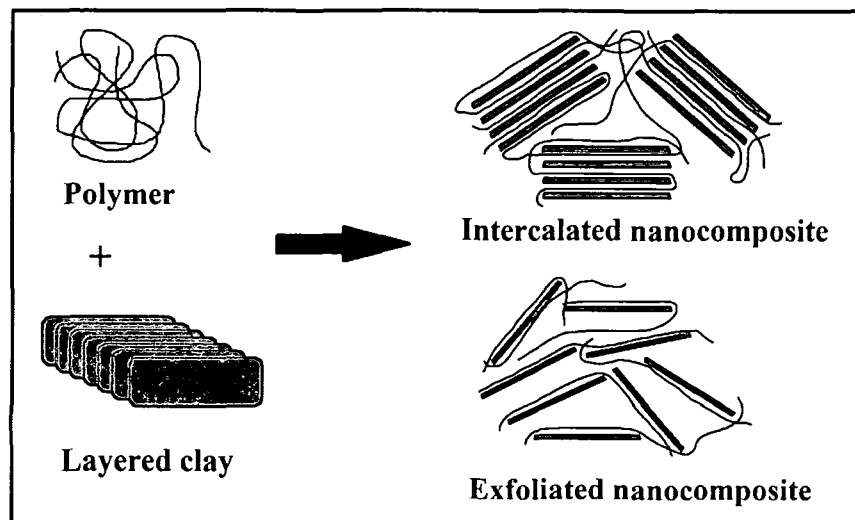


Fig. 1.1: Different states of polymer/clay nanocomposites

1.4. Materials and Methods

1.4.1. Materials

In polymer nanocomposite, there are nanomaterials and other necessary additives along with the polymer matrix. Depending on the technique of preparation, sometimes solvent or other auxiliary chemicals are also employed. It has already been stated that a large number of polymer matrices and nanomaterials are utilized to obtain a variety of polymer nanocomposites. In the present investigation, as epoxy will be used as the matrix and nanoclay, metal nanoparticles and carbon nanotube shall be the nanofillers, so the discussion is restricted within these materials only.

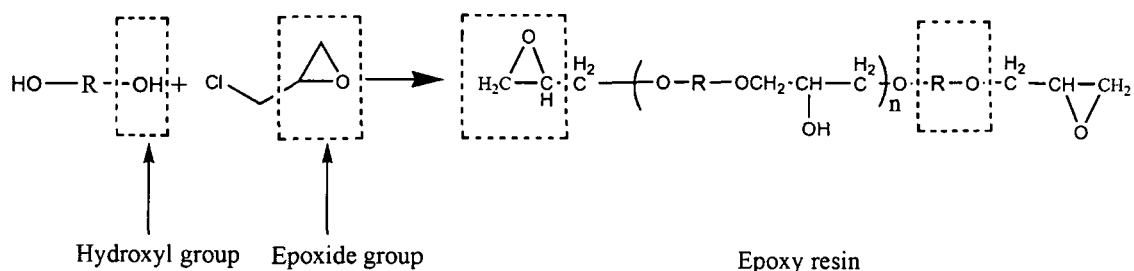
1.4.1.1. Epoxy

Epoxy resins are being used as matrix for the preparation of both conventional composites as well as nanocomposites. The epoxy resins are usually synthesized by direct reaction of the aromatic or aliphatic diols and epichlorohydrin through polycondensation reaction (Scheme 1.1). In case of epoxidized oil it is generally synthesized by *in-situ* peroxidation with organic and inorganic peroxides,⁵¹ with halohydrins and molecular oxygen. However, the epoxidation of unsaturated moiety having electron deficient double bonds with halohydrins is environmentally unfriendly.

A brief description of the different compounds used for synthesis of epoxy resins and epoxidized oil are presented below.

Aromatic diols

A short list of different aromatic diols, which are generally used in preparation of epoxy resins is given in Table 1.1.



Scheme 1.1: Formation of epoxy resin

Bisphenol-A (2,2-bis(4-hydroxyphenyl)propane or BPA) is one of the most widely used aromatic diols for the synthesis of epoxy resin. One of the first reports on synthesis of epoxy resin utilized BPA and epichlorohydrin.⁴⁶ The resins are commonly used as lacquers to coat metal products such as food ‘can’, bottle tops and water supply. There are also reports on the uses of bis(4-hydroxyphenyl) sulfone or bisphenol-S

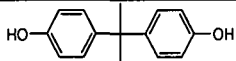
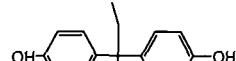
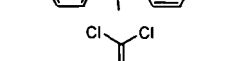
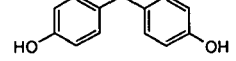
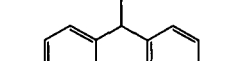
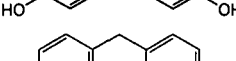
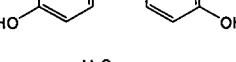
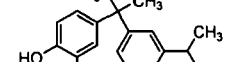
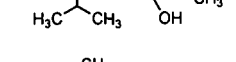
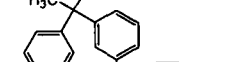
(BPS) in the synthesis of epoxy resin. The advantages of resistance to deformation by heat and improvement of thermal stability were observed for such epoxy resins.⁵²⁻⁵³ The presence of sulfone group in the epoxy resin exhibits better gel time than BPA based epoxy.⁵⁴⁻⁵⁵ Another important diol i.e. bis(4-hydroxydiphenyl)methane or bisphenol-F (BPF) is used for the synthesis of low viscosity epoxy resins. BPF generally comprises of several isomers such as bis(2-hydroxyphenyl)methane (i.e. ortho-ortho isomer), bis(4-hydroxyphenyl)methane (i.e. para-para isomer) and 4-hydroxyphenyl-2'-hydroxyphenylmethane (i.e. ortho-para isomer). However those based on para-para isomers are reported to exhibit improved solution/melt viscosity and other physical properties. Epoxy resins based on bisphenol-F are used primarily as functional diluents where low viscosity is required and high performance resin systems (e.g. solvent-free coatings). High functionality epoxy resin are also synthesized by using multifunctional aromatic moiety such as phenol novolac and o-cresol novolac as reported by Dow and Ciba Products Co. while Shell introduced polyglycidyl ethers of tetrafunctional phenols whereas Union Carbide developed triglycidyl *p*-aminophenol resin.⁵⁶ Bisphenol-C is another important diol which is widely used for preparation of flame retardant epoxy resin. The other important diol which finds wide application in synthesis of flame retardant epoxy thermosets is 4,4'-isopropylidene bis(2,6-dibromophenol) (tetrabromobisphenol-A, TBPA). The primary use of TBPA is as a reactive flame retardant⁵⁷ in epoxy resin based circuit boards and in electronic enclosures made of polycarbonate-acrylonitrile butadiene-styrene (PC-ABS), etc.⁵⁸ Hexafluorobisphenol-A (bisphenol-AF, hexafluoroisopropylidene diphenol) has also been used for the synthesis of fluorinated epoxy resin aiming at the anticorrosion coatings market for industrial vessels and pipes. The key disadvantages of fluorinated epoxies are their relatively high costs and low T_g , which limit their commercialization.⁵⁹⁻⁶¹

Epoxidized oil

Vegetable oils are potential sources for substituting BPA based epoxy resin. Commercially available vegetable oils are primarily obtained from oil seed plants through extraction of flaked oil seeds with non-polar solvents such as hexanes.⁶² Triglycerides form the largest component of the extracted vegetable oils. Triglycerides are comprised of three fatty acid molecules attached to one molecule of glycerol through ester bonds. The functional properties, oxidative stability, and the nutritional

value of oils are determined by fatty acid composition, geometric configuration, and positional distribution.

Table 1.1: Different aromatic diols with their structures and a few physical properties

Name	Structure	Melting point (°C)	Boiling point (°C)	Density (g/cm ³)
Bisphenol A		158-159	220	1.20
Bisphenol B		124 - 125	412	1.19
Bisphenol C		213-217	239	1.28
Bisphenol E		123-127	224	1.19
Bisphenol F		159-161	314	1.17
Bisphenol G		98	422.7	1.04
Bisphenol M		135-139	495.9	1.107
Bisphenol S		245-250	505.3	1.43
Tetra bromo bisphenol-A		178	250	2.12
4,4'-bis Bisphenol AF		159-163	316-664	1.37

Fats and oils are renewable resources that can be chemically or enzymatically treated to obtain epoxidized oil.⁶³⁻⁶⁷ Epoxidation of fatty acids is a reaction of a carbon-carbon double bond with active oxygen, which results in the addition of an oxygen atom, converting the original double bond into a three membered epoxide (oxirane) ring. In general, olefins can be epoxidized with various peracids, of which peracetic acid is most often used.

Epihalohydrin

Epihalohydrin are compound with an oxirane ring. It is colorless liquid with a pungent garlic like odor, moderately soluble in water but miscible with most polar organic solvents.^{45,47} Epichlorohydrin is a highly reactive compound and is used in the production of epoxy resin.

Catalysts

Various types of catalyst are used for the polycondensation reaction of diols with epichlorohydrin. The catalysts facilitate the reaction by generating an anion from the hydroxyl containing compounds. This catalyst is preferably any heterogeneous or homogenous compound or resin which removes a hydrogen atom from the active hydrogen containing compound under the used reaction conditions. The useful base compounds include alkali and alkaline earth metal bicarbonates, carbonates, hydroxides or hydrides or alkoxides, etc. A few of such compounds are sodium carbonate (Na_2CO_3), potassium carbonate (K_2CO_3), lithium carbonate (Li_2CO_3), calcium carbonate (Ca_2CO_3), sodium hydroxide (NaOH), potassium hydroxide (KOH), lithium hydroxide (LiOH), calcium hydroxide (CaOH), sodium bicarbonate (NaHCO_3), potassium bicarbonate (KHCO_3), lithium bicarbonate (LiHCO_3), calcium bicarbonate ($\text{Ca}(\text{HCO}_3)_2$), or any combination of any two or more such base compounds and the like. However, the most preferred base compounds are sodium carbonate and sodium hydroxide.^{47,68-71}

Alternatively tertiary amines, phosphines and quaternary ammonium salts are established as addition reaction catalysts instead of sodium hydroxide or the addition and the dehydrohalogenation reactions are separated from each other.⁶⁹⁻⁷⁰ Sodium hydroxide is introduced in the second step, after 40-90% of the phenol groups of bisphenol-A have already reacted and after the excess of epichlorohydrin was removed under reduced pressure. Sometimes, two different ammonium catalysts are used in both steps of the process, or sodium hydroxide is partly added with ammonium salts. In all cases, when supplementary catalysts were applied, both stages of the reaction were separated.

The epoxidation of the vegetable oils can be carried out by four different methods such as (a) epoxidation with percarboxylic acids, can be catalyzed by acids or by enzymes, (b) epoxidation with organic and inorganic peroxides, catalyzed by transition metal catalyst, (c) epoxidation with halohydrines, using hypohalous acids (HOX) and

their salts and (d) epoxidation with molecular oxygen. However the oxidation of the double bond by employing organic peracids are by far the most industrially accepted one and therefore the discussion is limited to this methods only. Such acids are, for example, formic, acetic, propionic, n-butyric, isobutyric, 3-methylbutanoic, 2,2-dimethylpropanoic, n-valeric, n-caproic, n-heptoic, caprylic, n-nonylic, capric, undecylic, lauric, tridecylic, myristic, pentadecylic, palmitic, margaric, and stearic acids. Though, the most preferred acids for this purpose are formic and acetic because of their ready availability at relatively low price in liquid form at room temperature. The order of reactivity of some of the peracides is m-chloroperbenzoic > performic > perbenzoic > peracetic. The presence of electron withdrawing groups promotes the reaction. More work has been published on the synthesis of epoxidized oil by peracetic acid than that of any other organic peracid.^{62-64,72-73}

Various types of inorganic catalysts are used in conjunction with organic acids for the peracid formation. The liquid inorganic acids used as catalysts for epoxidation are H₂SO₄, HNO₃, H₃PO₄, and HCl.^{62-64,72}

Curing Agents

Curing agents play an important role in the curing process of epoxy resin because they relate to the curing kinetics, reaction rate, gel time, degree of curing, viscosity, curing cycle, and the final properties of the cured products. Thus many researchers have been studying the effects of curing agents on the curing process. An overview of the epoxy curing agents and modifiers was highlighted by Mike and Bauer in 1988.⁷⁴ There are mainly three types of curing agents. The first type of curing agents includes active hydrogen containing compounds and their derivatives.^{75,76} Compounds with amine, amide, hydroxyl, acid or acid anhydride groups belong to this category. They usually react with epoxy resin by polyaddition and resulted in amine, ether, or ester linkages. Aliphatic and aromatic polyamines, polyamides, and their derivatives are the commonly used amine type curing agents. The liquid aliphatic polyamines such as polyethylene polyamines (PEPAs) were some of the first curing agents used for epoxies. The low equivalent weights of the ethylene amines give tightly crosslinked networks with good physical properties, including excellent chemical and solvent resistance but limited flexibility and toughness. They offer good RT (room temperature) cures with bisphenol-A diglycidyl-type resins. The aliphatic amines are very reactive and have a short lifetime. Their applications are limited because they are

usually volatile, toxic or irritating to eyes and skin, and thus cause serious health problems.^{45,47,75} Polyetheramines, most commonly amine terminated polyoxypropylene, are less volatile and are available in a range of molecular weights including low (230 g/mol) and high (2,000 g/mol) molecular weight oligomers.⁷⁷ Incorporation of these amines also increases the flexibility of the network. The etheramine reactivity is lower than that of the alkylene amine so they are often used in combination with other amine curing agents. Another type of amine curing agent are the aromatic amines, compared to aliphatic amine, aromatic amines are less reactive, less harmful to people, and need higher curing temperature and longer curing time. Hydroxyl and anhydride curing agents are usually less reactive than amines and require a higher cure temperature and more cure time.⁷⁸ They have longer lifetimes. Polyphenols are the more frequently used hydroxyl type curing agents.⁷⁶ Polybasic acids and acid anhydrides are the acid and anhydride type curing agents that are widely used in the coating field.^{79,80} Table 1.2 gives a list of commonly used curing agents and their chemical structures. Polyamides are extremely versatile curing agents. The polyamides react with the epoxide group through the amine functionality in the polyamide backbone. Whereas, the unreacted amide -NH groups in the backbone provide good intercoat adhesion and the fatty acid structures offer good moisture resistance and mechanical properties. The wetting of surfaces by polyamide cured epoxy thermosets is excellent. As a result of their relatively higher molecular weight, the ratio of polyamide to epoxy is more forgiving than with low molecular polyamines. They are inexpensive, less toxic to handle; give no blushing; exhibit readily workable pot lives; and cure under mild conditions. Polyamides are mainly used in coating and adhesive formulations in industrial maintenance and in civil engineering applications. Amidoamines have all the properties of polyamides, except for a significantly low viscosity, which make them useful in high solids and solvent-free coating formulations. They are prepared by the reaction of a monofunctional acid like tall oil fatty acid with a multifunctional amine such as diethyl triamine (DETA), resulting in a mixture of amidoamines and imidazolines.

The second type of curing agents includes anionic and cationic initiators. They are used to catalyze the homopolymerization of epoxy resins. Molecules, which can provide an anion such as tertiary amines, secondary amines, and metal alkoxides are the effective anionic initiators for epoxy resins. Molecules that can provide a cation, such as the halides of tin, zinc, iron and the fluoroborates of these metals are the effective cationic initiators. The most important types of cationic initiators are the complexes of

BF_3 like boron trifluoride monoethylamine ($\text{BF}_3 \cdot \text{NH}_2\text{C}_2\text{H}_5$), a crystalline material which is a commonly used catalyst, cures epoxy resins at 80–100 °C.

The third type of curing agents is called reactive crosslinkers. They usually have higher equivalent weights and crosslink with the second hydroxyls of the epoxy resins or by self-condensation. Examples of this type of curing agents are melamine, phenol, and urea formaldehyde resins. Among the above three types of curing agents, compounds with active hydrogen are the most frequently used curing agents and have gained wide commercial success. Most anionic and cationic initiators have not been used commercially because of their long curing cycles and other poor cured product properties. Reactive crosslinkers are mainly used for surface coatings and usually are cured at high temperatures to produce films having good physical and chemical properties.

1.4.1.2. Nanomaterials

By definition materials whose at least one of the dimension is within 100 nm are called nanomaterials (Fig. 1.2). The specific surface area of the materials increases with the decrease in grain size, which results markedly different physico-chemical properties that are dominated by the physics of the bulk materials.

The nanomaterials generally used in the preparation of nanocomposites to enhance the desired performance of pristine polymer systems are divided into three types depending on the dimensions are discussed briefly below.

Nanolayers

Among all the potential nanocomposite precursors, those based on clay and layered silicates have been most widely investigated, probably because the starting clay materials are easily available and because their intercalation chemistry has been studied for a long time.^{1,49} This type of nanomaterial has only one dimension in the nanometer range. They possess a platelet like structure in the form of sheets or layers. The lateral dimension may be in the range of several hundred nanometers to microns, while the thickness is usually less than 100 nm. They may be both natural and synthetic minerals, consisting of very thin layers that are usually bound together with counter-ions. Their basic building blocks are tetrahedral sheets in which silicon is surrounded by four oxygen atoms, and octahedral sheets in which a metal like aluminum is surrounded by eight oxygen atoms. Examples of such layered nanofillers, which are potential candidates for preparing polymer nanocomposites are phyllosilicates {kaolinite, dickite,

nacrite, halloysite, chrysotile, antigorite, lizardite, montmorillonite, bentonite, nontronite, beidellite, hectorite, colknskonite, pyrophyllite, talc, vermiculite, illite, glauconite, muscovite, celadonite, phlogopite, taenolite, margarite (brittle mica), palygorskite, sepiolite, clinochlore}, layered silicic acids {kanemite, makamite,

Table 1.2: Different curing agent with their physical properties

Name	Structure	Melting point (°C)	Boiling point (°C)	Density (g/cm ³)
Hexamethylene diamine		42	205	0.84
Diamino diphenyl sulfone		131	295	1.53
Diamino diphenyl methane		89	398-399	1.14
4,4-methylene bis(3-chloro-2,6-diethylaniline)		87	506.4	1.15
Methylaniline		-57	200.4	0.99
Dicyandiamide		208 - 211	229.8	1.4
Fatty amido amines		-4	>350	0.987

octosilicate, magadite, kenyaite, layered organo-silicates}, mineral-layered hydroxides {brucite (Mg(OH)₂), gibbsite (Al(OH)₃)}, layered double hydroxides (LDH) {M₆Al₂(OH)₁₆CO₃·nH₂O (M: Al, Zn)}, layered alumino-phosphates {berlinite, vantasselite (Al₄(PO₄)₃(OH)₃·9H₂O)}, metal (M⁴⁺) phosphates {M⁴⁺: Zr, Ti or Sn; Zr(HPO₄)}, phosphonates {HUO₂PO₄·4H₂O, Na(UO₂PO₄)·nH₂O}, chlorides {FeCl₃,

CdCl₂}, oxyhalides {FeOCl, VOCl, CrOCl} metal chalcogenides {(PbS)_{1.18}(TiS₂)₂, TiS₂, MoS₂, MoS₃}, cyanides {Ni(CN)₂}.

The crystal lattice of 2:1 layered silicates (or 2:1 phyllosilicates), consists of two-dimensional layers where a central octahedral sheet of alumina is fused to two external silica tetrahedra by the tip, so that the oxygen ions of the octahedral sheet also belong to the tetrahedral sheets, as shown in Fig. 1.3. The layer thickness is around 1 nm and the lateral dimensions may vary from 0.03 μm to several microns, and even larger, depending on the particulate silicate, the source of the clay and the method of preparation (e.g. clays prepared by milling typically have lateral platelet dimensions of approximately 0.1–1.0 nm). Therefore, the aspect ratio of these layers (ratio of length/thickness) is particularly high, with values greater than 1000.^{49,81-82} These layers are attracted by van der Waals forces. Stacking of the layers leads to a regular van der Waals gap between the layers called the interlayer or gallery. Isomorphous substitution within the layers (for example, Al³⁺ is replaced by Mg²⁺ or Fe²⁺, or Mg²⁺ is replaced by Li⁺) generates negative charges that are counterbalanced by alkali and alkaline earth cations (Na⁺, K⁺, Ca²⁺ and Mg²⁺) situated inside the galleries. These pristine clay minerals are generally hydrophilic in nature.⁸³ Inorganic clays are incompatible with most of the polymers, so to render layered silicates miscible with hydrophobic polymeric matrices. Thus one must convert the hydrophilic silicate surface to an organophilic one. Traditionally cation-exchange reactions have been exploited as an effective method to replace these inorganic ions with organic cationic surfactant molecules which intercalate into the clay gallery, resulting in expansion of the interlayer spacing thereby leading to an increase in the basal spacing. These organic cations render the clay mineral hydrophobic at the surface while also increasing its wettability and thermodynamically favorable interactions with polymer molecules. The most widely used organic cation for the modification of organonano clay is the alkylammonium species such as quaternary ammonium compounds containing alkyl, phenyl, benzyl and pyridyl groups (Table 1.3). In some cases, a mixture of alkyl and alkenylammonium ions is also used. Alkylphosphonium cations have also gained wide significance for such modifications. Alkylammonium or alkylphosphonium cations in the organosilicates lower the surface energy of the inorganic host and improve the wetting characteristics of the polymer matrix and result in a larger interlayer spacing.

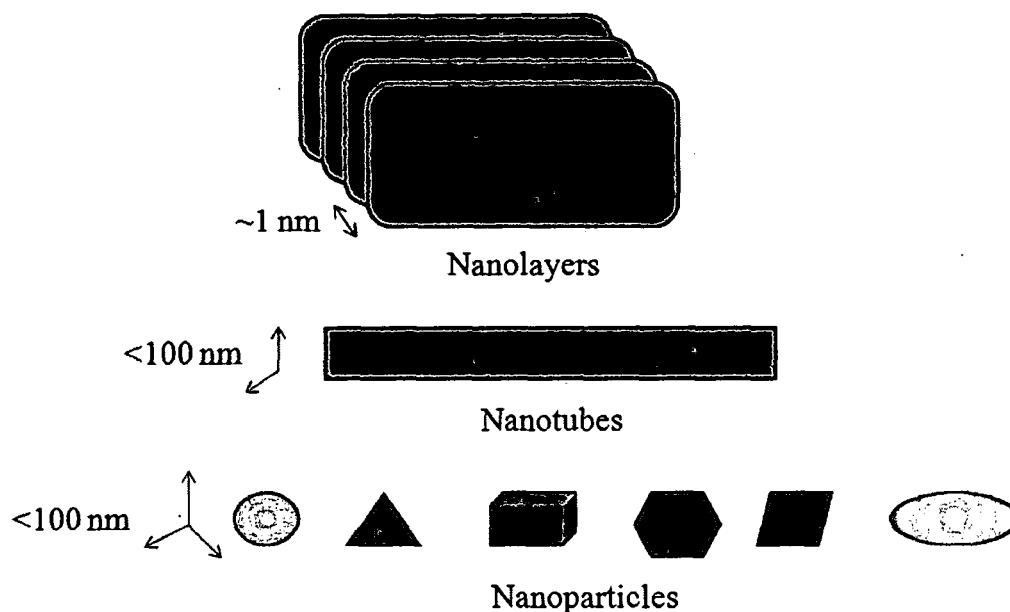


Fig. 1.2: Different types of nanomaterials

Additionally, the alkylammonium or alkylphosphonium cations can provide functional groups that can react with the polymer matrix, or in some cases initiate the polymerization of monomers to improve the strength of the interface between the inorganic and the polymer matrix.⁸³ These organophilic montmorillonite (OMMT) clays whose surface energy is lowered and are more compatible with organic polymers may intercalate under well defined conditions by the polymer chains.

Nanotubes

The second type of nanomaterials has two dimensions in the nanometer scale while the third dimension is a few hundred nanometers in size. Carbon nanotubes (CNTs) and nanofibres fall in this category. They possess an elongated structure. They are found in cylindrical or tubular form and are known as nanotubes or nanofibers/whisker/nanorods, carbon nanotubes, carbon nanofibers, exfoliated graphite (graphene), cellulose nanofibers and cellulose whiskers belong to this category. Carbon nanotubes consist of rolled graphene where each carbon atom is sp^2 hybridized and covalently bonded to three neighboring carbon atoms. These consists of sheets with diameters in the nanometre range and lengths in the micrometre range, and are useful materials with unique physicochemical properties different from those of other carbon allotropes, such as graphite, diamond, and fullerenes. The atoms are arranged in same manners as in graphite.⁸⁷ The graphitic carbon layers and the tubes typically have an internal diameter of *ca.* 5 nm and external diameter of *ca.* 10 nm (Fig. 1.4). Nanofibres

of diameter up to 200 nm are also being produced. There are two main types of carbon nanotubes that can have high structural perfection. Single-walled nanotubes (SWCNTs) consist of a single graphite sheet seamlessly wrapped into a cylindrical tube. In contrast, multi-walled nanotubes (MWCNTs) comprise an array of such nanotubes that are concentrically nested like rings of a tree trunk (Fig. 1.4).

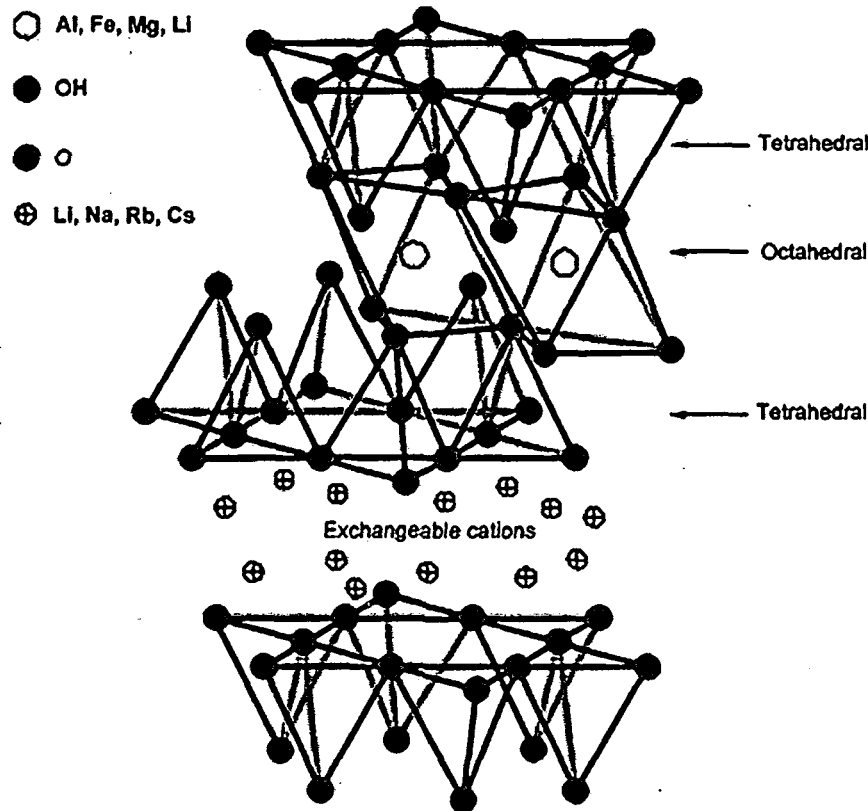


Fig. 1.3: Structure of clay (2:1 phyllosilicates)

They usually have a diameter from a few angstroms to tens of nanometers and can have lengths up to several microns. Both SWCNTs and MWCNTs have physical characteristics of solids and are micro-crystals with high aspect ratios. The atomic arrangements, diameter and length of the nanotubes, morphology or nanostructure predict the properties of the carbon nanotubes. The carbon nanotubes are one of the strongest and stiffest material, the young modulus of these are as high as 1 to 4 TPa. This strength results from the covalent sp^2 bonds formed between the individual carbon atoms.

They also show high optical, electrical and thermal properties. The strong interfacial adhesion between CNTs and polymer matrix is improved by the

modification of CNTs, which leads to well dispersed and a stable nanocomposites with enhanced properties.⁸⁸

Table 1.3: Different quaternary ammonium and phosphonium ions used for modification of hydrophilic clay

Quaternary cation'	Chemical structure	Ref.
Trimethylammonium bromide		84
Octadecyl triethylammonium bromide		84
Tetrabutyl phosphonium bromide		85
Tributyl hexadecylphosphonium bromide		85
Propyl triphenylphosphonium bromide		85
Cetyl trimethylammonium bromide		84
Bis(2-hydroxyethyl) lauryl(vinylbenzyl) ammonium chloride		86
Octadecylammonium chloride		86
Dodecyl pyridinium chloride		85
1-ethyl 3-methyl imidazolium bromide		85
1-hexyl 3-methyl imidazolium chloride		85

Another important example in this category is tube-like nanoscale particles called cellulose nanofibers. Cellulose is a biopolymer which consists of β -1-4-linked D-anhydroglucopyranose units (Fig. 1.4). The degree of polymerization (DP) for cellulose nanofibers varies from 1000 to 15000 glucopyranose units depending upon the source of their origin. Cellulose nanofibers are linear polymer which exhibits high stiffness

and strength due to the extensive inter- and intra-molecular hydrogen bonds between the molecules. They are often referred to as cellulosic fibers, related to the main chemical component cellulose, or as lignocellulosic fibers, since the fibers usually contain a natural polyphenolic polymer, lignin also, in their structure. After defibrillation, they are mostly produced as stiff rodlike particles called whiskers or nanofibers.⁸⁹ Generally, their geometrical characteristics depend on the origin of cellulose microfibrils and acid hydrolysis process conditions such as time, temperature and purity of materials.

Nanoparticles

The different metal nanoparticles like silver, copper, magnetic iron etc. and spherical silica where all the three dimensions are in nanometer scale are the examples of this class. The nanoparticles are also often named as equi-axed or nanogranules or nanocrystals. They have different shapes depending on their sizes and the same nanoparticles may have different shape, size and behavior. Nanoparticles are generally thermodynamically unstable. To produce stable nanoparticles, they must be arrested during the preparation either by adding surface protecting reagents, such as organic ligands or inorganic capping materials, or by placing them in an inert environment such as an inorganic matrix or polymers. In general, the nanoparticles are obtained by different routes such as sol process, chemical precipitation, sol-gel process, hydrothermal/solvothermal synthesis, reaction in confined space, pyrolysis, vapor deposition etc. however, for preparing monodisperse nanostructures, the process requires a single, temporally short nucleation event followed by slower growth on the existing nuclei.

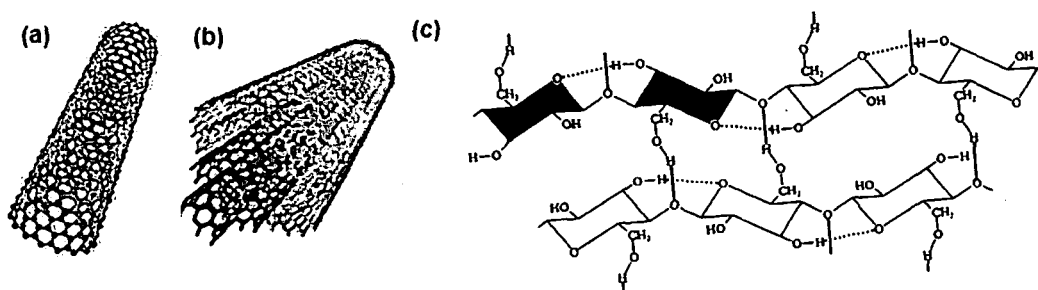


Fig. 1.4: Structures of (a) SWCNTs, (b) MWCNTs and (c) cellulose chain

1.4.2. Methods

1.4.2.1. Epoxy Matrix

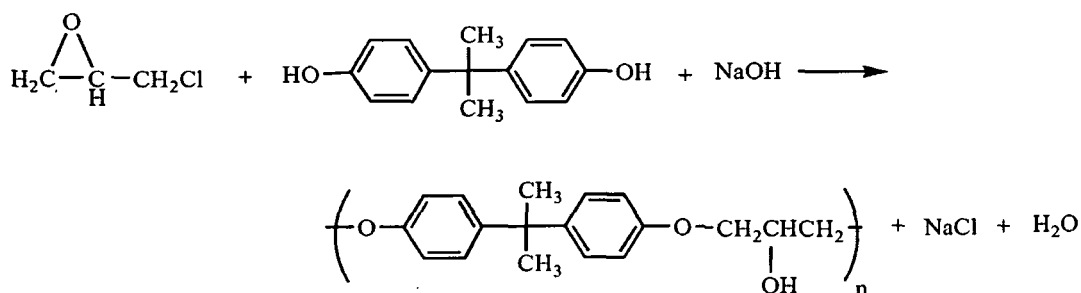
The matrix epoxy resin can be prepared by the following methods

Taffy Process

According to this process, bisphenol-A is reacted directly with epichlorohydrin in the presence of a stoichiometric amount of NaOH and the molecular weight of the product is controlled by the ratio of ECH to BPA. In the typical *taffy* process, resins with rather small polycondensation degree from 1 to 4 are obtained. The term *taffy* is derived from the appearance of the advanced epoxy resin prior to its separation from water and precipitated salts (Scheme 1.2).

In the *taffy* process, a calculated excess of epichlorohydrin governs the degree of polymerization. However, preparation of the higher molecular weight species is subject to practical limitations of handling and agitation of highly viscous materials and is largely governed by the effect of epichlorohydrin to bisphenol-A (ECH-BPA) ratio.

In commercial practice, the *taffy* method is used to prepare lower molecular weight solid resins, i.e. those with maximum epoxide equivalent weight (EEW) values of about 1000 (type "4"). Upon completion of the polymerization, the mixture consists of an alkaline brine solution and a water-resin emulsion. The product is recovered by separating the phases, washing the *taffy* resin with water, and removing the water under vacuum. One disadvantage of the *taffy* process is the formation of insoluble polymers, which create handling and disposal problems.



Scheme 1.2: Synthesis of epoxy resin by *taffy* process

In this process, caustic is used as a catalyst for the nucleophilic ring-opening (coupling reaction) of the epoxide group on the primary carbon atom of epichlorohydrin by the phenolic hydroxyl group and in caustic coupling processes, caustic (20–50% sodium hydroxide in water) is slowly added to an agitated mixture of epichlorohydrin and bisphenol-A. The highly exothermic coupling reaction proceeds

during the initial stages. As the coupling reaction nears completion, dehydrochlorination becomes the predominant reaction.

Alternatively, the coupling reaction and dehydrochlorination can be performed separately by using phase-transfer coupling catalysts, such as quaternary ammonium salts,⁹⁰ which are not strong enough bases to promote dehydrochlorination. Once the coupling reaction is completed, caustic is added to carry out the dehydrochlorination step. Higher yields of the $n = 0$ monomer (>90%) are readily available via this method. Many variations of these two basic processes are described in process patents,⁹¹ including the use of co-solvents and azeotropic removal of water to facilitate the reactions and to minimize undesirable by-products such as insoluble polymers. The original batch methods have been modified to allow for continuous or semicontinuous production. New developments have been focused on improving manufacturing yield and resin purity.

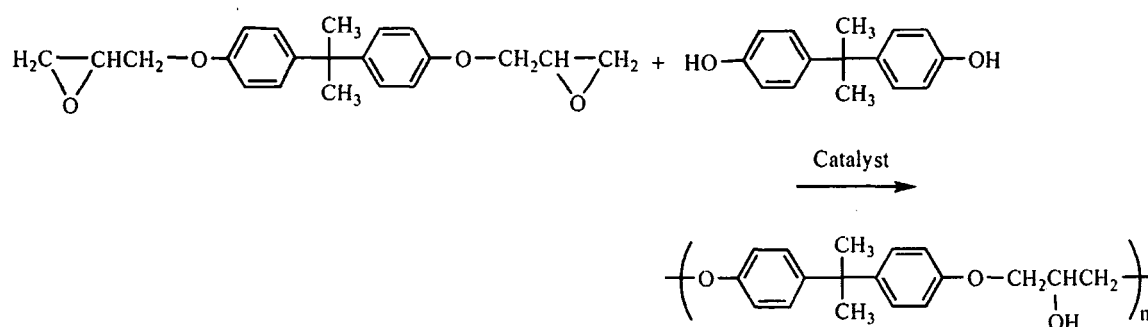
Kinck and Ditrych⁹² have synthesized epoxy resin ester of bisphenol-C, epichlorohydrin, by *taffy* process in organic solvents at 80-100 °C. The resin obtained had an ester equivalent of 180, content of epoxy groups 0.11 mol/100 g, and number of -OH groups 0.33 mol/100 g.

Advancement Process

The advancement method often referred to as the fusion process is the reaction of compounds containing 2 to 4 phenolic hydroxyl groups with a stoichiometric excess of low molecular weight epoxy resin or polyepoxide (Epoxy Value = 0.58–0.35 mol/100 g; $M_n = 370$ –500) or middle molecular weight epoxy resin (Epoxy Value = 0.30–0.15 mol/100 g; $M_n = 500$ –1,000) in the presence of a catalyst, the reaction proceeds as a step-growth polymerization process and hence the name advancement process (Scheme 1.3).

The advancement process is more widely used in commercial practice. Isolation of the polymerized product is simpler, since removal of copious amounts of NaCl is unnecessary. The reaction can be carried out with or without solvents. In a typical advancement process, dihydric or polyhydric phenols and a liquid polyepoxides resin (175–185, Epoxide Equivalent Weight, EEW) are heated to about 150–190 °C in the presence of a catalyst. The oligomerization is exothermic and proceeds rapidly to near completion. The exotherm temperatures are dependent upon the targeted EEW and the

reaction mass. The exotherm temperatures of >200 °C are routinely encountered in case of epoxy resin of high molecular weight.



Scheme 1.3: Synthesis of high molecular weight epoxy resin

Many compounds have been suggested or described as catalysts for the advancement reaction. The catalysts play a major role in determining the final structure of the resin. Many of the catalysts used result in branching or crosslinking while others are ineffective in promoting the highly exotherm reactions at the practices rates to obtain a satisfactory linear solid epoxy resin. Conventional advancement catalysts include basic inorganic reagents, e.g. NaOH, KOH, Na_2CO_3 , or LiOH, and amines and quaternary ammonium salts. One key disadvantage of catalysts based on inorganic bases and salts is the increased ionic impurities added to the resin, which is not desirable in certain applications. Alternative to the traditional catalysts phosphonium halide such as methyl or ethyl triphenyl phosphonium iodide or bromide or organic phosphine catalysts such as triphenyl phosphine or tributylphosphine or phosphonium salt of carboxylic acids such as ethyl triphenylphosphonium acetate exhibits sufficient selectivity and reactivity towards advancement reactions.

1.4.2.2. Nanocomposites

The preparative methods of polymer nanocomposites can broadly be categorized into three sub categories namely, *in-situ* polymerization, solution and melt-mixing techniques. Briefly, these methods are discussed below.

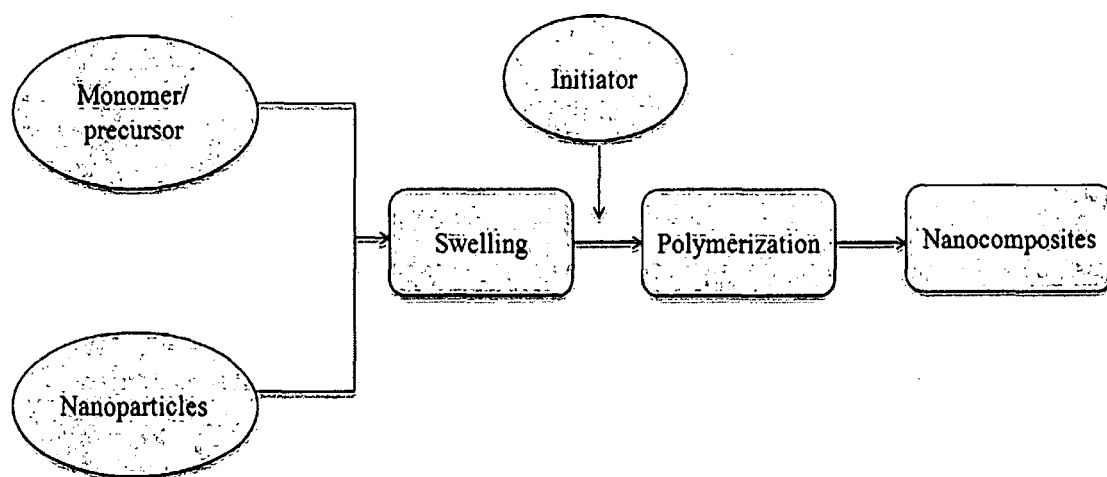
In-situ Polymerization

In-situ polymerization was the first reported method to prepare the polymer/clay nanocomposites.⁹³⁻⁹⁴ It is one of the most accepted methods for the preparation of nanocomposites. In this technique the nanoparticles are first swelled or dispersed in the monomer or precursor and subsequently polymerization is carried out. The

polymerization can be initiated either by heat or radiation, by the diffusion of a suitable initiator, or by appropriate organic initiator or catalyst fixed through cation exchange inside the interlayer before the swelling step. The low viscosity of the monomers and pre-polymers results in better diffusion in between the nanoparticles resulting in breaking down of the particle agglomerates. Consequently, the use of high shear force results in uniform mixing of the two phases as compared to other techniques. This method is capable of producing well exfoliated nanocomposite and has been applied to a wide range of polymer systems. The driving force of this technique is related to the secondary interactions of the monomers. In the swelling state due to the high surface energy, the nanomaterials attract the monomer molecules so that they diffuse between the layers or tube structure of nanomaterials. After reaching the equilibrium the diffusion of the monomer is stopped and the nanomaterials are swelled. On starting of the polymerization, the polymer chains start to grow within the nanomaterials and ultimately result the exfoliated structure. A schematic diagram for preparation of nanocomposite through *in-situ* polymerization technique is shown in Scheme 1.4.

Solution Method

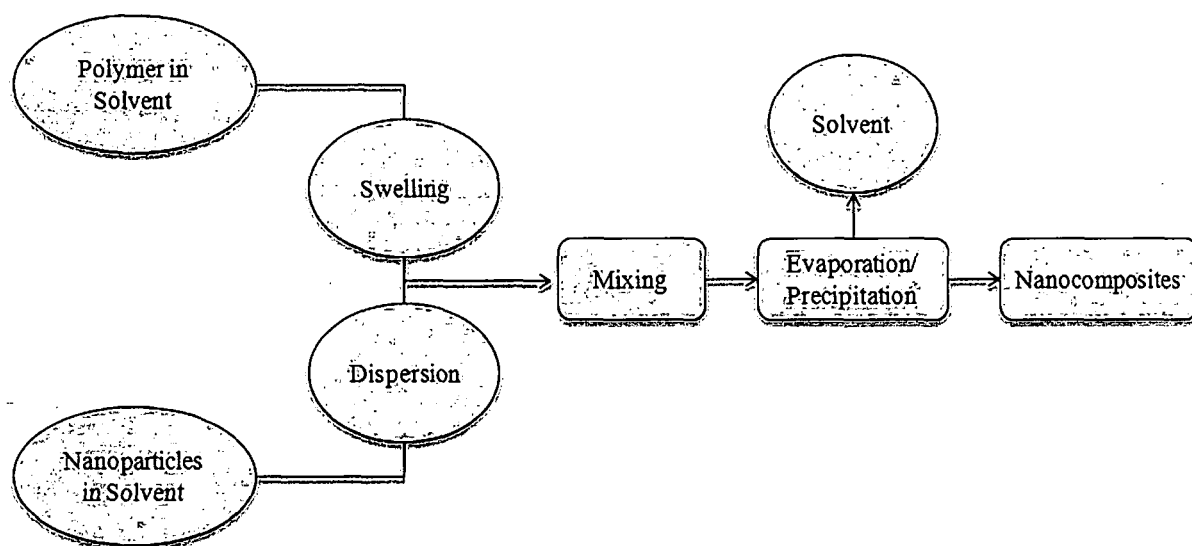
The preparation of polymer nanocomposites by solution technique involves dispersion of the polymer and nanomaterials in an appropriate solvent or a mixture of miscible



Scheme 1.4: Schematic diagram for the preparation of polymer nanocomposites by *in-situ* polymerization technique

solvents followed by evaporation of the solvent or by precipitation (Scheme 1.5).⁹⁵⁻⁹⁶ The solution techniques follows a two step process, initially the solvent molecules help

to swell and/or disperse the nanomaterials into the polymer solution and finally the polymer chains substitute the solvent molecules in the final stage. Such a replacement requires a negative variation in the Gibbs free energy. It is thought that the diminished entropy due to the confinement of the polymer is compensated by an increase due to desorption of intercalated solvent molecules. In other words, the entropy gained by desorption of solvent molecules is the driving force for polymer intercalation from solution. In case of polymer/layered silicate nanocomposites, at first the weakly stack layers are easily dispersed in a suitable solvent. Delamination of the weakly stacked silicate layers occur only in the second stage by the insertion of the polymer chains. However the resultant structure of the nanocomposites i.e. intercalated or exfoliated is largely govern by the nature of the interaction between the clay layers and the polymer chains. However, during solvent evaporation (or the mixture precipitated), the layers can reassemble to reform an ordered multilayer structure with polymer chains sandwiched in between forming a well ordered intercalated nanocomposite. It is a good way to intercalate polymers with little or no polarity into layered structures, and facilitates production of thin films of polymer with oriented-clay intercalated layers. The chance of forming exfoliated nanocomposites is very low by this technique.



Scheme 1.5: Schematic diagram for the preparation of polymer nanocomposites by solution method

Though this technique is used in many cases for preparation of nanocomposite, from the commercial production point of view it is not a well accepted method. This is due to the copious use of organic solvents and phase separation of the prepared

products. The solvents, usually are environmentally unfriendly and economically prohibitive.⁹⁷ The advantage of this technique is that it offers the possibility to synthesize intercalated nanocomposite based on polymers with even or no polarity.

Melt Mixing

Nanocomposite synthesized via polymer melt intercalation involves annealing, usually under shear, of a mixture of polymer and nanomaterials like layered silicate above the softening point of the polymer. During annealing, polymer chains diffuse from the bulk polymer melt into the nanomaterials galleries.

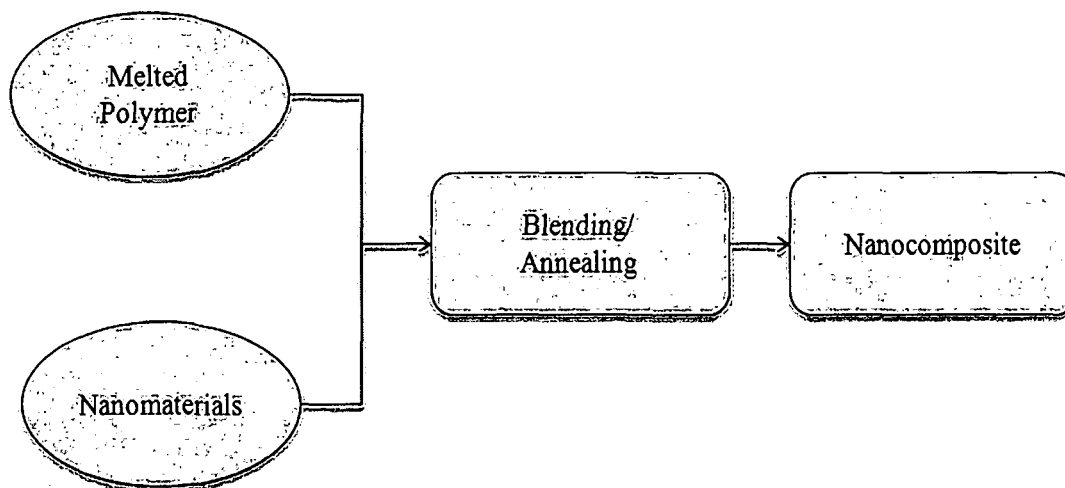
The advantages of forming nanocomposites by melt processing are quite appealing, rendering this technique a promising new approach that would greatly expand the commercial opportunities for nanocomposites technology.⁹⁸⁻¹⁰⁰ At the melting state the chosen polymer should be sufficiently compatible with the nanomaterials to form the nanocomposite. Therefore to optimize the interaction, the process may require several judicious experiments with different compatibilizers. Generally the temperature is kept below the decomposition temperature of all the components of the nanocomposite. In this technique, processing conditions play important roles on the structure and property of polymer nanocomposite. Melt processing allows nanocomposites to be formulated directly using ordinary compounding devices such as extruders or mixers, without the necessary involvement of resin production. Therefore, it shifts nanocomposite production downstream, giving end-use manufacturers many degrees of freedom with regard to final product specifications (e.g. selection of polymer grade, choice of nanomaterial, level of reinforcement etc.). At the same time, melt processing is environmentally sound since no solvents are required and it enhances the specificity for the intercalation of polymer, by eliminating the competing host-solvent and polymer-solvent interactions.^{99,100}

The fact that polymer chains can undergo centre of mass transport in between the nanomaterials is surprising because, the unperturbed radius of gyration of the polymer is roughly an order of magnitude greater than the interlamellar spacing. The polymer chains possess a dramatic loss of conformational entropy during the intercalation. In this case, the believed driving force is the enthalpic contribution that comes from the interaction between the matrix and nanomaterials during blending and annealing steps. The different steps of melt mixing process are presented in Scheme 1.6.

Besides the above methods there are other techniques too, which are used sometimes to prepare polymer nanocomposites. Among these template synthesis and sol-gel process are the most important and hence discussed below.

Template Synthesis

This is a bottom up approach and is different from above described methods. This



Scheme 1.6: Schematic diagram for preparation of nanocomposites by the melt mixing technique

method is also called as *in-situ* hydrothermal crystallization. In this method, nanomaterials are synthesized from precursor solution using polymers as template and hence the nanocomposites are formed *in-situ*. This method is widely used for the synthesis of double layered hydroxide based nanocomposites. Theoretically this method has potential of promoting the dispersion of nanomaterials in the polymer matrix in a one-step process. The compounds obtained by template synthesis are of great interest in view of the preparation of inorganic porous materials. But this does not hold for all the nanomaterials.^{49,101}

Sol-gel Process

In this technique, the nanoparticles are synthesized within the polymer matrix, using an aqueous solution (or gel) containing the polymer and the precursor or building blocks of the nanomaterials. During the process, the polymer aids the nucleation and growth of the inorganic host crystals and gets trapped within the layers as they grow. Most of the colloidal nanocomposites are prepared by this technique, where the silica precursors are precipitated in controlled manner onto the polymer core particles to form silica coated

hybrid colloids. Although theoretically this method has the potential of promoting the dispersion of the silicate layers in a one-step process, without needing the presence of the onium ion, it presents serious disadvantages. First of all, the synthesis of clay minerals generally requires high temperatures, which decompose the polymers. An exception is the synthesis of hectorite-type clay minerals which can be performed under relatively mild conditions. Another problem is the aggregation tendency of the growing silicate layers. Therefore, this technique, although widely used for the synthesis of double-layer hydroxide-based nanocomposites, is far less developed for layered silicates and will not be considered in the following discussion.

Again, the preparation of polymer/metal nanocomposites falls either in *in-situ* (nanoparticles are prepared inside the matrix system) or *ex-situ* (nanoparticles are prepared outside the matrix system) approaches, where metal nanoparticles are incorporated in the polymer matrix by using solution, *in-situ* or melt mixing techniques. Indeed, large varieties of other techniques are also employed for the preparation of polymer nanocomposites. These include cryogenic ball milling, thermal spraying, plasma induced polymerization, evaporation of elemental metal with its deposition on polymeric matrices, thermal decompositions of metal ions using different procedures etc. However, to achieve the uniform distribution of the nanoparticles through these techniques is very difficult and thus they are not used, in general. Sonication is often used for homogenization of the nanomaterials in the polymer matrix.

1.5. Characterization

1.5.1. Epoxy Matrix

The characterization tools such as analytical or spectroscopic techniques used for epoxy resin are similar to other polymers. One of the most immediate information of the epoxy formation is obtained by the determination of epoxy equivalent. Other characteristics such as hydroxyl value, viscosity, volatile matter content, specific gravity etc. are also important and determined by employing the standard methods.¹⁰²⁻¹⁰⁴ Structural confirmation, molecular weight determination, rheological behavior and thermal characterization are generally carried out by using instruments like Fourier transform infra-red (FTIR)/nuclear magnetic resonance (NMR), gel permeation chromatography (GPC), rheometer/dynamic mechanical analyzer (DMA) and thermogravimetric analyzer (TGA)/differential scanning calorimetry (DSC)/thermo-mechanical analyzer (TMA) etc.¹⁰⁵⁻¹⁰⁹ Crystallinity and morphology of the matrix are

characterized by X-ray diffractometer (XRD) and scanning electron microscopy (SEM) respectively.

Analytical Techniques

Epoxy equivalent is defined as the amount of resin in gram required to obtain one equivalent of epoxy group. The epoxy equivalent indicates the presence of epoxy group, lower is the epoxy equivalent, easier is curing. Hydroxyl value of a polymer is a measure of the hydroxyl content and is defined as the numbers of milligram of KOH equivalent to the hydroxyl content of one gram of the polymer.¹⁰² The results of hydroxyl value and viscosity¹⁰² indicate the free -OH groups and processability, respectively.

1.5.2. Nanocomposites

Characterization tools are crucial to comprehend the basic physical and chemical properties of polymer nanocomposites. For structural applications, it facilitates the study of emerging materials by giving information on some intrinsic properties.²⁰ Various techniques for characterization have been used extensively in polymer nanocomposite research.²⁰ The commonly used powerful techniques are wide-angle X-ray diffraction (WAXD), small-angle X-ray scattering (SAXS), scanning electron microscopy (SEM), and transmission electron microscopy (TEM).^{49,110}

XRD is most commonly used to probe the nanocomposite structure and occasionally to study the kinetics of polymer melt intercalation.¹¹⁰ This technique allows the determination of the spaces between layers of the silicate utilizing Bragg's law: $\sin\theta = n\lambda/2d$, where λ corresponds to the wave length of the X-ray radiation used in the diffraction experiment, d the spacing between diffractive lattice planes and θ is the measured diffraction angle or glancing angle.^{1,49}

Due to the easiness and availability, WAXD is the most commonly used to probe the nanocomposite structure¹¹⁰ and occasionally to study the kinetics of the polymer melt intercalation by employing *in-situ* synchrotron XRD experiments.¹⁰⁸ In many cases, XRD serves to characterize the crystal structure of the nanoparticles, estimate their size and shape and individuate lattice defects. On the other hand, in layered silicate nanocomposite systems, a fully exfoliated system may be characterized by the absence of intensity peaks in WAXD pattern e.g. in the range $1.5^\circ \leq 2\theta \leq 10^\circ$ which corresponds to a d -spacing of at least 6 nm. Therefore, a WAXD pattern concerning the mechanism of nanocomposite formation and their structure are tentative issues for

making any conclusion. SAXS, can be more informative and somewhat quantitative as explained by numerous authors.^{110,111-116} SAXS is typically used to observe structures on the order of 10 Å or larger, in the range of 0° or 0.5–5°.

The SEM provides images of surface features associated with a sample. However, there are two other microscopies, scanning probe microscopy (SPM) and scanning tunneling microscopies (STM), which are indispensable in nanotube research.¹¹⁷ The SPM uses the interaction between a sharp tip and a surface to obtain an image. In STM, a sharp conducting tip is held sufficiently close to a surface (typically about 0.5 nm), such that electrons can 'tunnel' across the gap. This method provides surface structural and electronic information at atomic level. The invention of the STM inspired the development of other 'scanning probe' microscopes, such as the atomic force microscope (AFM). The AFM uses a sharp tip to scan across the sample.

Scanning probe microscopes (SPM) have emerged as powerful techniques capable of characterizing surface morphological features at ambient conditions and generating three dimensional, images of the surface topography with nanometer resolution¹¹⁸ So, they are extensively used for imaging in most of the disciplines including materials science as in nanocomposites. SPMs are not only used for surface morphological characterization, but also for proximity measurements of magnetic, electrical, chemical, optical, thermal, spectroscopy, friction, wear, and other mechanical properties.

The most important members of this family of SPMs are AFM and STM. AFM has an added advantage for the high-resolution profiling of nonconducting surfaces. Also, AFM is a non-destructive technique and it does not require any specific sample preparation. Furthermore, the resolution capabilities of the AFM are near or equal to those of electron microscopes though AFM differs from electron microscopes. AFM does not have a lens, does not require coating or staining, and can be operated at atmospheric pressure, in fluids, under vacuum, low temperatures, and high temperatures. It has been reported that although AFM identifies the dispersion of nanoparticles, it is still necessary to subsidize the structure and dispersion of nanoparticles with other characterization techniques like small angle neutron scattering (SANS) and neutron scattering.

Transmission electron microscopy (TEM) is fashioned after a traditional light microscope. However, instead of transmitting light it uses electron beams which can give a higher resolution picture due to the decrease in wavelength. An electron gun emits an electron beam which moves through a condenser aperture and then bombards

the specimen. The beam that passes through the sample is then filtered and magnified. The electrons impact a phosphor screen which allows for the viewing of the image. This analytical tool can be used to view samples in three dimensions. The scanning electron microscope differs from the TEM by the fact that the beam is used to scan across the surface of the specimen. Secondary electrons are released from the specimen due to the increased energy are then detected by a phosphor screen producing the image shown. TEM allows a qualitative understanding of the internal structure, spatial distribution of the various phases, and views of the defective structure through direct visualization, in some cases of individual atoms. TEM analysis gives visible information on the extent of particle separation in the nanocomposites depending on the surface modification over a broad scale range including especially large sized aggregates.

For thermal characterization and to study the curing behavior (typically for thermoset resin systems) of polymer nanocomposites, the commonly used techniques are differential scanning calorimeter (DSC). DSC is a valuable tool to evaluate the thermal properties of the nanocomposites.¹¹⁸ The change of glass transition temperature (T_g), crystallization behavior, crosslinking kinetics for thermosetting polymers etc. on incorporation of the nanomaterials can be studied by DSC. Other thermal characterization tools such as thermogravimetric analysis (TGA) and thermomechanical analysis (TMA) are also used to characterize thermal behavior of nanocomposites.

Solid-state nuclear magnetic resonance spectroscopy is a powerful tool capable of providing information both about the structure of materials and the dynamics of processes occurring within those materials. Further, more structural information can be drawn from solid state NMR study. Characterization of polymer/layered silicate nanocomposites by ^{13}C solid-state nuclear magnetic resonance (^{13}C NMR) has also been proposed. van der Hart et al.¹¹⁹⁻¹²¹ first used this technique as a tool for gaining greater insight about the morphology, surface chemistry, and to a very limited extent, the dynamics of exfoliated polymer nanocomposites. They used this technique on polyamide-6 nanocomposites and showed that the paramagnetic Fe^{3+} ions in the crystal lattice of the montmorillonite provide an additional relaxation mechanism of the protons. It is this additional relaxation which is determined by the average Fe^{3+} -H distance (and therefore by Fe^{3+} ion and clay concentration). Solid-state NMR measurement generally connects the measured longitudinal relaxations, T^1 s, of proton (and ^{13}C nuclei) with the quality of clay dispersion. The ^{29}Si solid state NMR further

gives the information on the distribution of silica nanoparticles in silica based polymer nanocomposites.⁷⁵ Due to the high polarizability, the xenon atom is particularly sensitive to the density of its microenvironment and thus ^{129}Xe NMR spectroscopy was used to investigate the enhancement of free volume in polymer nanocomposites.¹²² Positron annihilation lifetime spectroscopy (PALS) technique is also used for the same purpose.

Fourier transform infrared spectroscopy (FTIR) is also used to elucidate the structure of the nanocomposites.¹²³⁻¹²⁴ FTIR identifies the differences between the bonding in a mixture and the bonding in a related nanocomposite. For example, the appearance of the bands $\sim 1130\text{ cm}^{-1}$ and $\sim 820\text{ cm}^{-1}$ corresponds to the Si-O-Si and Si-OH bond stretching in the polymer/clay nanocomposites. These spectra are also useful to predict existence/disappearance of hydrogen-bonding between the nanomaterials and matrix. Attenuated total reflection infrared (ATR-IR) spectroscopy is used to characterize the nanocomposites of too thick or too strong absorbing samples.

The rheometric study and dynamic mechanical analysis (DMA) are utilized to measure the viscous and elastic components of polymer nanocomposite in terms of storage (G') and loss modulus (G''), which in turn help in determination of state of dispersion of nanofillers in matrix. The well dispersed nanofillers caused shifting of G' and T_g values of the nanocomposite. They also measure the stiffness of nanocomposite quantitatively.¹²⁵

SANS, disk centrifuge photosedimentometry (DCP), dynamic light scattering (DLS) etc. have also found to use in determining the structural aspect and sometimes the conformation of the nanocomposites. To assess the surface compositions, X-ray photoelectron spectroscopy (XPS) surface analytical technique have also been widely used. The TEM studies of the ultramicrotomed particles combined with the XPS data can further illuminate the particle morphology. The other techniques such as determination of mechanical properties, chemical resistance, flame retardancy, water vapor barrier property etc. are same as that of the conventional polymer composites.

1.6. Properties

The incorporation of nanofiller ($\leq 5\text{ wt}\%$) significantly enhances the various properties as compared to pristine polymer system and is the prime attraction of industrial and scientific fraternities. The various properties of polymer nanocomposites are briefly discussed here.

1.6.1. Mechanical

The mechanical behavior of polymer nanocomposite has been the subject of considerable attention in such studies. Mechanical properties are, indeed, of relevance for all applications of polymer nanocomposite in industry.¹²⁶ Tensile strength is one of the best judges of the mechanical properties of polymer nanocomposites. The tensile strength shows a gradual variation with the nanofiller content, in most of the cases it increases with increase in filler content. However after attaining a critical concentration of nanofiller the increment becomes stagnant and in most of the cases it decreases. The type of nanocomposite structure (intercalated or exfoliated) and orientation of the nanofiller significantly influence on the mechanical properties. The declining of the properties at high concentration of nanofiller is mainly due to the formation of agglomerates. As the degree of exfoliation increases the effective surface area of the filler increases which in turn increases filler matrix contact. Therefore, the polymer, particularly that adjacent to the filler particles, becomes highly restrained mechanically. This enables a significant portion of an applied load to be carried by the filler, assuming, of course, that the bonding between the two phases is adequate.¹²⁷ Thus it becomes obvious that the larger the surface of the filler in contact with the polymer, the greater the reinforcing effect will be. On the other hand, the elongation at break values of nanocomposites generally decreases but sometimes it remains constant or even increased.¹²⁸⁻¹²⁹ The increased restricted movement of polymer chains attributed to decrease of elongation at break but the increase of elongation at break value may be due to formation of nano domain shear zones under stress and strain. Impact resistance is another important mechanical property for many end application of polymers. It is a combined effect of flexibility and strength of materials.

Hardness of polymer nanocomposites is important from application point of view as it refers to the resistant to change of shape when force is applied. The hardness of polymer nanocomposite depends on type of nanofillers and the interfacial interactions between fillers and polymer chains.

1.6.2. Dynamic Mechanical

Dynamic mechanical property is the response of a material to a cyclic deformation or stress (usually tension or three-point bending type deformation) as a function of the temperature. These are the storage modulus (G' or E'), corresponding to the elastic response to the deformation, the loss modulus (G'' or E''), corresponding to the plastic

response to the deformation and phase angle ($\tan \delta$), useful for determining the occurrence of molecular mobility transitions such as the T_g .¹³⁰⁻¹³¹ The G' increases with the formation of exfoliated and well dispersed nanocomposite. Enhancement of G'' has also been reported for different nanocomposites. The $\tan \delta$ values depend not only on the dispersion state of nanofillers but also on the type of matrix used. The dynamic mechanical properties of polymer nanocomposites can also be measured by dynamic thermal mechanical analysis (DMTA).

1.6.3. Barrier

Polymer nanocomposites are generally characterized by very good enhancements of their barrier properties. The spectacular improvement in barrier properties of polymer nanocomposites depends both on the degree of dispersion of the amount of nanomaterial incorporated in the polymer, and the aspect ratio of the nanomaterial. In particular, aspect ratio is shown to have a major effect, with high ratios (and hence tendencies towards filler incorporation at the nano-level) quite dramatically enhance gas barrier properties. The impermeable nanomaterials force the permeating molecules to wiggle around them in a random walk and hence diffuse by a tortuous pathway in the polymer matrix. It becomes obvious from this expression that a sheet-like morphology is particularly efficient at maximizing the path length, due to the large length-to-width ratio, as compared to other filler shapes. There are several models for predicting this behavior. Nielsen, Bicerano and Bharadwaj, Fredrickson etc. models can be exemplified, for instance. The different polymer nanocomposites show enhanced barrier property to various gases, liquids, water vapor and chemical molecules. Improvements in capability of the polymer nanocomposite based membranes for gas separation have also been achieved.¹³²

1.6.4. Thermal

Thermal properties are key aspect of nanocomposites describing the materials response to temperature. The thermal stability of nanocomposite, nature of degradation, T_g , degree of crystallinity, specific heats etc. of polymers are influenced by incorporation of nanomaterials into them. Generally, the incorporation of nanofillers like nanolayers and nanofibers into the polymer matrix was found to enhance the thermal stability by acting as a superior insulator and mass transport barrier to the volatile masses produced during decomposition and assisting in formation of char after thermal decomposition.¹³³ However, in certain cases the thermal stability of the polymer may deteriorate too after

nanocomposite formation. DSC is used to determine the various thermal transition behaviors such as T_g , crystallization temperature (T_c), melting temperature (T_m), etc. of nanocomposite. T_g is generally shifted or diminished due to the restricted motion of the polymer chains by the nanofillers. Thermally stimulated depolarization current is a recent dielectric technique used extensively to study relaxation mechanisms in polymeric nanocomposites to characterize the T_g in more details.

1.6.5. Rheological

The rheology is the study of the deformation and flow of matter under the influence of an applied external force. The determination of rheological properties is helpful to know the physical properties during and after processing of nanocomposites. Since for polymer nanocomposite the rheological properties are responsive to the size, shape and surface properties of the fillers, therefore rheology can be envisaged to assess the state of dispersion of fillers in matrix.¹³⁴ Generally nanocomposites show increased viscosity at low shear rates known as solid-like behavior and shear thinning behavior at high shear rates. The alignment of nanofillers towards the flow direction at high shear rates attributed to this fact.¹³⁴

1.6.6. Flame Retardancy

Increased flammability resistance has been noted as an important property enhancement involving nanoplatelet/nanofiber modification of polymeric matrices. The improvement in flame retardancy has been investigated using both thermoplastic and thermosetting resins. The flame retardant property of nanocomposite is studied by measuring limiting oxygen index (LOI), UL 94 test and cone calorimetry. The flammability behavior of a polymer nanocomposite can be defined by parameters like burning rates, spread rates, ignition characteristics etc. The nanofillers blended into the liquid resin must ensure consistent flame retardant properties throughout the polymer. There exists a common mechanism of thermal stability and flammability reduction, and it was found that addition of nanofillers can substantially reduce the flame retardancy by encouraging the formation of a carbonaceous char in the condensed phase.¹³⁵⁻¹³⁷ This effectively reduces the amount of flammable small molecules into vapor phase and decreases the heat release rate. The char also helps in maintaining the material structural integrity and preventing fire spreading. The carbonaceous char builds up on the surface during burning and insulates the underlying materials. This limits the passage of degradation products from the matrix which supports the continuous fueling of the fire. Synergistic

effect on enhancing flame retardancy can also be achieved by incorporation of atoms like halogens, sulfur, nitrogen and phosphorous into polymer precursor along with nanofillers.

1.6.7. Optical

The optical properties are mainly transparency, refractive index, fluorescence, luminescence etc. Polymer nanocomposites with polymer containing optical functional group or material exhibits interesting optical properties.¹³⁸ In polymer nanocomposite, generally the nano-sized filler enhance the optical properties while the polymer acts as stabilizer to the fillers. In the nanocomposite the transparency of the pristine polymers is retained as there is no marked decrease in the clarity due to the nano dispersed fillers.

1.6.8. Electrical

The electrical properties of polymer nanocomposite encountered are the conductivity and dielectric properties. The electrical properties generally are expected vary with the inclusion of nanofillers. The variation results from the quantum effects which are prominent at nano region and the interparticle spacing which decreases for the same volume fraction compared with the bulk. In addition, the decrease of rate of resistivity is lower than in micrometer scale fillers.

1.6.9. Magnetic

Magnetic nanoparticles has attracted considerable attention from the researchers especially its application in the medical sectors. Targeted drug delivery is an important application of the magnetic nanoparticles based systems as they can be manipulated by an external magnetic field gradient to control a targeted delivery. Cell separation, drug targeting, enzyme immunoassay etc. are some of the fields where polymer coated magnetic nanoparticles have attracted more and more attention. This is because of the fact that the magnetic separations are comparatively easy, rapid, and require simple equipment as compared to other separation procedures.¹³⁹

1.6.10. Catalytic Activity

The catalytic activity differs for different polymer nanocomposite systems. For example vegetable oil based hyperbranched polyurethane/ silver nanocomposites can act as heterogeneous catalyst to convert the 4-nitrophenol to 4-aminophenol.¹⁴⁰ However catalytic activity of nanoparticles generally reduces with the increase in cycles of its use. Polymer/clay nanocomposite has been known for its catalytic activity.¹⁴¹ The

highly active and large surface area of nanomaterials result their effective catalytic activity.

1.6.11. Biodegradation

The significant enhancement of biodegradation of polymer after nanocomposites is another interesting and exciting aspect of their utility. The improved biodegradability of the nanocomposites may be attributed to manifold catalytic role played by the nanomaterials in the biodegradation process. The biodegradation process can be categorized into four main steps viz. water absorption, ester cleavage and formation of oligomer fragments, solubilization of oligomer fragments, and ultimately removal of soluble oligomers by microorganisms.¹⁴¹ Therefore any factor which influences the hydrolysis tendency may control the biodegradation process. In case of polymer/clay nanocomposites the terminal hydroxyl groups of silicate layers is one of the reasons for improvement of biodegradation ability of polymers.¹⁴²

1.7. Applications

As described above, polymer nanocomposite often exhibits properties superior to conventional composites, such as strength, stiffness, thermal and oxidative stability, barrier properties, as well as flame retardant behavior compared to pristine polymeric system and conventional composites.^{1,49} These improved properties are generally attained at low filler content in comparison with conventionally filled systems. Therefore, polymer nanocomposites are far lighter in weight than a conventional composite, which makes them quite competitive for specific applications (Fig. 1.5).¹¹⁰ The potential of nanocomposites in various sectors of research and application is promising and attracting increasing investment from Governments and business in many parts of the world. While there are some niche applications where nanotechnology has penetrated the market, the major impact will be at least a decade away.²

Another unique aspect of nanocomposites is the lack of property trade-offs. Traditionally, blend or composite formulations require trade-offs between desired performance, mechanical properties, cost and processability. However, polymer nanocomposite technology provides a route around these traditional limitations, and offers, for the first time, the opportunity to design materials without the compromises typically found in conventionally filled polymers.¹⁴³⁻¹⁴⁴

The significant weight reduction, reduced materials density and high fuel efficiency suggest polymer nanocomposites a variety of possible industrial applications such as automotive (gas tanks, bumpers, interior and exterior panels), construction (building sections and structural panels), aerospace (flame retardant panels and high performance components), food packaging, textile etc.

The first commercial product of clay based polymer nanocomposites was the timing-belt cover made from nylon clay nanocomposites by Toyota Motors in the early 1990s. This timing-belt cover exhibited good rigidity, excellent thermal stability and no wrap. It also saved weight by up to 25%.¹⁴⁵ Later, General Motors and partners Basell, Southern Clay Products and Black hawk Automotive Plastics designed external automotive body parts (step-assist) made from thermoplastic, olefin layered silicate nanocomposites.

Besides, polymer nanocomposites are also used as oil reservoir tank, engine cover and fuel hoses in the automotive industry due to their extraordinary increase in heat distortion temperature and enhanced barrier properties together with their improved mechanical properties. Thus polymer nanocomposites can be utilized as potential materials in various vehicles for external and internal parts such as mirror housings, door handles and under-the-hood parts. The lighter weight characteristics of polymer nanocomposites could have added advantage on environmental protection and material recycling. Epoxy nanocomposites have also their own niche in automotive industries.

Another domain where polymer nanocomposites have been used extensively is the packaging industry. They have been viewed as the future for the global packaging industry. The widespread interests generate from the reduction in weight, low production cost, excellent barrier properties resulted considerable enhancement of shelf-life for many types of packaged food compared to the conventional composites systems. The advantages that nanocomposites offer far outweigh the costs and concerns. The outstanding properties of polymer nanocomposite film make them acceptable widely in packaging industries as wrapping films and beverage containers, such as processed meats, cheese, confectionery, cereals, fruit juice and dairy products, beer and carbonated drinks bottles.¹⁴⁵ For example, Bayer has recently developed a new grade of plastic films for food packaging which are made from nylon-6/clay based exfoliated nanocomposites.

Renewable resource based epoxy resin has been widely used as reactive diluents in paints. In such an application the oil functions, on the one hand, as a solvent, making

dispersion or solubilization of the formulation with volatile organic solvents superfluous, while, on the other hand, the oil reacts with other components in the formulation to form an integral part of the dried coating. Qureshi et al.¹⁴⁶ and Barrett et al.¹⁴⁷ used *Euphorbia lagascae* and *Vernonia species* epoxidized oils as include coatings relying on the formation of interpenetrating polymer networks and flexible baked coatings on metals.¹⁴⁸ These coatings showed excellent flexibility, adhesion to substrate, chemical resistance, cohesive film properties and resistance to chipping.¹⁴⁹ The use of epoxidized functional fatty acid i.e. vernolic acid as reactive diluent in radiation curable coating compositions has been reported by Samuelsson et al.¹⁵⁰ The coating compositions comprises of hydroxyl functional hyperbranched polyether and 30 wt% vernolic methyl ester as reactive diluent. The coating exhibits sufficient flexibility after the use of epoxy functional fatty acid as indicated by the T_g 's which gets lowered by 10 °C only at 10 wt% of reactive diluents. Further they found significant enhancement in the flow behavior for 30 wt% (viscosity reduces from 4100 mPas to 460 mPas) of reactive diluents composition.

Koo and Pilato¹⁵¹ investigated the epoxy nanocomposite for high-temperature applications and described the feasibility of using these materials for fire retardant coatings, rocket propulsion insulation, rocket nozzle ablative materials, damage tolerant performance, etc. Timmerman et al.¹⁵² used nanoclays in carbon fiber/epoxy reinforced composites for cryogenic storage systems with improved mechanical and thermal expansion (CTE) characteristics thereby avoiding micro cracking and thermal cycling. Ren et al.¹⁵³ investigated the fatigue behavior (under repeated mechanical loads) of unidirectional, aligned SWCNTs reinforced epoxy composite, which is demonstrated in long-term structural applications as well as in aerospace application. Gibson et al. investigated epoxy based adhesives formulated with silver coated and uncoated vapor grown carbon nanofibers for several aerospace applications such as electrical conductivity, thermal transport, and mechanical properties.¹⁵⁴

The combination of hardness, scratch resistance and flexibility is a highly desired feature in many surface coating applications. The structure of epoxy-based coatings leads to high chemical resistance, thermal stability, good adhesion, and superior toughness. Some epoxies offer greater chemical and corrosion resistance than alkyd resins. Epoxy based coatings are used as a primer upon which a polyurethane topcoat is placed. Use of epoxy resins in traffic marking paint is increasing due to a 2 to 3 year life expectancy. Traffic marking coatings are two components in that the resin and

catalyst are mixed at the nozzle of the applicator. Many reports are found which have developed the polymer nanocomposites for coating purposes. Epoxy nanocomposites with different type of nanofillers such as nanoclay, metals nanoparticles etc. are used to obtain highly hydrophobic, antimicrobial, flame retardant, high performance and

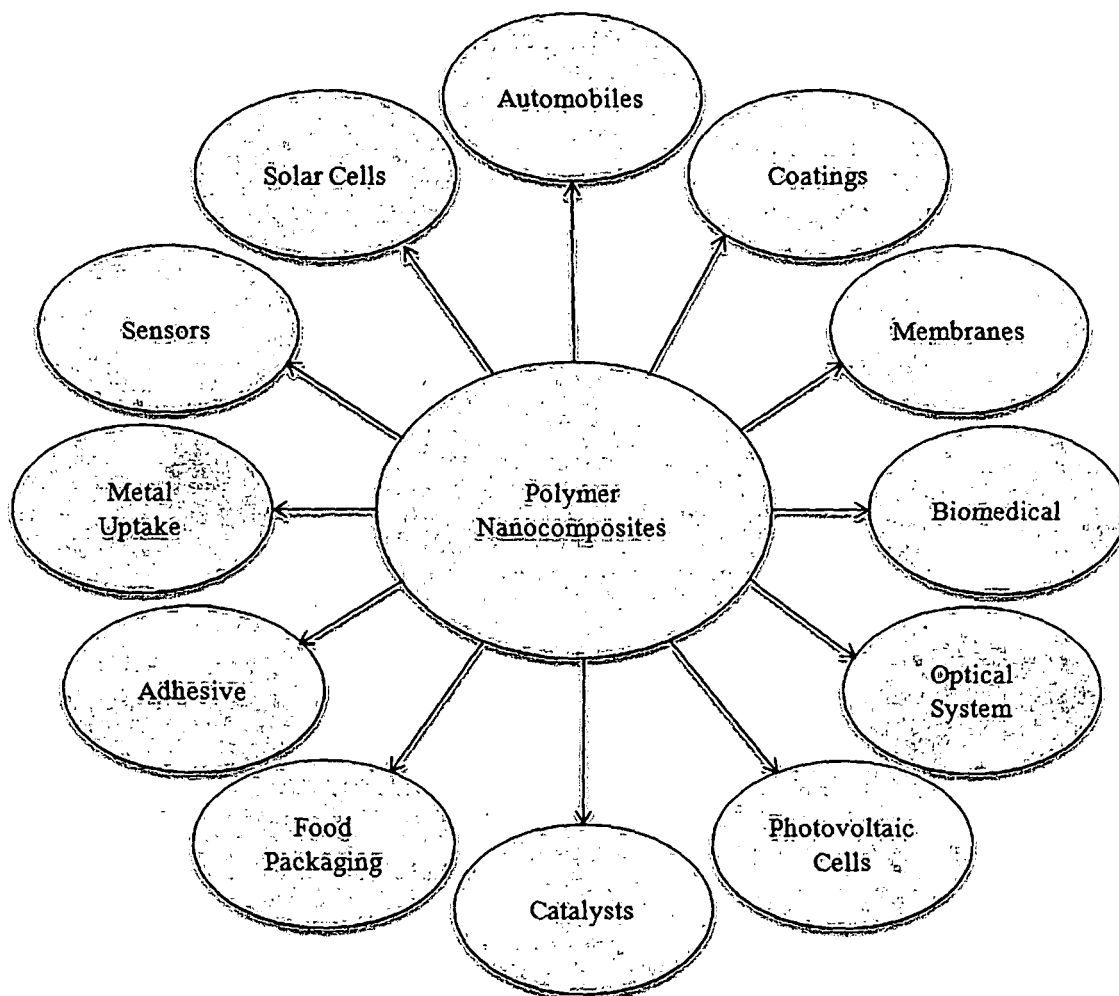


Fig. 1.5: Different fields of applications of polymer nanocomposites

thermostable surface coatings. Besides surface coating materials the polymer nanocomposites are also used as adhesive and sealant. Chisholm et al.¹⁵⁵ introduced micro and nanosized SiC in an epoxy matrix system and studied the thermal and mechanical properties of the nanocomposites. Lin et al.¹⁵⁶ investigated a low velocity impact test with improved impact strength using TiO₂ and nanoclay in an epoxy system. Tsujimoto et al.¹⁵⁷ reported that presence of nano silica in the epoxidized natural oils resulted in highly transparent and glossy coating. They further observed the enhancement of hardness and Young's modulus of the nanocomposite coatings in the presence of silane coupling agent as compared to the pristine epoxidized natural oils.

Ge et al.¹⁵⁸ develop anticorrosive epoxy coating for steel. They studied the effect of PANI's content on anticorrosion property of the composite coatings by using the electrochemical impedance spectroscopy (EIS). Benfarhi et al.¹⁵⁹ developed various photocurable nanocomposites using epoxide, vinyl ether and acrylate with organically modified clays. They found increased in the flexibility (low T_g) and impact resistant for the nanocomposites.

Another important applicability of polymer nanotechnology and nanocomposites is the biomedical/biotechnological applications. One area of intense research involves electrospinning for producing bioresorbable nanofiber scaffolds for tissue engineering applications. Another area also involving nanofibers is the utilization of electrically conducting nanofibers based on conjugated polymers for regeneration of nerve growth in a biological living system. Nanoparticle silver, silver oxide and silver salts have been incorporated into polymer matrices to provide antimicrobial/biocidal activity.¹⁶⁰⁻¹⁶² Polymer nanocomposites based on hydroxyapatite ($\text{Ca}_{10}(\text{PO}_4)_6(\text{OH})_2$) have been investigated for bone repair and implantation.¹⁶³ The resultant scaffold structure contained both nano and micro sized pores offering a combination of cell growth and blood vessel invasion microdimensions along with nanodimensions for nutrient and metabolic waste transport. Polymer nanocomposites also finds usage in artificial muscles and rapid actuators based on property enhancement like, especially on heat responsivity, swelling-de-swelling rate and molecular diffusion.¹⁶⁴

One of the most interesting applications of polymer nanocomposites is in the field of electronics and optoelectronics. The utility of polymer based nanocomposites in these areas is quite diverse involving many potential applications. The potential applications include electromagnetic interference shielding, transparent conductive coatings, electrostatic dissipation, supercapacitors, electromechanical actuators and various electrode applications.¹⁶⁵⁻¹⁶⁶ The remarkable electrochemical behavior of conducting polymers associated with nanomaterials attracts potential applications in these fields such as modified electrodes biosensors, solid-state batteries, smart windows and other electrochemical devices. Tuncer et al.¹⁶⁷ investigate the electrical properties of epoxy nanocomposites using as nano and sub-micron-scale barium titanate and calcium copper titanate nanoparticles for electrical insulation applications.

The sensor technology is highly utilizing the advantages of nanotechnology.¹⁶⁸ The polymer nanocomposites are utilized for sensitivity of gas, humidity, toxic-chemicals,

metals etc. The factors like accuracy of sensitivity, selectivity, reproducibility, scanning time etc. are dependent directly on the sensing capability of the membrane.

1.8. Short Review on Vegetable Oil Based Epoxy Nanocomposites

Introduction

The markets for vegetable oil based materials are growing due to the economical, environmental, societal and availability advantages. The vegetable oil-based materials are also recognized as sustainable which could contribute to reduce global warming effects.¹

Renewable resource based polymers can replace petroleum based polymers, and hence, compete or even surpass the existing petroleum based materials on the basis of cost-performance and eco-friendliness nature. There is a growing urgency to develop and commercialize new biobased products that can unhook widespread dependence on petroleum.

The products based on vegetable oils are developed keeping two criteria in mind. First, the products must meet the same technical and industrial standards as demanded for conventional industrial products, e.g. durability, fastness to exposure, resistance to chemicals etc. of paints. Secondly, the products must also meet all ecologically relevant standards. For producers of natural paints, ecological compatibility comprises both environmental aspects and human health risk factors.¹⁶⁹

Polymers are quantitatively the most important products of the chemical industry that are used in diverse applications in everyday life. Almost all current polymers are produced from fossil sources. The consumption of material and energy resources is not the only issue surrounding polymeric products. Because of their widespread use and the dominant consumption patterns, in which materials and products are used only once and then discarded, polymers also make a significant contribution to the increasing amount of solid waste due to a very large percentage of the plastics produced from fossil fuel feedstock being non-biodegradable. Further, the vegetable oil based polymers have much lower mechanical strength than that of conventional petroleum based polymers. Therefore, there is constantly a need for stronger, lighter, less expensive and more versatile polymeric systems to meet the demands of many industrial consumers. In the last two decades there is a continuous increase of research for improvement of the properties of materials by employing nanometric engineered structures i.e. nanomaterials with inherent high surface area/volume ratio. Therefore the

development of polymer nanocomposites has attracted much attention in recent years due to their dramatic improvements in their desired properties at relatively low loadings of nanofillers and without the property trade-offs commonly that are encountered in conventional microcomposite systems. This is mainly due to their extremely small interparticles distance and the interaction that lies between the interface of polymer and fillers in nanoscale.¹⁷⁰ The polymer nanocomposites are also extending the applications of physics, chemistry, biology, engineering and technology into previously unapproached infinitesimal length scales.¹⁷¹ Now, at nanoscale one enters a world where physics, chemistry meet biology and material science together and develop novel properties of matter.

Background

The first resins based on vegetable oil are reported by Kienle and Hovey in 1925,¹⁷² though potentiality of vegetable oil industrially is first reported by Kane in 1911.¹⁷³ Since, the first report of vegetable oil based epoxy by Swern et al. in 1951,¹⁷⁴ different types of vegetable oils are being used for manufacturing of epoxies. In the formation of sustainable epoxy resins, epoxidized plant oils and fatty acids have been largely utilized as reported in the literature.¹⁷⁵⁻¹⁷⁶ Traditionally, epoxidized plant oils are used as plasticizers and stabilizers for PVC, but also in the painting and coating formulations.¹⁷⁷ On industrial scale, the unsaturated fatty compounds are converted into epoxidized oils by the *in-situ* peracid method.¹⁷⁸ However, the use of strong mineral acid has proved to be non-selective, leading to undesirable by-products, such as ring-opened epoxides.¹⁷⁹ In this respect, different catalysts have been employed, including transition metal complexes, ion exchange resins, venturillo's catalyst, crown ethers and enzymes.¹⁸⁰⁻¹⁸¹ However, none of these methods has achieved industrial significance.¹⁷⁸ Natural epoxidized plant oil that contains 60-65% vernolic acid is available in *Vernonia galamensis* and other *Vernonia species* have gained significance in recent times, however due to their low epoxide content wide spread use is still limited.¹⁸²

To meet the demand for more sustainable and tough epoxy material numerous approaches has been employed. The modifications of the bisphenol-A based epoxy resin, by epoxidized oil or esterification of the resins are among the various alternatives. The esterification of epoxy resins with commercial fatty acids is a well known process that has been employed for industrial coatings for many years. The carboxylic acids are esterified with the terminal epoxy groups or the pendant hydroxyls

on the polymer chain. A wide variety of saturated and unsaturated fatty acids are utilized to confer properties useful in air-dried, protective, and decorative coatings. Even if there are adequate amount of epoxidized vegetable oils available at the present time, Clayton¹⁸³ and Meyer et al.¹⁸⁴ agreed that those vegetable oils with relatively high iodine value or high content of unsaturated fatty acid especially soybean and linseed oils are only chosen to produce high epoxy functionality epoxides. The developments in this field are due to the research work of Greenlee and described in a number of patents. These include work on the modification of epoxy resins with glycerol, the esterification with drying oil acids and reaction with phenolic and amino resins. Devoe and Reynolds Co. Inc.¹⁸⁵ have reported coatings of epoxy resin and dimeric fatty acids. Aliphatic polyepoxides or dihydric phenol react at 150 °C with dimeric unsaturated fatty acids, especially dilinoleic acid so that all carboxylic groups react only with epoxy groups to give high molecular weight linear polyether-polyester resins with epoxy end group for each carboxylic group. Such resins give coatings after baking in the presence of amine catalysts together with phenol or urea HCHO resins. Parzuchowski¹⁸⁶ utilized carbonated soybean oil (CSO) containing five-membered cyclic carbonate groups for modification of bisphenol-A based epoxy resin. Goldblatt and Lucien¹⁸⁷ reported the esterification of epoxy resin by tung oil using zinc resinate as the esterification catalyst. They further reported that the protective coating obtained from such modified epoxy resins system exhibited outstanding adhesion, chemical resistance, extreme flexibility and hardness. The presence of triene structure of the fatty acids further provided the coatings with rapid drying abilities without the use of any metal based drier. The amalgamation of peculiar structural characteristic of synthetic raw materials and the benefits of vegetable oils in the field of polymer nanocomposites are described below.

Materials

The versatility of the epoxy nanocomposites are enhanced when the matrix is vegetable oil based epoxy. The presence of triglyceride moiety of the vegetable oil enhanced the chemical and physical properties in the epoxy matrix. The vegetable oil based epoxies possesses properties like adequate flexibility, high gloss, good toughness and adhesion etc. Most importantly, since one of the starting material is renewable resource based and is largely available, so compared to petroleum based epoxy the overall cost of the raw materials and processing are also relatively lower. Again being renewable resource based these materials they are eco-friendly and biodegradable in nature.

Vegetable Oils

Vegetable oils have fixed composition and boiling point (b.p.) hence is commonly known as fixed oils. Compared to the mineral oils found in petroleum fractions, they are non-volatile and unstable at high temperature. Whereas the essential oils found in stems, flowers, leaves are generally volatile in nature. Vegetable oils are triglyceride esters of fatty acids (95–98%) and complex mixtures of minor compounds (2–5%) of a wide range of chemical nature,¹⁴⁸ the general structure of which is shown in Fig. 1.6. They possess different degrees of unsaturation. Triglycerides comprise three fatty acids joined by a glycerol center.¹⁸⁸ Most of the common oil contains fatty acids that vary from 14 to 22 carbons in length, with 1 to 3 double bonds. The fatty acid distribution of several common oils is shown in Table 1.4.¹⁸⁸ In addition, there are some oils that comprise fatty acids with other types of functionalities (e.g. epoxies, hydroxyls, cyclic groups and furanoid groups).¹⁸⁹ It is apparent that on a molecular level, these oils are composed of many different types of triglyceride, with numerous levels of unsaturation. In addition to their application in the food industry, triglyceride oils have been used for the production of coatings, inks, plasticizers, lubricants and agrochemicals.¹⁹⁰⁻¹⁹³ Depending on the distribution of fatty acid, different vegetable oils possess different physical and chemical properties. The various saturated fatty acids such as lauric, arachidic, palmitic, stearic etc. and unsaturated fatty acids such as oleic, linoleic,

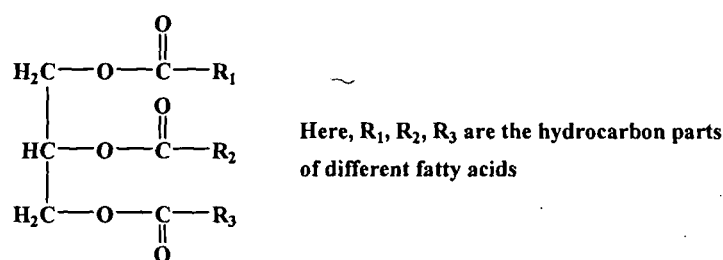


Fig. 1.6: Structure of triglyceride of fatty acid

linolenic etc. are generally found in different triglycerides. A few vegetable oils also comprise ricinoleic, myristic, behenic, capric, caproic, eleostearic, erucic, licanic, isanic, caprylic etc. fatty acids.

The physical state of vegetable oils depends on both the nature and the distribution of the fatty acids. Most vegetable oils are liquid at room temperature. Generally, higher melting point vegetable oils are obtained with more carbons in the fatty acid chain, a lower number of carbon–carbon double bonds, and an *E* (*trans*) configuration and conjugation of the carbon–carbon double bonds. The physical properties like boiling

point (b.p.), melting point (m.p.) and density of some important fatty acids¹⁹⁴ along with their structures are given in Table 1.4. The fatty acid composition of the vegetable oils is fixed and acts as its “finger print” (Table 1.4) that can be used to differentiate the vegetable oils from one another.

The vegetable oils may be of different types depending on the film forming ability, edibility (or toxicity) and yellowing tendency (linolenic acid content). The iodine value i.e. the unsaturation content measures the film forming ability of a vegetable oil.

The oils are generally classified as drying, semi-drying and non-drying depending upon the unsaturation present. In general, the oils with iodine value greater than 150 are termed as drying oils (linseed, perilla, tung, oiticica, walnut etc. oils), in between 120-150 are termed as semi-drying (safflower, sunflower, soybean, watermelon, rubber seed, nigerseed, tobacco seed etc. oils) and under 120 are called as non-drying oils (castor, cottonseed, coconut, rapeseed, olive, karanja, ground nut, sesame, rice bran etc. oils).

In general, drying oils (these can polymerize in air to form a tough elastic film) are the most widely used oils in industries, although the semi-drying oils (these partially harden when exposed to air) also find use in some applications. However for non-conjugated oils, the drying rates are more closely related to the average number of methylene groups adjacent to two double bonds per oil molecule (f_n) instead of their iodine values. Thus double bonds are separated by a methylene group, which makes them less reactive. Oil with f_n value > 2.2 is said to be a drying oil, whereas oil with f_n value less than 2.2 is semi-drying. This method cannot be used to classify conjugated systems, though this method is superior and more reliable than the conventional iodine value method.¹⁹⁵

Non-conjugated oils are classified based on their drying index values which, $\text{Drying index} = \% \text{ linoleic acid} + 2 \times (\% \text{ linolenic acid})$. If the drying index is greater than 70 then oils are said to be drying. Again, depending on the linolenic acid content the vegetable oils are industrially classified as yellowing or non-yellowing. Generally, the drying oils are yellowing and semi-drying and non-drying oils are non-yellowing.

The vegetable oils may be edible and non-edible based on edibility which depends on odor, taste and toxicity. The common edible oil includes cotton seed, peanut, olive, mustard, corn etc. while perilla, castor, tung, oiticicca oils falls into the non-edible category. Some oils such as sunflower, safflower, soybean etc. are used for dual

purpose.¹⁹⁶ A few important vegetable oils used to prepare epoxy resins and epoxidized oil are given in Table 1.5 with their physical properties and major fatty acids contents.

Extraction and Purification of Vegetable Oils

Prior to their use the vegetable oils are extracted and purified. The four general methods used to extract oils from the seeds are mechanical pressing, solvent extraction, enzymatic process and high pressure CO₂ extraction process.¹⁹⁶ In the mechanical pressing method oil is squeeze out from the protein meal of the pretreated seeds by hydraulics pressing or screw pressing. In solvent extraction technique, the pretreated seeds are first immersed in a suitable solvent system for a sufficient period at 60-80 °C and then distillation is done to collect the oil. However, the process involves use of copious amount of solvent and also loss of solvent is another major concern. In the enzymatic process, the pretreated seeds are boiled in water and mixed with a suitable enzyme viz. cellulase, α-amylase, protease etc. which digest the solid material from the seed. The oil is then extracted by liquid-liquid centrifugal method. In the high pressure CO₂ method, the pretreated seeds are mixed with CO₂ under high pressure, which dissolves the oil. Then the pressure is released which makes liquid CO₂ gaseous and hence the oil gets separated. The yields of the last two methods viz. enzymatic and high pressure CO₂ method are quite high and hence are adopted largely in commercial scale. In order to avoid the hydrolysis of the oil to free fatty acids by moisture present in the atmosphere, the extracted oil is kept at low temperature. Again, care should be taken during storage and handling to minimize the chances of contamination by oxygen. The best way to keep the oil without losing quality and stability is under nitrogenous atmosphere.^{194, 196}

Generally, the oil extracted contains certain impurities such as phosphatides, gums, resins, free fatty acids and colored substances. Prior to their utilization for industrial and edible purposes, the oil should be refined in order to remove the impurities. Heavier impurities such as dirt's can be removed by settling or by simple filtration technique. Gums are removed by degumming which exploits the affinity of phosphatides towards water by converting them to hydrated gums by treatment with water, salt solution, acid etc. As a result, gums coagulate and are separated by a centrifugal separator.¹⁹⁶

The alkali refining technique is the most effective refining process which removes free fatty acid contents and causes efficient removal of color without excessive

Table 1.4: Chemical structure and physical properties of a few fatty acids of vegetable oils

Name of fatty acid	Structure	Density (g/cm ³) at 25 °C	m.p. (°C)	b.p. (°C)
Arachidic		0.8240	74-76	328
Behenic		0.822	75-80	306
Capric		0.888	31-32	269
Caproic		0.92	-3	202
Caprylic		0.910	16-17	237
Eleostearic		0.924	48	390.6
Eicosenoic		0.895	25-32	430.5
Gadoleic		1.01	-	161-162
Heptadecanoic		0.853	59-61	227
Heptadecenoic		0.902	-	388.3
Isanic		0.930	39.5	-
Lauric		0.880	44-46	299
Licanic		-	75	-
Linoleic		0.9	-5	229
Linolenic		0.914	-11	230-232
Myristic		0.862	58.8	250
Myristoleic		0.9	-4.5	144
Oleic		0.895	13-14	360
Palmitic		0.853	63-64	351
Palmitoleic		-	33	162
Ricinoleic		0.94	5.5	245
Stearic		0.83-0.94	66-70	365-370

saponification of the oil and without loss of oil by emulsification.¹⁹⁴ The technique involves the use of a very dilute caustic soda solution in sufficient quantity to neutralize the free fatty acids. Depending on the type of oil, the color required and impurities present the quantity of caustic soda is varied.^{194,196}

Sometimes, acid refining technique is also used although color removal in the process is not suitable as in alkali refining technique. In this process, the cold oil is stirred with concentrated sulphuric acid solution. On settling, the impurities are drawn off and the oil is washed to make free from impurities. As a finishing step of the refining process, bleaching should be done for partial or complete removal of color.

Bleaching can be done either by chemical or by physical means. The chemical method is disadvantageous as the oil suffers oxidation during the process. However, in the physical method, the oil is heated with an adsorbent such as fullers earth, activated carbon, silica, bentonite etc. in the absence of oxygen. The process is generally carried out at about 110 °C with 0.2-2.5% solution of the adsorbent for duration of ca. 30-60 min.¹⁹⁴

Preparation of Epoxy Resins from Vegetable Oil

In-situ Epoxidation with Peracid

The epoxidation using peracids is one of the most industrially viable techniques; the process of epoxide synthesis gives stereospecific oxirane formations thus a *cis* olefin leads to a *cis* epoxide and a *trans* olefin leads to a *trans* epoxide. The order of reactivity of some of the peracids are *m*-chloroperbenzoic acid > performic acids > perbenzoic acids > peracetic acids.¹⁹⁷

Table 1.5: *A few important vegetable oils used to prepare epoxy resin with their physical properties and major fatty acids contents*

Name of oil	Major fatty acids (% of total)	Saponification value (mg KOH/g)	Iodine value (g I ₂ /100 g)
Linseed oil	Linolenic (50-61)/ linoleic (13-15)	192-195	175-204
Castor oil	Ricinoleic (80-90)/ linoleic (3-4)	180	82-88
Tung oil	Elaeostearic (77-88)/ oleic (4-10)	193	155-175
Soybean oil	Linoleic (54.5)/ oleic (22.3)	189-195	125-140
Sunflower oil	Linoleic (69)/ oleic (18.3)	188-194	119 - 135
Safflower oil	Linoleic (75)/ oleic (14)	135-190	140-150
Tobacco seed oil	Linoleic (66-76)/ oleic (17-27)	193	135
Oiticica oil	Licanic (73-76)/ linoleic (8-10)	150	179-218
Perilla oil	Linolenic (46.5)/ linoleic (37)	182-205	192-208
Coconut oil	Lauric (48.2)/ myristic (16.6)	252-284	8-10
Rubber seed oil	Linoleic (39.6)/ oleic (24.6)	192	155

Electron withdrawing groups promote the reaction. The carboxylic acid produced is a stronger acid than the strongly hydrogen bonded peracid and may lead to

subsequent ring opening reactions especially in the case of formic acid. Small scale reactions are carried out with *m*-chloroperbenzoic acid in a halocarbon or aromatic solvent, in the presence of bicarbonate to neutralize the carboxylic acid as it is formed.¹⁹⁸ Many studies have indicated the importance of using catalysts for epoxidation purposes.

It is possible to use either acetic acid or formic acid as the carboxylic acid in the epoxidation process. Acetic acid represents an inexpensive acid that is readily available and has high epoxidation efficiency. Predominately the role of acetic acid is as a catalyst in the formation of the oxirane ring¹⁹⁹ and as an oxygen carrier from the aqueous phase to the oil phase.⁶⁴ Mungroo et al.²⁰⁰ found that the use of acetic acid resulted in a 10% increase in the conversion of ethylenic unsaturation to oxirane than that formed by formic acid. Furthermore Dinda et al.⁶⁴ worked on the epoxidation kinetics of cottonseed oil using the aqueous H₂O₂ catalyzed by liquid inorganic acids, i.e. hydrochloric acid, sulphuric acid, nitric acid and phosphoric acid. It was found that the degree of conversion to oxirane in cottonseed oil with H₂SO₄ or H₃PO₄ as catalyst was higher than those with HCl and HNO₃. The greatest oxirane conversion (~70.4%) could be achieved in the shortest period of time (after 6 h) using H₂SO₄ as catalyst compared to those using H₃PO₄. Further they identified that acetic acid resulted in a higher ultimate conversion to oxirane with fewer undesired products formed. The increased formation of undesired products may be attributed to the decomposition of some hydrogen peroxide. This is a result of the active temperament of the formic acid thereby resulting in early onset oxygen depletion of the system.

Hilker et al.²⁰¹ and Cai et al.²⁰² reported that conventional epoxidation process, which required peracetic or performic acid for the transfer of oxygen to the unsaturated double bonds was less advantageous since these acids would eventually give rise to side reactions, followed by greatly reducing the selectivity to epoxidized products. Klass and Warwel²⁰³ mentioned that the selectivity of epoxidation of vegetable oils using conventional method seldom exceeded 80%. Furthermore, safety aspects and the difficulty in isolating the acid catalyst from the yield were other problems that arise during epoxidation using conventional Prileshajev peracid process.²⁰⁴

To minimize the drawback of using strong mineral acids such as concentrated sulphuric acid as catalysts in the conventional epoxidation method, it was suggested by Gurbanov and Mamedov²⁰⁵ to employ the ion-exchange resin as the catalyst to synthesize peroxy acids, followed by epoxidizing the unsaturated vegetable oil with the

in-situ formed peroxy acids. Being in the solid stage and insoluble, the ion-exchange resin as catalysts not only suppressed undesirable side reactions and improved selectivity, but also contributed to the easy separation of the catalysts from the reaction products.²⁰⁶ Mungroo et al.²⁰⁰ further reported that the epoxidation process of vegetable oils could be made more cleaner and environmental friendly by utilizing heterogeneous catalysts especially ion-exchange resin instead of conventional homogeneous catalysts.

Epoxidation with Organic and Inorganic Hydroperoxides

This method is generally catalyzed by a transition metal catalyst. The most common of these is nitrile hydrogen peroxide, which is an inorganic chemical.

Epoxidation with organic and inorganic hydroperoxides in homogeneous phase, the most active catalysts are soluble compounds of the early transition elements Ti^{IV} , V^V , Mo^{VI} and W^{VI} . With organic hydroperoxides the activity of these metals is in the order $Mo^{VI} \gg Ti^{IV} \sim V^V > W^{VI}$, but with anhydrous hydrogen peroxide W^{VI} catalysts are superior to the others. Some compounds of these metals have been successfully heterogenized but the heterogenization remarkably changes their relative activity.²⁰⁷⁻²⁰⁹ The epoxidation of olefins with organic hydroperoxides catalyzed by early transition elements involves a peroxometal mechanism in which the rate-limiting step is oxygen transfer from an electrophilic (alkyl) peroxometal species to the nucleophilic olefin. The metal center does not undergo any change in oxidation state during the catalytic cycle, it functions as a Lewis acid by withdrawing electrons from the O-O bond and thus increases the electrophilic character of the coordinated peroxide. Therefore, active catalysts are metals which are strong Lewis acids and relatively weak oxidants (to avoid one electron oxidation of the peroxide), in their highest oxidation state.

Epoxidation with Molecular Oxygen

Epoxidations with molecular oxygen which are catalyzed by compounds containing elements from groups IV-VI B show high selectivity but low activity.^{201,210} With elements from groups I, VII and VIII B the epoxidations are more active but less selective. Silver is a unique catalyst for the heterogeneous epoxidation of ethylene with molecular oxygen, but the reaction is mainly restricted to a few substrates like ethylene and butadiene, the epoxidation of other alkenes results in very low yields.²¹¹ Liquid phase oxidations with molecular oxygen are generally free radical autoxidations, the intermediate alkylperoxy and alkoxy radicals are largely indiscriminate in their reactivity and selective oxidations are generally observed only with relatively simple

substrates containing one reactive group. Thus, although O_2 is a cheap oxidant with no waste problems its scope is limited to a rather small number of simple petrochemicals.^{211,179,181} For the particular case of vegetable oils, the oxidation with O_2 leads to the degradation of the oils to smaller volatile compounds such as ketones and aldehydes as well as short-chain dicarboxylic acids. Therefore, it is not an adequate method to epoxidize vegetable oils.

Epoxidation with Halohydrins

Halohydrins are prepared by the addition of hypohalous acids to olefins, subsequently; their treatment with alkali produces the epoxide.²¹¹ This is a highly environmentally unfriendly system: apart from being a classical stoichiometric synthesis which is characterized by an extensive use of reactants, dihalides, halogen ethers and salts are produced.

Chemo-Enzymatic Epoxidation

With the intention to eliminate the practice of using strong acid as catalyst which would lead to side reactions to catalyze peroxy acid formation during the epoxidation process and to make the process more environmentally friendly, Klass and Warwel²⁰³ studied on the epoxidation of plant oils such as rapeseed, sunflower, soybean and linseed using immobilized lipase-catalyzed perhydrolysis process. An approximately 5 mol% of free fatty acids related to C=C bond was incorporated into the system. The final mixture generated comprised of only the epoxidized free acids and epoxidized triglycerides without the presence of any by-products. In addition, it was explored that this chemo-enzymatic 'self' epoxidation using lipase biocatalyst was highly selective and conversion rate of epoxidation usually exceeded 90%. Ursula et al.²¹² had reported that the lipase catalyst not only exhibited excellent stability and activity during the epoxidation process, but also could be utilized several times without scarifying its activity.

Vegetable Oil based Epoxy Resins and Epoxidized Vegetable Oils

With respect to the environmental issues, waste disposal problems as well as depletion of non-biodegradable oleochemical-based resources in late, plenty of biobased natural polymer products such as polyhydroxy alkonate, polylactic acid, cellulose plastics, thermoplastic starch and vegetable oil based polymers have been widely developed and commercialized.^{213,214} Among these, there has been a growing trend in utilizing the

vegetable oils extensively as raw material in various applications due to their inherent biodegradability, low cost, societal favorably advantages and availability.²¹⁵⁻²¹⁶ Due to curiosity as to the versatility of vegetable oil constituents that are made up of complex multi-component mixtures of fatty acids and glycerol ester, various researches have been conducted to make full use of linseed, castor, soya, safflower or tall oils in oleoresinous production. In general, advances in oleochemistry technology today make possible for researchers to chemically modify and hence, plenty of researches on the epoxidation of triglyceride oils have been conducted worldwide in order to optimize the conversion rate of epoxidation and increase the epoxy yield. Even if there are adequate amount of epoxidized vegetable oils available at the present time, Clayton¹⁸³ and Meyer et al.¹⁸⁴ found that the vegetable oils with relatively high iodine value i.e. high content of unsaturated fatty acid especially soybean and linseed oils are the best to produce epoxy resins with high epoxy functionality epoxides. Although plenty of investigations indicated that formation of epoxy ring, transform the triglycerides into polymerizable monomer via epoxidation, metathesis of double bonds, acrylation of epoxies, reaction with maleic anhydride or transesterification.²¹⁷ Among those reactions, epoxidation is a commercially important reaction in organic synthesis since the high reactivity of oxirane rings makes them to be readily transformed into desired functionality.²¹⁸

Czub²¹⁹ reported a method of synthesis of liquid high molecular weight epoxy resins from modified vegetable oils such as epoxidized soybean, rapeseed, linseed, and sunflower oils as well as hydroxylated soybean and rapeseed oils using the advancement process. The advancement reaction was carried out with bisphenol-A based epoxy resin with hydroxylated natural oils in the presence of different catalysts (i.e. LiCl, 2-methylimidazole, triphenylphosphine, and triethanolamine) in the temperature range of 130–160 °C (depending on the catalyst type), and under nitrogen for minimization of the oxidative degradation.

Although plenty of investigations indicated that epoxidized vegetable oils (EVO) which possess functional epoxy groups on their triglycerides backbone chains own the capability to produce a flexible, semi-flexible or rigid elastomeric network structure when subjected to anhydride curing, amine curing or UV curing,²²⁰⁻²²² however, it was discovered that EVO with its relatively low oxirane value tended to impart poor properties to the biobased system.²²³ Hence, there is a growing trend of blending the petrochemical based epoxies with EVO in the presence of appropriate curing agents in order to produce biobased epoxy system with satisfactory properties. In addition, there

are also lots of attempt carried out to toughen the epoxy resins which are brittle in nature by incorporating relatively low cost and readily biodegradable EVO into the epoxy system.²²⁴

Gerbase et al.²²⁵ investigated the mechanical and thermal behaviour of epoxidized soybean oil (ESO) cured with various cyclic acid anhydrides in the presence of tertiary amines. Five different types of anhydrides viz. succinic anhydride (SUC), hexahydrophthalic anhydride (CH), phthalic anhydride (PA), maleic anhydride (MA) and dodecenylsuccinic anhydride (DDS) and three types of initiators triethylamine (TEA), N,N'-dimethylaniline (ARO) and 1,4-diazobi-cyclo [2,2,2] octane (DABCO) were investigated in the study. The ESO anhydride-amine system tended to show high T_g and crosslink density when the systems was cured with PA, MA or CH anhydrides that are made up of rigid chemical backbone structures. From the dynamic mechanical analysis (DMA) results, it was found that the PA or MA cured systems exhibited better dynamic mechanical properties (i.e. storage modulus) as compared with the SUC or DDS-cured systems. In term of the epoxidation level on the dynamic mechanical properties, it was proven experimentally that the reactivity of partially ESO was relatively low and hence, the networks showed lower T_g and crosslink density. Studies on the thermal and rheological properties of vegetable oil-based epoxy resins cured with N-benzylquinoxalinium hexafluoroantimonate (BQH) thermal latent initiator has been conducted by Jin and Park.²²⁶ For the preparation of epoxidized soybean oil ESO-BQH and epoxidized castor oil (ECO)-BQH epoxy networks, these systems were cured at 110 °C for 1 h, then 140 °C for 2 h and finally at 170 °C for 2 h. Experimental evidence from dynamic differential scanning calorimetry (DSC) thermograms proved that the peak maximum temperature and cure activation energy (E_a) of the ESO-BQH system were greater than the ECO-BQH system whereas thermogravimetric analysis (TGA) thermograms indicated that the initial decomposition temperature (IDT) and the temperature at the maximum degradation rate (T_{max}) of the ESO-BQH system were higher than the ECO/BQH system.

Park et al.²²⁷ found that N-benzylpyrazinium hexafluoroantimonate (BPH) initiator was only miscible with ESO and ECO resins completely at ambient temperature. Although the polymerization reaction of both ESO and ECO were incapable to be initiated by BPH below 80 °C and 50 °C respectively, both of the cationic polymerization reactions took place swiftly exceeding these temperatures. DMA results

also proved that the crosslink density and storage modulus @ 30 °C of the ESO-BPH system were greater than the ECO/BPH system.

A kinetic study of the acceleration effect of mono, di and trisubstituted alcohols on the cationic photopolymerization rate of epoxidized natural oil, i.e. soybean, linseed, sunflower and corn oil, have been conducted by Ortiz et al.²¹⁷ It was observed that the rate of conversion of the four different types of epoxidized oils were relatively low, but the polymerization rate of these epoxy systems were accelerated using alcohols. The addition of approximately 20% of 2,5-dimethoxybenzyl alcohol into ESO tended to maximize the photopolymerization rate.

Lligadas et al.²²⁸ synthesized novel phosphorous containing fatty acid derivatives which they used monomers in the designing of flame retardant epoxy thermosetting materials. The phosphorus containing epoxy thermosets exhibited good flame retardancy. When heated, these phosphorous moiety leads to the formation of a protective phosphorous rich layer that shields the underlying polymer from attack by oxygen and radiant heat. This layer further prevents the escaping of any volatiles from feeding into the flame. However the epoxy thermosets exhibited limited thermal and mechanical properties because of the low reactivity of epoxy groups and the tendency for intramolecular bonding.

Most of the epoxidized oils do not exhibit sufficient mechanical properties to be useful in many applications. By the help of reactions like co-polymerization, chain extension by reactive diluents, side chain modification the desired properties can be achieved. A lot of research work has been done to improve the required parameters of epoxy resins through modifications in both the backbone and pendant groups.

The developments in this field are due to the research work of Greenlee and described in a number of patents. These include work on the modification of epoxy resins with glycerol, the esterification with drying oil acids and reaction with phenolic and amino resins. Greenlee²²⁹ prepared the rapid drying composition from diphenols and epichlorohydrin and esterified the product with Tall oil.

Castan and Gandillon²³⁰ have reported esterified epoxy resin of phenol formaldehyde with long chain fatty acids, which may be unsaturated, and found that dehydration is affected with acid catalyst to produce rapid drying films. Cobalt or Lead naphthenate were also used. The resulting films were relatively resistant to alkali. The use of saturated acids in the esterification step gives resins, which can be hardened in the kiln.

Narracott²³¹ has esterified epoxy resins with drying fatty acids (Armours Neofat No. 3, comprising 50% linoleic acid, 40% oleic acid and 10% stearic acid) in the presence of orthophosphoric acid catalyst and xylene for 10 h at 230–240 °C under nitrogen atmosphere (as a 50% xylene solution). They employed different types of polyhydric phenol to obtain the esterified epoxy resin. They also reported that the esterified product has the tendency of air drying when applied to metal surfaces by spraying or brushing. They further observed that the drying tendency enhances on incorporation of metal drier such as cobalt as naphthalene salt (0.1-0.2%).

Preparation of Nanocomposites

The methods are almost similar to the methods as described in general section.

Characterization

Vegetable oil based epoxy nanocomposites are characterized by similar methods as discussed in the sub-section 1.5.2. XRD is a common tool that is frequently used to characterize the vegetable oil based polymer nanocomposites too. The shift of the reflection peak corresponding to {001} planes of nanoclay towards low angle value reveals the intercalation of clay galleries by the epoxy chains. The disappearance of this peak indicates the formation of exfoliated type structure, however TEM study is necessary to confirmed the above observation. The XRD spectra in the case of polymer/metal nanoparticles nanocomposites showed the appearance of new desired peaks which confirmed the formation of nanocomposites.

In the FTIR spectra of vegetable oil based epoxy nanocomposites, in addition to the characteristic bands for the nanomaterial, the bands for fatty acids were also distinct. The bands for epoxide group, ester carbonyl C=O , ether oxygen C-O-C etc. as well as bands for the stretching vibration of Si-O , Al-O and Si-O-Si for nanoclay are observed in the FTIR spectra of vegetable oil based epoxy/clay nanocomposites. For different metal nanoparticles the bands for metal oxides or metal hydroxides are obtained. For example, zirconia exhibits bands at 3771 cm^{-1} corresponding to terminal Zr-OH groups and at 3671 cm^{-1} for bridging or triple-bridging OH groups. The magnesium oxide shows weak adsorption band in the -OH stretching region at 3750 cm^{-1} . Also bands corresponding to fundamental skeletal vibrations for nanoparticles are also obtained at low frequency, whose band position mostly depends on the amount of the metal element and on the nature of the bond.²³²

For example band is found near 1000 cm^{-1} for alumina and titania, near 800 cm^{-1} for zirconia and 700 cm^{-1} for magnesia.

SEM technique is used to study the surface morphology of the vegetable oil based epoxy nanocomposites. The SEM micrographs indicate the dispersion pattern of different nanomaterials in the epoxy matrix. On the other hand TEM is used to get direct qualitative information of spatial distribution, structure and morphology of the various nanofillers as well as the defect structure of the epoxy nanocomposites.

The thermal characterization of vegetable oil based epoxy nanocomposites by TGA and DSC techniques are carried out in a similar manner as for other polymer nanocomposites. Higher thermal stability compared to the pristine epoxy matrix is reported by several authors after formation of nanocomposites by incorporation of nanoclay. This is attributed to the nanoclay which by virtue of its distribution in the matrix acts as a thermal insulator and mass transport barrier to the volatile generated during decomposition of the matrix. Similarly the T_g and melting enthalpy (ΔH_m) are also enhanced after nanocomposite formation.

DMA (DMTA) and TMA measurements are used to analyze the structure and morphology by determining the various transitions and relaxations processes (such as variation of G' and G'' with temperature).

Properties

Vegetable oil based epoxy nanocomposites exhibited properties which are comparable or even better in some cases than the petroleum based epoxy nanocomposites. The properties described in section 1.6. are also valid for vegetable oil based epoxy nanocomposites.

The incorporation of nanofillers has a profound effect on the mechanical properties of pristine polymeric systems in terms of tensile strength, scratch resistance, impact strength, toughness etc. of vegetable oil based epoxy nanocomposites. While in most of the cases the elongation at break value has been observed to decrease after nanocomposite formation though it may exhibit increase in value as observed in some cases. The imposed restriction in chain motion of the polymer by the nanomaterial results in the decreased value. However, Li⁴¹ observed an increasing trend of the elongation at break value after nanocomposite formation. The vegetable oil based epoxy exhibited enhanced flexibility and it retains in the nanocomposites. The presence

of long chain of fatty acid in the vegetable oil may be attributed to this flexibility in the nanocomposites.

The nanocomposites prepared by an acid-catalyzed curing of epoxidized soybean and linseed oil in the presence of silane coupling agents exhibited highly glossy character with retention of transparency. The hardness and Young's modulus of the nanocomposite coatings exhibited an improvement as compared with those only from the pristine system.¹⁵⁷ Enhancement in the storage modulus up to 14% with only 0.24 wt% of fluorinated SWCNT was observed for epoxidized linseed oil, whereas the fracture toughness exhibited an enhancement of 43% after nanocomposites formation. The excellent improvement of the modulus was achieved without sacrificing the fracture toughness.²³³

The vegetable oil based epoxy also exhibited enhancement in the thermal stability after incorporation of different nanofillers like nanoclay, nanometal, carbon nanotubes etc. The well dispersed nanofillers in the epoxy matrix restrict the segmental motion of the polymer chains thereby increasing the thermal stability. Also they hinder the diffusion of volatiles and assist in char formation after thermal decomposition.

The biodegradability of the vegetable oil based epoxy/clay nanocomposites show significant enhancement with increase of clay content. Although different mechanisms have been postulated for biodegradation, yet the exact pathway is not still confirmed. Vegetable oil based epoxy containing copper nanoparticles exhibited antimicrobial activity. Vegetable oil based epoxy are known for their sustainability and biocompatibility, and hence its nanocomposites. The red blood cell (RBC) haemolysis inhibition capacity of the vegetable oil based epoxy nanocomposites was studied to check their cytocompatibility. Dutta reported the RBC haemolysis inhibition capacity of the *Mesua ferrea* oil based PU/clay nanocomposites to state the cytocompatibility of the materials.¹⁹⁶ The bacterial degradation of the same is also studied by broth culture technique where the nanocomposites are exposed to microbial degradation.

The rheological study of vegetable oil based epoxy showed increase in the viscosity with the incorporation of nanomaterials. The interaction between nanofillers and the epoxy chains restricted the chains to relax. However with the increase of shear rates slight decrease in the viscosity was observed. These result the break down in network structure and the parallel alignment of the nanomaterials. Consequently orientating the nanomaterials in the flow direction, and contributes shear thinning behavior in the nanocomposites. Because of this shear thinning behavior, the

nanocomposites can be processed in the melt state using the conventional equipment available in a manufacturing line.

The metal nanocomposites have catalytic activity due to the high surface area of the nanoparticles, which can effectively catalyzed reactions where the matrix acts as support. Karak et al.¹⁴⁰ explored the catalytic activity of the sunflower oil based hyperbranched polyurethane/silver nanocomposite in the reduction of 4-nitrophenol to 4-aminophenol.

Applications

Almost all current polymers are produced from petroleum resources. Because of their widespread use and the dominant consumption patterns, in which materials and products are used only once and then discarded, polymers also make a significant contribution to the increasing amount of solid waste due to a very large percentage of the plastics produced from fossil-fuel feedstock are being non-biodegradable. Moreover, efforts such as recycling and combustion in incinerating plants have to be considered carefully from economic and ecological perspectives. In the search for sustainable chemistry, there are increasing demands for replacing petroleum-derived raw materials with renewable raw materials in the production of polymers.²³⁴⁻²³⁸ The importance of natural products for industrial applications becomes very clear from a social, environmental and energy standpoint, with the increasing emphasis on issues concerning waste disposal and depletion of non-renewable resources. Vegetable oils are one of cheap and available easily in large quantities, annually renewable natural resources and are now being used in an increasing number of industrial applications. In recent years, extensive work has been done to develop polymers with triglycerides of fatty acids as the main component.²³⁹⁻²⁴¹ The products have wide application in agricultural mulching films, hay binder twines, compostable waste bags and controlled release fertilizers. Future applications currently being evaluated are in agricultural packaging including stretch wrap films for hay and silage, in bird netting and animal feed bags.

1.9. Scopes and Objectives of the Present Investigation

From the main features of the above discussion, it has been found that many vegetable oils are widely used in place of petroleum based products as the raw materials. Among the vast varieties of widely grown plants and herbs that are available in India, *Mesua ferrea* L. (Nahar) is a plant that produces exceptionally high oil containing seeds. It is

available in different countries such as India, Sri Lanka, Bangladesh, Nepal, Indochina (Southeast Asia), Malay Peninsula etc. Reports deal with the utilization of this oil in the fields of medicine and biodiesel and as well in the field of polymer. Nevertheless, there is no report on utilization of this oil for synthesis of epoxy and its nanocomposites. Hence, the following questions may arise in this area.

- (i) Whether this oil can be utilized for the preparation of epoxy resins or epoxidized oil.
- (ii) Whether the performance characteristics of the epoxy resins can be improved by any physical or chemical means?
- (iii) Whether the virgin as well as the modified resins can be utilized as the matrix for the preparation of different types of nanocomposites?
- (iv) Whether the incorporation of different nanofillers into the epoxy matrix can lead to the genesis of advanced materials?

Under the above background, the main objectives of the present investigation are as follows:

- (i) To synthesize, characterize and evaluate various properties of *Mesua ferrea* L. seed oil based epoxidized oil and epoxy resins.
- (ii) To improve the performance of the vegetable oil based epoxies by blending with a suitable commercial polymer.
- (iii) To improve the performance characteristics of the epoxy systems by the formation of nanocomposites.
- (iv) To utilize different types of nanofillers for the preparation of various nanocomposites to achieve desire level of properties.
- (v) To study the rheological behavior for better understanding of nano-reinforcing mechanisms in the nanocomposites.
- (vi) To utilize the prepared nanocomposites as advanced materials in the field of surface coating, adhesive, flame retardancy, biodegradable biomaterial, antimicrobial etc.

1.10. Plans of Work

To fulfill the above objectives, the following plans of work have been adopted.

- (i) A state of art literature survey on the field of epoxy resin and their nanocomposites will be conducted.

- (ii) The epoxidized oil and epoxy resin from vegetable oil will be synthesized by the help of standard procedures reported in literature.
- (iii) The synthesized epoxidized oil/epoxy resin will be characterized by different analytical and spectroscopic techniques such as determination of hydroxyl value, saponification value, epoxy equivalent, FTIR, NMR, TGA, DSC etc.
- (iv) Epoxy nanocomposites will be prepared by the *ex-situ* technique as reported in the literature using epoxy resin and epoxidized oil/organophilic nanoclay/metal nanoparticles /MWCNTs etc.
- (v) The prepared nanocomposites will be characterized by UV, FTIR, XRD, TEM, SEM, rheometer etc. to study the structure, morphology and rheological behaviors.
- (vi) The performance characteristics of the nanocomposites will be investigated by determination of mechanical properties like, tensile strength, elongation at break, impact strength, scratch resistance, thermal properties such as T_g , thermostability and flame retardancy, chemical resistance in different chemical media etc. Further, the special properties like adhesive strength, antimicrobial behavior, cytocompatibility etc. will also be conducted depending on requirement.
- (vii) The performance characteristics of the nanocomposite will be optimized by manipulation of composition of raw materials, processing parameters etc. to find out the best nanocomposite in each category.

References

1. Pavlidoua, S., & Papaspyrides, C.D. A review on polymer-layered silicate nanocomposites, *Prog. Polym. Sci.* **33**, 1119–1198, 2008.
2. Fischer, H. Polymer nanocomposites: From fundamental research to specific applications, *Mater. Sci. Eng. C.* **23**, 763–72, 2003.
3. Winey, K.I., & Vaia, R.A. Polymer nanocomposites, *MRS Bull.* **32**, 314-322, 2007.
4. Ahmad, S., et al. Polyesteramide from *pongamia glabra* oil for biologically safe anticorrosive coating, *Prog. Org. Coat.* **47**, 95-102, 2003.
5. Aigbodion, A.I., et al. Synthesis, characterization and evaluation of heated rubber seed oil and rubber seed oil-modified alkyd resins as binders in surface coatings, *Ind. J. Chem. Technol.* **8**, 378-384, 2001.
6. Sharmin, E., et al. Synthesis, characterization, antibacterial and corrosion protective properties of epoxies, epoxy-polyols and epoxy-polyurethane coatings from linseed and *Pongamia glabra* seed oils, *Int. J. Bio. Macromol.* **40**, 407-422, 2007.
7. Ikhuoria, E.U., et al. Preparation and characterization of water-reducible alkyds with fumarized rubber seed oil, *Prog. Org. Coat.* **52**, 238-240, 2005.
8. Blayo, A., et al. Chemical and rheological characterizations of some vegetable oils derivatives commonly used in printing inks, *Ind. Crop. Prod.* **14**, 155-167, 2001.
9. Carrick, L.L. Vegetable oil paints, *J. Am. Oil. Chem. Soc.* **27**, 513-522, 1950.
10. Aigbodion, A.I., & Pillai, C.K.S. Preparation, analysis and applications of rubber seed oil and its derivatives in surface coatings, *Prog. Org. Coat.* **38**, 187-192, 2000.
11. Sabin, P., et al. Offset printing inks based on rapeseed and sunflower oil: Synthesis and characterization of rapeseed oil- and sunflower oil-modified alkyd resins, *J. Am. Oil. Chem. Soc.* **74**, 481-489, 1997.
12. Erhan, S.Z., & Bagby, M.O. Vegetable-oil-based printing ink formulation and degradation, *Ind. Crop. Prod.* **3**, 237-246, 1995.
13. Akram, D., et al. Synthesis and characterization of boron incorporated polyester polyol from linseed oil: A sustainable material, *Macromol. Symp.* **277**, 130-137, 2009.
14. Joseph, R., et al. Studies on epoxidized rubber seed oil as plasticizer for acrylonitrile butadiene rubber, *J. Appl. Polym. Sci.* **89**, 668-673, 2003.
15. Nandan, V., et al. Rubber seed oil: A multipurpose additive in NR and SBR compounds, *J. Appl. Polym. Sci.* **72**, 487-492, 1999.

16. Bisht, R.P., et al. Vegetable oils as lubricants and additives, *J. Sci. Ind. Res.* **48**, 174-180, 1989.
17. Ramadhas, A.S., et al. Use of vegetable oils as I.C. engine fuels-A review, *Renew. Energy* **29**, 727-742, 2004.
18. Ajiwe, V.I.E., et al. Characterization and applications of oils extracted from *Canarium schweinfurttii*, *Vitex doniana* and *Xylopi aethiopica* fruits/seeds, *Bioresour. Technol.* **64**, 249-252, 1998.
19. Aigbodion, A.I., et al. Utilization of maleinized rubber seed oil and its alkyd resin as binder in water-borne coatings, *Prog. Org. Coat.* **46**, 28-31, 2003.
20. Akintayo, C.O., & Akintayo, E.T. Synthesis and characterization of arylated polyetheramide based coating from *Albizia benth* seed oil, *World Appl. Sci. J.* **11**, 1408-1415, 2010.
21. Mondhe, O.P.S., & Rao, J.T. Studies on *Jatropha Curcas* seed oil incorporated alkyd dyes. II. Preparation and application of azo alkyd dyes, *Colourage* **40**, 51-53, 1993.
22. Chahande, P.P., & Gogte, B.B. Ecofriendly primers based on very short oil novel alkyd, *Paintindia* **57**, 61-64, 2007.
23. Hassanein, M.M.M. Studies on non-traditional oils: I. Detailed studies on different lipid profiles of some *Rosaceae* kernel oils, *Int. J. Fats Oils* **50**, 379-384, 1999.
24. Abd El-Aal, M.H., et al. Apricot kernel oil: Characterization, chemical composition and utilization in some baked products, *Food Chem.* **19**, 287-298, 1986.
25. Panda, S., & Kar, A. *Annona squamosa* seed extract in the regulation of hyperthyroidism and lipid-peroxidation in mice: Possible involvement of quercetin, *Phytomedicine* **14**, 799-805, 2007.
26. Igwe, I.O., & Ogbobe, O. Studies on the properties of polyesters and polyester blends of selected vegetable oils, *J. Appl. Polym. Sci.* **75**, 1441-1446, 2000.
27. Sharmin, E., et al. Characterization, antibacterial and corrosion protective properties of epoxies, epoxy-polyols and epoxy-polyurethane coatings from linseed and *Pongamia glabra* seed oils, *Int. J. Bio. Macromol.* **40**, 407-422, 2007.
28. Aigbodion, A.I., & Okieimen, F.E. An investigation of the utilization of African locustbean seed oil in the preparation of alkyd resins, *Ind. Crop. Prod.* **13**, 29-34, 2001.
29. Ajiwe, V.I.E., et al. Extraction and utilization of *Azzeria Africana* seed oil, *Bioresour. Technol.* **53**, 89-90, 1995.

30. Wen, J., & Wilkes, G.L. Organic/inorganic hybrid network materials by the sol-gel approach, *Chem. Mater.* **8**, 1667–1681, 1996.
31. Paul, D.R., & Robeson, L.M. Polymer nanotechnology: Nanocomposites, *Polymer* **49**, 3187–3204, 2008.
32. Njuguna, J., et al. Nanofiller-reinforced polymer nanocomposites, *Polym. Adv. Technol.* **19**, 947-959, 2008.
33. Lagaly, G. Introduction: from clay mineral-polymer interactions to clay mineral-polymer nanocomposites, *Appl. Clay. Sci.* **15**, 1–9, 1999.
34. Cho, J.W., & Paul, D.R. Nylon 6 nanocomposites by melt compounding, *Polymer* **42**, 1083–94, 2001.
35. Bower, C.A. Studies on the form and availability of organic soil phosphorous, *IOWA Agric. Exp. Station. Res. Bull.* **362**, 39–42, 1949.
36. Theng, B.K.G. Interactions of clay minerals with organic polymers. Some practical applications, *Clay Miner.* **18**, 357-362, 1970.
37. Hess, P.H., & Parker, P.H. Polymers for stabilization of colloidal cobalt particles, *J. Appl. Polym. Sci.* **10**, 1915-1927, 1966.
38. Karak, N. Polymer (epoxy) clay nanocomposites. *J. Polym. Mater.* **23**, 1-20, 2006.
39. Kojima, Y., et al. Sorption of water in nylon 6-clay hybrid, *J. Appl. Polym. Sci.* **49**, 1259-1264, 1993.
40. Jia, Q.M., et al. Synthesis and characterization of polyurethane/epoxy interpenetrating network nanocomposites with organoclays, *Polym. Bull.* **54**, 65-73, 2005.
41. Li, J. High performance epoxy resin nanocomposites containing both organic montmorillonite and castor oil-polyurethane, *Polym. Bull.* **56**, 377-384, 2006.
42. Jia, Q., et al. Tribological performance and thermal behavior of epoxy resin nanocomposites containing polyurethane and organoclay, *Polym. Adv. Technol.* **19**, 859-864, 2008.
43. Astruc, A., et al. Incorporation of kaolin fillers into an epoxy/polyamidoamine matrix for coatings, *Prog. Org. Coat.* **65**, 158-168, 2009.
44. Becker, O., & Simon, G.P. *Epoxy Layered Silicate Nanocomposites*, Advances in Polymer Sciences, Springer-Verlag, Berlin, 2005, 29–82.
45. Pascault, J.P. & Williams, R.J.J. *Epoxy Polymers*, Wiley-VCH, Weinheim, 2010.
46. Hartman, S.J. *The Epoxy Resin Formulators Training Manual*, The Society of the Plastics Industry Inc., New York, 1984, 1.

47. Lee, H. & Neville, K. *Handbook of Epoxy Resins*, McGraw-Hill Inc., New York, 1967, reprinted 1982.
48. Ishida, H., et al. General approach to nanocomposite preparation, *Chem. Mater.* **12**, 1260-1267, 2000.
49. Alexandre, M., & Dubois, P. Polymer-layered silicate nanocomposites: preparation, properties and uses of a new class of materials, *Mater. Sci. Eng. R* **28**, 1-63, 2000.
50. Beyer, G. Nanocomposites: A new class of flame retardants for polymers, *Plast. Addit. Comp.* **4**, 22-7, 2002.
51. Goud, V.V., et al. Kinetics of epoxidation of jatropha oil with peroxyacetic and peroxyformic acid catalyzed by acidic ion exchange resin, *Chem. Eng. Sci.* **62**, 4065-4076, 2007.
52. Chiu, Y.C., et al. Preparation and thermal properties of diglycidylether sulfone epoxy, *Polym. Degrad. Stab.* **93**, 668-676, 2008.
53. Gao, J., & Li, Y. Curing kinetics and thermal property characterization of a bisphenol-S epoxy resin and DDS system, *Polym. Int.* **49**, 1590-1595, 2000.
54. Bansal, R., et al. Epoxy resins VIII. Thermal properties of 4,4'-sulfonyldiphenol and bisphenol a epoxy resins, *Macromol. Mater. Eng.* **117**, 211-218, 1983.
55. Liaw, D.J., & Shen, W.C. Synthesis of epoxy resins based on bisphenol-S and its derivatives, *Angew. Makromol. Chem.* **199**, 171-190, 1992.
56. Mark, H.F. *Encyclopedia of Polymer Science and Technology*, John Wiley & Sons, Weinheim, 2004.
57. Birnbaum, L.S., & Staskal, D.F. Brominated flame retardants: Cause for concern?, *Environ. Health Perspect.* **112**, 9-17, 2004.
58. Saroop, U.K., et al. Effects of various process variables on resin characteristics of brominated epoxy polymers, *Eur. Polym. J.* **30**, 557-560, 1994.
59. Twardowski, T.E., & Geil, P.H. A highly fluorinated epoxy resin. III. Behavior in composite and fiber-coating applications, *J. Appl. Polym. Sci.* **42**, 1721-1726, 1991.
60. Twardowski, T.E., & Geil, P.H. A highly fluorinated epoxy resin: Post-curing and transition behavior, *J. Appl. Polym. Sci.* **41**, 1047-1054, 1990.
61. Twardowski, T.E., & Geil, P.H. Highly fluorinated epoxy resin. II. Behavior in blend applications, *J. Appl. Polym. Sci.* **42**, 69-74, 1991.
62. Salunkhe, D.K., et al. Legume lipids, in *Chemistry and biochemistry of Legumes*, S.K. Arora ed., Edward Arnold Pub. Ltd., London, 1983.

63. Goud, V.V., et al. Studies on the epoxidation of mahua oil (*Madhumica Indica*) by hydrogen peroxide, *Bioresour. Technol.* **97**, 1365–1371, 2006.
64. Dinda, S., et al. Epoxidation of cottonseed oil by aqueous hydrogen peroxide catalyzed by liquid inorganic acids, *Bioresour. Technol.* **99**, 3737–3744, 2008.
65. Vlcek, T., & Petrovic, Z.S. Optimization of the chemoenzymatic epoxidation of soybean oil, *J. Am. Oil Chem. Soc.* **83**, 247-252, 2006.
66. Piazza, G.J., & Foglia, T.A. One-pot synthesis of fatty acid epoxides from triacylglycerols using enzymes present in oat seeds, *J. Am. Oil Chem. Soc.* **83**, 1021-1025, 2006.
67. Hilker, I., et al. Chemo-enzymatic epoxidation of unsaturated plant oils, *Chemical Engineering Science*, 16th International Conference on Chemical Reactor Engineering, **56**, 2001, 427-432.
68. Ting, R.Y. *Epoxy Resins Chemistry and Technology*, 2nd ed., C.A. May et al. eds., Marcel Dekker Inc., New York, 1988, 551-601.
69. Potter, W.G. *Epoxide Resins*, Springer-Verlag, New York, 1970.
70. Newley, H.A. and Shokal, E.C. *Glycidyl ether compositions and method of using same*, **US Patent No. 2575558** (to Shell Oil Co.), November 20, 1951.
71. Paul, S. *Surface Coatings*, 2nd ed., John Wiley & Sons, Chichester, England, 1997, 261-262.
72. Abdullah, B.M., & Salimon, J. Epoxidation of vegetable oils and fatty acids: Catalysts, methods and advantages, *J. Appl. Sci.* **10**, 1545-1553, 2010.
73. Milchert, E. et al. Optimization of the epoxidation of rapeseed oil with peracetic acid, *Org. Process Res. Dev.* **14**, 1094–1101, 2010
74. Mika, T.F. & Bauer, R.S. Curing Agents and Modifiers, in *Epoxy Resins Chemistry and Technology*, 2nd ed., C.A. May ed., Marcel Dekker Inc., New York, 1988, 465.
75. Tanaka, Y. & Bauer, R.S. Curing Reactions, Synthesis and Characteristics of Epoxides, in *Epoxy Resins: Chemistry and Technology*, C.A. May ed., Marcel Dekker Inc., New York, 1988.
76. Lee, H. & Neville, K. *Epoxy Resins Their Applications and Technology*, McGraw-Hill Book Company Inc., New York, 1967.
77. Ashcroft, W.R. Curing Agents for Epoxy Resins, in *Chemistry and Technology of Epoxy Resins*, 1st ed., B. Ellis ed., Chapman & Hall, New York, 1993, 37-71.
78. Shechter, L., et al. Glycidyl ether reactions with amines, *Ind. Eng. Chem.* **48**, 94–97, 1956.

79. Potter, W.G. *Epoxide Resins*, Springer-Verlag, New York, 1970.
80. Shechter, L., & Wynstra, J. Glycidyl ether reactions with alcohols, phenols, carboxylic acids, and acid anhydrides, *Ind. Eng. Chem.* **48**, 86–93, 1956.
81. Beyer, G. Nanocomposites: A new class of flame retardants for polymers, *Plast. Addit. Compd.* **4**, 22–7, 2002.
82. McNally, T., et al. Polyamide-12 layered silicate nanocomposites by melt blending, *Polymer* **44**, 2761–2772, 2003.
83. Jordan, J., Experimental trends in polymer nanocomposites-A review, *Mater. Sci. Eng. A* **393**, 1-11, 2005.
84. Lee, J.Y., & Lee, H.K. Characterization of organobentonite used for polymer nanocomposites, *Mater. Chem. Phys.* **85**, 410–415, 2004.
85. Patel, H.A., et al. Preparation and characterization of phosphonium montmorillonite with enhanced thermal stability, *Appl. Clay Sci.* **35**, 194–200, 2007.
86. Someya, Y., & Shibata, M. Morphology, thermal, and mechanical properties of vinyl ester resin nanocomposites with various organo-modified montmorillonites, *Polym. Eng. Sci.* **44**, 2041–2046, 2004.
87. Grobert, N. Carbon nanotubes-becoming clean, *Mater. Today* **10**, 28-35, 2007.
88. Spitalsky, Z., et al. Carbon nanotube-polymer composites: Chemistry, processing, mechanical and electrical properties, *Prog. Polym. Sci.* **35**, 357-401, 2010.
89. Tasis, D., et al. Chemistry of carbon nanotubes, *Chem. Rev.* **106**, 1105-1136, 2006.
90. Reinking, N.H. *Process for preparing glycidyl polyethers of polyhydric phenols*, **US Patent No. 2943095** (to Union Carbide Corp.), June 28, 1960
91. Wang, C.S., Pham, H.Q. and Bertram, J.L. *Preparation of epoxy resin*, **US Patent No. 4499255** (to the Dow Chemical Co.), February 12, 1985.
92. Kincl, J. and Ditrych, Z. *Epoxy resin esters*, **Czech Patent No. 101431**, October 15, 1961.
93. Blumstein, A. Study of the absorbed layered polymerizations I, *Bull. Chem. Soc. France* 899–906, 1961.
94. Blumstein, R., et al. Polymerisation of monomolecular layers adsorbed on montmorillonite: cyclization in polyacrylonitrile and polymethacrylonitrile, *Appl. Polym. Symp.* **25**, 81–88, 1974.
95. Ruiz-Hitzky, E., & Aranda, P. Polymer-salt intercalation complexes in layer silicates, *Adv. Mater.* **2**, 545–547, 1990.

96. Wu, J., & Lerner, M.M. Structural, thermal, and electrical characterization of layered nanocomposites derived from Na-montmorillonite and polyethers, *Chem. Mater.* **5**, 835–838, 1993.
97. Vaia, R.A., & Giannelis, E.P. Lattice model of polymer melt intercalation in organically-modified layered silicates, *Macromolecules* **30**, 7990-7999, 1997.
98. Giannelis, E.P. Polymer layered silicate nanocomposites, *Adv. Mater.* **8**, 29–35, 1996.
99. Fornes, T.D., et al. Nylon 6 nanocomposites: The effect of matrix molecular weight, *Polymer* **42**, 9929–40, 2001.
100. Lepoittevin, B. Polymer/layered silicate nanocomposites by combined intercalative polymerization and melt intercalation: A masterbatch process, *Polymer* **44**, 2033-2040, 2003.
101. Carrado, K.A. Synthetic organo and polymer–clays: preparation, characterization, and materials applications, *Appl. Clay Sci.* **17**, 1-23, 2000.
102. Oil and Colour Chemist's Association of Australia, *Surface Coatings*, Vol. 1, Chapman and Hall, London, 1981.
103. Jahn, H. & Goetzky, P. *Epoxy Resins Chemistry and Technology*, C.A. May et al. eds., 2nd ed., Marcel Dekker Inc., New York, 1988, 1049-1087.
104. Annual Book ASTM Standard Section 8 (Plastics), Web site: <http://www.astm.org>.
105. Silverstein, R.M., Bassler, G.C. & Morrill, T.C. *Spectroscopic Identification of Organic Compounds*, 5th ed., John Wiley & Sons, New York, 1991.
106. Kemp, W. *Organic Spectroscopy*, 3rd ed., ELBS, Hampshire, 1991.
107. Crompton, T.R. *Analysis of Polymers*, Pergamon Press, New York, 1989.
108. Hunt, B.J. & James, M.I. (eds.). *Polymer Characterization*, Blackie Academic & Professional, New York, 1993.
109. Ibbett, R.N. (ed.). *NMR Spectroscopy of Polymers*, Blackie Academic & Professional, New York, 1993.
110. Ray, S.S., & Okamoto, M. Polymer–layered silicate nanocomposite: A review from preparation to processing, *Prog. Polym. Sci.* **28**, 1539–641, 2003.
111. Vaia, R.A., et al. Microstructural evolution of melt intercalated polymer-organically modified layered silicates nanocomposites, *Chem. Mater.* **8**, 2628-2635, 1996.

112. Lincoln, D.M., et al. Isothermal crystallization of nylon-6/montmorillonite nanocomposites, *Macromolecules* **37**, 4554–61, 2004.
113. Hernandez, M., et al. The effect of dispersion state on PMMA/epoxy/clay ternary blends : In situ study and final morphologies, *Polymer* **48**, 2007, 4075-4086.
114. Lincoln, D.M., et al. Secondary structure and elevated temperature crystallite morphology of nylon-6/layered silicate nanocomposites, *Polymer* **42**, 1621–31, 2001.
115. Vaia, R.A., et al. Analysis of small-angle scattering of suspensions of organically modified montmorillonite: Implications to phase behavior of polymer nanocomposites, *J. Polym. Sci. Part B Polym. Phys.* **41**, 3214–36, 2003.
116. Justice, R.S., et al. Interface morphology and phase separation in polymer-dispersed liquid crystal composites, *Polymer* **46**, 4465–73. 2005.
117. Meyyappan, M. (ed.). *Carbon Nanotubes, Science and Application*, CRC Press, New York, USA, 2006.
118. Zanetti, M., et al. Polymer layered silicate nanocomposites, *Macromol. Mater. Eng.* **279**, 1-9, 2000.
119. vanderHart, D.L., et al. NMR measurements related to clay dispersion quality and organic-modifier stability in nylon 6/clay nanocomposites, *Macromolecules* **34**, 819– 22, 2001.
120. vanderHart, D.L., et al. Solid-state NMR investigation of paramagnetic nylon 6 clay nanocomposites. 2. Measurement of clay dispersion, crystal stratification, and stability of organic modifiers, *Chem. Mater.* **13**, 3796–809, 2001.
121. vanderHart, D.L., et al. Solid-state NMR investigation of paramagnetic nylon 6 clay nanocomposites. 1. Crystallinity, morphology, and the direct influence of Fe³⁺ on nuclear spins, *Chem. Mater.* **13**, 3781–95, 2001.
122. Merkel, T.C., et al. Investigation of enhanced free volume in nanosilica-filled poly(1-trimethylsilyl-1-propyne) by ¹²⁹Xe NMR spectroscopy, *Macromolecules* **36**, 353-358, 2003.
123. Loo, L.S., & Gleason, K.K. Fourier transforms infrared investigation of the deformation behavior of montmorillonite in nylon 6/nanoclay nanocomposite, *Macromolecules* **36**, 2587–90, 2003.
124. Wu, H.D. Chain conformation and crystallization behavior of the syndiotactic polystyrene nanocomposites studied using Fourier transform infrared analysis, *Macromolecules* **34**, 2992–9, 2001.

125. Liu, X., & Wu, Q. PP/clay nanocomposites prepared by grafting-melt intercalation, *Polymer* **42**, 10013-10019, 2001.
126. Crosby, A.J., & Lee, J.Y. Polymer nanocomposites: The "nano" effect on mechanical properties, *Polym. Rev.* **47**, 217-229, 2007.
127. Fornes, T.D., & Paul, D.R. Modelling properties of nylon 6/clay nanocomposites using composite theories, *Polymer* **44**, 4993-5013, 2003
128. LeBaron, P.C., et al. Polymer-layered silicate nanocomposites: An overview, *Appl. Clay.Sci.* **15**, 11-29, 1999.
129. Jia, Q.M., et al. The mechanical properties and tribological behavior of epoxy resin composites modified by different shape nanofillers, *Polym. Adv. Technol.* **17**,168-173, 2006.
130. Romo-uribe, A., et al. Microstructure and dynamic mechanical analysis of extruded layered silicate PVC nanocomposites, *Polym. Adv. Technol.* **19**, 1168-1176, 2008.
131. Michler, G.H. & Balta-Calleja, F.J. (eds.). *Mechanical Properties of Polymers Based on Nanostructure and Morphology*, CRC press, Boca Raton, 2005.
132. Cong, H., et al. Polymer-inorganic nanocomposite membranes for gas separation, *Sep. Purif. Technol.* **55**, 281-291, 2007.
133. Becker, O. Thermal stability and water uptake of high performance epoxy silicate nanocomposites, *Eur. Polym. J.* **40**, 187-195, 2004.
134. Mohan, T.P., et al. Rheology and curing characteristics of epoxy-clay nanocomposites, *Polym. Int.* **54**, 1653-1659, 2005.
135. Kaynak, C., et al. Mechanical properties, flammability and char morphology of epoxy resin/montmorillonite nanocomposites, *Appl. Clay Sci.* **46**, 319-324, 2009.
136. Kashiwagi, T., et al. Nanoparticle networks reduce the flammability of polymer nanocomposites, *Nature Mater.* **4**, 928-933, 2005.
137. Kashiwagi, T., et al. Flame retardant mechanism of polyamide 6-clay nanocomposites, *Polymer* **45**, 881-91, 2004.
138. Beecroft, L.L., & Ober, C.K. Nanocomposite materials for optical applications, *Chem. Mater.* **9**, 1302-1317, 1997.
139. Zou, H., et al. Polymer/silica nanocomposites: Preparation, characterization, properties and applications, *Chem. Rev.* **108**, 3893-3957, 2008.

140. Karak, N., et al. Catalytically active vegetable-oil-based thermoplastic hyperbranched polyurethane/silver nanocomposites, *Macromol. Mater. Eng.* **295**, 159-169, 2010.
141. Dubey, A., & Mishra, B.G. Selective liquid phase oxidation of aromatics over silica-polymer nanocomposite materials, *Catal. Commun.* **8**, 1507-1510, 2007.
142. Bordes, P., et al. Nano-biocomposites: Biodegradable polyester/nanoclay systems, *Prog. Polym. Sci.* **34**, 125-155, 2009.
143. Schmidt, D., et al. New advances in polymer/layered silicate nanocomposites, *Curr. Opin. Solid State Mater.* **6**, 205-12, 2002.
144. Kim, J.H., et al. Preparation and characterization of polypropylene/layered silicate nanocomposites using an antioxidant, *Polymer* **45**, 7719-27, 2004.
145. Zeng, Q.H., et al. Clay-based polymer nanocomposites: Research and commercial development, *J. Nanosci. Nanotechnol.* **5**, 1574-92, 2005.
146. Qureshi, S., et al. New polymers from botanical oils, *Org. Coat. Plast. Chem.* **45**, 649-653, 1981.
147. Barrett, L.W., et al. Naturally functionalized triglyceride oils in interpenetrating polymer networks, *J. Am. Oil Chem. Soc.*, **70**, 523-534, 1993.
148. Carlson, K.D., & Chang, S.P. Chemical epoxidation of a natural unsaturated epoxy seed oil from *Vernonia galamensis* and a look at epoxy oil markets, *J. Am. Oil Chem. Soc.* **62**, 934-939, 1985.
149. Carlson, K.D., Schneider, W.J., Chang, S.P. & Princen, L.H. New Sources of Fats and Oils, in *AOCS Monograph 9*, E.H. Pryde et al. eds., American Oil Chemists Society, Champaign, 1981, 297.
150. Samuelsson, J., et al. Synthesis and polymerization of a radiation curable hyperbranched resin based on epoxy functional fatty acids, *Prog. Org. Coat.* **50**, 193-198, 2004.
151. Koo, J., et al. Polymer nanostructured materials for high temperature applications, *SAMPE J.* **41**, 7-19, 2005.
152. Timmerman, J., et al. Nanoclay reinforcement effects on the cryogenic micro cracking of carbon fiber/epoxy composites, *Compos. Sci. Technol.* **62**, 1249-1258, 2002.
153. Ren, Y., et al. Fatigue behaviour of unidirectional single-walled carbon nanotube reinforced epoxy composite under tensile load, *Adv. Compos. Lett.* **12**, 19-24, 2003.

154. Gibson, T., Rice, B., & Ragland, W. Formulation and evaluation of carbon nanofiber based conductive adhesives, SAMPE, Longbeach, CA, 2005.
155. Chisholm, N., et al. Fabrication and mechanical characterization of carbon/SiC-epoxy nanocomposites, *Compos. Struct.* **67**, 115–124, 2005.
156. Lin, J.C., et al. Mechanical behavior of various nanoparticle filled composites at low-velocity impact, *Compos. Struct.* **74**, 30–60, 2006.
157. Tsujimoto, T., et al. Synthesis of high-performance green nanocomposites from renewable natural oils, *Polym. Degrad. Stab.* **95**, 1399-1405, 2010.
158. Ge, C.Y., et al. Synthesis of polyaniline nanofiber and anticorrosion property of polyaniline-epoxy composite coating for Q235 steel, *J. Coat. Technol. Res.* 2011, DOI 10.1007/s11998-010-9316-8.
159. Benfarhi, S., et al. Synthesis of clay nanocomposite materials by light-induced crosslinking polymerization, *Eur. Polym. J.* **40**, 493–501, 2004.
160. Hung, H.S., & Hsu, S.H. Biological performances of poly(ether)urethane-silver nanocomposites, *Nanotechnology* **18**, 475101 (pp. 9), 2007.
161. Chen, C.Z., & Cooper, S.L. Recent advances in antimicrobial dendrimers, *Adv. Mater.* **12**, 843–846, 2000.
162. Damm, C., et al. The antimicrobial efficacy of polyamide 6/silver-nano and microcomposites, *Mater. Chem. Phys.* **108**, 61–6, 2008.
163. Hule, R.A., & Pochan, D.J. Polymer nanocomposites for biomedical applications, *MRS Bull.* **32**, 354–8, 2007.
164. Zeng, Q.H., et al. Clay-based polymer nanocomposites: Research and commercial development, *J. Nanosci. Nanotechnol.* **5**, 1574-1592, 2005.
165. Baughman, R.H., et al. Carbon nanotubes-the route toward applications, *Science* **297**, 787–792, 2002.
166. Moniruzzaman, M., & Winey, K.I. Polymer Nanocomposites containing carbon nanotubes, *Macromolecules* **39**, 5194–205, 2006.
167. Tuncer, E., et al. Electrical properties of epoxy resin based nanocomposites, *Nanotechnology* **18**, 025703 (pp. 6), 2007.
168. Rajesh, et al. Recent progress in the development of nano-structured conducting polymer/nanocomposites for sensor applications, *Sens. Actuators B: Chem.* **136**, 275-286, 2009.
169. Burgess, J.G. The Development of a marine natural product-based antifouling paint, *Biofouling* **19**, 197-205, 2003.

170. Raman, N., et al. Synthesis and structural reactivity of inorganic-organic hybrid nanocomposites: A review, *J. Saudi Chem. Soc.* 2011, DOI: 10.1016/j.jscs.2011.01.012.
171. Kumar, A.P., et al. Nanoscale particles for polymer degradation and stabilization-Trends and future perspectives, *Prog. Polym. Sci.* **34**, 479-515, 2009.
172. Bringi, N.V. (ed.), *Non-traditional oil seeds and oils in India*, Oxford & IBH Publishing Co. Pvt. Ltd., New Delhi, 1987.
173. Konwar, U. *Development of Polyester Nanocomposites*, PhD Thesis, Tezpur University, India, 2011.
174. Swern, D. and Findley, T.W. *Epoxidized oil*, **US Patent No. 2569502**, October 02, 1951.
175. Biermann, U., et al. New syntheses with oils and fats as renewable raw materials for the chemical industry, *Angew. Chem. Int. Ed.* **39**, 2206–2224, 2000.
176. Puglisi, J.S. and Chaudhari, M.A. Epoxies (EP), in *Engineered Materials Handbook*, J.N. Epel et al. eds., OH ASM International, Material Park, USA, 1988, 240–1.
177. Crivello, J.V., et al. Fabrication and mechanical characterization of glass fiber reinforced UV-cured composites from epoxidized vegetable oils, *J. Appl. Polym. Sci.* **64**, 2073–87, 1997.
178. Kaplan, D.L. *Biopolymers from Renewable Resources*, Springer, Berlin, 1998, 267.
179. Goud, V.V., et al. Epoxidation of karanja (*Pongamia glabra*) oil by H₂O₂, *J. Am. Oil Chem. Soc.* **83**, 635–40, 2006.
180. Lu, H., et al., Enzymatic epoxidation of soybean oil methyl esters in the presence of free fatty acids, *Eur. J. Lipid Sci. Technol.* **112**, 1101–1105, 2010.
181. Goud, V.V., et al. Epoxidation of karanja (*Pongamia glabra*) oil catalyzed of acidic ion exchange ion exchange resin, *Eur. J. Lipid Sci. Technol.* **109**, 575–84, 2007.
182. Sperling, L.H., et al. Tough plastics and reinforced elastomers from renewable resource industrial oils. A short review, *Ing. Eng. Chem. Prod. Res.* **20**, 163–6, 1981.
183. Clayton, A.M. *Epoxy Resins: Chemistry and Technology*, CRC Press, Boca Raton, FL, 1988, 1–4.

184. Meyer, P.P., et al. Epoxidation of soybean oil and jatropha oil, *Thammasat Int. J. Sci. Technol.* **13**, 1–5, 2008.
185. Masters, J.E. *Dicarboxylic acid modified triglyceride oil-modified epoxide compositions*, **US Patent No. 3027340**, March 27, 1962
186. Pawel, G., et al. Epoxy resin modified with soybean oil containing cyclic carbonate groups, *J. Appl. Polym. Sci.* **102**, 2904–2914, 2006.
187. Goldblatt, L.A. and Lucien, L. *Epoxy esters containing tung oil fatty acids*, **US Patent No. 3079354**, February 26, 1963.
188. Khot, S.N., et al. Development and application of triglyceride-based polymers and composites, *J. Appl. Polym. Sci.* **82**, 703–23, 2001.
189. Gunstone, F. *Fatty acid & lipid chemistry*, Blackie Academic & Professional, New York, 1996.
190. Salunkhe, D.K. *World oil seeds: Chemistry, Technology and Utilization*, Van Nostrand Reinhold, New York, 1992.
191. Force, C.G. and Starr, F.S. *Vegetable oil adducts as emollients in skin and hair care products*, **US Patent No. 4740367**, April 26, 1988.
192. Trecker, D.J., Borden, G.W., and Smith, O.W. *Method for curing acrylated epoxidized soybean oil amine compositions*, **US Patent No. 3979270**, September 07, 1976.
193. Trecker, D.J., Borden, G.W., and Smith, O.W. *Acrylated epoxidized soybean oil amine compositions and method*, **US Patent No. 3931075**, January 06, 1976.
194. Dutta, N. *Development of Polyester Resins from Mesua ferrea L. Seed Oil*, PhD Thesis, Tezpur University, India, 2006.
195. Hayes, D.G. Enzyme-Catalyzed modification of oilseed materials to produce eco-friendly products. *J. Am. Oil Chem. Soc.* **81**, 1077-1103, 2004.
196. Dutta, S. *Development of Mesua ferrea L. Seed Oil Based Polyurethane Resins*, PhD Thesis, Tezpur University, India, 2009.
197. Chlebicki, J., & Matyschok, H. Synthesis and epoxidation of ethyl esters of unsaturated fatty acids and use of the products in the manufacture of surfactants, *Przemysl Chemiczny* **84**, 933–938, 2005.
198. Schwartz, N.N., & Blumbergs, J.H. Epoxidations with m-chloroperbenzoic acid *J. Org. Chem.* **29**, 1976–1979, 1964.

199. Petrovic, Z.S., et al. Epoxidation of soybean oil in toluene with peroxyacetic and peroxyformic acid—kinetics and side reactions, *Eur. J. Lipid Sci. Technol.* **104**, 293–299, 2002.
200. Mungroo, R. Epoxidation of canola oil with hydrogen peroxide catalyzed by acidic ion exchange resin, *J. Am. Chem. Soc.* **85**, 887–896, 2008.
201. Hilker, I., et al. Chemo-enzymatic epoxidation of unsaturated plant oils, *Chem. Eng. Sci.*, **56**, 427–432, 2001.
202. Cai, C.S., et al. Studies on the kinetics of in situ epoxidation of vegetable oils, *Eur. J. Lipid Sci. Technol.* **110**, 341–346, 2008.
203. Klass, M., & Warwel, S. Complete and partial epoxidation of plant oils by lipase-catalyzed perhydrolysis, *Ind. Crops Prod.* **9**, 125–132, 1999.
204. Gerhard, K. & Johannes, T.P.D. *Recent developments in the synthesis of fatty acid derivatives*, AOCS Press, USA, 1999, 157.
205. Gurbanov, M.S., & Mamedov, B.A. Epoxidation of flax oil with hydrogen peroxide in a conjugate system in the presence of acetic acid and chlorinated cation exchanger KU-2x8 as catalyst, *Russ. J. Appl. Chem.* **82**, 1483–1487, 2009.
206. Sinadinovic, F.S., et al. Kinetics of in situ epoxidation of soybean oil in bulk catalyzed by ion exchange resin, *J. Am. Oil Chem. Soc.* **78**, 725–731, 2001.
207. Sobczak, J.M., & Ziolkowski, J.J. Molybdenum complex-catalyzed epoxidation of unsaturated fatty acids by organic hydroperoxides, *Appl. Cat. A: Gen.* **248**, 261–268, 2003.
208. Maiti, S.K., et al. Selective epoxidation of olefins catalyzed by oxidiperoxomolybdenum (VI) complexes immobilized over highly ordered 2D-hexagonal mesoporous silica, *J. Mol. Catal. A Chem.* **287**, 135–141, 2008.
209. Mohamed, T.B., et al. Kinetics of tungsten-catalyzed sunflower oil epoxidation studied by ¹H NMR, *Eur. J. Lipid Sci. Technol.* **109**, 1186–1193, 2007.
210. Kockritz, A., et al. Epoxidation of methyl oleate with molecular oxygen in the presence of aldehydes, *Eur. J. Lipid Sci. Technol.* **110**, 581–586, 2008.
211. Guenter, S., Rieth, R. & Rowbottom, K.T. *Ullmanns Encyclopedia of Industrial Chemistry*, 6th ed., Wiley-VCH, Weinheim, 2003, 269–284.
212. Ursula, B., et al. New syntheses with oils and fats as renewable raw materials for the chemical industry, *Angew. Chem. Int. Ed.* **39**, 2206–2224, 2000.
213. Miyagawa, H., et al. Biobased epoxy/clay nanocomposites as a new matrix for CFRP, *Compos. Part A* **37**, 54–62, 2006.

214. Mohamed, A.S., et al. Synthesis and characterization of bismaleimide-modified, soy-based epoxy matrices for flame-retardant application, *High Perform. Polym.* **22**, 328–344, 2010.
215. Bo, L., et al. Kinetic studies on oxirane cleavage of epoxidized soybean oil by methanol and characterization of polyols, *J. Am. Oil Chem. Soc.* **85**, 113–117, 2008.
216. Jue, L., & Wool, R.P. Additive toughening effects on new bio-based thermosetting resins from plant oils, *Compos. Sci. Technol.* **68**, 1025–1033, 2008.
217. Ortiz, R.A., et al. A Kinetic study of the acceleration effect of substituted benzyl alcohols on the cationic photopolymerization rate of epoxidized natural oils, *Polymer* **46**, 1535–1541, 2005.
218. Gerbase, A.E., et al. Epoxidation of soybean oil by the methyltrioxorhenium-CH₂-Cl₂-H₂O₂ catalytic biphasic system, *J. Am. Oil Chem. Soc.* **79**, 179–181, 2002.
219. Czub, P. Synthesis of high-molecular-weight epoxy resins from modified natural oils and bisphenol A or bisphenol A-based epoxy resins, *Polym. Adv. Technol.* **20**, 194–208, 2009.
220. Pan, X., et al. High biobased content epoxy-anhydride thermosets from epoxidized sucrose esters of fatty acids, *Biomacromolecules* **12**, 2416–28, 2011.
221. Chandrashekhara, K., et al. Affordable composites using renewable materials, *Mater. Sci. Eng. A* **412**, 2–6, 2005.
222. Cheong, M.Y., et al. Synthesis and characterization of palm-based resin for UV coating, *J. Appl. Polym. Sci.* **111**, 2353–2361, 2009.
223. Gunstone, F.D. & Fred, B.P. *Lipid Technologies and Applications*, CRC Press, Boca Raton, FL, 1997, 765.
224. Ratna, D., & Banthia, A.K. Rubber toughened epoxy, *Macromol. Res.* **12**, 11–21, 2004.
225. Gerbase, A.E., et al. Dynamic mechanical and thermal behavior of epoxy resins based on soybean oil, *J. Am. Oil Chem. Soc.* **79**, 797–802, 2002.
226. Jin, F.L., & Park, S.J. Thermal and rheological properties of vegetable oil-based epoxy resins cured with thermally latent initiator, *J. Ind. Eng. Chem.* **13**, 808–814, 2007.
227. Park, S.J., et al. Synthesis and thermal properties of epoxidized vegetable oil, *Macromol. Rapid Commun.* **25**, 724–727, 2004.

228. Lligadas, G., et al. Synthesis and properties of thermosetting polymers from a phosphorus-containing fatty acid derivative, *J. Polym. Sci. Part A: Polym. Chem.* **44**, 5630-5644, 2006.
229. Greenlee, S.O. *Tall-oil esters*, **US Patent No. 2493486**, January 03, 1950.
230. Castan, P. and Gandillon, C. *Process for the manufacture of synthetic resins obtained by condensation and esterification*, **US Patent No. 3028348**, April 03, 1962.
231. Narracott, E.S. *Epoxy resin esterified with drying oil fatty acids and phosphoric acid*, **US Patent No. 2709690**, May 31, 1955.
232. Riccio, M., et al. An IR study of the chemistry of triethoxysilane at the surface of metal oxides, *Colloids Surf. A* **294**, 181-190, 2007.
233. Miyagawa, H., et al. Nanocomposites from biobased epoxy and single-wall carbon nanotubes: synthesis, and mechanical and thermophysical properties evaluation, *Nanotechnology* **16**, 118 (pp.7), 2005.
234. Belgacem, M.N. & Gandini, A. (eds.). *Monomers, polymers and composites from renewable resources*, Elsevier, Amsterdam (The Netherlands), 2008.
235. Williams, C.K., & Hillmeyer, M.A. Polymers from renewable resources: A perspective for a special issue of polymer reviews, *Polym. Rev.* **48**, 1-10, 2008.
236. Gandini, A. Polymers from renewable resources: A challenge for the future of macromolecular materials, *Macromolecules* **41**, 9491-9504, 2008.
237. Ragauskas, A.J., et al. The path forward for biofuels and biomaterials, *Science* **27**, 484-489, 2006.
238. Clark, J.H., et al. Green chemistry and the biorefinery: A partnership for a sustainable future, *Green Chem.* **8**, 853-860, 2006.
239. Guner, F.S., et al. Polymers from triglyceride oils, *Prog. Polym. Sci.* **31**, 633-670, 2006.
240. Sharma, V., & Kundu, P.P. Addition polymers from natural oils. A review, *Prog. Polym. Sci.* **31**, 983-1008, 2006.
241. Sharma, V., & Kundu, P.P. Condensation polymers from natural oils, *Prog. Polym. Sci.* **33**, 1199-1215, 2008.

CHAPTER 2

Synthesis and Characterization of *Mesua ferrea* L. seed oil based Epoxy resin and Epoxidized oil

2.1. Introduction

From the discussion in the first chapter, it is cleared that the utilization of renewable resources in energy and material applications is receiving increasing attentions in both industrial and academic settings, due to concerns regarding environmental sustainability.^{1,2} Nowadays, most of the commercially available polymers are derived from non-renewable resources and account worldwide for approximately 7% of all oil and gas used.² With the continuous depletion of fossil oils, dramatic fluctuations in the price of oil and worldwide environmental concerns, there is an urgent need to develop polymeric materials from renewable resources.³ Renewable resources can provide an interesting sustainable platform to substitute partially, and to some extent totally, petroleum based polymers through the design of biobased polymers that can compete or even surpass the existing petroleum based materials on a cost-performance basis with high eco-friendliness values.^{4,5} In non-food applications, the most widely applied renewable resources include vegetable oils, polysaccharides (mainly cellulose and starch), and proteins.⁶ Vegetable oils are now being considered as the most important renewable raw materials for the production of biobased polymeric materials.⁷ Among the diverse types of such natural resources, vegetable oils represent one of the most environmentally benign and abundant renewable feed stocks and thereby expected to be an alternative feasible raw material for production of important industrial products including polymers.⁸ The products obtained from vegetable oils play significant roles for many industrial applications such as surface coatings, paints, varnishes, printing inks, soaps, shoe polishes, cosmetics, pharmaceuticals, multipurpose additives etc.

Since from the previous chapter it is cleared that *Mesua ferrea* L. seed oil has the potential to be used as raw material for preparation of various industrial resins⁹⁻¹² so in the present investigation this oil will be utilized. The plant oil is available in different countries especially in India. The seeds contain remarkably large amount of oil (75%). The oil comprises of oleic (52.3%) and linoleic (22.3%) acids as unsaturated,

and palmitic (15.9%) and stearic acids (9.5%) as saturated fatty acids.⁹ This fatty acid composition indicates its potentiality as feedstock in the development of different types of industrially important polymers. This has already been proved by the preparation of various types of polymers like polyester, polyurethane, poly(ester amide), etc. from the same laboratory.¹⁰⁻¹² Among the various industrial resins, epoxy resins have many advantages over other industrially used resins for different applications. A number of both traditional and non-traditional vegetable oils are being utilized for the preparation of epoxy resins.¹³⁻¹⁵

Different bisphenols based epoxides are utilized for many applications due to the versatility imparted by the strained oxirane ring.¹⁶⁻¹⁸ Epoxides can be crosslinked via homopolymerization or reaction with crosslinking agents. A large number of backbone structures can be incorporated into the epoxy oligomer and a variety of crosslinking reagents can be used to cure these resins. However, the most of the bisphenol based epoxides are brittle in nature and are non-biodegradable. In such research various diepoxide has been prepared using bisphenol-A (BPA), bisphenol-S (BPS), tetrabromobisphenol-A (TBPA) or combination thereof with epichlorohydrin. The bisphenol-A based epoxy resin is characterized by its outstanding performance characteristics such as rigidity, adhesive strength and elevated temperature performance. The ether linkages and aromatic moiety provides good chemical resistance, the hydroxyl and epoxy groups impart high adhesive strength and reactivity with a wide variety of chemical curing agents.¹⁹ On the other hand epoxy resin based on bisphenol-S has the advantage of resistance to deformation by heat and thermal stability. Such improved epoxy resins from bisphenol-S have other advantages like short gel periods, rapid development of mechanical properties on curing, good resistance to organic solvents attack, high dimensional stability and good wetting characteristics.²⁰ The diglycidyl ether of TBPA (ca 50 wt% Br) is used for critical electrical/electronic encapsulation where flame retardancy is required. Brominated epoxies are also used to produce epoxy vinyl esters for structural applications. The high molecular weight brominated epoxies are used as flame-retardant additives to engineering thermoplastics for computer housing application too.²¹ Monoglyceride of the different vegetable oils may also be used as one of the versatile diols for epoxy resins as it has already been widely used for the preparation of various other resins viz. polyester, polyurethane etc. The presence of monoglyceride in the structure of epoxide will not only impart flexibility but also biodegradability. Hence in the present

investigation emphasis is given to derive biobased diglycidyl epoxy resins, using above aromatic and *Mesua ferrea* L. seed oil based diols. Further, as epoxidized vegetable oil have also captured a significant place as industrial products for various applications^{2,4} so epoxidized *Mesua ferrea* L. seed oil is also prepared in the present investigation. The prepared resins will be characterized by analytical techniques such as epoxy equivalent, hydroxyl value, saponification value etc. and spectroscopic techniques like FTIR, ¹H NMR, ¹³C NMR etc.

2.2. Experimental

2.2.1. Materials

The *Mesua ferrea* L. seed oil used in the present investigation was extracted from the matured seeds, which were collected from Jamugurihat, Assam, India. The seeds were obtained from the plant, which is a medium size tree with a conical crown and is about 3 to 15 m in height. It is found in different countries like India, Sri Lanka, Nepal, Bangladesh, Indochina (South-East Asia), Malay Peninsula etc. In India²²⁻²⁴ it is mainly found in North-East region, West Bengal, Karnataka, Kerala etc. The oil is brownish color viscous liquid with a characteristic odor. The flower blossoms between April and July, and fruits between October and November. The average yield of seeds per tree is around 10-15 kg per annum. The oil content in the seeds is about 70-75%. The availability of the seeds in India per year is 5,690 tonnes.²⁵ In this study solvent soaking technique using petroleum ether (Merck, India) as the solvent was employed to extract oil from the dried powdered seeds. The oil was purified by degumming it with water followed by alkali refining technique using 0.01% aqueous NaOH solution, and then washed with distilled water followed by drying under vacuum.²⁶⁻²⁷

Glycerol was obtained from Merck, India with density 1.26 g/mL, maximum sulphated ash 0.005% and minimum assay 99%. Other impurities present are glycerol tributyrate 0.05%, chloride 0.0001%, sulphate 0.0005% and heavy metals 0.0002%. Glycerol is used as a prochiral building block in organic synthesis (Fig. 2.1). It is generally used in the production of hydrogen gas, citric acid, propylene glycol, acrolein, ethanol, epichlorohydrin etc. It is also used in pharmaceutical and medical sectors. In the present investigation, it was used as a triol (alcoholizing reagent) for converting triglyceride ester of *Mesua ferrea* L. seed oil into monoglyceride. It was used after drying under vacuum.

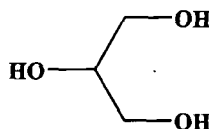


Fig. 2.1: Structure of glycerol

Lead mono-oxide (PbO) was obtained from Loba Chemie, India with minimum assay 99%, and maximum limit of impurities contain chloride 0.02%, copper 0.005% and iron 0.01%. It is generally used in lead paints, lead-acid batteries, vulcanization of rubber and as catalysts in many organic condensation reactions. Herein, it was used as a catalyst for trans-esterification reaction of triglyceride with glycerol. It was utilized as received.

4,4'-Isopropylidene diphenol, bisphenol-A (BPA) (Fig. 2.2.) was obtained from Burgoyne India, Mumbai. It was recrystallized from toluene before used. The melting point (m.p.) of the purified compound is 157 °C and molecular weight is (M_w) 228.29 g/mol.

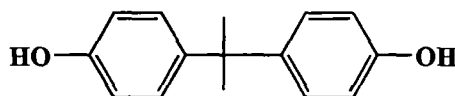


Fig. 2.2: Structure of bisphenol-A

BPA is mainly used in the synthesis of epoxy resins and polycarbonates. Due to the non-toxic nature of BPA, these plastics are used in packaging applications for many foods and drinks items. While the resins are commonly used as lacquers to coat metal products such as food 'can', bottle tops and water supply. Some polymers used in dental treatment contain BPA. Here it is used as an aromatic diol.

4,4'-Isopropylidene bis(2,6-dibromophenol) (tetrabromobisphenol-A, TBPA) (Fig. 2.3.) was collected from Aldrich Chemie, Germany. The compound has melting point of (m.p.) 178 °C, purity 97% and molecular weight (M_w) 543.9 g/mol. It was used as received. TBPA is commercially available both as an epoxy resin grade and a high quality polycarbonate grade compound. The primary use of TBPA is as a reactive flame retardant in epoxy resin based circuit boards and in electronic enclosures made of polycarbonate-acrylonitrile butadiene-styrene (PC-ABS).

Other applications of TBPA includes its use as a flame retardant additive for plastics paper and textiles, as a plasticizer in coating and as chemical intermediates for

the synthesis other flame retardants (e.g. TBPA-allyl ether). Here it is used as a bromine-containing aromatic diol.

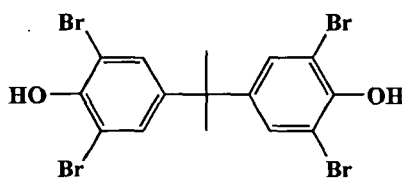


Fig. 2.3: Structure of tetrabromobisphenol-A

4,4'-sulfonyl diphenol, (bisphenol-S) (BPS) (Fig. 2.4.) was obtained from Aldrich Chemie, Germany. The compound has melting point (m.p.) 245 °C, purity 98% and molecular weight (M_w) 250.27 g/mol. It was used as received. This compound is generally used in preparation of thermostable epoxy resin as an aromatic diol. Here also it is used as a thermostable aromatic diol.

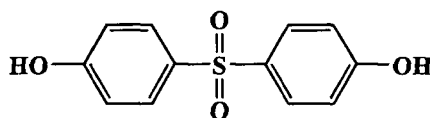


Fig. 2.4: Structure of bisphenol-S

Molecular sieve 4A x 1.5 mm has procured from Merck, Mumbai. Its equilibrium capacity for water at 30 °C, 75% relative air humidity is $\geq 20\%$ and bulk density is 650-700 g/cm³. It was used as received.

Epichlorohydrin (Fig. 2.5.) was obtained from Across, it has a molecular weight of 92.52 g/mol with density of 1.18 g/cm³ and a boiling point of 115 °C. Epichlorohydrin is mainly used to prepare diglycidyl ether of bisphenol-A, a building block in the manufacture of epoxy resins. It is also a precursor to monomer for other resins and polymers. Epichlorohydrin is also used in paper reinforcement (used for instance in the food industry to manufacture tea bags, coffee filters, and sausage/salami casings) and water purification. Here it is used as a reactant for epoxy resin synthesis.

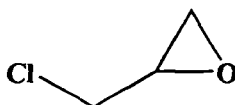


Fig. 2.5: Structure of epichlorohydrin

Tetrahydrofuran GR was obtained from Merck, India. It has a boiling point of 65-67 °C, density 0.886-0.88 g/cm³, minimum purity 99.5% and maximum limit of impurities contain Cu 0.0001%, Fe 0.0001%, Pb 0.0001% and non-volatiles substances 0.002%. Another main application of THF is as an industrial solvent for PVC and

in varnishes.⁶ It is an aprotic solvent with a dielectric constant of 7.6. It is a moderately polar solvent and can dissolve a wide range of non-polar and polar compounds. THF is water miscible, and can form solid clathrate hydrate structures with water at low temperature. Here it is used as a solvent

Glacial acetic acid was obtained from Merck, India with a molecular weight of 60.05 g and density of 1.048-1.051 g/cm³. It has a boiling point of 118-119 °C with maximum purity of 99% and maximum limit of impurities of chloride 0.0005% and Pb 0.0005%. Acetic acid is a reagent used for the production of other compounds. The largest single use of acetic acid is in the production of vinyl acetate monomer, closely followed by acetic anhydride and ester production. It is widely used in the industry as acid catalysts for the synthesis epoxy resin. Here it is used as a weak acid for the generation of peracid.

Hydrogen peroxide was purchased from Ranbaxy fine Chemicals Ltd. New Delhi, India. It was obtained as 50% solution (w/v) with a density of 1.10 g/cm³ and a boiling point of 150 °C. It has a assay of 50% and maximum limits of impurities of H₂SO₄ 0.2%, Fe 0.0001%, Pb 0.001 and Cu 0.00001. It is most widely used in the pulp and paper industry as bleaching agent. Other bleaching applications are becoming more important as hydrogen peroxide is seen as an environmentally benign alternative to chlorine-based bleaches. Hydrogen peroxide is also used in the oil and gas exploration industry to oxidize rock matrix in preparation for micro-fossil analysis. It has also been used to synthesize propylene oxide and is an environmentally benign process. Hydrogen peroxide has also played important roles as a signaling molecule in the regulation of a variety of biological processes. It also plays an important role in aging and cancer. Here it is used as a oxidizing agent which helps generation of peracid.

Sodium sulfate (anhydrous) was obtained from Merck India, it has a molecular weight of 142.04 g/mol and density of 2.664 g/cm³. It has a minimum assay of 99.5% and other impurities present are free acid (H₂SO₄) 0.005%, free alkali (as NaOH) 0.004%, chloride 0.001%, phosphate 0.002%, ammonium 0.0005%, arsenic 0.00004%, calcium 0.01%, copper 0.0005%, Fe 0.0005%, Pb 0.01%, Mg 0.01% and K 0.01%. Sodium sulfate is a very cheap compound. The largest use is as filler in powdered home laundry detergents. The glass industry provides another significant application for sodium sulfate, as second largest application in Europe. Sodium sulfate is used as a fining agent, to help remove small air bubbles from molten glass. It fluxes the glass,

and prevents scum formation of the glass melt during refining. In the laboratory, anhydrous sodium sulfate is widely used as an inert drying agent, for removing traces of water from organic solutions. It is more efficient, but slower-acting drying agent, than the similar agent magnesium sulfate. It is only effective below about 30 °C, but it can be used with a variety of compounds since it is chemically fairly inert.

Sodium chloride crystals was obtained from Merck, India, it has a molecular weight of 58.44 g/mol. It has a minimum assay of 99.5% with a density of 2.16 g/cm³, boiling point of 1413 °C and melting point of 801 °C. It has maximum impurities of bromide 0.005%, iodide 0.001%, sulfate 0.002% phosphate 0.0005%, Pb 0.0005%, iron 0.0001%, Mg 0.001% and Ca 0.002%. Sodium chloride is sometimes used as a cheap and safe desiccant because of its hygroscopic properties, making salting an effective method of food preservation historically; the salt draws water out of bacteria through osmotic pressure, keeping it from reproducing, a major source of food spoilage. The industrial uses of salt include, in descending order of quantity consumed, various applications, oil and gas exploration, textiles and dyeing, pulp and paper, metal processing, tanning and leather treatment, and rubber manufacture. Here it is used as a desiccant.

Sodium hydroxide (NaOH) was obtained from Merck, Mumbai and was used as received. It has molecular weight (M_w) 40.0 g/mol and purity > 97%.

Hydrochloric acid was obtained from Merck, Mumbai and was used as received. It has formula weight (F_w) 36.46 g/mol, purity \geq 35% and density at 20 °C of 1.16-1.18 g/cm³.

Bisphenol-A based epoxy resin (Araldite LY 250) and poly(amido amine) hardener (HY 840) were obtained from Hindustan Ciba Geigy Ltd. and used as received. The specifications of epoxy resin and hardener are given in Table 2.1.

Table 2.1: Technical specifications of epoxy resin and hardener

Name	Araldite LY 250 (Ciba Geigy)	Hardener HY 840 (Ciba Geigy)
Viscosity at 25 °C (mPas)	450-650	10000-25000
Epoxy equivalent (g/eq)	182-192	–
Epoxy content (eq/kg)	5.2-5.5	–
Amine value (eq/kg)	–	6.6-7.5
Density at 25 °C (g/cm ³)	1.15	0.98

2.2.2. Instruments and Methods

FTIR spectra of the epoxidized oil and epoxy resins were recorded in a FTIR spectrophotometer (Impact-410, Nicolet, USA) using KBr pellet. ^1H NMR spectra were recorded in a Varian 400 MHz NMR spectrometer (Shimadzu, Japan) using CDCl_3 and or deuterated dimethylsulphoxide (d_6 -DMSO) as the solvents and tetramethylsilane (TMS) as the internal standard.

The different physical properties such as acid value, saponification value, iodine value, hydroxyl value, drying time etc. of the epoxidized oil and epoxy resins were determined by the standard methods.^{28,29}

The rheological study of the epoxidized oil and epoxy resins were measured by Rheometer of Model CVO100 (Malvern, UK) with a parallel plate geometry (plate diameter = 20 mm). The relationships between viscosity and time at constant stress (100 Pa) and single shear, viscosity against shear stress (50-200 Pa) and viscosity versus temperature (25-100 °C) at constant stress of 20 Pa were determined from this study. The coating performance of the cured films was evaluated by the determination of various mechanical properties. The mechanical properties such as tensile strength and elongation at break were measured with the help of Universal Testing Machine, UTM (Zwick, Z010, Germany) with a 10 kN load cell and crosshead speed of 6 mm/s (ASTM D 412-51 T). Impact resistance was determined by falling weight impact tester (S.C. Dey Co., Kolkata) as per the standard falling weight (ball) method (ASTM D 1037). In this test a weight of 850 g was allowed to fall on the film coated on a mild steel plate from minimum to maximum falling heights. The maximum height was taken as the impact resistance up to which the film was not damaged. Gloss characteristic of the cured films was evaluated²⁸ using a glossmeter (Minigloss meter, Sheen, UK) over cured resin coated on mild steel plates at an angle of incidence of 60°. Scratch hardness (ASTM D5178/1991) of the cured films was measured by using scratch tester, Model no. 705, (Sheen Instrument Ltd., UK) with stylus accessory and a travel speed of 6 mm/s. The chemical resistance tests were performed in a number of different chemical media as per the ASTM D 543-67 standard procedure²⁹ by taking weighted amount of cured epoxy resin films in 250 mL beakers containing 150 mL of the individual chemical medium for specified periods. The chemical resistance was determined by making observations of visual changes in the films after the specified time.

The flame retardancy test of all the thermosets were carried out by measuring limiting oxygen index (LOI) value by a flammability tester (S.C. Dey Co., Kolkata) as

per the standard ASTM D 2863-77 procedure for self supported samples and also by UL 94 test method. In UL 94 method, samples were cut into 5" × 0.5" × 0.037" and then they were mounted vertically in such a way so that the gap between surgical cotton placed directly below the specimen is 12". Flame was introduced for 10 s to the specimen at an angle of 45°. A total of 5 tests were done for each specimen.

Swelling test was done by immersing weighted amount of the cured films in THF. After 48 h, the weight of the swelled films was taken. Swelling value (%) was determined by differences in weight between the dried film and the swelled film as follows: Swelling (%) = $[(W_s - W_d)/W_d] \times 100$ where, W_s and W_d are the weight of the swelled film and the dried film respectively.

The adhesive strength of the cured thin films was measured by lap-shear test as per the standard ASTM D3165-95 using plywood, aluminum (Al), and polypropylene sheets as the substrates. The plywood substrates were first washed with acetone to remove dirt and subsequently polished with sand paper of grit number 60 (250 mm) according to ASTM 906. The clean Al sheets were treated with hydrochloric acid (5% w/v) and then washed with distilled water and dried.

2.2.2.1. Synthesis of Epoxidized Oil and Epoxy Resin

Epoxidation of Mesua ferrea L. seed Oil

The purified oil was epoxidized by using *in-situ* peracid method.^{30,31} 40 g of the oil was taken in a three necked round bottom flask equipped with a mechanical stirrer and a thermometer. To the oil, 4.4 g of CH_3COOH and a required amount of H_2SO_4 (2% of the H_2O_2 - CH_3COOH mixture) were added and stirred for 30 min, then 13.4 g of 50% aqueous H_2O_2 was added for about half an hour. The reaction was then continued with constant stirring for 8 h. The temperature was maintained at 55-60 °C. The resulted product was washed with water until it was free from acid. Then the product was dried under vacuum to a constant weight. This product was coded as ENO.

Preparation of Monoglyceride of the Oil

A three-neck round bottom flask equipped with a mechanical stirrer, a thermometer, a nitrogen gas inlet and a dropping funnel, was flushed with nitrogen and charged with 34.73 g (0.04 mol) of *Mesua ferrea L.* seed oil, 7.36 g (0.08 mol) of glycerol and 0.017 g (0.05 wt% with respect to the oil) of lead mono-oxide under continuous stirring. The mixture was then heated upto (225±5) °C and continues until the monoglyceride was

formed. This was confirmed by checking its solubility in methanol (monoglyceride: methanol = 1:3 v/v) at ambient temperature.

Monoglyceride Based Epoxy Resin (MGE)

8 g (0.0230 mol) of monoglyceride and 8.51 g (0.092 mol) of epichlorohydrin were taken in a three necked round bottom flask fitted with a thermometer pocket, a condenser and a nitrogen inlet. The mixture was mixed together and refluxed for 1 h. The reaction temperature was maintained at that temperature, (115 ± 5) °C and to this reaction mixture 2.76 g of NaOH in the form of 30% aqueous solution was added at slow rate such that it was completed within 1 h. The reaction was then continued for about 14 h. After this period of time the reaction, the product was separated by a separating funnel, washed with brine solution and followed by distilled water. Then the content was vacuum dried to obtain the product with 80-90% yield.

Monoglyceride and Bisphenol-A based Epoxy Resin (BP AE)

Similar resinification reaction was carried out with required amount of BPA along with monoglyceride by maintaining the mole ratio the reactants at 75:25, while the mole ratio of epichlorohydrin with respect to total diol has been kept same as above. The reaction was carried out for 14 h keeping all others conditions same as mentioned above.

Flame Retardant Epoxy Resin (TBPAE)

A flame retardant epoxy resin was prepared from monoglyceride of the oil, BPA and TBPA with epichlorohydrin. Similar resinification reaction was carried out with required amount of BPA, TBPA along with monoglyceride by maintaining the mole ratio of these reactants at 50:25:25, with epichlorohydrin mol ratio kept as same as above. All others conditions remain the same, as above.

Synthesis of Bisphenol-S Epoxy Resin (BPSE)

The bisphenol-S based epoxy resin was prepared by using the similar method as described above. Monoglyceride of the oil (obtained by glycerolysis technique), epichlorohydrin, BPA and BPS were treated together by maintaining the mol ratio of 1:8:2:1 at (110 ± 5) °C for 8 h in alkaline medium same as above. After the completion of the reaction the product was separated in a separating funnel, washed with brine solution and distilled water. Then the product was vacuum dried. The yield of the product was 80-90%.

Another *Mesua ferrea* L. seed oil modified sulfone epoxy resin was prepared by similar method at molar ratio of 1:5:2:1 at (110±5) °C for 14 h in alkaline medium same as above. The purified and dried product was coded as MBPSE.

2.2.2.2. Curing of the Resins

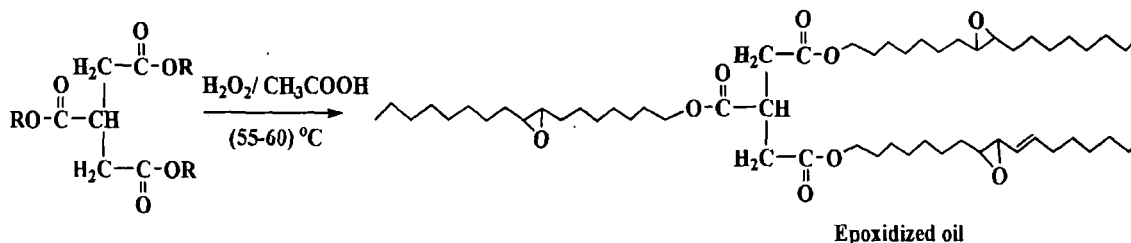
A homogenous mixture of each resin system with 50 phr (parts per hundred grams of resin) of poly(amido amine) hardener was prepared in a glass beaker at room temperature by constant stirring for 10-20 min. The thin film of the mixtures were casted on a glass plate, degassed for 15 min under vacuum and then heated at 100 °C in a muffle furnace to determine the touch free time (minimum time, when no impression will appear on touching the film) and hard dry time of the resin. The mixtures were also uniformly casted on mild steel plates (150 mm × 50 mm × 1.60 mm), tin plates (150 mm × 50 mm × 0.40 mm) and glass plates (75 mm × 25 mm × 1.75 mm) for impact resistance, gloss and chemical resistance tests.

2.3. Results and Discussion

2.3.1. Epoxidation

The epoxidation of the oil (*Mesua ferrea* L.) was directly carried out by *in-situ* epoxidation reaction using hydrogen peroxide with acetic acid at about (55-60) °C for a specified period of time in a single step process without using any solvent (Scheme 2.1.). As it is a bulk reaction so it avoids the limitations associated with solvents like removal, health hazards, flammability, etc. The hydroxylation reaction of the epoxy group occurs with the increase of reaction time but less than 8 h reaction is not possible to obtain desired product, so the reaction was carried up to 8 h for this study. In the epoxy synthesis from olefins, increased electron density in the double bond due to electron donating substituents increases the reactivity of the vinyl group with peroxy acids. While the activity of many peracids has been investigated, peracetic acid is commonly used in industry, as in the production of cycloaliphatic epoxy resins. The course of reaction is accelerated by strong mineral acids, most often by sulfuric acid.^{31,32} The selection of the process parameters, so that the epoxidation will proceed faster than the formation of peracid, is an important issue. Otherwise, generated peracid may decompose ineffectively under the reaction conditions, and the yield of epoxidation recalculated on the consumed hydrogen peroxide will be small.^{33,34} The reaction environment contains water, mineral (catalyst), and organic acids, which may

cause the decomposition of the epoxy groups due to the hydrolysis or acylation.^{33,35} This decreases the yield of epoxidized oil. However with proper control of parameters the resin was formed with reasonable time with relatively good yield (80-90%).



R is the hydrocarbon part of the fatty acids viz. oleic, linoleic, palmitic and stearic acids

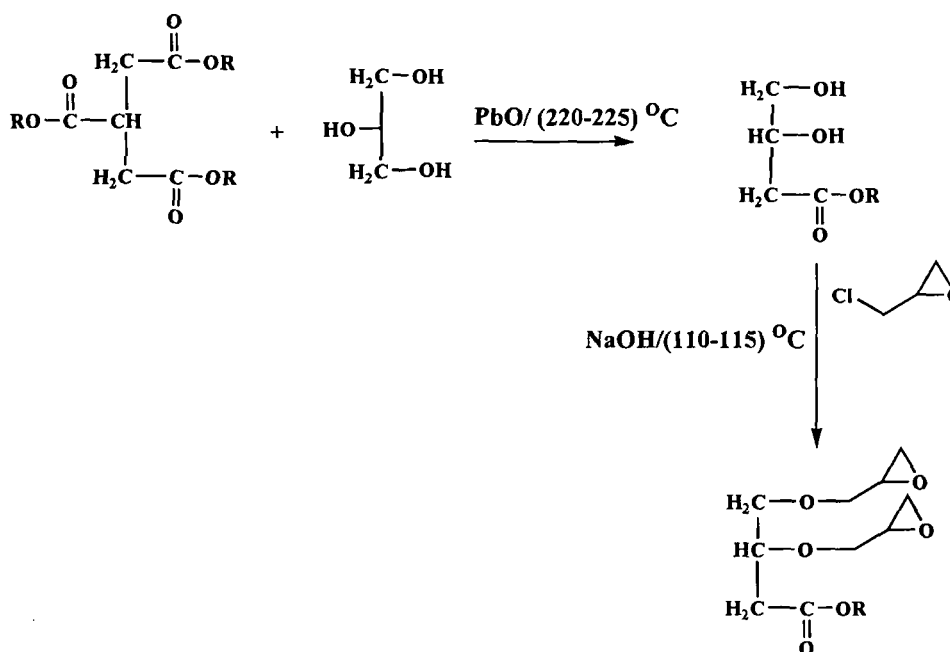
Scheme 2.1: Epoxidation of *Mesua ferrea* L. seed oil (ENO)

2.3.2. Resinification of Monoglyceride Based Epoxy Resin

Synthesis of epoxy resin from the monoglyceride of *Mesua ferrea* L. seeds oil has been carried out by using monoglyceride of the oil as one of the components to utilize a low cost product to a value added industrial resin. Three epoxy resins of the oil were prepared by condensation reaction of diol like monoglyceride (Scheme 2.2), combination of monoglyceride and bisphenol-A (Scheme 2.3), combination of monoglyceride, bisphenol-A and tetrabromobisphenol-A with epichlorohydrin (Scheme 2.4) and combination of monoglyceride, bisphenol-A and bisphenol-S with epichlorohydrin, separately (Scheme 2.5). The addition of aqueous NaOH was done in such a manner that the color of phenolphthalein should not vanishes otherwise undesirable products were formed.³⁶ In this process, the phenolate anion opens the oxirane ring of the halohydrin through a nucleophilic substitution reaction. Then subsequent intramolecular chloride elimination regenerates an oxirane ring. The substitution occurs most readily at the least substituted carbon, which is consistent with the SN² mechanism. Addition at the more substituted carbon or incomplete chloride elimination leads to the epoxy resin with unsubstituted chlorine, typically at a concentration of less than 1%.³⁷ More stable 'bound' chlorine results when the phenolate reacts at the more substituted epoxy containing ring carbon or when the secondary hydroxyl group of the intermediate reacts with epichlorohydrin.

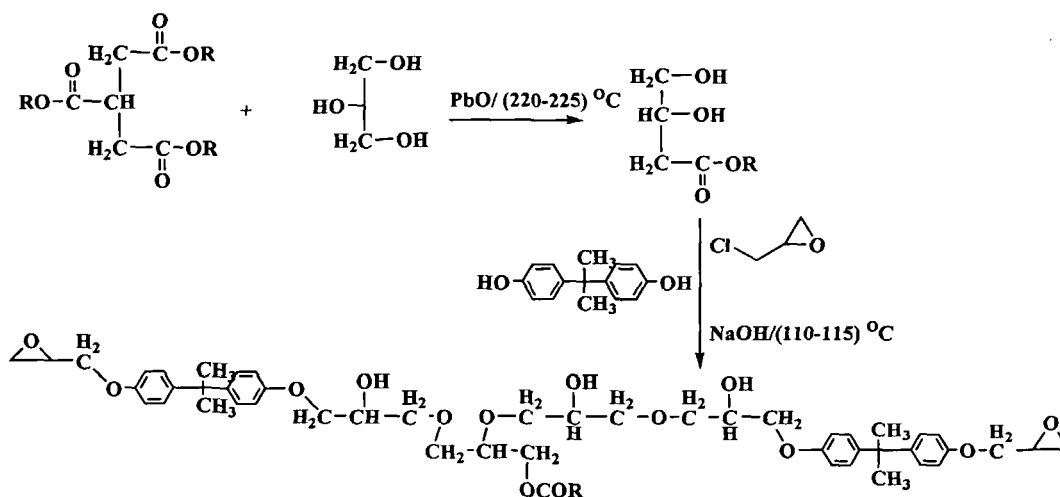
When reaction occurs at the more substituted carbon, the 1,3-chlorohydrin is formed and cannot undergo ring closure, resulting in chloromethyl groups. 'Hydrolyzable' is observed chlorine at reaction sites where the intermediate does not undergo the final chloride elimination step. The enhanced hydroxylation reaction of the

epoxy group with the increase of the reaction time from the optimum was observed, so the reactions should not be performed for over time (>14 h). It was also observed that with the increase of the reaction time the viscosity of the resin increase, so the reactions were not carried out for less than 14 h. By using this time period adequate viscosity with good epoxy equivalent of the resins was found.



R is the hydrocarbon part of the fatty acids viz. oleic, linoleic, stearic and palmitic acids

Scheme 2.2: Synthesis of MGE resin

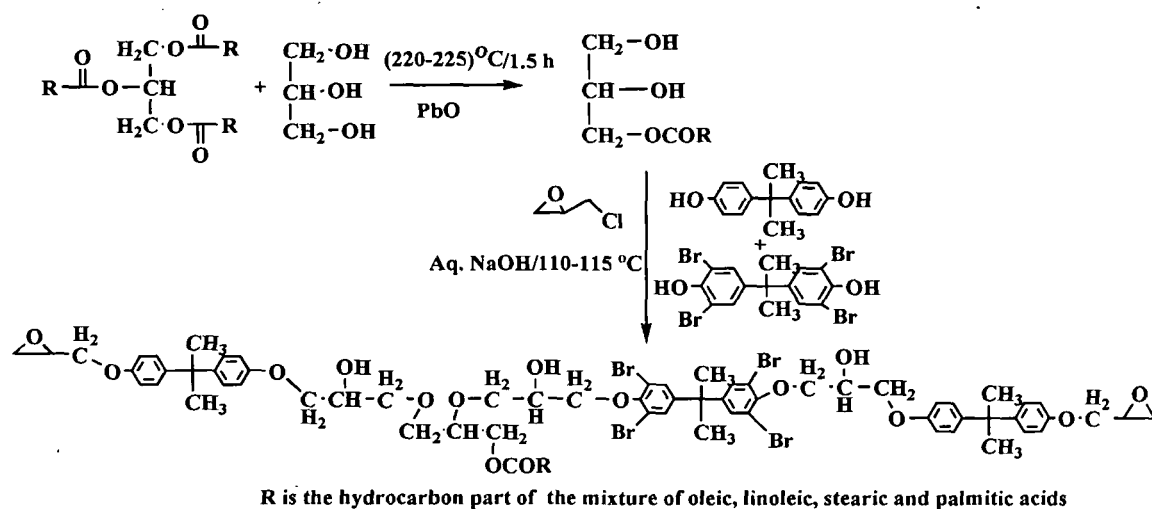


R is the hydrocarbon part of the fatty acids viz. oleic, linoleic, stearic and palmitic acids

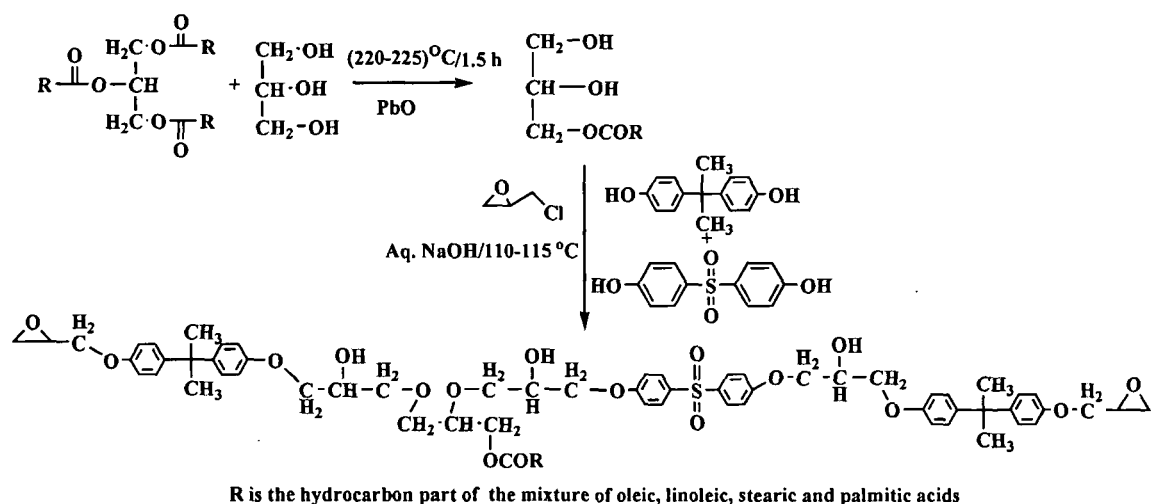
Scheme 2.3: Synthesis of BPAE resin

The excess of epichlorohydrin is used to minimize the degree of chain extension that occurs during epoxidation. Thus the resins were obtained with relatively good yield

(80-90%) under the used reaction conditions. No noticeable difference was observed during resinification reaction compared to the conventional BPA based epoxy resin due



Scheme 2.4: Synthesis of TBPAE resin



Scheme 2.5: Synthesis of sulfone epoxy resin (BPSE)

to the use of monoglyceride.

Most of the epoxy resins even though exhibit good performance characteristics, yet they suffer from the serious drawback of brittleness. This limits their uses in many advanced applications. The presence of sulfone group may impart thermal stability along with strength properties.^{38,39} In the present investigation monoglyceride of *Mesua ferrea* L. seeds oil has been utilized as one of the components to reduce the brittleness of the resin along with improved flexibility and toughness, good thermal stability of the synthesized resin is projected as the outcome because of inherent characteristics of the used components (such as monoglyceride of the oil and bisphenol-S). The reaction was

carried out for 8 h to acquire good epoxy equivalent with minimum hydroxylation. The basic catalyst (NaOH) neutralizes HCl and thereby accelerates conversion of the reaction. The synthesized resin is also expected to exhibit low viscosity. Further the resin was obtained with relatively good yield (80-90%) under the used reaction conditions.

2.3.3. Characterization of the Epoxy Resins

2.3.3.1. Physical Properties

The physical properties like acid value, saponification value, iodine value, hydroxyl value, and epoxy equivalent of the epoxidized oil are given in Table 2.2. From this table it can be observed that the iodine value decreases with epoxidation of the oil though the saponification and hydroxyl values increase with the same. The results indicate that the some amounts of unsaturation are utilized for oxirane ring formation which increases the molecular weight as indicated by the increase in saponification value. High hydroxyl value results from the slight hydrolysis of the oxirane ring during the resinification reaction. ENO was soluble was soluble in solvents like THF, ethyl acetate, diethyl ether, xylene, acetone etc.

Table 2.2: Physical property of oil and ENO

Property	Pure oil	ENO
Acid value(mg KOH/g)	14	12.46
Iodine value(g I ₂ /100 g)	89.28	35.59
Saponification value(mg KOH/g)	260	279.99
Hydroxyl value (mg KOH/g)	220	287.35
Epoxy Equivalent (g/eq. epoxy group)	-	500
Viscosity (Pas)	-	2.04

The physical properties like acid value, saponification value, hydroxyl value, and epoxy equivalent of the TBPAE, MGE, BPAE and BPSE resins are given in Table 2.3. TBPAE has the lowest epoxy equivalent value, whereas MGE has the highest. The saponification value decreases with the decrease in the amount of monoglyceride content in the resins (Table 2.3) as it is the only component containing ester linkage. TBPAE has the lowest epoxy equivalent value, whereas MGE has the highest. The results are again due to the variation of monoglyceride content. As the monoglyceride

may also contain some other components like triglyceride, diglyceride, etc. so the presence of epoxy groups is less in the structure (Table 2.3). The synthesized resins

Table 2.3: Physical property of epoxy resins

Property	TBPAE	BPAE	MGE	BPSE	MBPSE
Acid value (mg KOH/g)	20	18	15	12.46	15.23
Saponification value (mg KOH/g)	220	240	268	257	265
Hydroxyl value (mg KOH/g)	242	254	266	235	265
Epoxy Equivalent (g/eq. epoxy group)	225	463	784	387	462
Specific gravity @ 25 °C	1.4	0.85	0.8125	0.8701	0.89

were soluble in solvents like DMF, DMSO, THF, xylene, acetone etc.

2.3.3.2. FTIR and ¹H NMR Spectroscopic Studies

The FTIR spectrum of ENO shows band at 906 cm⁻¹ (Fig. 2.6) which was not observed for the oil.^{13,15} The other important characteristic bands (cm⁻¹) at 3466-3675, 2852–2923, 1747, 1163-1164 and 1617-1619 for -OH, aliphatic -C-H, -C=O of triglyceride esters, C-O-C of ester and C=C stretching vibrations respectively were also observed in FTIR spectrum for ENO before curing. The FTIR spectra of TBPAE, BPAE and MGE are presented in Figs. 2.7-2.9. The bands for asymmetric vibrations for epoxy ring

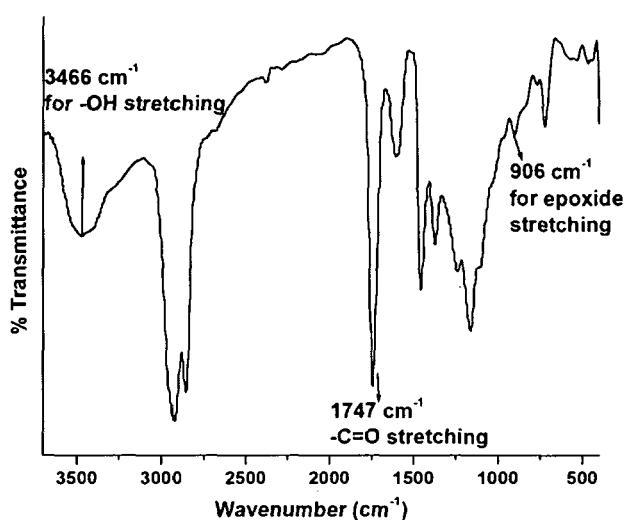


Fig. 2.6: FTIR spectrum of ENO

appeared at 912-834 cm⁻¹ for TBPAE, 928-832 cm⁻¹ for BPAE and 926-831 cm⁻¹ for MGE.^{17,19,21} The appearance of sharp bands at 740 cm⁻¹ and 660 cm⁻¹ indicates the

stretching vibrations of C-Br at the aromatic ring for TBPAE.²¹ The presence of a strong absorption band at 1038 cm^{-1} for TBPAE and 1042 cm^{-1} for BPAE confirmed the presence of alkyl-aryl ether group in the molecule. Similarly, strong absorption at

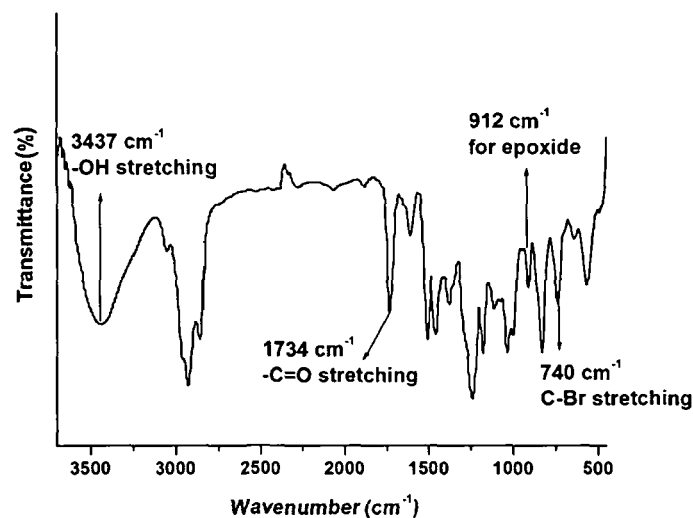


Fig. 2.7: FTIR spectrum of TBPAE

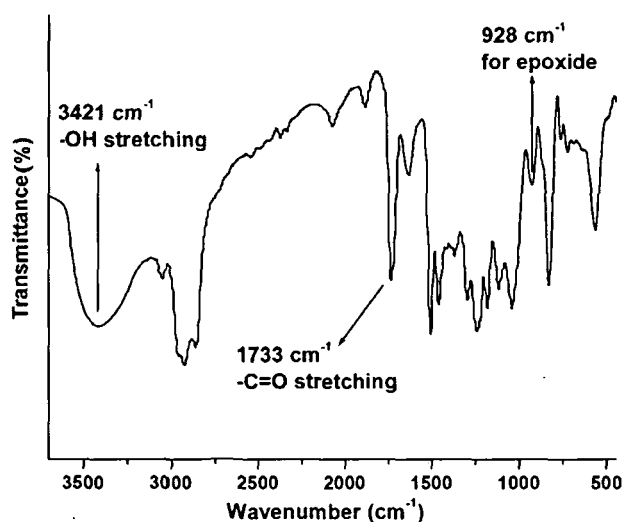


Fig. 2.8: FTIR spectrum of BPAE

1242 cm^{-1} for TBPAE and 1243 cm^{-1} for BPAE confirmed the presence of aryl ether linkage in the structure of the resins.¹⁶ The C=C stretching vibrations for TBPAE, BPAE and MGE were observed at around $1609\text{--}1458\text{ cm}^{-1}$, $1609\text{--}1461\text{ cm}^{-1}$ and $1607\text{--}1457\text{ cm}^{-1}$ respectively. Bands at 1734 cm^{-1} for TBPAE, 1733 cm^{-1} for BPAE and 1730 cm^{-1} for MGE in the spectra were observed due to the -C=O stretching vibrations of triglyceride esters in the resins. The presence of bands at 3437 cm^{-1} , 3421 cm^{-1} and 3415 cm^{-1} for TBPAE, BPAE and MGE respectively, are due to the O-H stretching vibrations.^{17,19,21}

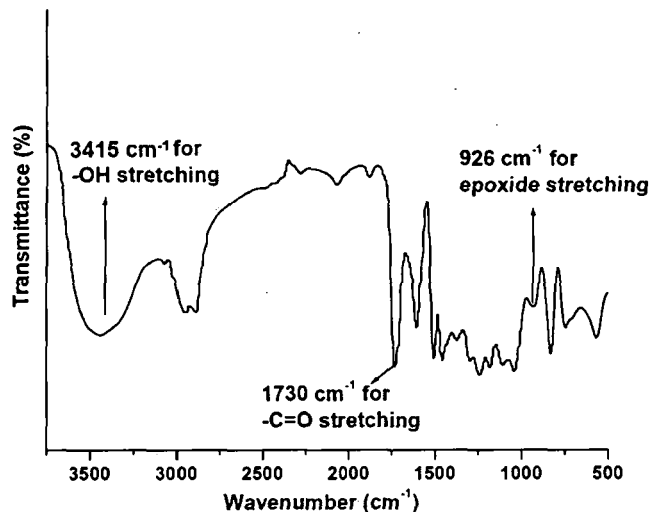


Fig. 2.9: FTIR spectrum of MGE

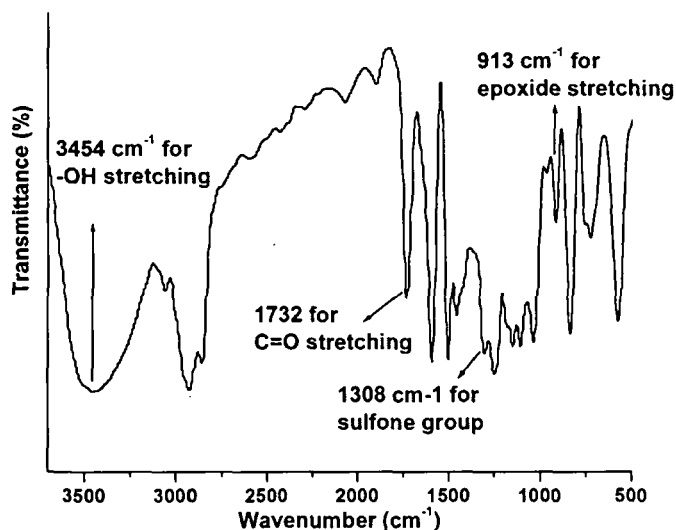


Fig. 2.10: FTIR spectrum of BPSE

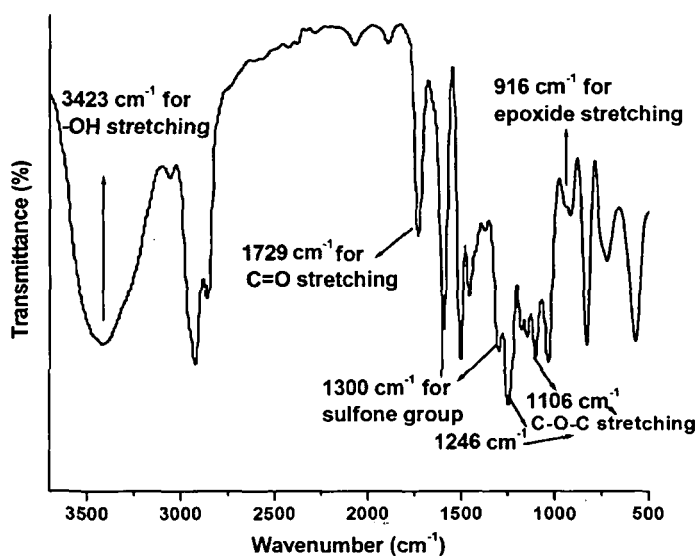


Fig. 2.11: FTIR spectrum of MBPSE

The FTIR spectra of BPSE and MBPSE exhibits oxirane ring stretching vibrations around 913 cm^{-1} and 916 cm^{-1} (Figs. 2.10-2.11). Notably, the two absorption bands around 1305 cm^{-1} , 1300 cm^{-1} and 1148 , 1149 cm^{-1} were observed in the spectra of BPSE and MBPSE due to the asymmetric structure of sulfone group, respectively.²⁰ The bands around 3065 , 3059 and 1454 , 1456 cm^{-1} indicated the presence of aromatic ring.²⁰ The other important characteristic bands (cm^{-1}) at 3454 , 3423 (-OH), 2866 – 2934 , 2868 - 2932 (-C-H), 1732 , 1729 (-C=O), 1249 , 1246 (aromatic ether), 1113 , 1106 (C-O-C of ester) and 1610 , 1605 (C=C) were observed in FTIR spectrum of BPSE and MBPSE respectively.

The $^1\text{H-NMR}$ spectra of TBPAE, BPAE and MGE are shown in the Figs. 2.12-2.14. Chemical shifts values observed at $\delta = 2.7$ - 2.9 ppm, 2.7 - 2.8 ppm and 2.5 ppm were due to the epoxy proton for TBPAE, BPAE and MGE, respectively.^{20,21} In the desired resins the shift values at $\delta = 7.0$ ppm and 6.80 ppm for TBPAE and 6.8 ppm and 7.1 ppm BPAE are due to the presence of two types of proton in the bisphenol-A ring. The higher value is due to ortho proton to isopropylidene and lower value is due to ortho proton to ether linkage in both the cases. But it was seen that the peak values were absent in MGE which suggested the presence of bisphenol-A moiety in both TBPAE and BPAE. The CH_2 protons attached with ether linkages of aliphatic and aromatic unit in the resins were observed at $\delta = 3.3$ - 3.38 , 3.34 , 3.5 - 3.7 ppm and $\delta = 3.5$ - 3.6 and 3.7 - 3.8 ppm for TBPAE, BPAE and MGE respectively.^{20,21} All the protons of monoglyceride were also observed in the $^1\text{H-NMR}$ spectra. The peaks at $\delta = 0.85$ – 0.88 ppm are for terminal methyl group of the fatty acids chains. The peaks at $\delta = 1.25$ – 1.30 ppm are for the protons of all the internal CH_2 groups present in the fatty acids chains.

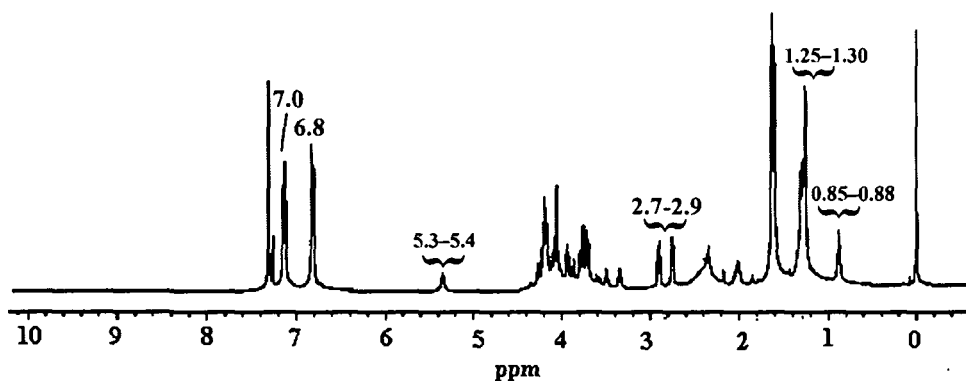


Fig. 2.12: $^1\text{H-NMR}$ spectrum of TBPAE

The peaks for protons of unsaturated moiety appear at $\delta = 5.3$ – 5.4 ppm. The $-\text{CH}_2$

protons attached with the double bonds are found at $\delta = 1.6-1.62$ ppm, whereas the protons for $-\text{CH}_2$ attached with ester groups were observed at $\delta = 4.0-4.3$ ppm.^{10,12}

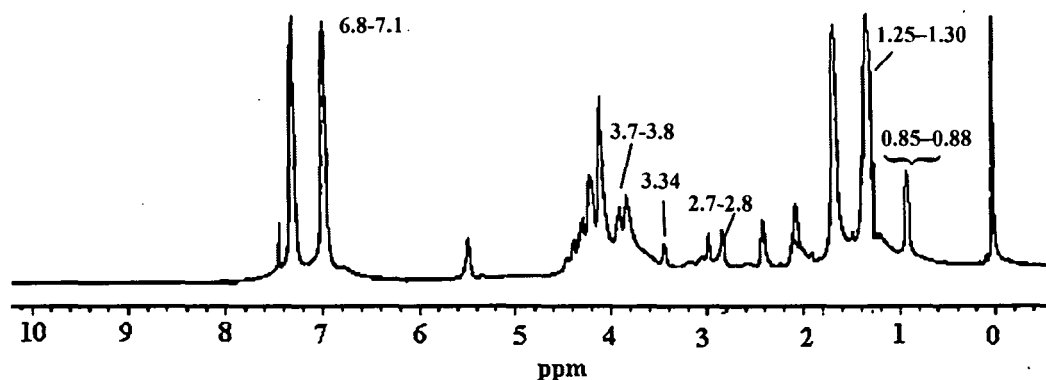


Fig. 2.13: ¹H NMR spectrum of BPAE

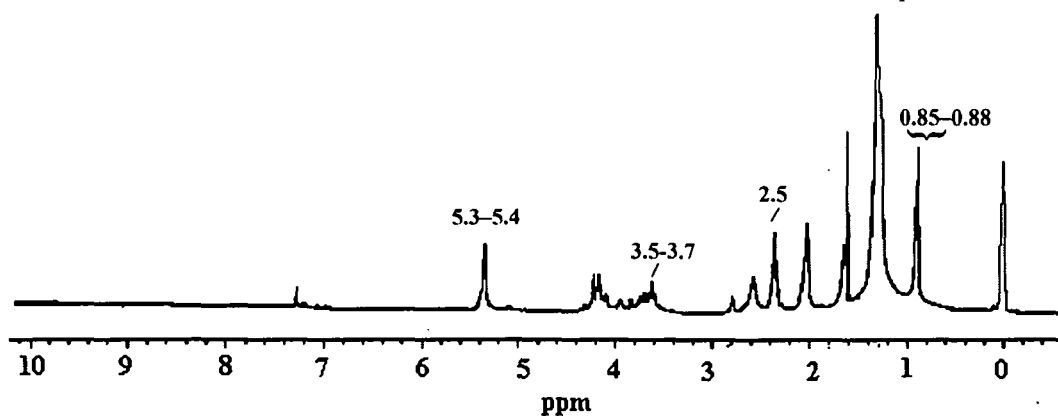


Fig. 2.14: ¹H NMR spectrum of MGE

The proton NMR spectrum of BPSE is shown in Fig. 2.15. The shift values as shown in the figure are: $\delta = 2.7-2.9$ ppm (for epoxy group proton), $\delta = 6.9$ ppm and 7.8

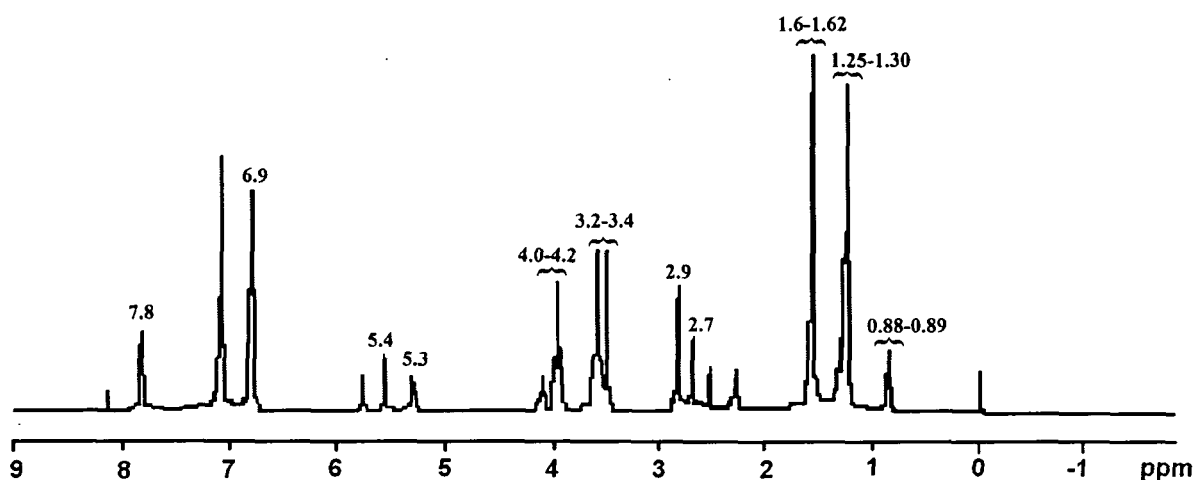


Fig. 2.15: ¹H NMR spectrum of BPSE

ppm (for aromatic protons), $\delta = 3.2$ and $\delta = 3.4$ ($-\text{CH}_2$ protons for ether linkages of aliphatic and aromatic unit).^{18,20} All the protons of monoglyceride were also observed in the ^1H NMR spectra, $\delta = 0.88\text{--}0.89$ ppm (terminal $-\text{CH}_2$ protons), $\delta = 1.25\text{--}1.30$ ppm (internal $-\text{CH}_2$ protons), $\delta = 5.3\text{--}5.4$ ppm (unsaturated moiety), $\delta = 1.6\text{--}1.62$ ppm ($-\text{CH}_2$ protons attached to double bond) and $\delta = 4.0\text{--}4.2$ ppm (protons of $-\text{CH}_2$ attached to ester groups).¹²

2.3.4. Rheological Behaviors

The rheological characteristics such as variation of viscosity against shear stress, temperature at constant stress and time of the resins were studied. Under a constant shear stress of 100 Pa, the viscosities remained almost constant; this indicates that all the resins exhibited Newtonian like behavior (Figs. 2.16-2.17). The average viscosity

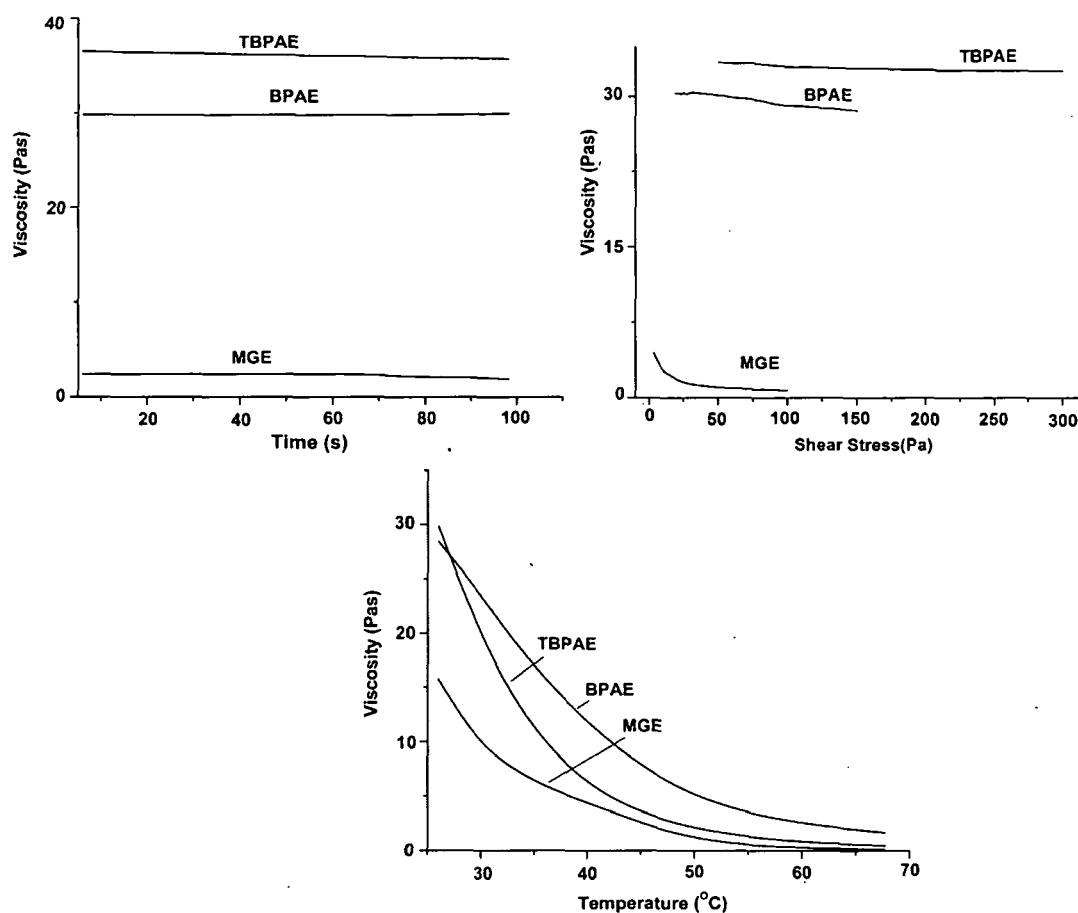


Fig. 2.16: Variation of viscosity against (a) time, (b) shear stress, and (c) temperature for MGE, TBPAE and BPAE

values are given in Table 2.4. MBPSE showed the highest viscosity, whereas MGE has the lowest value. This difference may result from the increase of the number of epoxy group, which may form hydrogen bonding. The viscosity decreased when a temperature

gradient was applied. This decrease may be due to the increase in the molecular mobility of the chains as kinetic energy of the system increases.

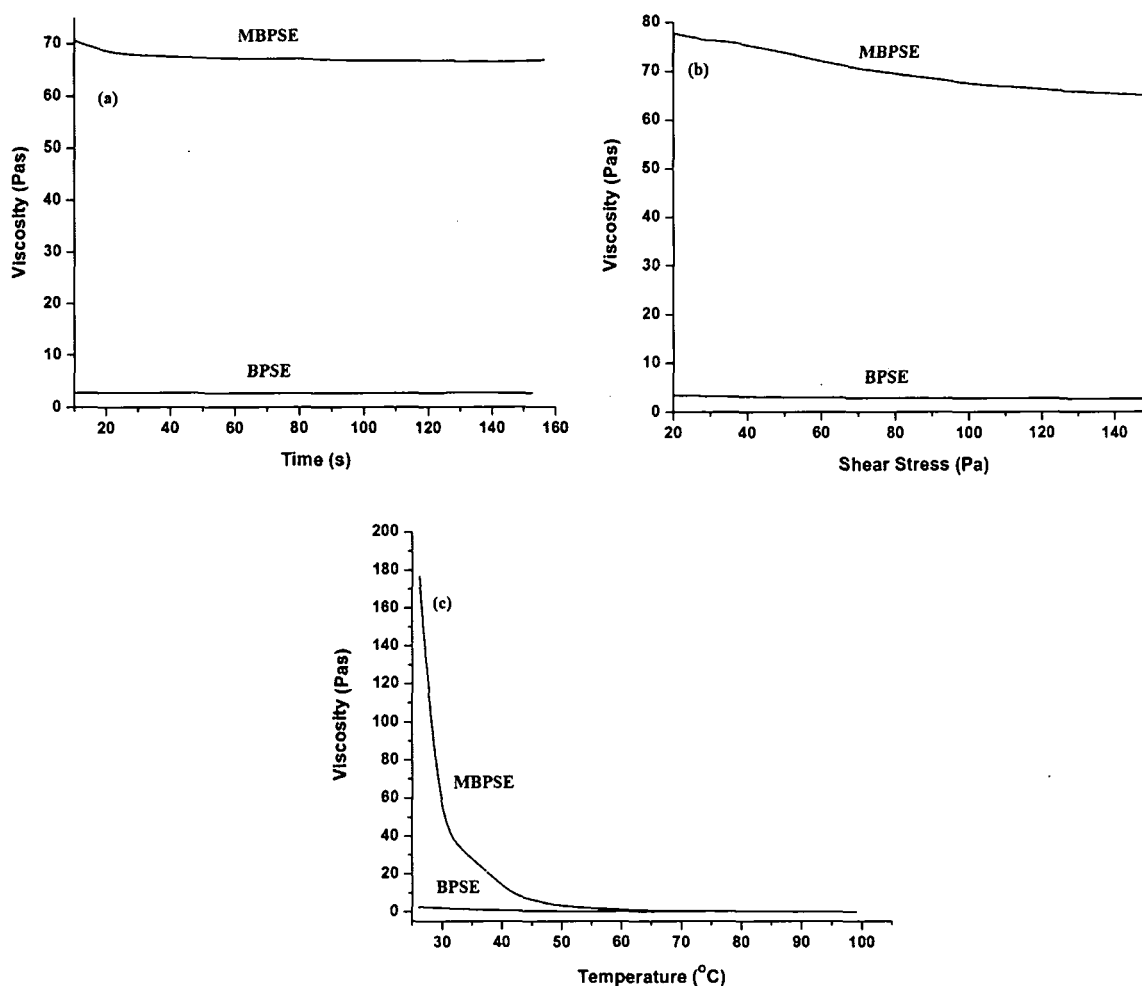


Fig. 2.17: Variation of viscosity against (a) time, (b) shear stress, and (c) temperature for BPSE and MBPSE

2.3.5. Curing Study for Epoxy Resins

In the drying process, the liquid resins are converted to solid form by chemical crosslinking reaction with hardener. The epoxy group (oxirane ring) of the resins is highly strain and is readily open up in the presence of active or labile atom like proton of amine or phenol/thiol. The hardener, poly(amido amine) contains labile amino protons which can readily react with epoxy groups under heat to form crosslinked three dimensional network structures. As in all the above resin systems, the amount of hardener and temperature are the same, so the rate of crosslinking or drying is dependent on the reactivity and amount of epoxy groups present in the resin. As the epoxy-amine curing is a nucleophilic addition reaction, the presence of any group which affect the electron density of the epoxide will accelerate the curing

process.^{27,28} Consequently, the presence of electron withdrawing group affects the epoxide group reactivity and accelerates the curing process. TBPAE required the lowest curing time, while MGE took the highest time for cure (Table 2.4). For TBPAE more number of epoxy groups (lowest epoxy equivalent, Table 2.4) took part in the curing reaction, also the reactivity of epoxy groups is the highest due to the presence of electronegative bromine atom in the structure, hence crosslinking reaction accelerated in this case. Similarly, for BPSE and MBPSE the presence of sulfonyl group enhanced the curing rate.⁴⁰ On the other hand, MGE exhibited the slowest cure rate, which can be attributed to the lowest amount of functionality (highest epoxy equivalent, Table 2.4) and also the epoxy groups are less reactive as they are not freely accessible because of the long hydrocarbon chains that are entangled and hence epoxy groups at interior are not taking part in for crosslinking reaction.

Table 2.4: *Drying time and viscosity of epoxy resins*

Sample code	Touch free time (min)	Hard dry time (min)	Viscosity (Pas)
BPSE	35	60	3
TBPAE	30	60	36.08
BPAAE	60	120	27.33
MGE	840	300	2.12
MBPSE	50	83	67.2

2.3.6. Performance Characteristics

The performance characteristics such as impact resistance, scratch resistance, gloss, tensile strength and adhesive strength values of the cured resins are tabulated in Table 2.5. From this table it has been found that with the increase of the epoxy content in the resins the impact resistance increases. The variation of impact resistance with the epoxy content of the resin may be explained from the angle of toughness of the films, which is the ability to absorb the applied external energy. Thus the impact resistance increases with the increase of mechanical strength and flexibility of the films (Table 2.5). However for MGE, the impact resistance was the lowest, which may be due to its low strength. The presence long hydrocarbon chains in the side group of MGE, causes enhancement on flexibility, which in turn makes the cured resin too soft to peel out. TBPAE exhibited the highest scratch resistance among the studied systems. This property can be related to the surface morphology and the toughness of the film. Highly

crosslinked film with good toughness shows high scratch resistance (Table 2.5). The high crosslink density is supported by the swelling values (Table 2.5). Thus the film with good toughness shows resistance to any plastic deformation. The gloss characteristics of the cured films were also measured. Generally, gloss refers to specular reflection of the light reflected at the same angle of incidence. The gloss generally depends on the quantity of light absorbed or transmitted by the coating surface, which is determined by the smoothness of the surface. All of the resins showed moderate gloss characteristic. TBPAE has good smooth film surface and hence exhibited the highest gloss value, whereas MGE film surface is not so smooth due to low dimensional stability and hence results in low gloss value. TBPAE also exhibited good adhesive strength. The adhesive strength of the resins on wood substrate depends on a wide range of variables such as surface smoothness of the substrate, presence of wood extractives, pH etc. The good adhesive strength in this case is due to the formation of hydrogen bonding, polar-polar and polar-induced polar interactions between hydroxyl, epoxy, ester, ether etc. groups of the resins and the hydroxyl groups of the cellulose plywood substrate.

Table 2.5: Performance characteristics of the epoxy resins

Samples	Impact resistance (cm)	Scratch hardness (kg)	Gloss (°)	Tensile strength (MPa)	Adhesive strength (Nm ⁻¹)	Elongation at break (%)	Swelling (%)
TBPAE	100	3.5	67	5.9	750.56	83.60	10.18
BPAAE	75	1	60	2.3	230.34	25.7	22.03
MGE	15	0.5	55	-	-	-	40.2
BPSE	100	2.7	55	4	90	70	25.7
MBPSE	100	3.4	60	6	100	95	30

2.3.7. Chemical Resistance

The chemical resistance of TBPAE to aqueous HCl, NaCl and ethanolic solution was found to be very good (Table 2.6), however to aqueous alkali the film remains intact though there is adhesion failure (as the film comes out from the surface of the glass plate). However, MGE and ENO shows very poor resistance to alkali solution, which may be due to presence of large number of hydrolyzable ester group of the fatty acids. Thus the overall chemical resistance of the cured resins was good though the alkali

resistance decreases with the increase of monoglyceride content due to the presence of hydrolysable ester group in it.

Table 2.6: Chemical resistance of the epoxy films

Types of media	TBPAE	BPAE	MGE	BPSE	MBPSE	ENO
0.5 wt% aqueous NaOH	F	F	PO	G	G	VP
10 wt% aqueous HCl	E	E	P	G	E	PO
10 wt% aqueous NaCl	E	G	G	E	G	G
Distilled water	E	E	G	G	E	G
Ethanol (20%)	E	E	F	G	E	PO

F=Fair, E=Excellent, PO= Peeled Off, G, Good, VP= Very Poor

2.3.8. Flame Retardancy

The flame retardancy rating of TBPAE was found out to be V1 as tested by UL 94. However for the MGE and BPAE it was found that they were combustible i.e. they burnt out completely on application of the flame (Table 2.7). This may be due to the presence of highly combustible hydrocarbon moiety, where C/H ratio is low. For TBPAE good flame retardant property can be attributed to the presence of TBPA moiety in the resin. TBPA moiety acts by hindering the spread of the fire, and gives precious extra time in the initial stages of a fire when it is much easier to escape. They could be involved to remove high-energy $\cdot\text{OH}$, $\cdot\text{H}$, $\cdot\text{O}$ and the like radicals generated during the burning process by the suppressions via bromine. Also it can produce the non-combustible HBr (25% Br content in the resin as measured by Schoniger method), which helps the inhibition of flame during the burning process though vapor phase mechanism. For BPSE flame retardancy characteristics can be endorsed to the existence

Table 2.7: Flame retardancy of epoxy resins

Samples	LOI value	UL94 ratings
TBPAE	37	V1
BPAE	25	Nil
MGE	20	Nil
BPSE	30.3	V 1
MBPSE	28.4	V2

of sulfone moiety in the resin. The presence of the sulfone group serves as a promoter for the formation of char. This may result flame retardancy, resulting from the decline in the amount of combustible gases and formation of barrier to heat transfer as the char was formed.

2.3.9. Thermal Study

The relative thermal stability of all the cured resins was compared from TGA thermogram (Fig. 2.18). From these curves, it can be seen that all the resins exhibited one-step degradation process. The onset temperature of degradation for TBP AE was 242 °C and for BPAE 265 °C, whereas for MGE it was 225 °C. For TBP AE due to the presence of the bromine containing moiety in the structure its degradation occurs at a lower temperature than BPAE. Since bromine is labile, so the major initial mass loss may be due to the loss of HBr from the structure. However, the enhanced stability of TBP AE over MGE may be due to the greater crosslinking density of the former than the latter because of the lower epoxy equivalent that is higher number of epoxy groups present in the TBP AE resin. Also in MGE the constituents are mainly aliphatic hydrocarbon, whereas in TBP AE sufficient amount of aromatic moieties are present. The highest thermal stability of BPAE compared to other two resins can be attributed to the presence of the aromatic group of BPA and absence of thermolabile bromine atoms in the structure. BPSE showed initial degradation temperature of 273 °C whereas MBPSE it was 280 °C. As the sulfone bond has greater heat resistance, hence in BPSE it provides a “shielding effect” to thermal degradation of the resin.³⁹

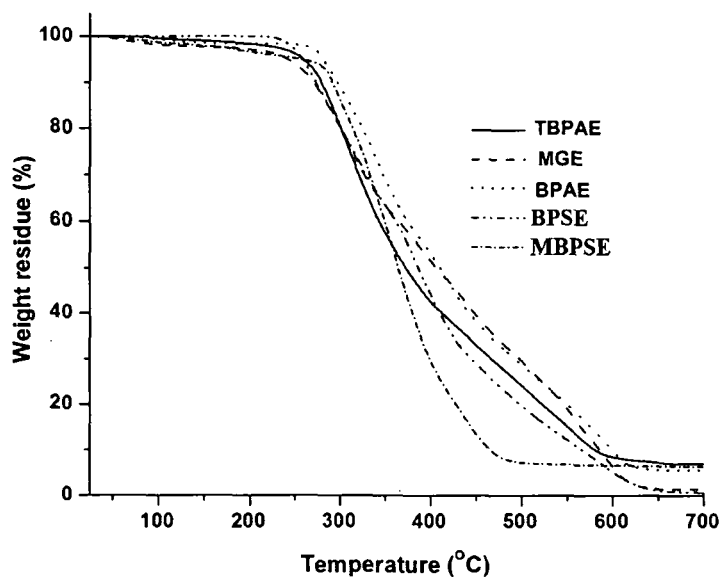


Fig. 2.18: TGA thermograms for epoxy resins

2.4. Conclusions

From this chapter, it can be concluded that *Mesua ferrea* L. seed oil is successfully epoxidized by peracid though the performance is not very encouraging. Further, along with monoglyceride of *Mesua ferrea* L. seed oil, BPA, TBPA and BPS resulted in different types of successful epoxy resins. These were characterized by various analytical and spectroscopic techniques. They exhibited good performance characteristics though the overall performance of MBPSE is the best, followed by TBP AE, BPSE and BPAE.

References

1. Bozell, J.J. Feedstocks for the future—Biorefinery production of chemicals from renewable carbon, *Clean: Soil, Air, Water* **36**, 641–647, 2008.
2. Williams, C.K., & Hillmyer, M.A. Polymers from renewable resources: A perspective for a special issue of polymer reviews, *Polym. Rev.* **48**, 1–10, 2008.
3. Eissen, M. et al. Ten Years after Rio—Concepts on the contribution of chemistry to a sustainable development, *Angew. Chem. Int. Ed.* **41**, 414–436, 2002.
4. Scott, G. Green polymers, *Polym. Degrad. Stab.* **68**, 1-7, 2000.
5. Bisht, R.P., et al. Vegetable oils as lubricants and additives, *J. Sci. Ind. Res.* **48**, 174-180, 1989.
6. Ramadhas, A.S., et al. Use of vegetable oils as I.C. engine fuels-A review. *Renew. Energy* **29**, 727-742, 2004.
7. Espinosa, L.M., & Meier, M.A.R. Plant oils: The perfect renewable resource for polymer science, *Eur. Polym. J.* **47**, 837-852, 2011.
8. Syed, H., & Nitin, V.P. Renewable materials in surface coatings, *Paintindia* **56**, 81-86, 2006.
9. Konwer, D., et al. Liquids from *Mesua ferrea* L. seed oil, *J. Am. Oil Chem. Soc.* **66**, 223-226, 1989.
10. Dutta, N., & Karak, N. Synthesis and characterization of polyester resins based on Nahar seed oil, *Prog. Org. Coat.* **49**, 146-152, 2004.
11. Dutta, S., & Karak, N. Synthesis, characterization of poly(urethane amide) resins from Nahar seed oil for surface coating applications, *Prog. Org. Coat.* **53**, 147-152, 2005.
12. Mahapatra, S.S., & Karak, N. Synthesis and characterization of polyesteramide resins from Nahar seed oil for surface coating applications, *Prog. Org. Coat.* **51**, 103-108, 2004.
13. Dinda, S., et al. Epoxidation of cottonseed oil by aqueous hydrogen peroxide catalyzed by liquid inorganic acids, *Bioresour. Technol.* **99**, 3737–3744, 2008.
14. Vlcek, T., & Petrovic, Z.S. Optimization of the chemoenzymatic epoxidation of soybean oil, *J. Am. Oil Chem. Soc.* **83**, 247-252, 2006.
15. Piazza, G.J., & Foglia, T.A. One-pot synthesis of fatty acid epoxides from triacylglycerols using enzymes present in oat seeds, *J. Am. Oil Chem. Soc.* **83**, 1021-1025, 2006.

16. Lee, H. & Neville, K. *Handbook of Epoxy Resins*, McGraw-Hill Inc., New York, 1967, reprinted 1982.
17. Anand, M., & Srivastava, A.L. Synthesis and characterization of epoxy resins containing transition metals, *Polymer* **34**, 2860-2864, 1993.
18. Anand, M., & Srivastava, A.K. Synthesis of zinc-containing epoxy resin, *J. Appl. Polym. Sci.* **51**, 203-211, 1994.
19. Chiu, Y.C., et al. Preparation and thermal properties of diglycidylether sulfone epoxy, *Polym. Degrad. Stab.* **93**, 668-676, 2008.
20. Liaw, D.J., & Shen, W.C. Curing kinetics of epoxy resins based on bisphenol-S and its derivatives, *Macromol. Mater. Eng.* **200**, 137-146, 1992.
21. Patel, B.K., & Patel, H.S. Interacting blends of flame-retardant acrylated poly(ester-amide) resins based on brominated epoxy resin with methyl methacrylate and styrene, *Polym. Plast. Technol. Eng.* **49**, 244-249, 2010.
22. Bringi, N.V. (ed.). *Non-Traditional Oil Seeds and Oils in India*, Oxford & IBH Publishing Co. Pvt. Ltd., New Delhi, 1987.
23. Dennis, T.J., & Kumar, K.A. Constituents of *Mesua ferrea* L., *Fitoterapia* **69**, 291-304, 1998.
24. Oil and Colour Chemist's Association of Australia, *Surface Coatings*, Vol. 1, Chapman and Hall, London, 1981.
25. Banerji, R., et al. Non-edible oil seeds potential raw material for industry, *J. Sci. Ind. Res.* **42**, 686-693, 1983.
26. Carr, R.A. Refining and degumming systems for edible fats and oils, *J. Am. Oil Chem. Soc.* **55**, 765-771, 1978.
27. Sharma, B.K. *Industrial Chemistry*, 10th ed., GOEL Publisher, Meerut, 1999.
28. Indian Standard, *Methods of Sampling and Test for Paints, Varnishes and Related Products* 101 (Part 4/Sec 4), 1988.
29. Annual Handbook of ASTM Standard, *The American Society for Testing Materials*, Philadelphia, 1973.
30. Okieimen, F.E., et al. Studies on the epoxidation of rubber seed oil, *Ind. Crop. Prod.* **15**, 139-144, 2002.
31. Goud, V.V., et al. Studies on the epoxidation of mahua oil (*Madhumica indica*) by hydrogen peroxide, *Bioresour. Technol.* **97**, 1365-1371, 2006.
32. Vleck, T., & Petrovic, Z.S. Optimization of the chemoenzymatic epoxidation of soybean oil *J. Am. Oil Chem. Soc.* **83**, 247-252, 2006.

33. Rios, L.A., et al. Mesoporous and amorphous Ti-silicas on the epoxidation of vegetable oils, *J. Catal.* **232**, 19-26, 2005.
34. Nowak, J.A., Zillner, T.A. and Mullin, L.P. *Thin-film epoxidation of an unsaturated oil or alkyl fatty acid ester*, US Patent No. 6734315, June 27, 2004.
35. Brojer, Z., Hertz, Z. & Penczek, P. *Zywiec epoksydowe*, WNT, Warszawa, 1972.
36. Rangarajan, B., et al. Kinetic parameters of a two-phase model for *in-situ* epoxidation of soybean oil, *J. Am. Oil Chem. Soc.* **72**, 1161-1169, 1995.
37. Charmas, W. Thioetherglycidyl resins: Synthesis, structure, and properties of glycidyl thioethers of aliphatic, aliphatic-aromatic, aromatic dithiols, and epichlorohydrin, *Int. J. Polym. Mater.* **52**, 101-117, 2003.
38. Gao, J., & Li, Y. Curing kinetics and thermal property characterization of a bisphenol-S epoxy resin and DDS system, *Polym. Int.* **49**, 1590-1595, 2000.
39. Li, Y., et al. Kinetics of 4,4'-diaminodiphenylmethane curing of bisphenol-S epoxy resin, **73**, 1799-1803, 1999.
40. Sykora, V., et al. Epoxy resin based on 4,4'-dihydroxydiphenylsulfone. I. Synthesis and reaction kinetics with 4,4'-diaminodiphenylmethane and 4,4'-diaminodiphenylsulfone, *J. Appl. Polym. Sci.* **54**, 1463-1467, 1994.

CHAPTER 3

Epoxy/Clay Nanocomposites

3.1. Introduction

It is cleared from Chapter 2 that vegetable oil based epoxy thermosets are attributed with weak performance characteristics, thus there is a strong demand for development of high performance advance materials for epoxy and these incline the scientists to develop high performance epoxy thermosets to fulfill the requirements of materials for the society. But the development of a new high performance epoxy is time consuming, laborious and is cost inefficient. In this context, the nanotechnology brings about a revolutionary era in material science. Nanocomposite represents itself as a multidisciplinary cutting edge genre of composite materials in the contemporary times and is challenging to the extreme.¹⁻⁴ In this domain, the polymer nanocomposites have been reported to be one of the best avenues to enhance the performance characteristics of the pristine polymers.⁵⁻⁹ Thus the improvement of performances by incorporation of the nanometer size organo-inorganic particles with a very low loading, generally ≤ 5 wt%, is a topic of today's interest.^{1,2} This is because of the fact that the formation of exfoliated nanocomposites results significant improvement of properties like dimension stability, strength, heat resistance, gas barrier capacity, biodegradability of biodegradable polymers without increase of specific gravity of the resulted products. Among the different nano reinforcing agents, nanoclay is still most accepted for preparation of polymer nanocomposites due to its combination of properties like high aspect ratio, relative low cost, easily modified and adequate availability. The enhancement of desirable properties by the formation of nanoclay based nanocomposite of epoxy resins has been well studied in literature.¹⁰⁻¹⁵

As it is observed from the earlier chapter that the vegetable oil based epoxy resin can be used as a reactive diluent in conjunction with the industrial resin for the reduction of viscosity and to increase the molecular mass of the latter. Since the reactive diluent acts as a solvent for the used resin system, so it permits to obtain high-solid and low VOC coatings.¹⁶

However the epoxidized oil doesn't have its own structural properties,

Parts of this work are published in: (i) Prog. Org. Coat. 66 (2009), 59–64, (ii) Polym. Degrad. Stab. 94 (2009), 1948-1954, (iii) Prog. Org. Coat. 69 (2010), 495-503, (iv) J. Appl. Polym. Sci. 2011 (proof corrected) and (v) Int. J. Polym. Mater. 2011 (communicated)

consequently it is used in conjunction with commercially available diglycidyl type epoxy resin and subsequent nanocomposite formation will enhance the mechanical properties. Hence in the present chapter, the nanoclay nanocomposites of BPA-based commercial epoxy resin in the presence of epoxidized *Mesua ferrea* L. seed oil-based reactive diluent are discussed.

Further, it has also been noticed that *Mesua ferrea* L. seed oil based different types of epoxy resins can be used in the fields of adhesives, coatings, composites etc. This is also the subject of multitude publications for different other types of epoxy resins. However, the studied epoxy resins are lacking to fulfill the demands for many advanced applications. These oil based epoxy resins are suffering from low mechanical strength, low thermal stability, low flammability, poor adhesive strength etc. similar to other vegetable oil based epoxy resins.¹⁴ Now as it is well established that by the formation of suitable nanocomposites with nanoscale inorganic materials especially nanoclay impressively enhances many properties including thermostability and flame retardancy without affecting the light weight characteristic of the pristine polymers,¹⁷ so the nanoclay based nanocomposites of the resins are also studied in the present chapter. Further, the use of the brominated flame retardant epoxy with nanoclay may result synergistic effect on its flame retardancy.¹⁸ As organo montmorillonite (OMMT) nanoclay is the most commonly used layered silicate for the preparation of polymer nanocomposites, so in the present study a flame-retardant epoxy/OMMT clay nanocomposite was investigated.

As it has been discussed earlier because of the ultrafine phase dimensions, nanocomposites exhibit new and improved properties in comparison with their microcomposite and macrocomposite counterparts. However for a true nanocomposite, the clay layer must be uniformly dispersed in the polymer matrix rather than aggregated as tactoids. The dispersion (intercalated or exfoliated structure) of clay mostly depends on thermodynamic compatibility between the different component present (polymer, clay and organic modifier) in the system. Hence, for a favorable free energy of nanocomposite formation, a proper choice of the cationic organic modifier is necessary.¹⁹ Alkylammonium ions are mostly used for this purpose, although other "onium" salts can be used, such as sulfonium and phosphonium.²⁰⁻²² Depending on the functionality, packing density, and length of the organic modifiers, the organo-modified layered silicates (organoclays) can be engineered to optimize their compatibility with a given polymer.^{19,23} The limited availability of commercial organoclays modified with

ammonium ions (which are mostly petroleum based aliphatic non-polar organics) provides the principal motivation for preparation of vegetable oil based polar organic modified nanoclays. This type of modification of montmorillonite may facilitate to control the final structure and end properties of polymer nanocomposites as well as in other applications.

The unique combination of the both polar and non-polar part in the structure may be an apt choice for use of the amido-amine as modifier for nanoclay. As already mention in Chapter 2 *Mesua ferrea* L. seed oil {70% (w/w) oil content} with its suitable fatty acid compositions represents an appropriate choice for synthesis of avant-garde materials. The fatty amido-amine of *Mesua ferrea* L. seed oil may involve in hydrogen-bonding or ionic bonding with the thin platelets of nanoclay and thereby manifesting in self-assembly process to form a super-hydrophobic surface. Conversely, the flexible alkyl groups tethered to the rigid platelet surface can offer higher degree of compatibility of the silicate layers with the polymers. Additionally the presence of amine in the layer structure may catalyze the homopolymerization and crosslinking processes of the matrices like epoxy resin. Thus fatty amido-amine of *Mesua ferrea* L. seed oil is utilized to modify hydrophilic (bentonite) and hydrophobic (OMMT) for improvement of compatibility with the studied epoxy resins. In the present chapter, the influence of insertion of s-triazine based hyperbranched polyurea into the OMMT gallery is also reported. This is due to the fact that the hyperbranched polymer with unique architectural features strongly influences the intercalation/exfoliation processes of nanoclay in polymer matrix, since intercalation of hyperbranched systems results larger gallery spacing as compared to linear systems with equivalent functional group densities.²⁴⁻²⁶

Therefore in the present chapter, the nanocomposites of ENO (epoxidized *Mesua ferrea* L. seed oil) with OMMT, *Mesua ferrea* L. seed oil based epoxy resins viz. TBPAE (tetrabromobisphenol A based epoxy) with OMMT, BPSE (bisphenol-S based epoxy) with OMMT, and MBPSE (modified BPSE) with OMMT, OMMT modified by fatty amido-amine of the oil, OMMT modified by hyperbranched polyurea, bentonite modified by fatty amido-amine of the oil, and hydrophilic bentonite have been prepared and the performance characteristics were evaluated.

3. 2. Experimental

3.2.1. Materials

Mesua ferrea L. oil, as described in Chapter 2, section 2.2.1. was used as the vegetable oil.

Montmorillonite {modified with 25-30% (w/w) of octadecylammonium ions, OMMT (Nanoclay Nanomer^R I.30E, Aldrich, Germany, CEC, cation exchange capacity 90 meqv/100 g} was used as received. Bisphenol-A based epoxy resin (Araldite LY 250) and poly(amido amine) hardener (HY 840) were obtained from Hindustan Ciba Geigy Ltd. and used as received. The specifications of epoxy resin and hardener are same as stated in Chapter 2, section 2.2.1.

Cyanuric chloride (Fig. 3.1) was purchased from Merck, Germany. It has melting point (m.p.) 144-147 °C, purity 99% and molecular weight (M_w) 184.41 g/mol. It was used after recrystallization from chloroform (< 30%).

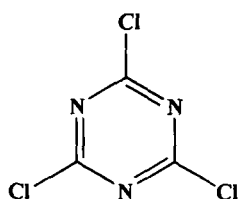


Fig. 3.1: Structure of cyanuric chloride

Cyanuric chloride is mainly used as an intermediate for manufacturing agrochemical, dyestuffs, optical brighteners, tanning agents, softening agents, pharmaceutical building block for plastics and additives. Here it is used as an A_3 monomer.

Urea (Fig. 3.2) was purchased from Merck, India. It has m.p. 132-135 °C, purity \geq 99.5% and M_w 60.06 g/mol. Interestingly, urea was known to be the first natural compound to be synthesized artificially using inorganic compounds and this was a scientific breakthrough. Here, it was used as the A_2 monomer. Urea is very cheap and nontoxic chemical and therefore handling is very easy.

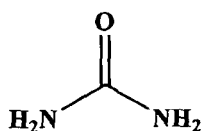


Fig. 3.2: Structure of urea

Diisopropylethylamine (DIPEA) (Fig. 3.3) was obtained from Merck, India. The compound has purity $\geq 98\%$ and M_w 410.52 g/mol. It was used as received. It is strong base and used as HCl scavenger.

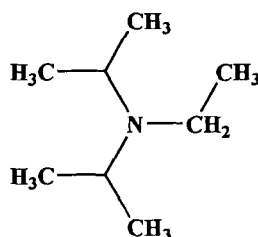


Fig. 3.3: Structure of diisopropylethylamine

N,N-Dimethylacetamide (DMAc) was purchased from Merck, India. Its purity is 99.5% with 0.1% water and 0.12% free acid as impurities. The density is 0.938-0.942 g/cm³ at 25 °C and b.p. 165-167 °C. It was purified by the following procedure. About 500 mL of DMAc was taken in a round bottom flask and 20 g of powder calcium oxide was added into it. The solution was kept for overnight. Then it was filtered and distilled under reduced pressure. This distillate obtained was kept in an amber bottle with 4A type molecular sieves.

Methanol (CH₃OH) was obtained from Merck, India. It has formula weight (F_w) 58.0 g/mol, purity $\geq 99.5\%$, density 0.971 g/cm³ and boiling point (b.p.) 56-57 °C. It is used as a solvent and also as a reagent to prepare sodium methoxide. Super dry methanol was used for this purpose, which was obtained as follows. An amount of about 4 g of purified dry Mg-turnings was taken in a 1000 mL single neck round bottom flask. A pinch of iodine was added into it and heated for 2-3 min. About 50 mL of distilled methanol was added into the above mixture. The flask was then fitted with a reflux condenser along with a guard tube containing anhydrous calcium chloride. The mixture was refluxed until the color of the iodine disappeared. Then about 600 mL of distilled methanol was added in the flask and it was refluxed until the color of the solution became milky white. This was then distilled. The distillate obtained was the super dry methanol and kept in an amber bottle using 4A type molecular sieves.

Sodium metal (Na) was obtained from Merck, Germany. It has atomic weight (A_w) 22.9 g/mol and purity 98.8% with chloride (0.01%), silica (0.002%), calcium (0.1%) and iron (0.01%) as impurities. It was kept in paraffin oil and used as received after cutting into small pieces.

Magnesium turning (Mg-turning) was purchased from SRL, Mumbai, India. It has atomic weight (A_w) 24.31 g/mol and purity 99.8% with maximum 0.05% iron as impurity. It was purified by thorough washing with dilute HCl followed by washing with distilled water. The process is repeated for several times until the turnings became shining. Finally it was washed with acetone and dried under vacuum at 45 °C for 4-5 h. The dried turnings were used in the same day.

3.2.2. Instruments and Methods

The FTIR and TGA analyses were carried out using the same instruments under the same conditions as mentioned in Chapter 2, section 2.2.2. The X-ray diffraction study was carried out at room temperature (~ 27 °C) by a Rigaku, Miniflex, UK, X-ray diffractometer at scanning rate of 2.0/min over the range of $2\theta = 1-35^\circ$. The X-ray was derived from nickel-filtered Cu-K α ($\lambda = 0.154$ nm) radiation in a sealed tube operated at 40 kV and 40 mA. The surface morphology of the samples was studied by a scanning electron microscope (SEM, JEOL, JSM-6390LV, Japan) after platinum coating on the surface of the samples. The size and distribution of OMMT layers in the nanocomposites were studied by using transmission electron microscope (TEM, JEOL, JEMCXII, JEM-100 CX and JEM-2100, Japan,) operated with an accelerating voltage of 100-200 kV, and equipped with a digital camera. The dilute polymer nanocomposite solution was transferred to a carbon-coated copper grid before analysis. The mechanical properties were tested by the same methods as stated in Chapter 2, section 2.2.2. The measurement of gloss, impact resistance, scratch hardness and chemical resistance was done according to the standard methods as mentioned earlier (Chapter 2, section 2.2.2.). Ultrasonicator (Hielscher, UP200S, Germany) was used to mix the epoxy resin with the nanoclays at 60% of amplitude and a half cycle for 10-20 min. The rheological studies of the nanocomposites were carried out as mentioned in Chapter 2, section 2.2.2.

The adhesive strength of the cured thin films was measured by lap-shear test as per the standard ASTM D3165-95 using plywood, aluminium (Al), and polypropylene sheets as the substrates as mentioned in Chapter 2, section 2.2.2.

Mesua ferrea L. seed oil was extracted from the matured seeds by the same method as described in Chapter 2, section 2.2.1.

3.2.2.1. Preparation of Sodium Methoxide

In a completely dried 100 mL three neck round bottom flask fitted with a water condenser and a nitrogen inlet about 50 mL 'super dry' methanol was taken. The

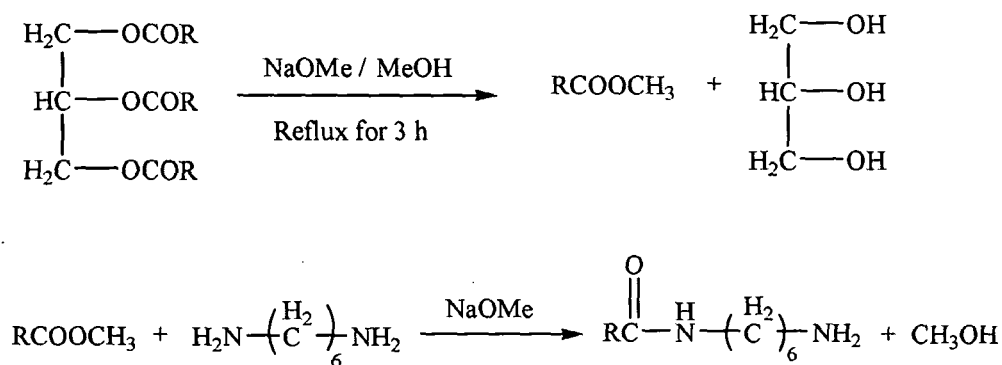
reaction flask was placed in an ice-water bath to maintain the temperature of the reaction, (0-5) °C. About 10 g of pure and dry sodium metal as small pieces was added very slowly with vigorous stirring into the flask. After completion of addition the reaction mixture was refluxed for 2 h. Finally the excess methanol was removed by vacuum distillation. A white powder of sodium methoxide was obtained, which was stored in a desiccator.

3.2.2.2. Preparation of Methyl Ester of *Mesua ferrea* L. seed Oil

The methyl ester of the oil was prepared as reported in the earlier published report.²⁷ Briefly, 25 g of oil in 50 mL super dry methanol and 0.5% sodium methoxide (with respect to the oil) were refluxed for 3 h in 250 mL round bottom flask under the nitrogen atmosphere. The contents of flask were then cooled to room temperature and kept for overnight. The excess methanol was removed by distillation and the methyl esters were extracted by petroleum ether (b.p. 60–80 °C) followed by washing with 15% aqueous NaCl solution and finally dried over anhydrous sodium sulfate. The methyl esters of the mixed fatty acids were purified from petroleum ether by distillation (Scheme 3.1).

3.2.2.3. Preparation of *Mesua ferrea* L. seed Oil based Fatty Amido-Amine (AMNO)

Mesua ferrea L. seed oil based fatty amido-amine was obtained from the methyl ester of the oil by the following procedure. 0.0585 mol methyl ester and sodium methoxide (0.5% (w/w) as catalyst) were taken into a three necked round bottom flask equipped with a condenser, a thermometer and a nitrogen gas inlet. Then 0.064 mol of 1,6-diaminohexane was added to the reaction mixture slowly. The reaction was then



R= hydrocarbon part of mixtures of oleic, linoleic, stearic and palmitic acid

Scheme 3.1: Synthesis of fatty amido-amine

continued at room temperature for 2 h followed by heating at (50-60) °C for 1 h with constant stirring. The product was purified by washing it with petroleum ether to remove any unreacted methyl ester followed by double distilled water for two to three times, and finally by extracting it with THF and distilling under vacuum. Further it was kept in a vacuum oven at (35-40) °C for 24 h before use. The product obtained was in quantitative yield. The product was coded as AMNO (Scheme 3.1).

3.2.2.4. *Modification of Organo-MMT (OMMT) by Fatty Amido-Amine*

The dispersed OMMT in THF (10% v/w) and AMNO (30% by weight with respect to OMMT) was mixed together by magnetic stirrer under refluxed condition. It was continued for 3 h. The product was vacuum dried for overnight at (35-40) °C. This product was coded as mOMMT.

3.2.2.5. *Modification of Hydrophilic Bentonite (MMT) by Fatty Amido-Amine*

0.5 g of clay was dispersed in 50 mL of double distilled water for 6 h at (50-60) °C using a magnetic stirrer with a reflux condenser. The salt of AMNO was prepared by neutralizing it with 1N HCl for 12 h at (60-65) °C. The above two solutions were mixed together by magnetic stirring at 70 °C. The heating was continued for 24 h. The resulting product was filtered and washed with double distilled water until chloride ion is completely removed. The product was dried under vacuum for 24 h at 40 °C. This product was coded as mMMT.

3.2.2.6. *Modification of organo-MMT (OMMT) by Hyperbranched Polyurea*

The hyperbranched polyurea was prepared as reported elsewhere.²⁸ This hyperbranched polyurea was used to modify the OMMT (organically modified MMT). The OMMT was modified by the following process. 1 g of the prepared hyperbranched polyurea was dissolved in 5 mL of DMF and mixed with a solution of OMMT (2 g) in 10 mL of DMF. The mixture was vigorously stirred for 4 h and finally sonicated for 15 min. Then the mixture was dried in a vacuum oven at (40-45) °C for 24 h.

3.2.2.7. *Preparation of Nanocomposites of Epoxidized Oil Modified Araldite LY 250 by OMMT*

The epoxidation of *Mesua ferrea* L. seed oil has been prepared as described in Chapter 2, section 2.2.2.1. Epoxidized oil and bisphenol-A-based commercial epoxy (Araldite LY 250) resins were mixed by mechanical stirring for 10 min at ambient temperature. The hardener was added in each case by maintaining the ratio of epoxy to hardener 2:1.

The mixtures were prepared by addition of epoxidized oil (ENO) with Araldite LY 250 in the ratio of 75:25, 50:50 and 25:75 (w/w) for ENO75, ENO50 and ENO25, respectively (Table 3.1).

Table 3.1: Composition of ENO modified Araldite LY 250 and OMMT nanocomposites

Sample Code	ENO (g)	Araldite LY 250 (g)	OMMT (g)	Hardener (phr)*
ENO	100	0	0	0
ENO75	75	25	0	50
ENO50	50	50	0	50
ENO25	25	75	0	50
ENC1	50	50	1	50
ENC2.5	50	50	2.5	50
ENC5	50	50	5	50

*Parts per hundred resin (epoxide)

The nanocomposites were prepared by *ex-situ* technique²³ by taking the mixed resin system, ENO50. Organically modified clay was added to the resin system at 80 °C and mixed by a mechanical stirrer for about 2 h. Then the mixture was sonicated for 30 min followed by degassing for 15 min under vacuum. The prepared nanocomposites were coded as ECN1, ECN2.5 and ECN5 for clay loadings of 1, 2.5 and 5 wt% respectively (Table 3.1).

3.2.2.8. Preparation of Nanocomposites of TBPAE and BPSE by OMMT

The nanocomposites were prepared by incorporation of OMMT nanoclay in TBPAE and BPSE matrix at 80 °C with constant mechanical stirring (at 1000 rpm) for about 2 h followed by sonication (pulse cycle 0.5 and amplitude 60%) for another 30 min at room temperature. To avoid the rise of temperature during the mixing, water bath was used so that the temperature is maintained at (25-30) °C. The dispersed nanoclay/resin system was degassed for 30 min under vacuum before further processing. The prepared nanocomposites for TBPAE were coded as TBPAEN1, TBPAEN2.5 and TBPAEN5 and for BPSE it was coded as BPSEN1, BPSEN2.5 and BPSEN5 for clay loadings of 1, 2.5 and 5 wt% respectively.

3.2.2.9. Preparation of Nanocomposites of MBPSE by OMMT, mOMMT, m-bentonite (mMMT), bentonite (MMT) and Hyperbranched Polyurea modified OMMT

At first the clay was vacuum dried at (35-45) °C for overnight. The nanocomposites were then prepared by incorporation of pre-calculated amount of OMMT, mOMMT, m-bentonite (mMMT), bentonite (MMT) and hyperbranched polyurea modified OMMT in the MBPSE matrix. The components were then mixed together as stated in the previous section. The prepared nanocomposites were coded as ENMC1, ENMC2, ENMC3 and ENC for mOMMT, OMMT, mMMT and MMT nanoclays respectively with 3 wt% of nanoclay with respect to resin. Whereas for hyperbranched polyurea modified nanoclay the nanocomposites were coded as HBPA1, HBPA3 and HBPA5 for 1, 3 and 5 wt% of hyperbranched polymer modified OMMT, respectively.

3.2.2.10. Curing of the Resins and Nanocomposites

A homogenous mixture of each resins and nanocomposite system with 50 phr (parts per hundred grams of resin) of poly(amido amine) hardener was prepared in a glass beaker at room temperature by constant stirring for 10 min similarly as described in Chapter 2, section 2.2.2.2. Then the mixtures were uniformly spread on mild steel plates (150 mm × 50 mm × 1.60 mm), tin plates (150 mm × 50 mm × 0.40 mm.) and glass plates (75 mm × 25 mm × 1.75 mm) for impact resistance, gloss and chemical resistance tests. The plates were cured at 100 °C for specified period of time and post cured at 150 °C.

3.3. Results and Discussion

3.3.1. Modification of Nanoclay

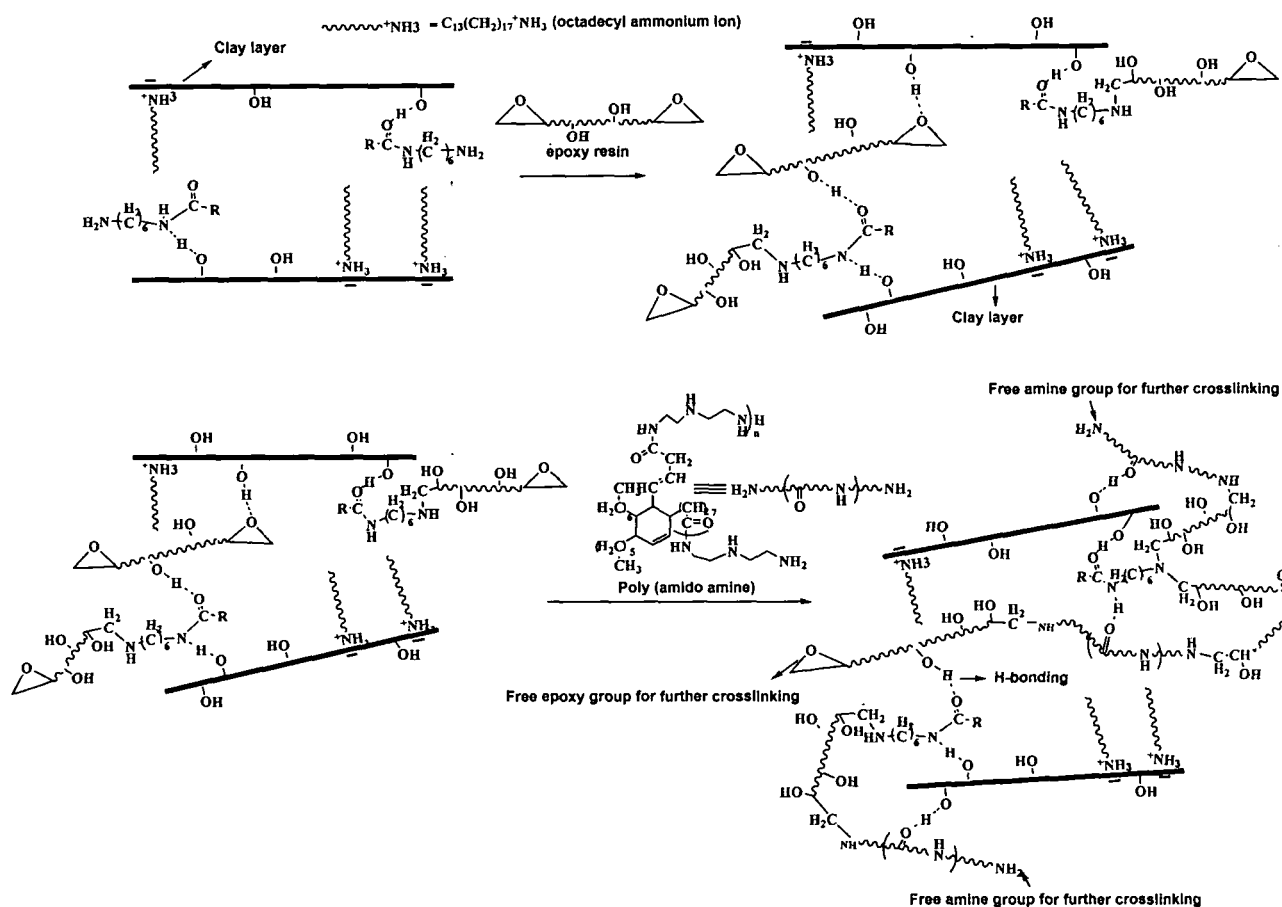
Organically modified layered-silicates or nanoclays become an attractive class of organic-inorganic hybrid materials because of their potential use in wide range of applications such as in polymer nanocomposites, rheological modifier in paints, inks, greases and cosmetics, adsorbent for toxic gases, effluent treatment and drug delivery carrier.²⁰ The generic term, layered silicates, refers to natural clays as well as synthesized layered silicates such as montmorillonite, laponite and hectorite. The most commonly used clay in the synthesis of polymer nanocomposites is montmorillonite which is the major constituent of bentonite. It is well known that filler anisotropy, i.e. large length to diameter ratio (aspect ratio), is especially favorable in matrix reinforcement. Due to unique structure of montmorillonite, the mineral platelet thickness is only one nanometer, although its dimensions in length and width can be measured in hundreds of nanometers, with a majority of platelets in 200–400 nm range after purification.^{21,22} Due to very small size and thickness of the platelets, a single

gram of clay contains over a million individual platelets. The inherent incompatibility between the hydrophilic layered silicate and hydrophobic polymer matrix greatly hinders the reinforcement ability of the layered silicate. Surface modification of hydrophilic clay was employed by long chain fatty amido-amine using cation exchange reaction. Further, organophilic clay was also co-intercalated by the fatty amido-amine (Scheme 3.2). There are two main objectives for clay modifications. The first one is to increase the basal spacing between clay layers by weakening the polar-polar interaction between adjacent layers, which is a prerequisite for polymer chains to intercalate into the clay galleries. Whereas the second objective is to enhance the compatibility between polymer and clay, which provides a driving force for polymers to migrate into the silicate galleries. Preparation of organophilic clay and the property of polar organic surfactant play a crucial role in the formation of the structure and morphology of polymer nanocomposites.²⁸

The *Mesua ferrea* L. seed oil based amido-amine containing a long hydrocarbon chain and polar groups can be effective in reducing the surface energy of the clay thereby improving the compatibility between the polymer and the layer silicates. Similarly the hyperbranched polyurea strongly influences the intercalation/exfoliation processes of nanoclay in the epoxy matrix, since intercalation of hyperbranched systems results larger gallery spacing as compared to linear systems with equivalent functional group densities.^{24,25,26}

3.3.2. Formation of Nanocomposites

Nanocomposite preparation essentially involves the dispersion or mixing of nanomaterial into a continuous phase termed as the matrix. Polymers have been widely used as matrices for these nanomaterials, since they prevent agglomeration and settling of the nanomaterials. Among all the potential nanocomposite precursors, those based on clay and layered silicates have been most widely investigated, probably because the starting clay materials are easily available and because their intercalation chemistry has been studied for a long time.²⁹⁻³¹ Amongst the vast nano-reinforcements available for fabricating polymer nanocomposites, clays have been focused and studied the most, because they are naturally occurring minerals, exhibit a layered morphology with high aspect ratios, and have substantial cation exchange capacities. The processing of polymers with various reinforcing nanofillers becomes a key technology to obtain advanced materials for the next generation. However, the nanolayers are not easily



Scheme 3.2: Probable interactions in epoxy nanocomposites

dispersed in most polymers due to their preferred face-to-face stacking in agglomerated tactoids. In fact, it has been well-demonstrated that the replacement of the inorganic exchange cations in the cavities or galleries of the native clay silicate structure by alkylammonium surfactants can compatibilize the surface chemistry of the clay and a hydrophobic polymer matrix (as discussed in the previous section).³² Thus the key factor in the polymer–organoclay interaction is the affinity of the polymer segments for the silicate surface. The incorporation of nanoclay to the biobased polymers or their blends to form nanocomposites can widened the scope of applications of these new materials as it improves their desired properties.³³⁻³⁶

Fundamentally the nanocomposites formation involves the dispersion of the modified as well as unmodified clay into the biobased epoxy matrix. Under the applied conditions delamination of the modified clay into individual silicate layers occurs, which ultimately become dispersed within the epoxy matrix. The separation of silicates into individual layers occurs by heating the clay and epoxy resin followed by sonication, addition of curing agent, and curing of the network at a prescribed set of temperatures. Ultrasonication can produce tiny bubbles, which can collapse violently,

releasing significant energy that can be used to exfoliate OMMT layers. The increase of gallery space during modification of the clay facilitates diffusion of the epoxy chains into the clay layers. Further the presence of alkylammonium ion in the gallery space may catalyze epoxy homopolymerization as well as crosslinking reactions. As the polymerization proceeds further more epoxy molecules migrate in between the layers.^{37,38} This causes the clay layers to move further apart from each other. The driving force for the intercalation/exfoliation process is believed to be the high surface energy of the clay which results in diffusion of polar species such as epoxy molecules between the layers. However in the absence of polymerization the system would reach a thermodynamic equilibrium and the layers could not be separated further. Since epoxy molecules react in the proposed homopolymerization process, they lower the polarity of clay and displace the equilibrium. Consequently, new polar epoxy molecules are driven between the layers in order to restore the equilibrium.^{39,40} As this mechanism proceeds, the organic molecules are driven between the layers to separate the clay. For unmodified clay the hydrophilic character and the confined layer spacing prevents the diffusion of the epoxy chains. Thus the high aspect ratio of clay in a delaminated structure offers an extensive filler-matrix contact, which may improve thermal, physical and mechanical properties at low loading of organoclay.

3.3.3. Characterization of Modified Nanoclay

3.3.3.1. FTIR Analysis

The FTIR spectra of AMNO, OMMT, mOMMT, MMT and mMMT are shown in Fig. 3.4. The presence of amine group in the structure of AMNO was characterized by the appearance of two weak absorption bands around 3428-3312 cm^{-1} . The absorption band around 3428 cm^{-1} and 3312 cm^{-1} are for primary and secondary -NH stretching vibrations. The band around 1636 cm^{-1} is attributed to stretching frequency of amide carbonyl of the fatty acid. Other characteristic bands observed in the spectra were 2923-2854 cm^{-1} (-CH₂ stretching), 1542 cm^{-1} (-NH bending) and 1053 cm^{-1} (C-N stretching).⁴¹ The spectrum of OMMT showed the presence of bands (cm^{-1}) at 3485 for -OH stretching, 2926 for -CH₂ stretching of modifying hydrocarbon, 3263 for -NH stretching, 1619 for -OH bending, 1045-980 and 524-429 for oxide bands of metals (Al, Mg, Si, etc.) present in the clay.³³ Multiple broad bands were detected for OMMT in the range 3627-3403 cm^{-1} that are attributed to the -OH stretching frequencies.

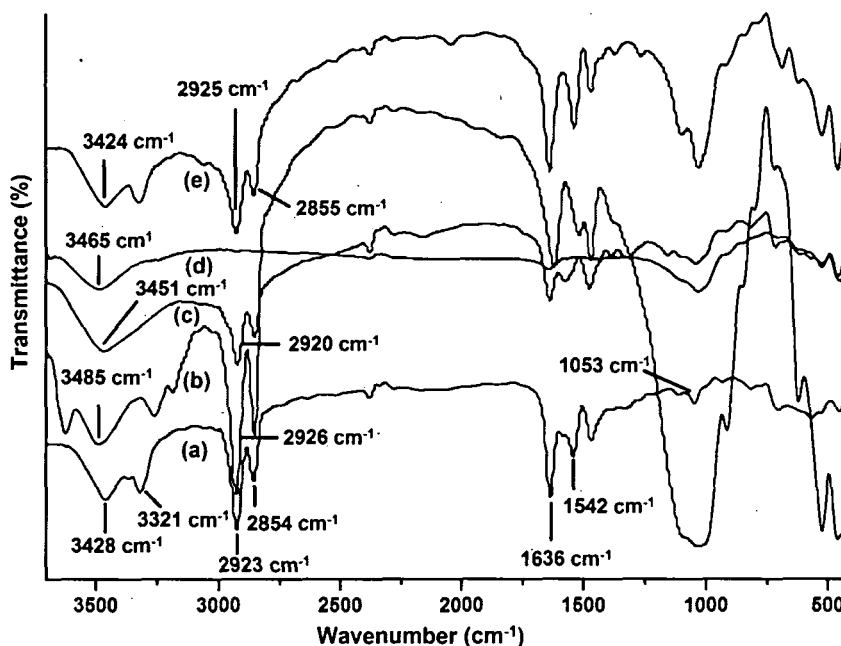


Fig. 3.4: FTIR spectra of (a) AMNO, (b) OMMT, (c) mOMMT, (d) MMT and (e) mMMT

For mOMMT, the -OH stretching vibration band showed a shift of 34 cm^{-1} , while the -CH_2 stretching vibration exhibited a shift of 6 cm^{-1} . These indicated that the modifying hydrocarbon of the fatty acids influences the arrangement of the octadecylammonium ion in the clay layers, consequently these affects the interlayer spacings. A decrease in the intensity of the -CH_2 absorption from 2926 cm^{-1} to 2920 cm^{-1} (asymmetric stretching) indicates an increase in the packing density for mOMMT.^{23,42} Further in the spectra, the band for amide carbonyl stretching was also observed at 1638 cm^{-1} for mOMMT, while the -NH deformation band exhibited a shift to 1577 cm^{-1} . This is indicative of the intercalation of the fatty amido-amine in the clay layers. In case of unmodified bentonite (MMT) the spectrum was quite similar to OMMT. Characteristics bands for the hydrophilic bentonite were observed at 3465 cm^{-1} (-OH stretching), 1640 cm^{-1} (-OH bending vibrations), 1032 (Si-O or Mg-O stretching) and $520\text{--}424\text{ cm}^{-1}$ for oxide bands of metals (Al, Mg, Si, etc.). For mMMT, the -OH stretching frequency was observed at around 3424 cm^{-1} , this shift may result from the hydrogen-bonding of the hydroxyl group of the clay with the amide carbonyl (-CONH) or secondary -NH group of the fatty amido-ammonium ion. Further the N^+H_3 ion may be involved in ionic interaction with the surface oxygen resulting in the shift of the -OH absorption band with respect to the pristine clay.²³ In the spectrum of mMMT,

additional bands (cm^{-1}) at 3314 (-NH stretching), 2925-2855 (-CH₂ stretching) and 1538 (-NH deformations) were also observed.

3.3.3.2. XRD Analysis

The basal spacing of the hydrophilic clay and the organophilic clay can be identified from the XRD spectra (Fig. 3.5). OMMT showed basal reflection at 4.15° corresponding to the {001} plane, this resulted in a basal spacing of about 6.4 nm. However, the surface modified OMMT by AMNO resulted in splitting of the peak into two. One peak appeared at 2° corresponding to a basal spacing of about 10 nm, while other peak was seen in the spectrum at about 5.9° .⁴³ This may be due to the presence of two different components in the organoclay. The intercalation of the clay by AMNO further increases the interlayer spacing. However complete modification of OMMT was not achieved as can be observed from the XRD spectra.

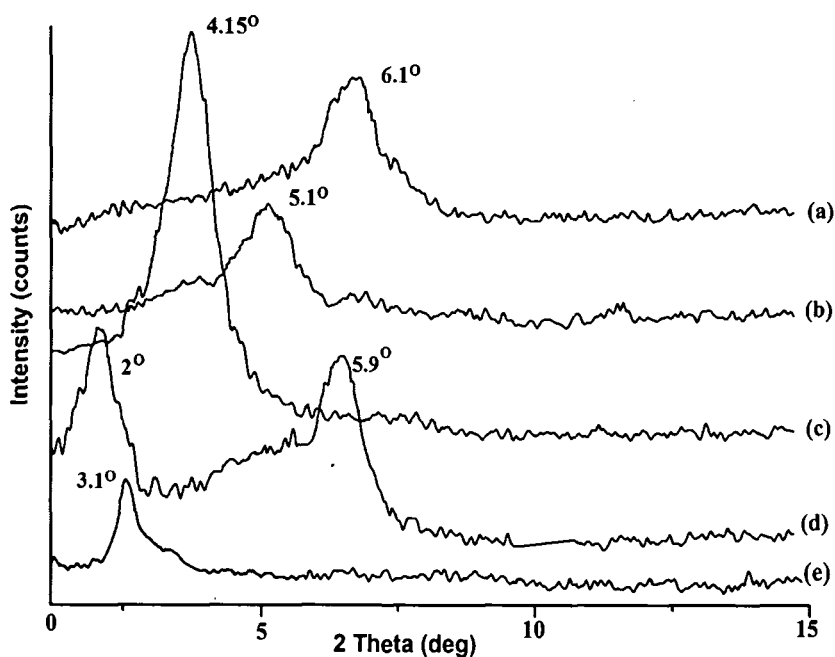


Fig. 3.5: XRD patterns of (a) MMT, (b) mMMT, (c) OMMT, (d) mOMMT and (e) hyperbranched polyurea modified OMMT

The diffraction patterns of MMT and mMMT are shown in Fig. 3.5. It can be seen from the figure that sharp peaks around 6.15° (d -spacing of about 3.6 nm) for hydrophilic bentonite and around 5.1° (d -spacing value is ~ 4.7 nm) for AMNO modified bentonite were appeared in the spectra. These results indicate that the modification was not sufficient to increase the interlayer spacing of the clay,

significantly. However, the above results confirmed the fatty amido-ammonium ion can modify the hydrophilic bentonite by cation exchange technique.

Thus higher basal spacing of mOMMT compared to mMMT may be attributed to the presence of the octadecyl ammonium ion in the clay galleries and also due to the use of proper modification methodology. This aids to the further expansion of the clay galleries by insertion of the fatty amido-amine. The presence of more number of functional group provides a greater degree of interaction, also the long chains surfactant tethered away from the surface pushes the clay layers apart.

The basal spacing of OMMT was also found to increase by co-intercalation with hyperbranched polyurea (Fig. 3.5). The modified nanoclay exhibited basal reflection at $2\theta \approx 3.01^\circ$.²⁸ The hyperbranched polymer influences the layer spacing by virtue of its globular structure.²⁸ The presence of numerous surface functionalities on the surface of hyperbranched polyurea helps in close interaction with the nanoclay surface, thereby providing an greater level of anchorage.

3.3.4. Characterization of Nanocomposites

3.3.4.1. FTIR Analysis

The FTIR spectra of ENO, ENO50 and its nanocomposites are shown in Fig. 3.6. The spectra revealed the absence of epoxide stretching band at 906 cm^{-1} after curing (Fig. 3.6), which confirmed the crosslinking reaction. This was also supported by the decrease in the intensity of -OH stretching band in the cured spectra, both for ENO50 and the nanocomposite (ECN2.5). The spectrum of organically modified nanoclay showed the presence of bands (cm^{-1}) at 3690-3420 for -OH stretching, 2930-2820 for -C-H stretching of modifying hydrocarbon, 1640 for -OH bending, 1045-980 and 538-486 for oxide bands of metals (Al, Mg, Si, etc.) of the clay, which agreed well with the reported values. But the intensities of these bands particularly for -OH , were reduced drastically in the nanocomposite (Fig. 3.6), which confirmed the participation of -OH group of clay in crosslinking of epoxy resin.

The representative FTIR spectra of the TBPAE and TBPAEN5 are shown in the Fig. 3.7. The interaction of the clay with the molecular chains of the epoxy resin can be understood by FTIR. As discussed in Chapter 2, section 2.3.3.2. TBPAE exhibited -OH stretching band at 3437 cm^{-1} . In TBPAEN5 a shift of the band was observed to 3412 cm^{-1} , these shifts primarily occur due to the formation of intermolecular hydrogen bonding with -OH groups of epoxy resin. For TBPAE and TBPAEN5 the complete

disappearance of the band at 834 cm^{-1} was observed suggesting that the epoxy group of the resin have been involved in bond ($-\text{CH}_2\text{-O}-$) formation with other epoxy groups, and $-\text{OH}$ groups of epoxy resin and also of the nanoclay.^{44,45}

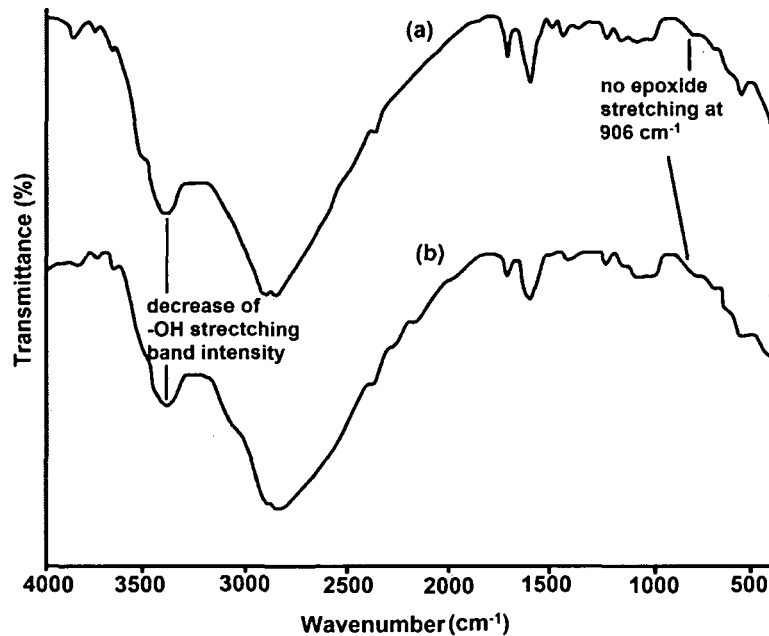


Fig. 3.6: FTIR spectra of (a) ENO50 and (c) ECN2.5

Fig. 3.8 shows the FTIR spectra of BPSE and its nanocomposite (BPSEN2.5). A shift of the $-\text{OH}$ band from 3454 cm^{-1} (BPSE) to 3421 cm^{-1} indicates (for BPSEN2.5) the formation of intermolecular hydrogen bonding with $-\text{OH}$ groups of the epoxy resin and nanoclay as discussed above. The band for the epoxy ring around 913 cm^{-1}

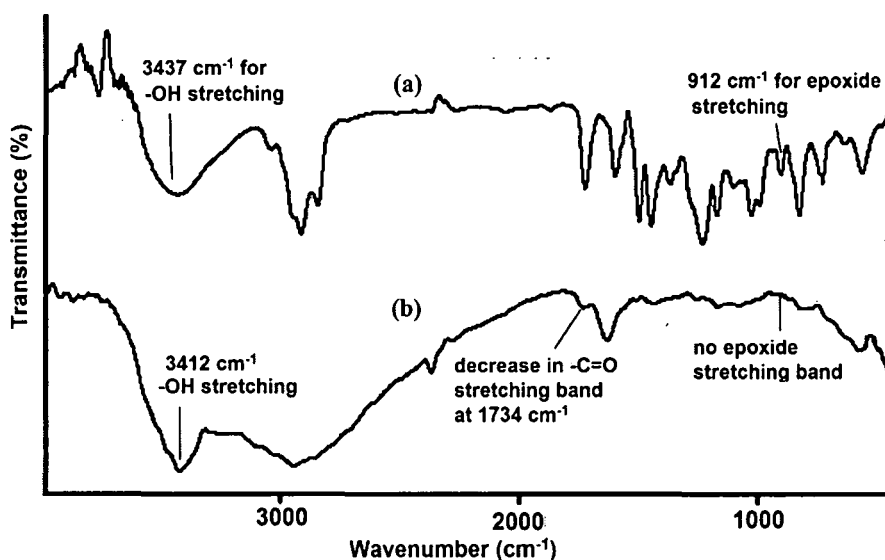


Fig. 3.7: FTIR spectra of (a) TBP AE and (b) TBP AEN5

almost disappeared in all the nanocomposites indicating the completion of the curing process (i.e. oxide-ring opening polymerizations) between epoxy rings of BPSE and amine group of the poly(amido amine) hardener. Further, the epoxy group of the resin may involve in bond other groups as well as nanoclay (as discussed above).⁴⁴

The FTIR spectrum of MBPSE, ENMC1, ENMC2, ENMC3 and ENC are shown in Fig. 3.9. The characteristics absorption bands (cm^{-1}) for MBPSE have already been discussed in details in Chapter 2, section 2.3.3.2. The $-\text{OH}$ stretching vibrations in all the nanocomposites showed significant shifts. The band was shifted from 3423 cm^{-1} to 3436 cm^{-1} for ENMC1, to 3433 cm^{-1} for ENMC2, to 3428 cm^{-1} for ENMC3 and to 3408 cm^{-1} for ENC due to the presence of significant interaction between the matrix and OMMT, which are similar to the above cases. The disappearance of the peak for the epoxy ring around 916 cm^{-1} in all the nanocomposites indicated the completion of the oxide-ring opening reaction of epoxy rings of MBPSE in the presence of amine group of the poly(amido amine) hardener.

The interaction of the hyperbranched modified clay with the epoxy matrix can be depicted from the FTIR spectra (Fig. 3.10). The broadened $-\text{OH}$ stretching band in the nanocomposites showed a red shifting of about $17\text{-}19 \text{ cm}^{-1}$ from that of the epoxy matrix.

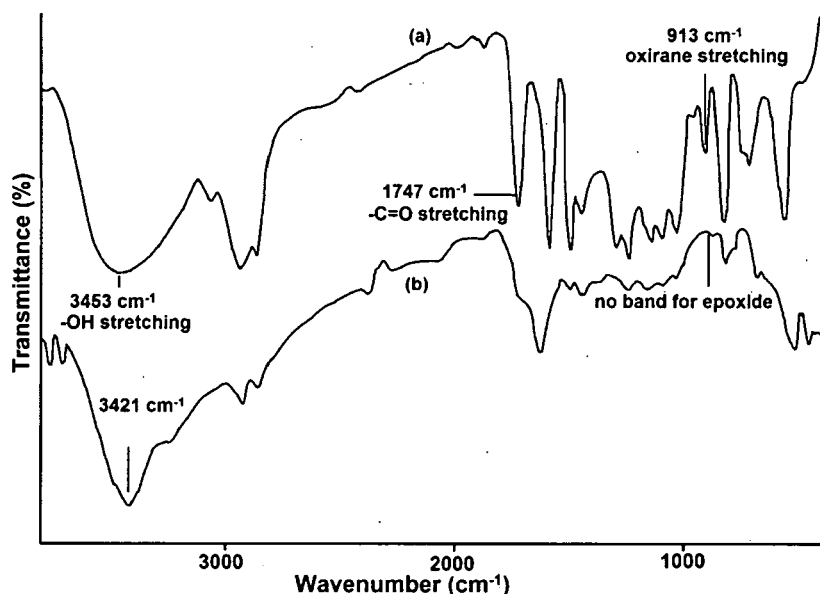


Fig. 3.8: FTIR spectra of (a) BPSE and (b) BPSEN2.5

The broadening resulted from the overlapping of $-\text{NH}$ stretching band of the clay (around $3391\text{-}3242 \text{ cm}^{-1}$) with the $-\text{OH}$ stretching band of the epoxy resin.²⁸ The $-\text{C}=\text{O}$ stretching vibrations band showed decrease in intensity after the incorporation of the

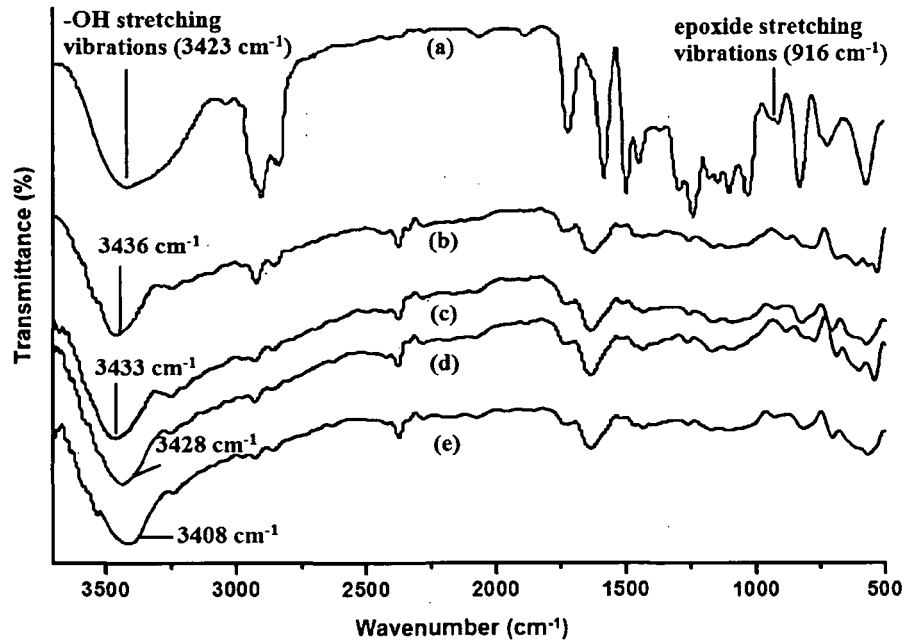


Fig. 3.9: FTIR spectra of (a) MBPSE, (b) ENMC1, (c) ENMC2, (d) ENMC3 and (e) ENC

modified nanoclay. The bands around 1034 cm^{-1} and 527 cm^{-1} due to the Si-O and Al-O stretching elements in the spectra for clay get suppressed in the nanocomposites indicating the interaction with the epoxy matrix.⁴⁶ The oxirane stretching vibration at

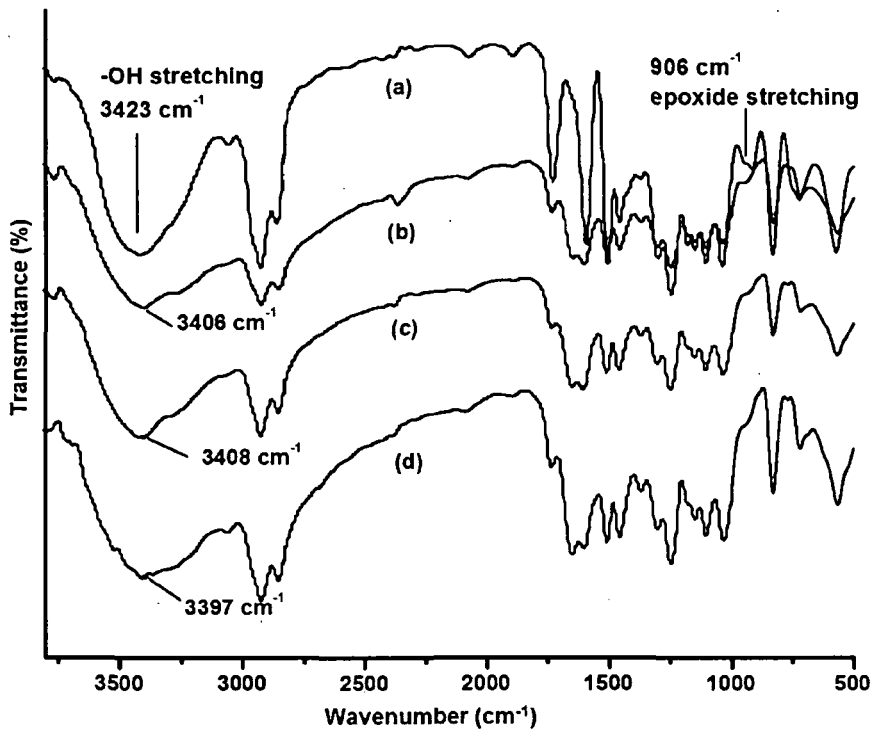


Fig. 3.10: FTIR spectra of (a) MBPSE, (b) HBPA1, (c) HBPA3 and (d) HBPA5

around 916 cm^{-1} disappeared in the spectra of the nanocomposites, indicating the crosslinking reaction of the epoxy with the hardener.

The above observations indicates extensive amount of interactions (dipole-dipole, dipole-induced dipole and hydrogen-bonding etc) present between the different functionalities of the epoxy resins and the modified nanoclays. However in such systems the interaction via hydrogen bonding largely depends on the amount of hydrocarbon segments present both in epoxy and in modified nanoclay systems. The $-\text{CH}_2$ moiety of the monoglyceride part in epoxy does not take part in the hydrogen bonding, but influences the bonding of other groups. Steric shielding of functional groups due to the presence of bulky side groups, steric crowding of hydrogen-bonded linkages due to limited spacing between the linkages on a polymer chain, and intramolecular screening due to flexible chains bending back upon themselves are some of the important factors that must be considered.

3.3.4.2. XRD Analysis

The formation of epoxy/clay nanocomposite is first understood from the XRD studies (Figs. 3.11-3.13). The XRD patterns of the nanocomposites with different clay loading and pure nanoclay are shown in Figs. 3.11-3.13. The nanocomposites (ENO/Araldite LY 250/OMMT, TBPAE/OMMT and BPSE/OMMT nanocomposites) exhibited only a very broad peak at around $15\text{-}28^\circ$ with no sharp peak near 4.15° . This broad peak may be due to amorphous character of the polymer and this result is the first sign of exfoliated nanocomposite formation. However, it cannot be confirmed from this study only.

For the nanocomposites with 1, 2.5 and 5 wt% clay contents, no clear peak was observed, which suggested that silicate layers of organoclay may be exfoliated in the polymer matrix. Thus the nanocomposites cured at 100°C with vigorous stirring results in the insertion of polymer chains in between the gallery space. These subsequently cause the galleries to expand and partially exfoliated nanocomposites are formed.

The XRD pattern of all the MBPSE its mOMMT, OMMT and mMMT nanocomposites exhibited no basal spacing corresponding to $\{001\}$ plane in the spectra (Fig. 3.14) except for ENC (small peak at around 5.9°). However a broad peak as discussed above in the earlier case was also observed in this case around 19.9° , which is due to the increase of basal spacing in case of mOMMT that helps the epoxy resin chains to intercalate in between the clay layers. Upon intercalation of the OMMT by

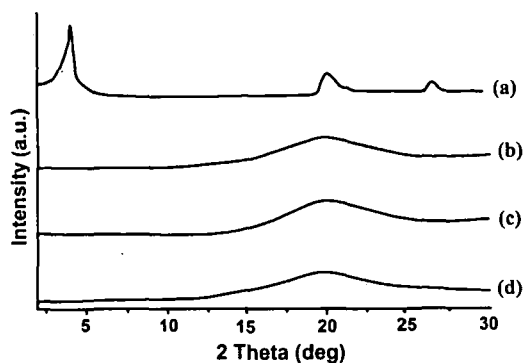


Fig. 3.11: XRD patterns for, epoxidized oil modified Araldite LY 250 nanocomposites (a) OMMT, (b) ECN1, (c) ECN2.5 and (d) ECN5

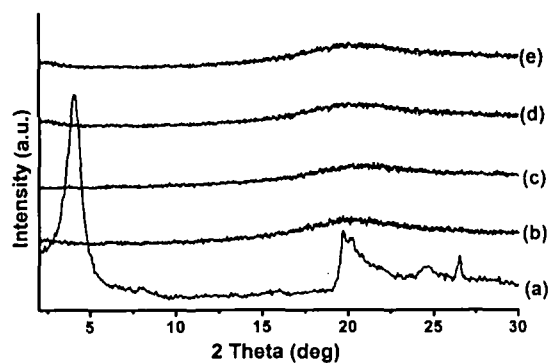


Fig. 3.12: XRD patterns for (a) OMMT (b) TBPAEN5, (c) TBPAEN2.5, (d) TBPAEN1 and (e) TBPAE

AMNO, the gallery cations reorient from their initial monolayer, lateral bilayer, or inclined paraffin structure to a more perpendicular orientation.^{23,32} The basal spacings suggest that an all *trans* configuration might be adopted by the alkylammonium chain. A related reorientation of alkyl ammonium ions has been observed previously for ϵ -caprolactam intercalated clay intermediates formed in the preparation of nylon-6-exfoliated clay nanocomposites.⁴⁷ Thus, the ability of the onium ion chains to reorient into a vertical position in order to optimize solvation interactions with the epoxy chains may achieve better layer separation upon intragallery polymerization in the nanocomposites.

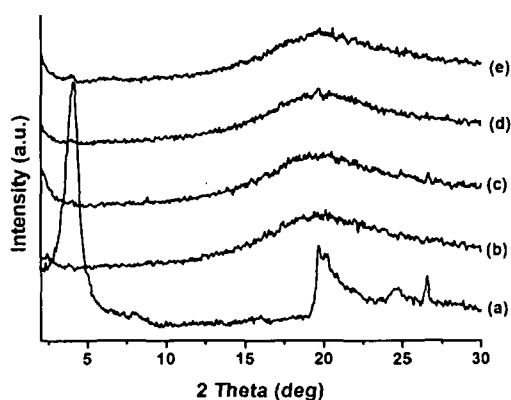


Fig. 3.13: XRD patterns for (a) MMT, (b) BPSE, (c) BPSEN1, (d) BPSEN2.5 and (e) BPSEN5

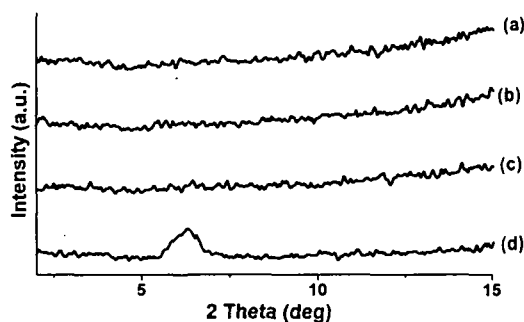


Fig. 3.14: XRD patterns for (a) ENMC1, (b) ENMC2, (c) ENMC3 and (d) ENC

The XRD spectra of hyperbranched polyurea modified OMMT nanocomposites are shown in Fig. 3.15. The spectra of the nanocomposites however showed no

basal reflection corresponding to the {001} plane (similar to the earlier cases).

The globular shape of hyperbranched modifying agent eases the insertion of epoxy chains into the clay galleries and its high surface functionality provides sites for interactions with clay and epoxy matrix. Several literatures described that insertion of polymer chain resulted an increment of gallery distance up to 8Å. Helical conformation or double layer planar zigzag disposition models are used to explain such phenomena.⁴⁸

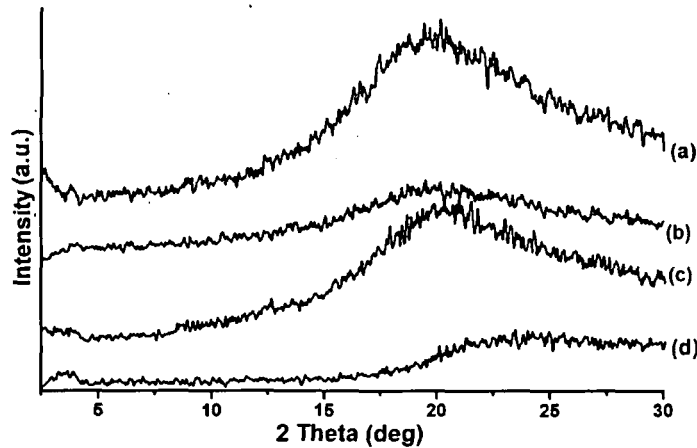


Fig. 3.15: XRD patterns for (a) MBPSE, (b) HBPA1, (c) HBPA3 and (d) HBPA5

This high interlayer spacing of clay surface end groups provide more wetting capacity of the epoxy chains to the clay layers through physical (such as hydrogen bonding, polar-polar interactions etc.) or chemical interactions. The interactions primarily occur through bridge loop and tail linkages of the polymer chains with the clay layers and consequently contributed to the formation of well dispersed clay layers.²⁶ The absence of Bragg scattering is the indication of delamination of the clay tactoids as the disappearance is not due to the limitation of the instrument since the concentration of clay in the matrix is in the range of detection and also there is no heavy element present in the systems.⁴⁹

However the exact distribution of the nanoclay in the epoxy matrix cannot be identified only XRD alone and hence the help of TEM is necessary.

3.3.5. Curing Study

The curing of the epoxy with the amine hardener is a well known process. Under the attack of amine group of the hardener the epoxy rings open up during the curing process, this in turn reduces the epoxide content of the resins dramatically. It was found that with the increase of Araldite LY 250 in the mixture of epoxidized oil and

commercial epoxy, the drying time decreases (Table 3.2). This may be due to the increase of epoxy functionality in the matrix i.e., due to higher epoxy content of commercial epoxy than the epoxidized oil. The long drying time of 100% ENO is due to very low epoxy value. However, decrease of curing time by the addition of ENO may be explained by the fact that because of much lower viscosity of ENO than Araldite LY 250 (Table 3.2), the dispersion and diffusion of the hardener is much better for crosslinking reactions. But again when the amount of ENO increases the curing time also increases as overall epoxy equivalent decreases. The long drying time of ENO indicates that *Mesua ferrea* L. seed oil based epoxy cannot be used as sole epoxy resin.

Table 3.2: Drying time of ENO modified Araldite LY 250/OMMT nanocomposites

Sample code	Touch free time (min)	Hard dry time (min)	Swelling (%)
ENO50	20	45	32
ECN1	18	45	29
ECN2.5	16	40	27
ECN5	15	35	24

The curing process of the epoxy/clay system is the crosslinking of linear macromolecules with a very complicated mechanism. The hydroxyl groups of the clay and the amine group of the hardener synergistically decrease the cure rate. It can be seen from Tables 3.2-3.4 that with the increase of clay loadings from 0 to 5 wt%, the curing rate as measured by touch free time and hard drying time decreases for ENO/Araldite LY 250/OMMT, TBPAE/OMMT and BPSE/OMMT nanocomposites. The specific intragallery onium ions can interact with reactants and precursors and can catalyze the epoxy curing reaction, thus leading to favorable curing conditions for obtaining exfoliated epoxy based clay nanocomposites.⁵⁰⁻⁵² The alkylammonium ions present in organoclay are most probably responsible for the catalytic acceleration of the epoxy curing reaction and thus enhancing the cure rate. Also, the catalytic effect of hydroxyl groups of nanoclay on the oxirane ring is also likely to play important role for this enhanced rate of curing.⁵³⁻⁵⁵

As discussed above the onium ion of the nanoclay plays a catalytic role in enhancing the cure rate wherein etherification via the cationic homopolymerization is initiated.⁵⁶ The onium ions may interact with reactants and precursors and thus catalyze

the epoxy curing reaction, leading to favorable curing conditions for obtaining exfoliated/intercalated epoxy based clay nanocomposites. Possibly, the high reactivity of the ammonium surface modifier of nanoclay in the nanocomposites increases the cure rate in proportion to nanoclay loading (touch free time).

Table 3.3: Drying time of TBPAE and nanocomposites

Sample code	Touch free time (min)	Hard dry time (min)	Swelling (%)
TBPAE	30	60	22
TBPAEN1	20	40	21
TBPAEN2.5	15	35	19
TBPAEN5	15	30	17

However, it is also possible that both the cationic and anionic sites of the clay could initiate polymerization, thereby aiding to decrease in the curing time. The curing reaction was also studied using only octadecyl amine to see the affect of the octadecyl amine on this process (Table 3.4). It was found that the presence of the amine affects the curing process. BPSE exhibited lower curing time when free octadecyl amine was taken than that of the nanoclay. This observation supports the above facts where decrease in curing time was observed with the increase of clay loadings of nanocomposites.

Table 3.4: Drying time of BPSE and nanocomposites

Sample code	Touch free time (min)	Hard dry time (min)	Swelling (%)
BPSE	35	60	25
BPSEN1	30	40	22
BPSEN2.5	20	35	20
BPSEN5	15	30	13
BPSE0	23	32	24

The curing characteristics of MBPSE and its nanocomposite with OMMT, OMMT modified by AMNO, MMT modified AMNO, MMT and mMMT are shown in Table 3.5. From Table 3.5 it can be seen that ENMC1 took the lowest and the pristine took the highest time for curing. The mechanisms for this increase rate might involve

hydrogen transfer from the donor to the epoxy, or hydrogen bonding of both the epoxy and the amine. These long-chain alkylammonium exchanged montmorillonite co-intercalated by AMNO provides a hydrophobic environment for the hardener to migrate into the clay interlayer region. Under the curing conditions more epoxy and hardener penetrate the gallery space and intragallery polymerization can occur at a rate that is comparable to extragallery polymerization. However, considerable interaction of the hydroxyl containing material with the reactants may accelerate the epoxy/diamine curing in all the cases.

Table 3.5: *Drying time of MBPSE and nanocomposites*

Sample code	Touch free time (min)	Hard dry time (min)	Swelling (%)
MBPSE	50	80	30
ENMC1	34	30	15
ENMC2	38	35	17
ENMC3	40	47	21
ENC	47	65	26

3.3.6. SEM Study

SEM is an essential tool for illuminating the distribution pattern of the nanoclay in the polymer matrix. SEM micrographs (Figs. 3.16-3.18) indicate uniform distribution of clay particles in the matrix.

Figs. 3.16-3.18 show the SEM micrographs of the surfaces corresponding to ENO/Araldite LY 250/OMMT, TBPAE/OMMT and BPSE/OMMT nanocomposites. It was seen that the surface of the pure epoxy is rather smooth and no significant amount of roughness was present. Whereas in case of nanocomposites some tiny white lines from the surface were found bulging out. In other words, the nanoclay present inside the epoxy acted like grid lines. When the weight percentage of nanoclay inside the epoxy samples was increased, the number of grid lines also seems to increase. Consequently, with the incorporation of the nanoclay the surface becomes rough indicating that clay layers has been dispersed uniformly in the matrix.⁵⁷

Fig. 3.19 shows the SEM micrographs of the surfaces corresponding to ENMC1, ENMC2, ENMC3 and ENC nanocomposites. From the images it can be seen that there is uniform distribution of the clay layers in the polymer matrix. ENMC1 showed the best dispersion of the clay in the matrix among the studied nanocomposites.

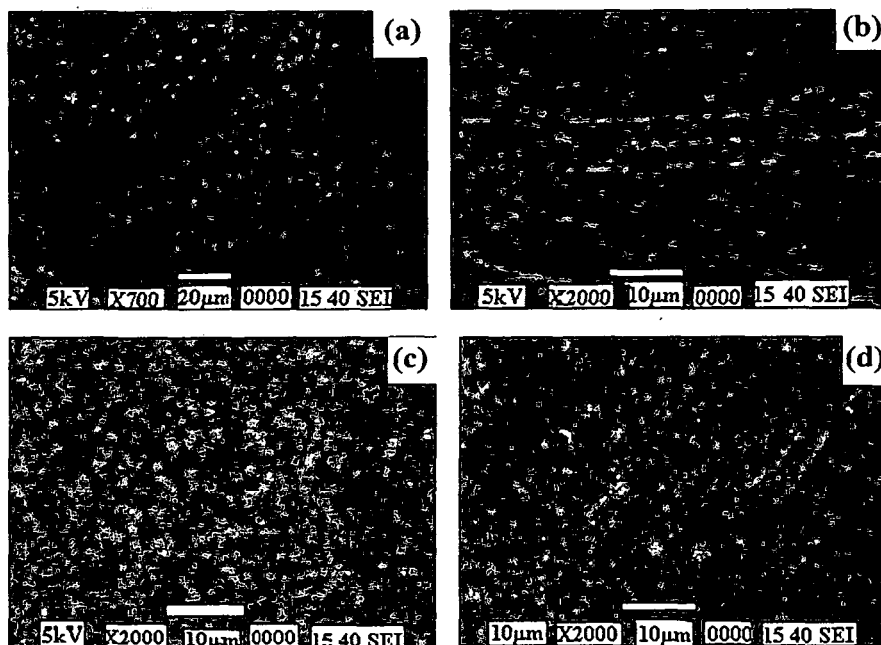


Fig. 3.16: SEM micrographs for (a) ENO50, (b) ECN1, (c) ECN2.5 and (d) ECN5

The clay layers were delaminated in the matrix. The formation of exfoliated clay nanocomposites is dependent on the nature of the alkylammonium exchanged clays. The presence of longer linear alkyl chains of *Mesua ferrea* L. seed oil facilitated the formation of exfoliated nanocomposite. Thus, the exfoliation of the clay is caused by intragallery polymer formation. In the case of AMNO modified bentonite, the hydrophobicity of the galleries is relatively low, and the amount of intercalated epoxide is insufficient to achieve exfoliation.

Fig. 3.20 shows the representative SEM images of the nanocomposites of the MBPSE and hyperbranched polyurea modified OMMT. Several factors such as chemical miscibility of the two components, method of mixing, interfacial interaction and crosslinking density affects the morphology of a two-component system at a given composition. The SEM image of the HBPA3 (Fig. 3.20) revealed uniform distribution of the clay layers in the epoxy matrix. The good dispersion results from the extensive interaction of hydroxyl groups of the clay layers with hydroxyl and ester groups of epoxy resin along with normal crosslinking of hydroxyl or epoxy groups of MBPSE by poly(amido amine) hardener. Along with this, there is the possibility of hydrogen-bonding between $-C=O$ of polyurea with the $-OH$ group of epoxy resin. Thus, the amine hardener acted as a compatibilizing agent for these systems. The SEM image of HBPA3 showed an uneven surface morphology, wherein some protruding white dots or lines can be visualized on the surface. Observation of protruding dots or lines indicated

that the embedded clay layers were well adhered to the polymeric surface. As observed for the pristine polymeric system the surface is rather smooth. The thicknesses of the ribbon like lines in the nanocomposites are in the range of a few nanometers.

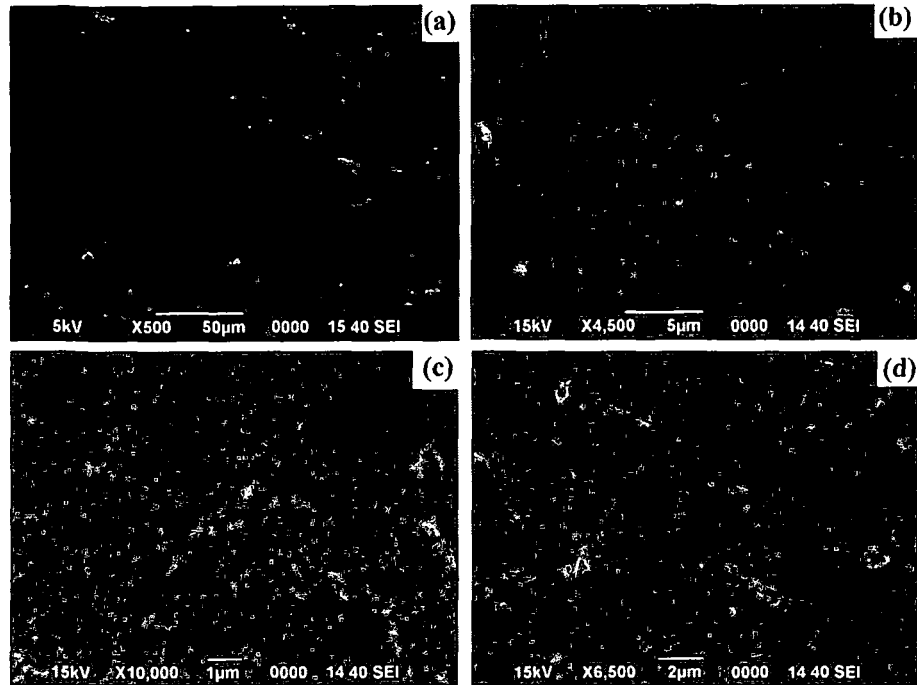


Fig. 3.17: SEM micrographs for (a) TBPAE, (b) TBPAEN1, (c) TBPAEN2.5 and (d) TBPAEN5

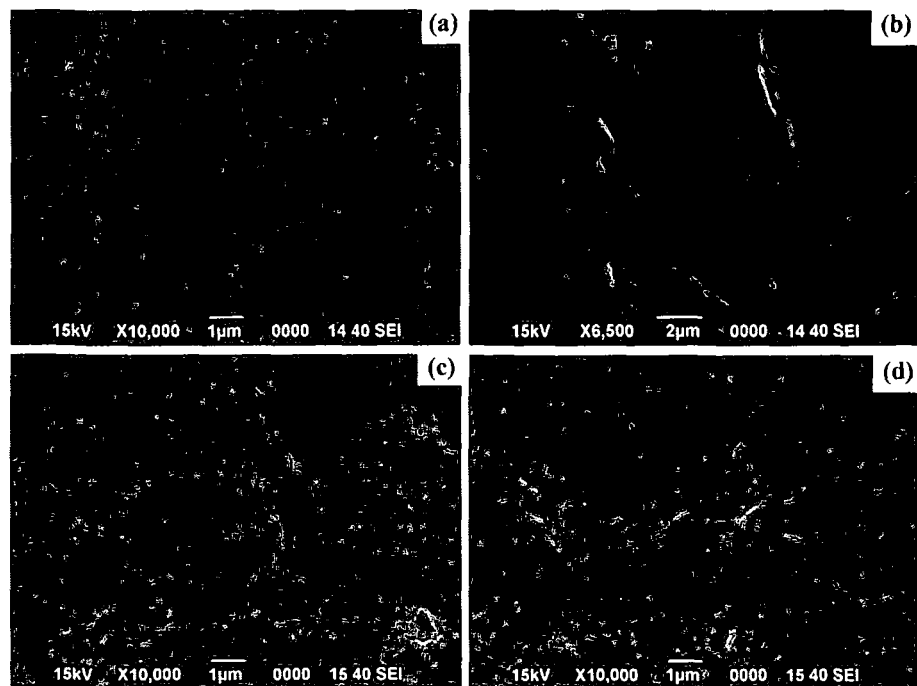


Fig. 3.18: SEM micrographs for (a) BPSE, (b) BPSEN1, (c) BPSEN2.5 and (d) BPSEN5

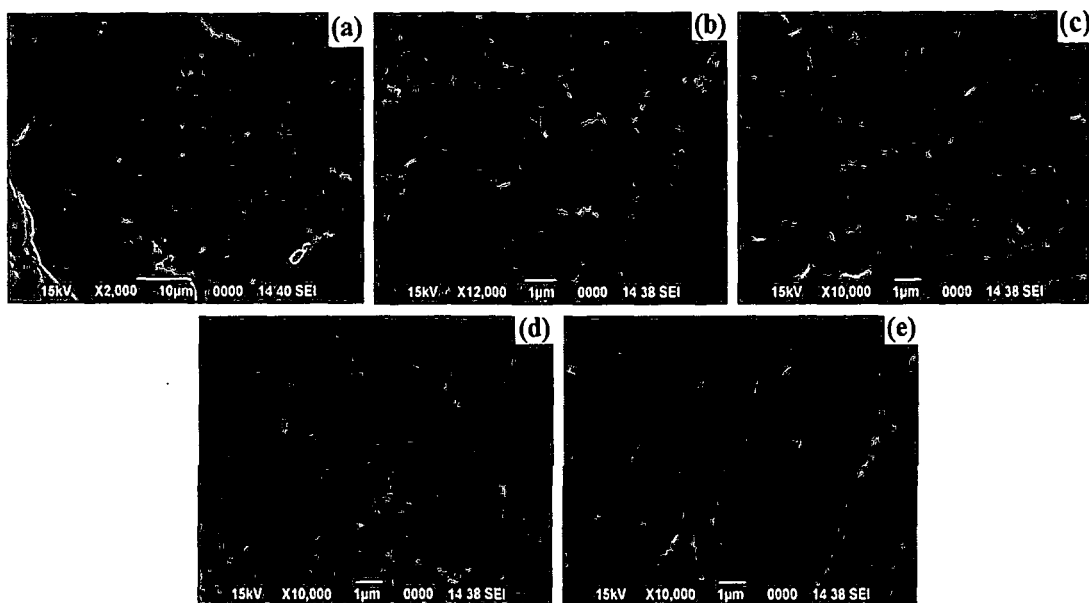


Fig. 3.19: SEM micrographs for (a) MBPSE, (b) ENMC1, (c) ENMC2, (d) ENMC3 and (e) ENC

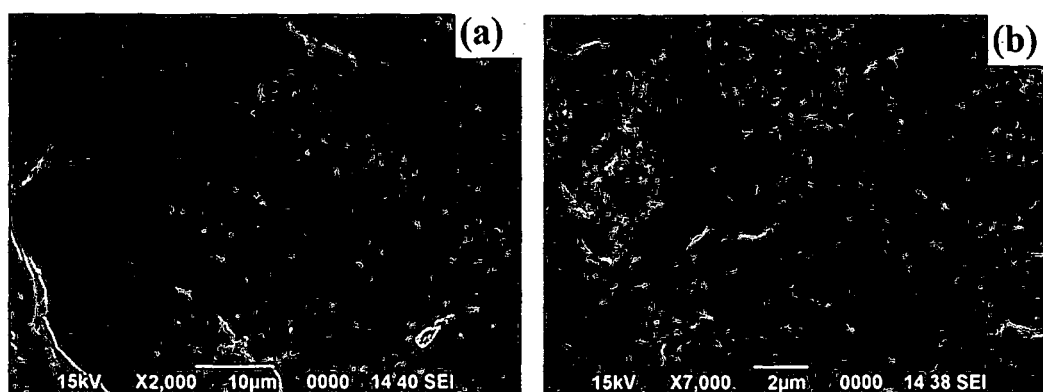


Fig. 3.20: SEM micrographs for (a) MBPSE and (b) HBPA3

3.3.7. TEM Study

TEM technique is necessary to confirm the state of dispersion of nanoclay in the matrix i.e. to understand the actual pattern of nanoclay layers dispersion and to evaluate visually the degree of intercalation, exfoliation and aggregation of the clay clusters and confirm the XRD results in the polymer matrix, so the TEM micrographs of the nanocomposites were recorded.

Figs. 3.21-3.23 show the TEM micrographs of ECN2.5, TBPAEN2.5 and BPSN2.5. The dark lines in the figure correspond to the silicate nanolayers. From the micrographs it can be seen that the clay was uniformly distributed in the polymer matrix with layer thickness of 5-10 nm. Thus TEM confirmed the partially exfoliated structure formation of nanoclay in the nanocomposites.



Fig. 3.21: TEM micrograph for ECN2.5

The good dispersion of the clay platelets in epoxy matrixes was achieved possibly due to use of high mechanical shear force and sonication. Layer spacing of the layers in the nanocomposites increases, wherein in some cases exfoliated structure were obtained. Thus coexistence of both partly intercalated and exfoliated clay layers can be visualized in the epoxy matrix.

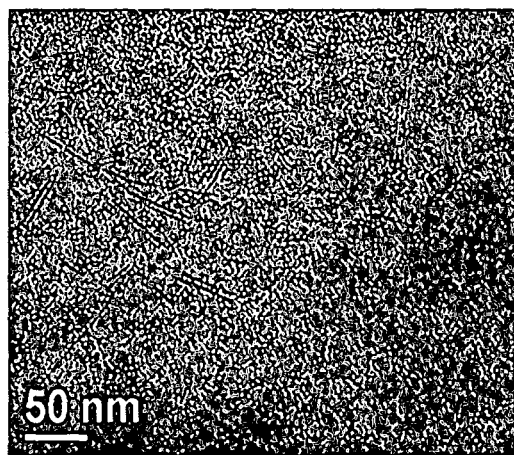
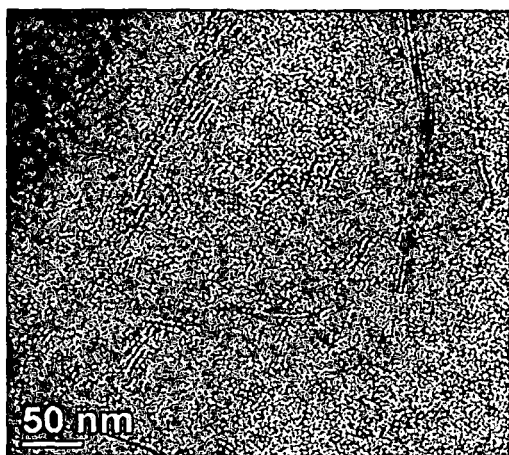


Fig. 3.22: TEM micrograph for TBPEN2.5 Fig. 3.23: TEM micrograph for BPSEN2.5

The curing agent, the curing temperature, and the amount and chemical structure of the onium ions can influence the exfoliation process. Additionally during curing, the viscosities raises to very high values through crosslinking and network formation which produces a rigid structure. Thus, further expansion of the interlayer space is hindered and a mixture of exfoliated and intercalated nanostructure is obtained rather than full exfoliation.⁵⁷ Fig. 3.24 shows the representative micrographs of ENMC1 and ENMC3. As discussed above the visibly dark lines in the figure corresponds to the silicate nanolayers. A good dispersion of the clay platelets was achieved in case of

ENMC1. The coexistence of both intercalated and exfoliated type structure can be visualized in the epoxy matrix.

The formation of partially exfoliated clay nanocomposites is dependent on the nature of the alkylammonium exchanged clays. The alkyl chains of *Mesua ferrea* L. seed oil facilitated the formation of partially exfoliated nanocomposite. Whereas for mMMT, the hydrophobicity of the galleries is relatively low, and the amount of intercalated epoxide is insufficient to achieve exfoliation. Therefore, only a portion of the clay was delaminated as evident from the TEM micrographs. Inorganic bentonite is hydrophilic and not readily swelled by epoxy monomers, making intragallery polymerization impossible. Therefore, a conventional type phase-separated composite was formed.

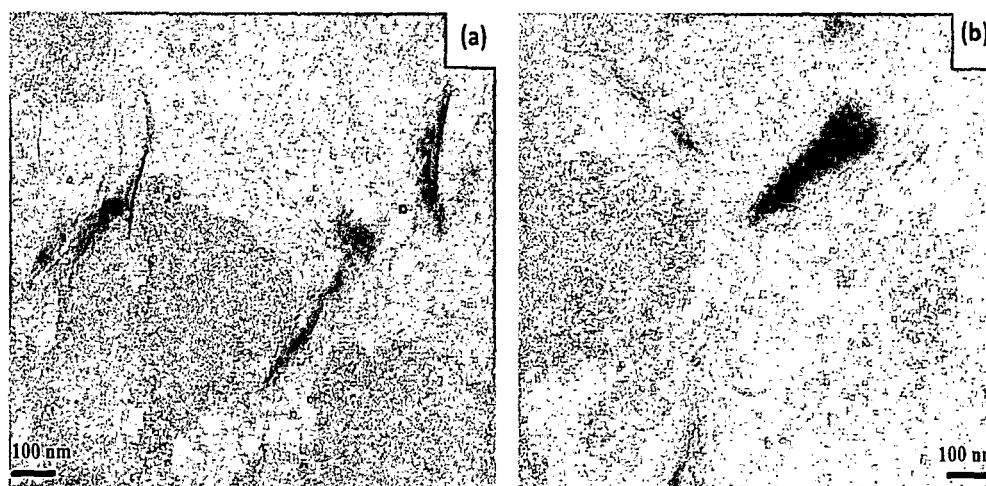


Fig. 3.24: TEM micrographs for (a) ENMC1 and (b) ENMC3

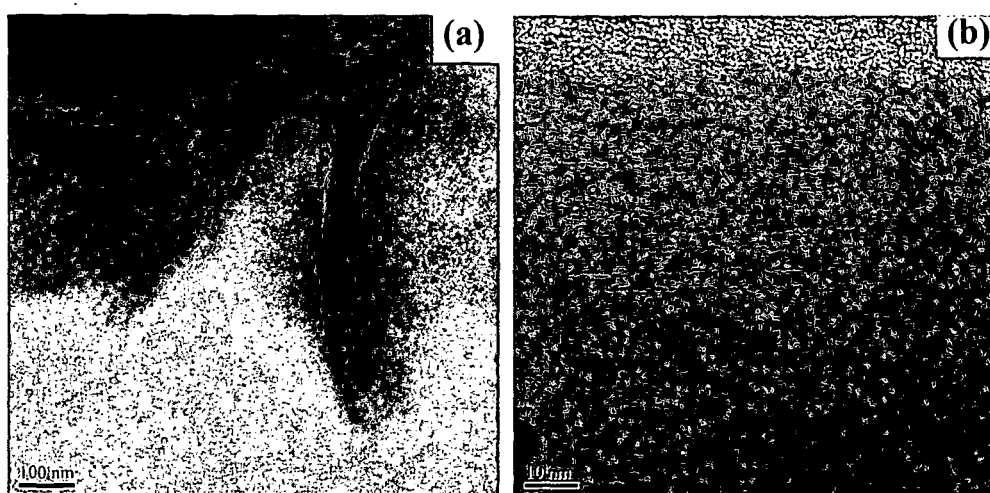


Fig. 3.25: TEM micrographs for HBPA3 at (a) 100 nm and (b) 10 nm scale

The TEM micrograph of HBPA3 exhibited a partially delaminated morphology in which partially exfoliated as well as intercalated structure exists (Fig. 3.25). Thus, the TEM micrographs confirmed the fine dispersion of the nanoclay in the epoxy matrix.

3.3.8. Rheological Behaviors

The variation of viscosity of the resins with time for ENO, ENO50 and ECN2.5 shows that the resin and the nanocomposite systems before curing exhibited a Newtonian fluid like behavior (Fig. 3.26). The viscosity of the Araldite LY 250 drastically decreases

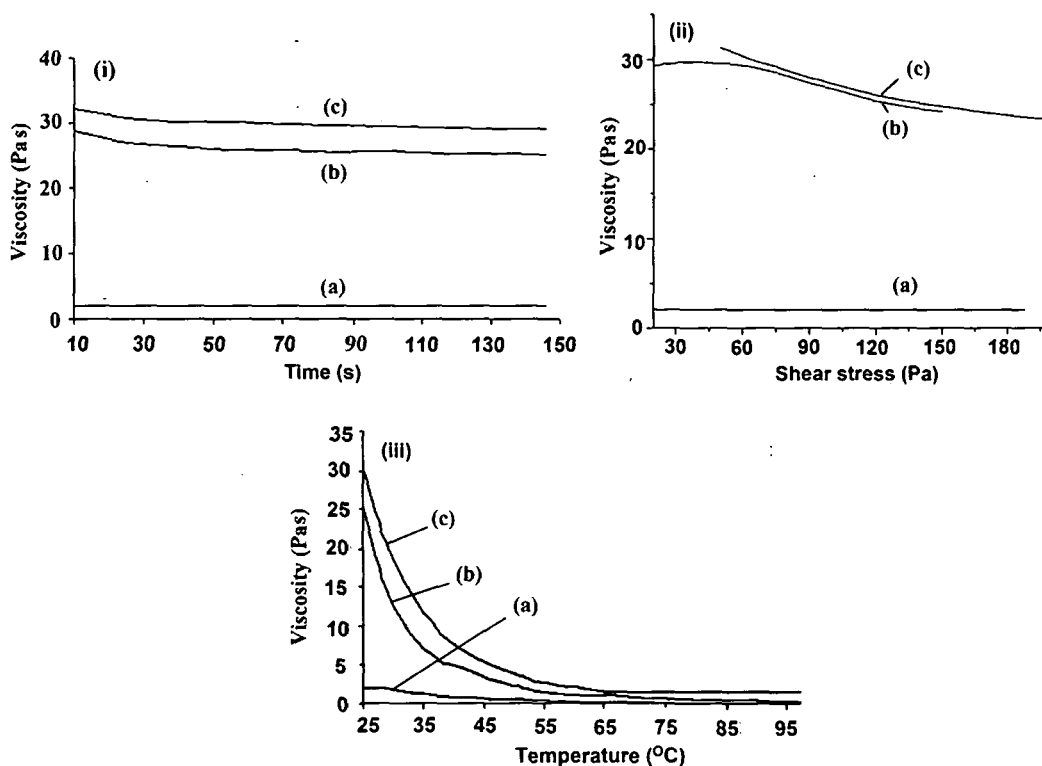


Fig. 3.26: Rheological characteristics of ENO modified Araldite LY 250 nanocomposites (a) ENO100, (b) ENO50 and (c) ECN2.5

with the addition of ENO, which supported the fact that the epoxidized oil can act as a reactive diluent for commercial epoxy resins. The rheological characteristics of the ENO/Araldite LY 250/OMMT, TBPAE/OMMT, BPSE/OMMT and MBPSE and OMMT, AMNO modified OMMT, AMNO modified MMT and mMMT nanocomposites are shown in Figs. 3.26-3.29. The rheological characteristics were studied for variation of viscosity against time, shear stress and temperature. It can be seen that the TBPAE, BPSE and MBPSE exhibited Newtonian like behavior. The viscosity showed an increase in trend with the clay loadings for TBPAE and BPSE and for MPBSE, the type of clay controls the viscosity, however, the nanocomposites still

exhibited Newtonian behavior (Figs. 3.26-3.29 (i)). ECN5, TBPAEN5, BPSEN5 and ENMC1 exhibited the highest viscosity among the different systems studied for their

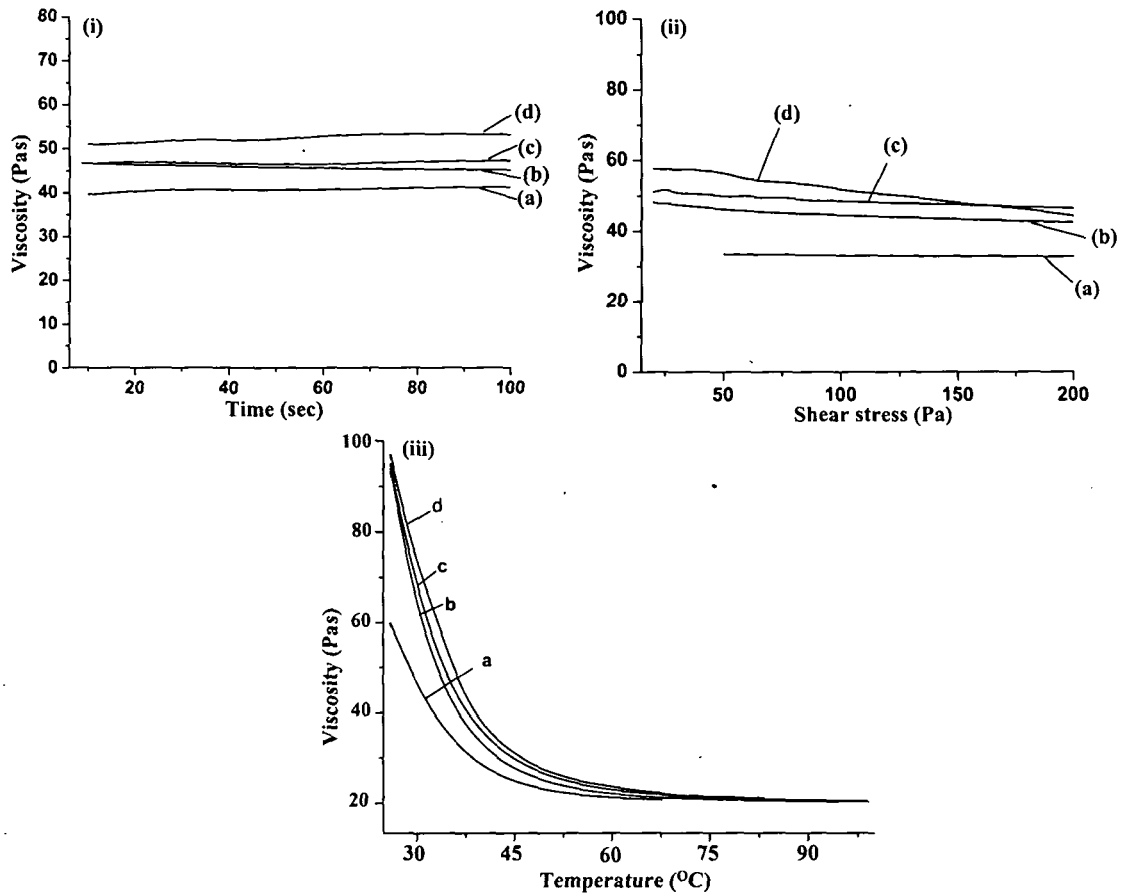


Fig. 3.27: Rheological characteristics of (a) TBPAE, (b) TBPAEN1, (c) TBPAEN2.5 and (d) TBPAEN5

respective cases. Due to uniform distribution (as shown by the SEM images) of the clay and its high aspect ratio the viscosity showed an increase in value.

The enhancement may also result from the interaction of the high surface functionalities of clay with the functional groups of TBPAE and BPSE (epoxy or ester or hydroxyl). Also matrix/clay interaction leads to the formation of an interphase and has the same effect as increase in clay content. For ENMC1 the enhanced viscosity is mainly attributed to the improved nanoscaled structure of clay tactoids, indicating that presence of AMNO is propitious to the well dispersion of clay.

Figs. 3.26-3.29 (ii) show the variation of viscosity with shear stress (20-200 Pa). It was observed that there was a slight decrease in viscosity in each case, however the decrease is negligible. This is due to good interaction of the clay layers with the polar functionality of the matrix and hence offers resistance to the applied force. This

prevents the preferential orientation and alignment of the silicate layers and the polymer chains to the direction of the flow.⁵⁸ The result indicated partially exfoliated structure associated with a good dispersion of the clay platelets which is then consistent with rheological results.⁵⁸⁻⁶⁰

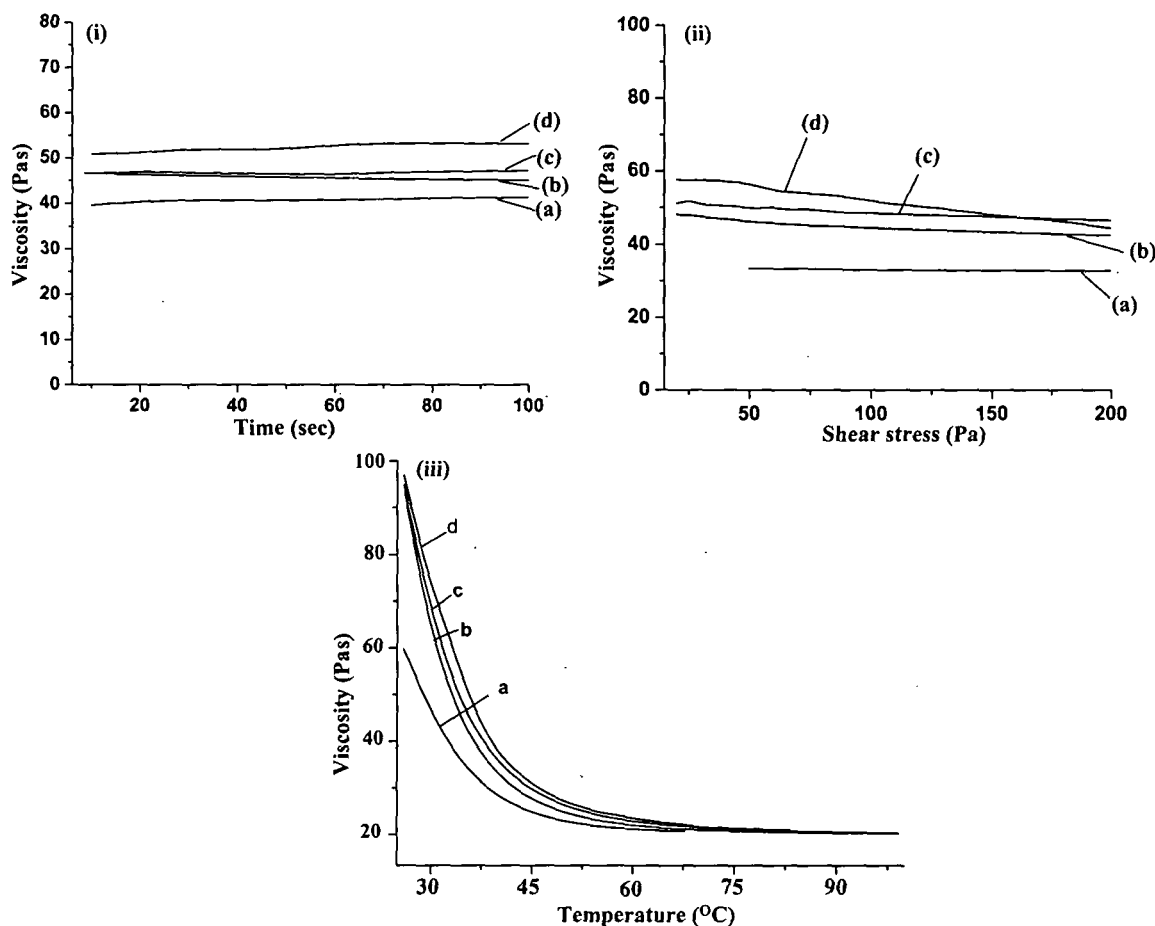


Fig. 3.28: Rheological characteristics of (a) BPSE, (b) BPSEN1, (c) BPSEN2.5, and (d) BPSEN5

The dependences of flow properties of the nanocomposites with respect to temperature are shown in Figs. 3.26-3.29 (iii) respectively. The temperature sensitivity of the shear viscosity has a profound effect on the choice of processing conditions. As can be seen from the figure shear viscosities of pure ENO50, TBPAE, BPSE, MBPSE and their nanocomposite decreases with the increase of temperature in the range of 25-100 °C at shear stress of 20 Pa, indicating that the increase of temperature improved the flow behavior of the system.

However, the effect of temperature on shear viscosity changes with the shear rate. It has been found that the temperature sensitivity of shear viscosity was higher in

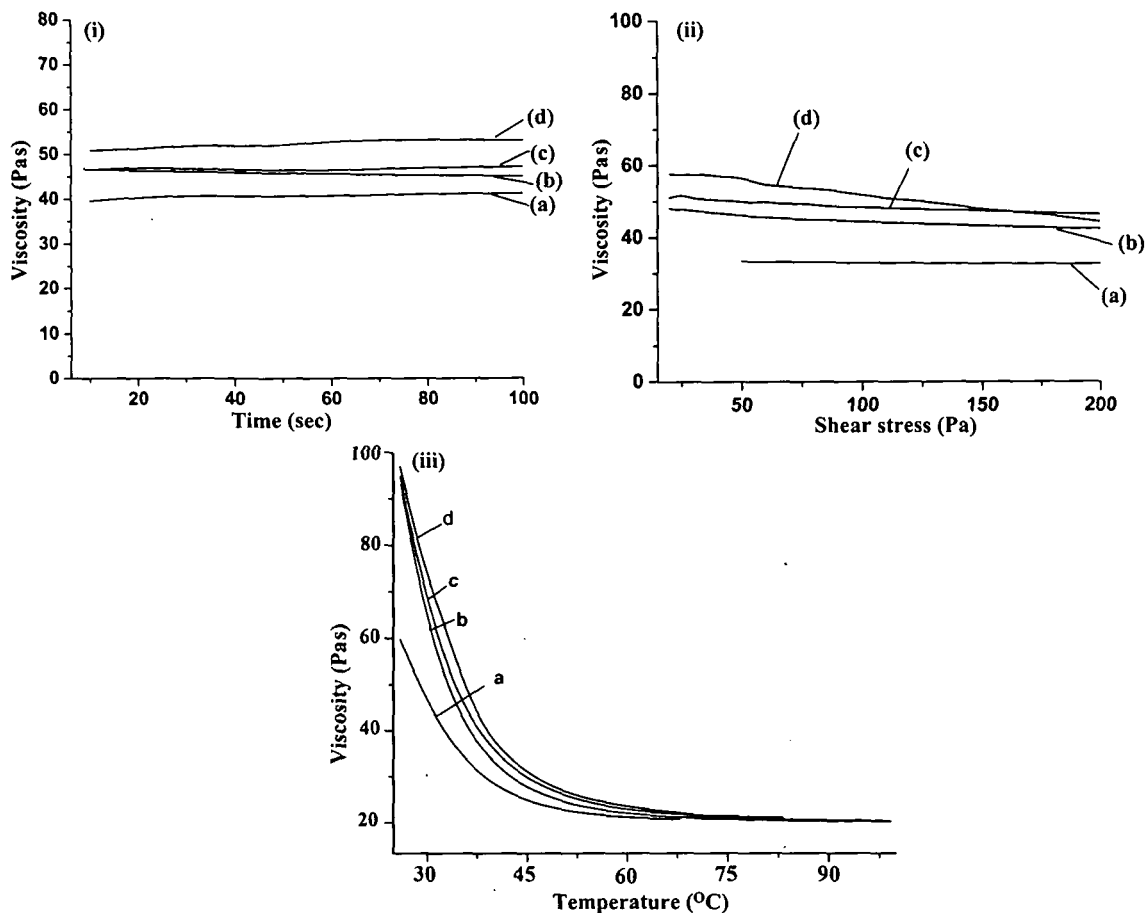


Fig. 3.29: Rheological characteristics of (a) MBPSE, (b) ENMC1, (c) ENMC2, (d) ENMC3 and (e) ENC

lower shear rate region, and drops at higher shear rates. This phenomenon is in agreement to the fact that elevating shear rate always accompanies by a rapid decrease of the entanglement density of macromolecules and the viscosity.⁵⁸

The hyperbranched polyurea modified OMMT/MBPSE nanocomposites showed a linear variation of viscosity with time indicating a Newtonian like flow behavior. The viscosity enhances after addition of hyperbranched polyurea modified OMMT (Fig. 3.30), the increased gallery spacings facilitates more matrix to nanoclay interactions. Further the presence of hyperbranched polyurea may interact with the MBPSE aiding to the enhancement.

The viscosity showed pseudoplastic like behavior with increase in the shear stress. However at higher shear value the viscosity becomes linear. The shear thinning behavior can be related to the unentanglement of the polymer chain when shear force was applied.

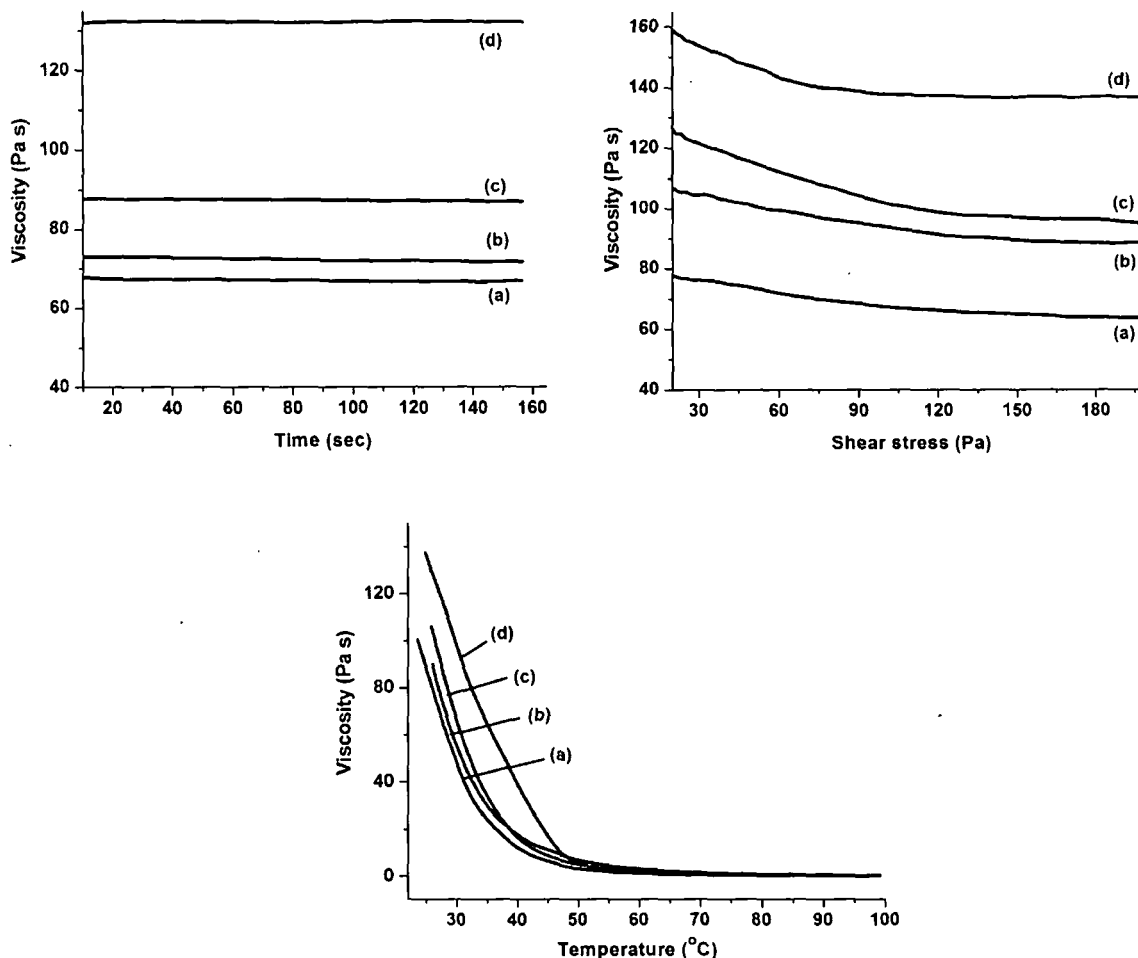


Fig. 3.30: Rheological characteristics of (a) MBPSE, (b) HBPA1, (c) HBPA3, and (d) HBPA5

Similar to the above cases the viscosities showed a decrease in trend with increase in temperature for hyperbranched polyurea modified OMMT nanocomposites. With the increase in temperature when shear force was applied, the interaction between the matrix and the filler decreases. As a result the shear flow can induce an increase of distance between filler particles or between the filler and resin matrix, resulting in destruction of the secondary bonds. Consequently, the array of particles becomes directional and the viscosity decreases.

3.3.9. Performance Characteristics

The performance characteristics such as impact resistance, scratch resistance, gloss, tensile strength and adhesive strength for ENO50/OMMT nanocomposites, TBPAE/OMMT nanocomposites, BPSE/OMMT nanocomposites, MBPSE/OMMT, mOMMT, mMMT, MMT and hyperbranched polyurea modified OMMT are given in Tables 3.6, 3.7, 3.8, 3.9 and 3.10 respectively.

For epoxidized oil modified Araldite LY 250 (Table 3.6) it was found that with the increase of the epoxy content in the mixture the impact resistance increases.

The incorporation of ENO provides flexibility to the film, hence the applied energy is absorbed by distribution throughout the matrix, which improved the impact resistance of the resulting materials. The tensile strength has been found to marginally increase with the amount of the Araldite LY 250 in the modified epoxy resins up to 50% dilution but at 75% dilution the strength property decreases a little due to low crosslinking density, as the epoxy equivalent of ENO is low. The increase in the tensile properties and the hardness can be explained from the fact that ENO helps in diffusion and uniform crosslinking by the hardener of the films.

The modified epoxy showed good adhesive characteristics with the incorporation of ENO may be due to polar functional groups, which promote the binding to the cellulosic plywood substrate. Also diffusion increases with ENO content in the materials which increases mechanical interlocking with the substrate. The gloss of the modified resin exhibited an improvement over the pristine resin. These improvements may be due to the better compatibility of the two components, higher crosslinking and smoothness of the surface compared to the pristine system.

The improvement of performance characteristics was observed through the formation of nanocomposites, though the rate of improvement up to 2.5 wt% was much better than at 5% loading. The improvement of properties resulted from the significant interaction of nanoclay particles with epoxy resin and this is facilitated by the presence of reactive diluent epoxidized oil. The improvement of tensile strength was almost double even at dose level of 2.5 wt% of nanoclay, which is a significant achievement from this study. Furthermore the elongation at break and impact resistances are also improved significantly which are rare to achieve. This may be due to diffusion of epoxy in the gallery of nanoclay by the presence of flexible diluent epoxidized oil compared to pristine system. This is also supported by adhesive strength value, where the increment is also significant.

The mechanical properties of TBP AE and BPSE (Table 3.7 and 3.8) exhibited enhancement on incorporation of nanoclay. The homogeneous dispersion of the individual layers shows an effective reinforcement to the polymer matrix. The nanodispersed clay with a high aspect ratio provides a higher stress-bearing capability and efficiency. Stronger interactions between nanoclay layers and the polymer chains as indicated by FTIR analysis (discussed in the previous section) associated with a

Table 3.6: Performance characteristics of ENO modified Araldite LY 250 nanocomposites

Sample code	Araldite LY 250	ENO25	ENO50	ENO75	ECN1	ECN2.5	ECN5
Tensile strength (MPa)	6.9	7.04	7.16	4.55	10.73	11.18	11.4
Elongation at break (%)	1.23	6	16.21	19.29	64.12	59.26	96.40
Impact resistance (cm)	>100	>100	>100	6	>100	>100	>100
Gloss (60°)	50.2	64.7	62.0	54.3	65.1	74.3	72.0
Adhesion (Nm ⁻¹)	684.2	1138.4	800.4	730.3	629.7	757.7	425.5
Scratch resistance (kg)	1.0	0.6	2.5	0.1	3	4	5.5

larger contact surface result in effective constraint of the motion of the polymer chains. It is believed that the presence of more polar groups and ionic interaction between polymer chains and silicate layers increased the tensile strength of the nanocomposites. The increase in the elongation at break with the increase of clay content may be caused by the presence of long hydrocarbon chains and the internal bond strength rather than crosslinking density. Elongation of polymers is a property influenced more seriously by chain breakage than chain slippage.⁵⁸

The scratch resistance also showed an increase in trend for the different weight percents of the clay loading. For 5 wt% of clay loading exhibited the highest value, the stiffness of the clay layers contributes to the presence of immobilized or partially immobilized polymer phases. It is also possible that the molecular orientations as well as clay layers contributed to the observed reinforcement effects. This altogether resulted in a tough surface that becomes more difficult for making any penetration or indentation.⁶⁰

The value of the impact resistance remained almost constant for all concentration of clay. This may be due to the fact that clay particles act as crack stoppers and form a tortuous crack propagation path and the presence of long flexible hydrocarbon chain of fatty acid moiety resulted in impact resistance almost same as the neat polymer. There may be some amount of the polymer chains of the polymer matrix that is physisorbed

Table 3.7: Performance characteristics of TBPAE and its OMMT nanocomposites

Sample code	TBPAE	TBPAEN1	TBPAEN2.5	TBPAEN5
Tensile strength (MPa)	5.99	7.52	10.31	12.14
Elongation at break (%)	83.60	54.15	40.34	45.5
Impact resistance (cm)	100	100	100	100
Gloss (60°)	67.0	69.6	78.8	80.0
Adhesion (Nm ⁻¹)	98.94	117.6	289.6	300.2
Scratch hardness (kg)	3.5	5	5	6

on the silicate surface, and is thus stiffened through its affinity for and adhesion to the filler surface. Thus the applied load to the polymer is transferred to the clay. However due to the limitations of the instrument further measurement of impact resistance was prevented. The gloss value of the nanocomposites increased with nanoclay content, the improved gloss characteristics of the film can be correlated to the good crosslinking of the cured films which results in a smooth surface. As large amount of light is being reflected from the surface due to the smooth texture, so the gloss value increases with the clay content in this case.

The adhesive strength of the nanocomposites was found to increase with the loading of clay (Table 3.7 and 3.8). The adhesive strength of the systems is due to the presence of large numbers of functionality (epoxy/hydroxyl/ester/amine/amide) of TBPAE and BPSE in the systems, which are interacting with the substrate. Uniformly dispersed nanoparticles may have some effects on the physical and chemical properties of the adhesion for epoxy adhesive. They provided stronger anchoring and hence increased adhesion strength by virtue of their positioning in the surface asperities of the wood surfaces. Also the increment of adhesive strength is due to the strong interactions of polar hydroxyl, epoxy, ether and other polar groups of the TBPAE, BPSE and clay with the hydroxyl groups of the substrate. The interactions are through hydrogen bonding, polar-polar and polar-induced-polar interactions, or/ and chemical bond formation. BPSE also shows good adhesion on to the metal substrate. Virtually all common metal surfaces exist as hydrated oxides. Thus the adhesive used for these materials must firmly interact with the metal oxide layer. The plausible explanation for good adhesion on to the steel substrate may be due to better interlocking and formations of secondary bonds with the rough surface of metal. Good adhesive

characteristics on the glass substrate may result due to better interaction of the nanoclay with the hydroxyl functionality on the glass surface through polar-polar or hydrogen bonding interactions.⁶¹

The mechanical properties of MBPSE and its nanocomposites are shown in Table 3.9. ENMC1 showed the highest tensile strength among the other systems (Table 3.9). The efficiency of clay in the reinforcement of polymer systems is dependent on their degree of dispersion in the organic medium. Better the dispersion of the clay layers in the matrix, greater is the surface area available for interaction with the polymer matrix, higher will be the strength. As discussed above the improved tensile strength of ENMC1 can be attributed to good dispersion of the clay in the matrix. The presence of

Table 3.8: Performance characteristics of BPSE and its OMMT nanocomposites

Sample code	BPSE	BPSN1	BPSN2.5	BPSN5
Scratch hardness (kg)	2.7	4.3	5.5	6.5
Tensile strength (MPa)	4	5.7	7	11.4
Elongation at break (%)	70	90	95	97
Gloss (60°)	55	63	70	77
Adhesion (Nm ⁻¹)	90	112	180	250

high functionality in mOMMT increases the interactions between the silicate layers and the epoxy matrix by hydrogen bonding or ionic bonding. This subsequently increases the tensile strength of the ENMC1.⁶² ENMC2 exhibited higher tensile strength than ENMC3.

The onium ion of the octadecyl amine has better intercalation ability than onium ion of AMNO. As seen from the XRD studies, mMMT has lower interlayer spacing compared to OMMT. Thus the interaction of OMMT with the epoxy chains is more than mMMT with epoxy (as can be seen from the XRD results, section 3.3.4.2). As a result ENMC2 has better interfacial reinforcing ability that leads to greater load bearing capability compared to ENMC3. However, ENC has tensile strength lower than the pristine polymer. This reduction in tensile strength is attributed to the stress concentration, which arises by the agglomeration of clay. The elongation at break remains almost unaffected in all the cases, though a slight increase was observed in the case of ENMC1. The presence of long hydrocarbon chains and the internal bond

Table 3.9: Performance characteristics of MBPSE and its *m*OMMT, OMMT, *m*MMT and MMT nanocomposites

Sample code	MBPSE	ENMC1	ENMC2	ENMC3	ENC
Tensile strength (MPa)	6	10	8.2	7.2	4
Elongation at break (%)	95	97	96	95	85
Impact resistance (cm)	100	100	100	100	90
Gloss (60°)	60	74	70	64	57
Scratch hardness (kg)	3.4	6.2	5.3	4.7	3.5

strength rather than crosslinking density aids to the increase in elongation value. Elongation is a property influenced more seriously by chain breakage than chain slippage. For ENMC1 the increase in scratch hardness may be attributed to the better dispersion of the clay in the matrix. In other words, with the gap between layers widening due to the AMNO modification of OMMT, the amount of epoxy inserted between layers also increases. This results in high interfacial adhesion between clay and the MBPSE matrix. Thus the uniformly distributed clay layers (as seen from SEM images) in the matrix with large surface areas would alter the local stress of surrounding matrix. This effective crack deflection by the clay platelets thereby increases the toughness of the matrix. This altogether resulted in a tough surface that becomes more difficult for making any penetration or indentation. The scratch hardness of ENC decreases compared to the pristine polymer, the presence of agglomerated structure of the nanofiller results in low scratch hardness. The impact resistance for all the nanocomposites including pristine system reached the maximum limit of the used instrument (maximum height of 100 cm). These results indicate that as such there is no deterioration of impact resistance by nanocomposites formation.

The gloss characteristics of the nanocomposites was also been found to increase significantly for ENMC1, ENMC2 and ENMC3, the improved gloss characteristics of the film can be correlated to the good crosslinking of the cured films (as supported by swelling data, Table 3.9) which results in a smooth surface. As large amount of light is being reflected from the surface due to the smooth texture, so the gloss value increases with the clay content in this case (Table 3.9).

Table 3.10 explicates the effect of the hyperbranched polyurea modified nanoclay on mechanical properties of MBPSE. The well dispersed nanoclay provides extensive filler to matrix wetting characteristics resulting in high interfacial interaction, this

behavior enhances with nanoclay loading. The nanocomposites showed an increment of tensile strength about 247 percent for 5 wt% of nanoclay loading. The interactions between surface modifier of nanoclay and epoxy chains per unit volume increase significantly with the intercalation of nanoclay because of high aspect ratio of the nanofiller. This feature of nano effect of reinforcing agent has a great influence on mechanical properties of polymers. The effect of formation of nanocomposite on elastic properties is much more than viscose properties under exfoliated condition. This leads the material to a solid-like behavior. Thus the applied stress can be effectively transferred to the nanoclay. On the other hand, the increased stiffness reduces the elongation at break value of the nanocomposites as can be observed with the increase of modified nanoclay loading. The addition of nanoclay has a pronounced effect on the hardness as measured by scratch hardness. The result revealed that all coatings have good adhesion to the substrate. The scratch hardness of a coating depends on several factors viz. mechanical properties of the coating, thickness, the friction between the indenter and the speed of the indenter etc.

The thickness of all the coating ranges between 60-70 micron, the friction between the coating and the indenter is largely control by the scratch velocity, however in this study the scratch velocity was kept constant (i.e. 6 mm/sec) and the load was varied. The stress generated at the tip interface and the coating surface is greatly reduced when nanoclay is present in the matrix. As discussed earlier there is good interaction between the clay and matrix. Thus the stress generated by the movement of the tip is partly absorbed by the hard silicate layers. At critical load the nanocomposites exhibits ductile ploughing. The deformation at low load is generally elastic type whereas at high load

Table 3.10: Performance characteristics of MBPSE and hyperbranched polyurea modified OMMT nanocomposites

Sample code	MBPSE	HBPA1	HBPA3	HPBA5
Tensile strength (MPa)	6	8.69	14.07	22.47
Elongation at break (%)	95	40.7	33.8	27.1
Impact resistance (cm)	100	90	87	65
Gloss (60°)	60	65	70	75
Scratch hardness (kg)	3.4	6	10	10

more plastic type deformation was observed. The impact resistance of the nanocomposites was observed to decrease with nanoclay loading. The decrease in the

impact resistance of the nanocomposites is mainly due to brittle fracture. The gloss characteristics of the nanocomposites were found to enhance with nanoclay loading similar to the earlier cases. The surface enhancement results in large amount of reflected light, and the gloss measured at 60° angle increases with nanoclay loading.

3.3.10. Thermal Study

The thermal stability of the polymer nanocomposites plays a vital role in determining the processing, as it affects the final properties of the materials. For the development of advanced materials it is necessary to study to thermal properties of the materials.

ENO50 exhibited a decrease in the initial thermal degradation temperature compared to Araldite LY 250 (Fig. 3.31). However with the incorporation of OMMT the degradation temperature increases as shown in the thermogram for ECNE2.5, the increase is due to the barrier imposed by the nanoclay on the conformations changes exhibited by the epoxy chains. Further as the nanoclay are distributed over the matrix they provide a shielding to the underlying matrix from decomposing.

The thermogravimetric profiles of TBPAE/OMMT nanocomposites, BPSE/OMMT nanocomposites and MBPSE/OMMT, mOMMT, mMMT and MMT nanocomposites are shown in Figs. 3.32-3.35.

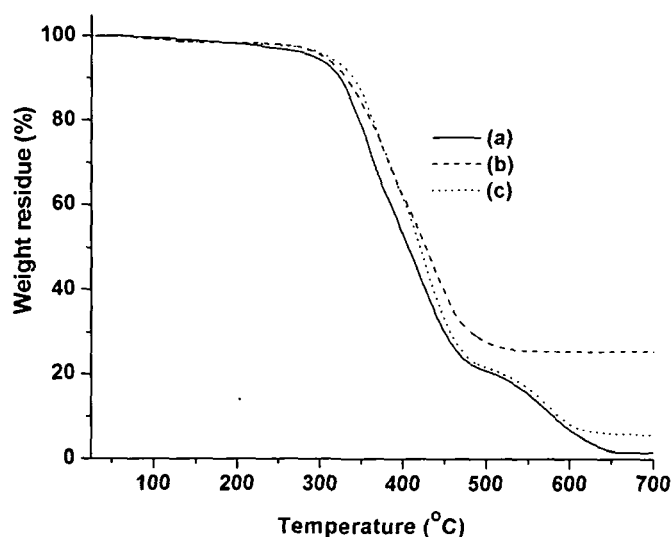


Fig. 3.31: TGA thermograms for (a) ENO50, (b) Araldite LY 250 and (c) ECNE2.5

It can be seen that the initial decomposition of TBPAE occurred at 242 °C, whereas the initial decomposition of BPSE was observed at 273 °C and in case of MBPSE it was at 282 °C. Generally, degradation of bromine containing polymers occurs at relatively

low temperature. Since bromine is labile so the major mass loss is due to the loss of HBr from the structure.

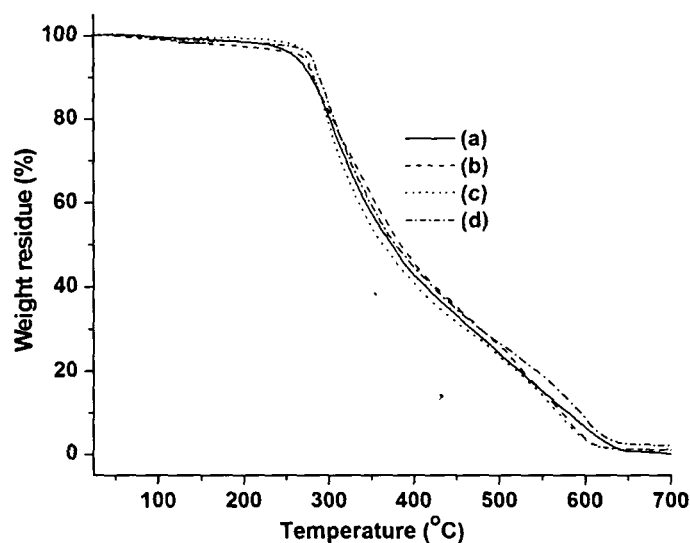


Fig. 3.32: TGA thermograms for (a) TBPAE, (b) TBPAEN1, (c) TBPAEN2.5 and (d) TBPAEN5

However, the stability up to 242 °C for TBPAE (Fig. 3.32) can be explained from the crosslinking between the free hydroxyl groups, which may present in the fatty acids or generated during the amine crosslinking reaction as well as good chemical interactions via hydrogen bonding and polar-polar interactions. As the sulfone bond has greater heat resistance, hence in BPSE it provides a “shielding effect” to thermal degradation of the resin.⁶³ Also the presence of thermostable aromatic moieties resulted in increase in degradation temperature. These have high rigidity and higher steric hindrance to molecular mobility, consequently resulting in increase in the degradation temperature.

The degradation of the epoxy network occurs by the elimination of water molecules which may result in the formation of C-C unsaturations. The C-O bond in β -positions with respect to these unsaturations becomes the weakest linkage. They ultimately break down to give fragments small enough to volatilize at such high temperature. The extensive breakdown of the epoxy network occurs with the progressive increase in temperature. At higher temperature the aromatic carbon bonds of the bisphenol-A ring may break down leading to volatilization. Also it was observed that the thermal stability enhances after the incorporation of clay. The increment of onset degradation temperature up to 25 °C was achieved for TBPAE/OMMT nanocomposites, TBPAEN1, TBPAEN2.5 and TBPAEN5 the

decomposition occurred at 250 °C, 264 °C and 269 °C respectively, while for BPSEN1, BPSEN2.5 and BPSEN5 (Fig. 3.33) the decomposition was at 280 °C, 286 °C and 292 °C respectively. While the initial decomposition for ENMC1, ENMC2,

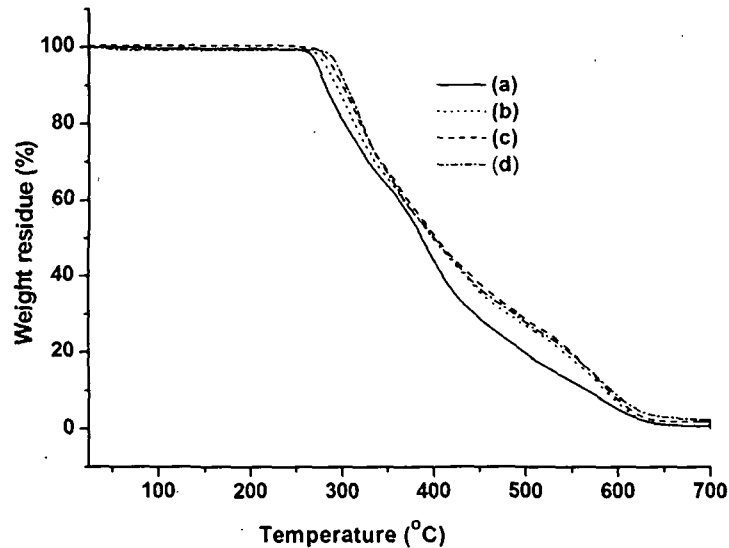


Fig. 3.33: TGA thermograms for (a) BPSE, (b) BPSEN1, (d) BPSEN2.5 and (d) BPSEN5

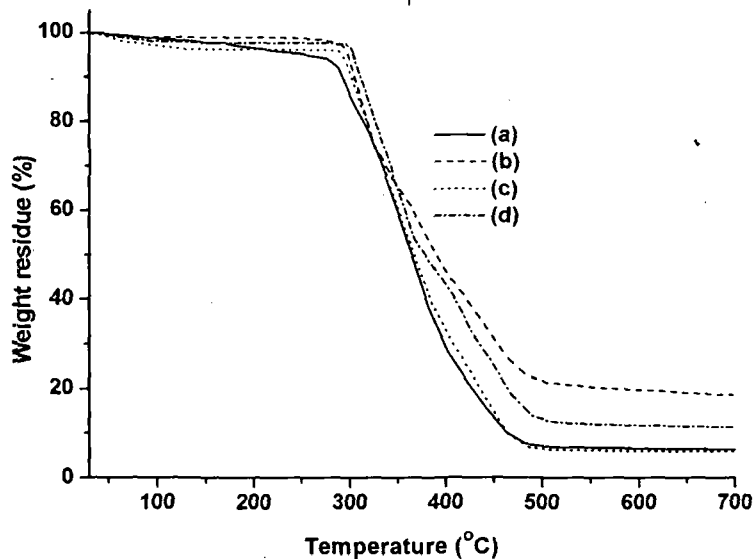


Fig. 3.34: TGA thermograms for (a) MBPSE, (b) ENMC2, (b) ENMC3 and (c) ENMC1

ENMC3 and ENC occurred at 301 °C, 296 °C, 291 °C and 285 °C (Fig. 3.34) respectively. However, there were no significant differences between peak temperatures at the various nanoclay contents. The increase in the initial decomposition temperatures for nanocomposites may be attributed to the protection of epoxy polymer

chains present between hard clay nanolayers that act as a blockade protecting from volatilizing the epoxy matrix. The network of polymer chains present between the clay layers are confined to a restricted segmental motion which is reflected in higher thermal stability properties than the pristine systems. The presence of inorganic phases like SiO_2 , Al_2O_3 , and MgO that dominates in the nanocomposites is responsible for such enhanced thermal stability of the systems. This observation suggests that the clay layers were well dispersed in the polymer matrix and hence was the enhancement in the thermal properties. Moreover the clay layers assists in the formation of char after thermal decomposition that could also enhance the overall thermal stability of the system.^{64,65}

In case of AMNO modified OMMT, AMNO reduces the hydrophilicity of the clay by reducing the cohesion between the stacks thereby prompting more amounts of polymer chains to enter into the galleries. This results in better dispersion of the clay in the matrix. The crosslinking of the epoxy with the hardener results in a more thermally stable structure.

The thermogravimetric profile of MBPSE and its hyperbranched polyurea modified clay nanocomposites is shown in Fig. 3.35. MBPSE exhibited initial degradation temperature of 282 °C, on incorporation of nanoclay thermal stability of the nanocomposites gets enhanced. The decomposition temperature of HBPA1, HBPA3 and HBPA5 were 290 °C, 299 °C and 318 °C, respectively. The hyperbranched modified nanoclay plays an important role in increasing the thermal stability.

The presence of the thermostable s-triazine moiety and nitrogen element in the clay layers further added to the increase in the thermal stability of the nanocomposites. The interaction between the clay layers and the polymer is facilitated by the presence of the hyperbranched polyurea moiety in the nanoclay layers. These results in reduced molecular mobility of the chains further aided by the crosslinking of the epoxy matrix.²⁸

The thermal stability exhibited dose dependent variation with nanoclay loadings, which was further confirmed by the weight residue obtained at 650 °C. HBPA5 exhibited a weight residue of 13.27%, whereas HBPA3 and HBPA1 showed weight residue of 11.83% and 9.67% respectively, however MBPSE showed residue of 7.50% only. The higher amount of carbonaceous char residue offers better heat shielding of the underlying polymer matrix from volatilizing, as a result HBPA5 shows the highest thermal stability in the present study.

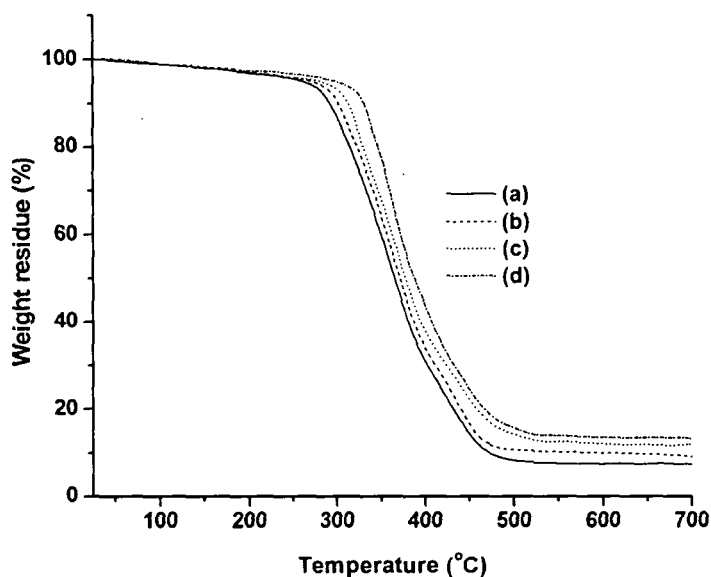


Fig. 3.35: TGA thermograms for (a) MBPSE, (b) HBPA1, (c) HPBA3 and (d) HBPA5

3.3.11. Flame Retardancy

Flame retardancy ratings of TBPAE/OMMT, BPSE/OMMT, MBPSE/OMMT, mOMMT, mMMT and MMT and MBPSE/hyperbranched modified OMMT nanocomposites are given in Tables 3.11-3.14. For TBPAE flame retardancy characteristics can be attributed to the presence of TBPA moiety in the resin. TBPA acts by hindering the spread of the fire and gives precious extra time in the initial stages. Hence TBPA slows down the initial burn rate and thereby helps in increase of the time to flashover, giving the occupants more time to escape. Both in case of BPSE and MBPSE flame retardancy characteristics can be endorsed to the existence of sulfone moiety in the resin. The presence of the sulfone group serves as a promoter for the formation of char.

Table 3.11: LOI values and UL 94 ratings of TBPAE/OMMT nanocomposites

Samples	LOI values	UL 94 ratings
TBPAE	37	V1
TBPAEN1	40	V0
TBPAEN2.5	42	V0
TBPAEN5	45	V0

This may result flame retardancy, resulting from the decline in the amount of combustible gases and formation of barrier to heat transfer as the char was formed. However no significant differences were observed in flame retardancy between BPSE

and MBPSE. However enhancement of flame retardancy after formation of nanocomposites was observed in all the cases. For TBPAE/OMMT the enhancement is due to the synergistic effect of bromine group and the OMMT. Further, the delaminated structure of the clay in the polymer matrix, which subsequently collapses during the combustion process, may act as an insulator and a mass transport barrier slowing the escapes of the volatile products as the epoxy matrix decomposes in all the cases of the nanocomposites. The ability of the clay to form char can also contribute to flame retardant properties, moreover, heat transfer during the initial stages may promote thermal decomposition of the organomodifier and the creation of strongly protonic catalytic sites onto the clay surface, which can catalyze the formation of a stable char residue, this char layer act as insulative layer to slow down heat transfer and retards movement of gases to feed the flame.⁶⁶⁻⁶⁸ Furthermore, the formation of gas bubbles enhances nanoclay migration to the surface, initiated by the decomposition of both the organomodifiers and the polymer chains.

Table 3.12: *LOI values and UL 94 ratings of BPSE/OMMT nanocomposites*

Samples	LOI values	UL 94 ratings
BPSE	27.0	V2
BPSen1	30.3	V1
BPSen2.5	31.7	V1
BPSen5	33.1	V1

Table 3.13: *LOI values and UL 94 ratings of MBPSE and mOMMT, OMMT, mMMT and MMT nanocomposites*

Samples	LOI value	UL 94 ratings
MBPSE	28.4	V2
ENMC1	32	V1
ENMC2	33	V1
ENMC3	30.5	V1
ENC	29.5	V2

Such gas bubbles may in fact be nucleated by the surface of the clay. These gas bubbles could also help in the convection of the clay sheets to the surface. For MBPSE/AMNO modified as well as unmodified nanoclay, ENMC1 exhibited the highest enhancement both in LOI value and UL 94 ratings among the studied

nanocomposites. This increase in the flame retardancy resulted from the good dispersion of the nanoclay in the matrix compared to other systems.

The low improvement of flame retardancy in case of ENC is attributed to the poor dispersion of the clay. This resulted in an ineffective barrier, which could not prevent the burning process and thereby low LOI value was observed.⁶⁷ Similar characteristics was also observed for MBPSE/hyperbranched polyurea modified OMMT; HBPA5 exhibited the highest flame retardant behavior among the other percentages in this case. As discussed above the modified clay plays manifold role in enhancing the flame retardancy of the nanocomposites, further the presence of the triazine moiety can also affect the flame retardancy of the nanocomposites.

Table 3.14: LOI values and UL 94 ratings of MBPSE and its hyperbranched polyurea modified OMMT nanocomposites

Samples	LOI value	UL 94 ratings
MBPSE	28.4	V2
HBPA1	33	V1
HBPA3	35	V1
HBPA5	36	V1

3.3.12. Chemical Resistance

The chemical resistances of all the samples excluding ENO and ENO75 are very good in all the tested media except in alkali medium (Table 3.15). The poor alkali resistance is due to the presence of hydrolyzable ester group of the fatty acids in the reactive diluent. However, the improvement of chemical resistance through the formation of nanocomposite is excellent for ECN2.5 and ECN5. The good alkali resistance of ECN1 indicates that 1 wt% nanoclay loading is sufficient to achieve the desired chemical resistance properties. Thus the overall chemical resistance of the cured resins and the nanocomposite are very good.

TBPAE/OMMT nanocomposites, BPSE/OMMT nanocomposites, MBPSE/AMNO modified as well unmodified nanoclay nanocomposites and MBPSE/hyperbranched polyurea modified OMMT nanocomposites showed good chemical resistance over the pristine polymer (Tables 3.16-3.19). The chemical resistance studies indicated that for different media the nanocomposites exhibited excellent resistance.

Table 3.15: Chemical resistance for ENO, ENO modified Araldite LY 250 and nanocomposites

Sample code	Aq. NaOH (0.5%)	Aq. HCl (10%)	Aq. NaCl (10%)	Distilled Water	Ethanol (20%)
Araldite LY 250	F	E	E	E	E
ENO25	P	E	E	E	E
ENO50	P	E	E	E	E
ENO75	O	F	G	F	G
ECN1	O	E	E	E	E
ECN2.5	E	E	E	E	E
ECN5	E	E	E	E	E

P=poor, O=peeled out, G= good, F=Fair and E= excellent

Table 3.16: Chemical resistance for TBPAE and nanocomposites in different media

Sample code	Aq. NaOH (0.5%)	Aq. HCl (10%)	Aq. NaCl (10%)	Distilled Water	Ethanol (20%)
TBPAE	G	F	G	F	G
TBPAEN1	G	E	G	E	F
TBPAEN2.5	E	E	E	E	G
TBPAEN5	E	E	E	E	E

P=poor, O=peeled out, G= good, F=Fair and E= excellent

Table 3.17: Chemical resistance for BPSE and nanocomposites in different media

Sample code	Aq. NaOH (0.5%)	Aq. HCl (10%)	Aq. NaCl (10%)	Distilled Water	Ethanol (20%)
BPSE	G	P	F	G	G
BPSEN1	G	F	E	E	G
BPSEN2.5	E	G	E	E	E
BPSEN5	E	E	E	E	E

P=poor, O=peeled out, G= good, F=Fair and E= excellent

In the case of nanocomposites the delaminated structure in the matrix reduces the permeability by formation of torturous pathway. Hence as a result the different ions or molecules present in the different media need more time to penetrate and thereby increasing the resistance.

The high moisture absorption of the epoxy network may be due to the presence of polar group in the network. The absorption of moisture was not significantly affected by nanocomposites formation.

Table 3.18: Chemical resistance for MBPSE and nanocomposites in different media

Sample code	Aq. NaOH (0.5%)	Aq. HCl (10%)	Aq. NaCl (10%)	Distilled Water	Ethanol (20%)
MBPSE	P	O	G	G	G
ENMC1	E	P	E	E	E
ENMC2	E	G	G	E	E
ENMC3	G	G	G	O	G
ENC	O	P	O	G	G

P=poor, O=peeled out, G= good and E= excellent

Table 3.19: Chemical resistance for MBPSE and hyperbranched polyurea modified OMMT in different media

Sample code	Aq. NaOH (0.5%)	Aq. HCl (10%)	Aq. NaCl (10%)	Distilled Water	Ethanol (20%)
MBPSE	P	O	G	G	G
HBPA1	E	E	E	E	G
HBPA3	E	G	E	E	E
HBPA5	E	E	E	E	E

P=poor, O=peeled out, G= good, F=Fair and E= excellent

3.4. Conclusions

From this Chapter it can be concluded that nanocomposites using OMMT, organo-bentonite, as well as AMNO modified nanoclays and hyperbranched polyurea modified OMMT with *Mesua ferrea* L. seed oil based epoxidized oil plasticized commercial epoxy resin and different types of monoglyceride epoxy resins has been successfully prepared. Further the study also revealed that the fatty amido-amine can be utilized as an effective modifier for OMMT to improve compatibility with the epoxy matrix. The modified nanoclays were characterized by XRD and spectroscopic technique. Further the formations of nanocomposites were confirmed by XRD, SEM, TEM and FTIR techniques. Significant enhancement in the performance characteristics of the nanocomposites were observed over the pristine polymer. Improvements in the thermal

stability of the nanocomposites were observed over the neat system. The UL 94 and LOI tests showed significant improvement in the flame retardancy of the nanocomposites compared to the pristine epoxy system. Thus the resultant system offers a potential high performance material for many advanced applications such as flame retardant, active thin film, surface coating etc.

References

1. Kojima, Y., et al. Mechanical properties of nylon 6-clay hybrid, *J. Mater. Res.* **8**, 1185-1189, 1993.
2. Wang, M.S., & Pinnavaia, T.J. Clay-polymer nanocomposites formed from acidic derivatives of montmorillonite and an epoxy resin, *Chem. Mater.* **6**, 468-474, 1994.
3. Liu, W., et al. Organoclay-modified high performance epoxy nanocomposites, *Compos. Sci. Technol.* **65**, 307-316, 2005.
4. Lan, T., et al. Mechanism of clay tactoid exfoliation in epoxy-clay nanocomposites, *Chem. Mater.* **7**, 2144-2150, 1995.
5. Haq, M., et al. Bio-based polymer nanocomposites from UPE/EML blends and nanoclay: Development, experimental characterization and limits to synergistic performance, *Compos. Part A: Appl. Sci. Manufactur.* **42**, 41-49, 2011.
6. Usuki, A., et al. Polymer-clay nanocomposites, *Adv. Polym. Sci.* **179**, 135-195, 2005.
7. Calvo, S., et al. Preparation and thermal-mechanical characterization of nanoclay-unsaturated polyester composites, *J. Nanosci. Nanotech.* **10**, 2863-2869, 2010.
8. Torre, L., et al. Compatibilization and development of layered silicate nanocomposites based of unsaturated polyester resin and customized intercalation agent, *J. Appl. Polym. Sci.* **115**, 3659-3666, 2010.
9. Ahmadi, S.J., et al. Synthetic routes, properties and future applications of polymer-layered silicate nanocomposites, *J. Mater. Sci.* **39**, 1919-1925, 2004.
10. Messersmith, P.B., & Giannelis, E.P. Synthesis and characterization of layered silicate-epoxy nanocomposites, *Chem. Mater.* **6**, 1719-1725, 1994.
11. Yang, J.P., et al. Cryogenic mechanical behaviors of MMT/epoxy nanocomposites, *Compos. Sci. Technol.* **67**, 2934-2940, 2007.
12. Ho, M.W., et al. Mechanical properties of epoxy-based composites using nanoclays, *Compos. Struct.* **75**, 415-421, 2006.
13. Wang, L., et al. Preparation, morphology and thermal/mechanical properties of epoxy/nanoclay composite, *Compos. Part A* **37**, 1890-1896, 2006.
14. Miyagawa, H., et al. Biobased epoxy/clay nanocomposites as a new matrix for CFRP, *Compos. Part A* **37**, 54-62, 2006.
15. Miyagawa, H., et al. Biobased epoxy/layered silicate nanocomposites: Thermophysical properties and fracture behavior evaluation, *J. Polym. Environ.* **13**, 87-96, 2005.

16. Johansson, K., & Johansson, M. Fatty acid methyl ester as reactive diluent in thermally cured solvent-borne coil-coatings—The effect of fatty acid pattern on the curing performance and final properties, *Prog. Org. Coat.* **63**, 155-159, 2008.
17. Paul, D.R., & Robeson, L.M. Polymer nanotechnology: Nanocomposites, *Polymer* **49**, 3187–3204, 2008.
18. Song, R., et al. Influences of catalysis and dispersion of organically modified montmorillonite on flame retardancy of polypropylene nanocomposites, *J. Appl. Polym. Sci.* **106**, 3488-3494, 2007.
19. Giannelis, E.P., et al. Polymer-silicate nanocomposites: Model systems for confined polymers and polymer brushes, *Adv. Polym. Sci.* **138**, 107-147, 1999.
20. Alexandre, M., & Dubois, P. Polymer-layered silicate nanocomposites: Preparation, properties and uses of a new classes of materials, *Mater. Sci. Eng. R: Rep.* **28**, 1-63, 2000.
21. Manias, E., et al. Polypropylene/montmorillonite nanocomposites. Review of the synthetic routes and materials properties, *Chem. Mater.* **13**, 3516-3523, 2001.
22. Zanetti, M., et al. Polymer layered silicate nanocomposites, *Macromol. Mater. Eng.* **279**, 1-9, 2000.
23. Vaia, R.A., et al. Interlayer structure and molecular environment of alkylammonium layered silicates, *Chem. Mater.* **6**, 1017-1022, 1994.
24. Plummer, C.J.G., et al. Hyperbranched polymer layered silicate nanocomposites, *Chem. Mater.* **14**, 486-488, 2002.
25. Frechet, J.M.J., et al. Dendrimers and hyperbranched polymers: Two families of three-dimensional macromolecules with similar but clearly distinct properties, *J. Macromol. Sci. Pure Appl. Chem.* **33**, 1399-1425, 1996.
26. Boogh, L., et al. Dendritic hyperbranched polymers as tougheners for epoxy resins, *Polymer* **40**, 2249-2261, 1999.
27. Mahapatra, S.S., & Karak, N. Hyperbranched polyamine: A promising curing agent for a vegetable oil-based poly (ester amide) resin, *Prog. Org. Coat.* **60**, 328-334, 2007.
28. Deka, H.K., & Karak, N. Influence of highly branched poly(amido amine) on the properties of hyperbranched polyurethane/clay nanocomposites, *Mater. Chem. Phys.* **124**, 120-128, 2010.

29. Kusmono, Z.A., et al. Effect of clay modification on the morphological, mechanical, and thermal properties of polyamide 6/polypropylene/montmorillonite nanocomposites, *Polym. Compos.* **31**, 1156, 2010.
30. Blumstein, A. Polymerization of absorbed monolayers: II. Thermal degradation of the inserted polymers, *J. Polym. Sci. A* **3**, 2665–1673, 1965.
31. Krishnamoorti, R., et al. Structure and dynamics of polymer-layered silicate nanocomposites, *Chem. Mater.* **8**, 1728–1734, 1996.
32. Patel, H.A., et al. Nanoclays for polymer nanocomposites, paints, inks, greases and cosmetics formulations, drug delivery vehicle and waste water treatment, *Bull. Mater. Sci.* **29**, 133–145, 2006.
33. Lu, J., et al. Bio-based nanocomposites from functionalized plant oils and layered silicate, *J. Polym. Sci. Part B: Polym. Phys.* **42**, 1441-1450, 2004.
34. Ray, S.S., & Bousmina, M. Biodegradable polymers and their layered silicate nanocomposites: In greening the 21st century materials world, *Prog. Mater. Sci.* **50**, 962-1079, 2005.
35. Miyagawa, H., et al. Novel biobased nanocomposites from functionalized vegetable oil and organically-modified layered silicate clay, *Polymer* **46**, 445-453, 2005.
36. Maiti, P., et al. New biodegradable polyhydroxybutyrate/layered silicate nanocomposites, *Biomacromolecules* **8**, 3393-3400, 2007.
37. Kamon, T., & Furakaw, H. Epoxy Resins and Composites IV, *Adv Polym Sci*, K. Dusek ed., Springer-Verlag, Berlin, 1986, 177.
38. Lan, T., & Pinnavaia, T.J. Clay-reinforced epoxy nanocomposites, *Chem. Mater.* **6**, 2216-2219, 1994.
39. Chen, B., et al. Synthesis of disordered and highly exfoliated epoxy/clay nanocomposites using organoclay with catalytic function via acetone–clay slurry method, *Chem. Mater.* **16**, 4864-4866, 2004.
40. Wang, K., et al. Epoxy nanocomposites with highly exfoliated clay: Mechanical properties and fracture mechanisms, *Macromolecules* **38**, 788-800, 2005
41. Kalsi, P.S. *Spectroscopy of Organic Compounds*, 6th ed., New Age International Limited, New Delhi, 2005.
42. Madejova, FTIR techniques in clay mineral studies, *J. Vibrat. Spectros.* **31**, 1-10, 2003.
43. Zhang, Y.Q., et al. Preparing PP/clay nanocomposites using a swelling agent, *Compos. Part B: Eng.* **35**, 133-138, 2004.

44. Dai, C.F., et al. Comparative studies for the effect of intercalating agent on the physical properties of epoxy resin-clay based nanocomposite materials, *Euro. Polym. J.* **44**, 2439–2447, 2008.
45. Zhang, W., et al. IR study on hydrogen bonding in epoxy resin–silica nanocomposites, *Prog. Nat. Sci.* **18**, 801–805, 2008.
46. Dutta, S., et al. Biocompatible epoxy modified bio-based polyurethane nanocomposites: Mechanical property, cytotoxicity and biodegradation, *Bioresour. Technol.* **100**, 6391–6397, 2009.
47. Sikdar, D., et al. A molecular model for ϵ -caprolactam-based intercalated polymer clay nanocomposite: Integrating modeling and experiments, *Langmuir* **22**, 7738–7747, 2006.
48. Yoon, K., et al. Modification of montmorillonite with oligomeric amine derivatives for polymer nanocomposite preparation, *Appl. Clay Sci.* **38**, 1–8, 2007.
49. Kim, M.S., et al. Shape memory and physical properties of poly(ethyl methacrylate)/Na-MMT nanocomposites prepared by macroazoinitiator intercalated in Na-MMT, *Compos. Sci. Technol.* **68**, 1919–1926, 2008.
50. Chen, D.Z., et al. Cure kinetics of epoxy-based nanocomposites analyzed by Avrami theory of phase change, *Polym. Test.* **22**, 689–697, 2003.
51. Pollard, M., & Kardos, J.L. Analysis of epoxy resin curing kinetics using the Avrami theory of phase change, *Polym. Eng. Sci.* **27**, 829–836, 1987.
52. He, P.S., & Li, C.E. Curing studies on epoxy system with fillers, *J. Mater. Sci.* **24**, 2951–2955, 1989.
53. Brown, J.M., et al. Thermoset-layered silicate nanocomposites. Quaternary ammonium montmorillonite with primary diamine cured epoxies, *Chem. Mater.* **12**, 3376–3384, 2000.
54. Okamoto, M., et al. Dispersed structure change of smectic clay/poly(methyl methacrylate) nanocomposites by copolymerization with polar comonomers, *Polymer* **42**, 1201–1206, 2001.
55. Bugnicourt, E., et al. Effect of sub-micron silica fillers on the mechanical performances of epoxy-based composites, *Polymer* **48**, 1596–605, 2007.
56. Carrasco, F., & Pages, P. Thermal degradation and stability of epoxy nanocomposites: Influence of montmorillonite content and cure temperature, *Polym. Degrad. Stab.* **93**, 1000–1007, 2008.

57. Arroyo, M., et al. Morphology/behaviour relationship of nanocomposites based on natural rubber/epoxidized natural rubber blends, *Compos. Sci. Technol.* **67**, 1330–1339, 2007.
58. Li, S.C., et al. Melt rheological properties of polypropylene-maleated polypropylene blends I. Steady flow by capillary, *J. Appl. Polym. Sci.* **71**, 1641–1648, 1999.
59. Khanbabaie, G., et al. Preparation and properties of epoxy-clay nanocomposites, *J. Macromol. Sci. Part B* **46**, 975-986, 2007.
60. Tjong, S.C., Structural and mechanical properties of polymer nanocomposites, *Mater. Sci. Eng. R: Rep.* **53**, 73–197, 2006.
61. Zhai, L., et al., The effect of nanoparticles on the adhesion of epoxy adhesive, *Mater. Lett.* **60**, 3031–3033, 2006
62. Tyan, H.L., et al. Effect of reactivity of organics-modified montmorillonite on the thermal and mechanical properties of montmorillonite/polyimide nanocomposites, *Chem. Mater.* **13**, 222-226, 2001.
63. Soni, H.K., et al. Studies on cure kinetics and thermal stability of liquid epoxy resin based on bisphenol-C and epichlorohydrin using different amines as curing agents, *Thermochim. Acta.* **191**, 307-316, 1991.
64. Park, J.H., et al. Intercalated polypropylene/clay nanocomposite and its physical characteristics, *J. Phys. Chem. Solids* **69**, 1375–1378, 2008.
65. Guo, B., et al. Effects of organo-montmorillonite dispersion on thermal stability of epoxy resin nanocomposites, *Eur. Polym. J.* **40**, 1743-1748, 2004.
66. Ribeiro, S.P.S. et al. Influence of clays on the flame retardancy and high temperature viscoelastic properties of polymeric intumescent formulations, *Polym. Degrad. Stab.* **94**, 421-431, 2009.
67. Jang, B.N., et al. The relationship between thermal degradation behavior of polymer and the fire retardancy of polymer/clay nanocomposites, *Polymer* **46**, 10678-10687, 2005.
68. Laoutid, F., New prospects in flame retardant polymer materials: From fundamentals to nanocomposites. *Mater. Sci. Eng. R* **63**, 100–125, 2009.

CHAPTER 4

Modified Epoxy and Clay Nanocomposites

4.1. Introduction

From the previous chapter it has been found that the formation of suitable nanocomposites of the virgin epoxy resins improved most of the desired properties to a significant extent. Further as epoxy resins are reactive towards diverse chemicals with different functionalities, such as hydroxy, amino, carboxylic etc. leading to extremely versatile materials that range from laminated circuit board, structural carbon fiber composites, electronic component encapsulations and adhesives.¹

As already discussed in previous chapters most of the polymeric materials are non-biodegradable petroleum based, which has besieged the environment. The subsequent decline of petroleum feedstock has forced to explore the naturally available renewable assets as alternating raw materials the resources for the polymer industry.² In view of the consequences of the damage to the environment and mounting environmental consciousness new environmental regulations right through the world have triggered the exploration for new opportunities for developing environment friendly materials.³⁻⁶

The use of vegetable oil based epoxy thermosetting materials is limited by their toughness properties i.e. weak mechanical attributes, which affect the durability (impact resistance, fatigue behavior, damage tolerance etc.). To increase the thermophysical and mechanical properties the vegetable oil epoxy resin modification or blending with other suitable resins such as polyurethane resin, amino resin, silicone resin, ketonic resin etc. can be done as these vegetable oil based epoxy resins exhibits good compatibility with a wide variety of other resins.⁷ The better compatibility comes from the relatively low viscosity of resin and from the structure of resin that contains a relatively polar and aromatic backbone as well as aliphatic side chains with low polarity. The modification of epoxies enhances the physical and mechanical properties and has been an active area of research for over a few decades. Various modification methods have been used to achieve a tougher and thermally strong epoxy system.⁸⁻¹⁰

The physical as well as chemical properties of the modified system however largely depend on the degree of compatibility of the used components in the formulation. Among the different types of physical modifications of epoxy resin,

blending is one of the most acceptable approaches. Even though immiscible or partially miscible blends have found commercial applications, the complete miscibility of the components for any system is most desirable because mixing on molecular scale results in superior physical as well as mechanical properties with change in composition.¹¹

Polyurethane is one of the most versatile polymer particularly when it is synthesized from naturally renewable resources like vegetable oils, and extensively used in different fields of applications such as coatings, adhesives, leathers, composites, elastomers, biomedical, etc.¹² The desirable level of properties of polyurethanes is due to the incompatibility of the hard and the soft segments and subsequent phase segregation into separate domains.¹³ Again, a lot of advantages are associated with hyperbranched structure of polyurethane.¹³ Thus, the use of hyperbranched polyurethane (HBPU) for the modification of epoxy resin may be an apt choice for generation of new avant-garde material with newer applications in the domain of material science.

However, the performance characteristics of the modified system are needed to be enhanced by formation of nanocomposites to meet the challenges of advanced polymeric materials. This nanocomposite material may find myriad of applications bestowed on their performance characteristics and biocompatibility. This chapter thus deals with the modification of MBPSE with hyperbranched polyurethane (HPBU) studied at different HBPU concentrations. Further, the nanocomposite with OMMT using the best combination of the modified system is also investigated.

4.2. Experimental

4.2.1. Materials

The isolation and purification of the oil was performed exactly the same way as described in Chapter 2, section 2.2.1. Monoglyceride of *Mesua ferrea* L. seed oil was prepared by glycerolysis process as described in Chapter 2, section 2.2.2.1. Bisphenol-A (BPA), bisphenol-S (BPS), epichlorohydrin and poly(amido-amine) hardener were used in this study and are described in details in Chapter 2, section 2.2.1. Montmorillonite (OMMT) used in this study is same and is described in Chapter 3, section 3.2.1.

Poly(ϵ -caprolactone) diol (PCL) (Fig. 4.1) was obtained from Solvay Co., UK. In the present investigation, it was used as a macroglycol in the synthesis of HBPU. PCL

has the density 1.071 g/cm^3 , hydroxyl number 37 mg KOH/g and number average molecular weight (M_n) 3000 g/mol . It was used after drying under vacuum at $45 \text{ }^\circ\text{C}$.

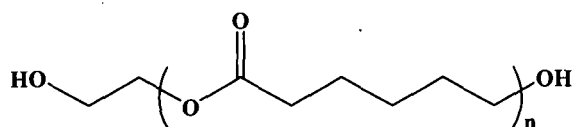


Fig. 4.1: Structure of poly(ϵ -caprolactone) diol

Toluene diisocyanate (TDI) (Fig. 4.2) was purchased from Sigma-Aldrich, Germany. It has formula weight (F_w) 174.16 g/mol , where 80% 2,4-isomer and 20% 2,6-isomer are present. It has density 1.214 g/cm^3 , m.p. $21.8 \text{ }^\circ\text{C}$ and b.p. $251 \text{ }^\circ\text{C}$. Herein, TDI was used as a diisocyanate in the polyurethane synthesis. It was used as received. Since TDI is highly reactive towards moisture, so it was cautiously used.

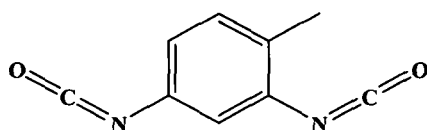


Fig. 4.2: Structure of toluene diisocyanate

Molecular sieve of 4A type was obtained from Merck, India. They often consist of alumino-silicate minerals, clays, porous glasses, microporous charcoals, zeolites, active carbons or synthetic compounds that have porous structure. Its equilibrium capacity for water at $30 \text{ }^\circ\text{C}$ and 75% relative air humidity is $\geq 20\%$ and bulk density is $650\text{-}700 \text{ g/cm}^3$. It was used as received to trap trace amount of moisture present in solvents.

N,N'-dimethylformamide (DMF) and methanol (CH_3OH) used here as solvent are same as mentioned in Chapter 3, section 3.2.1.

The minerals $(\text{NH}_4)_2\text{SO}_4$, Na_2HPO_4 , KH_2PO_4 , $\text{MgSO}_4 \cdot 7\text{H}_2\text{O}$, $\text{CaCl}_2 \cdot 2\text{H}_2\text{O}$, $\text{FeSO}_4 \cdot 7\text{H}_2\text{O}$, $\text{CuSO}_4 \cdot 7\text{H}_2\text{O}$, $\text{MnSO}_4 \cdot 5\text{H}_2\text{O}$, $\text{ZnSO}_4 \cdot 7\text{H}_2\text{O}$, $\text{H}_3\text{BO}_3 \cdot 5\text{H}_2\text{O}$ and MoO_3 used for the bacterial broth culture preparation were obtained from Merck, India and Triton X 100 used for RBC haemolysis tests was obtained from Fluka, Sigma Aldrich, USA. The bacterial strain of *Pseudomonas aeruginosa* MTCC 424 along with other ingredients required for biodegradation study was obtained from the Department of Molecular Biology and Biotechnology (Department of Biotechnology, DBT Centre, Government of India), Tezpur University.

4.2.2. Instruments and Methods

The FTIR and TGA analyses were carried out using same instruments and methods as described in Chapter 2, section 2.2.2. Ultrasonicator (Hielscher, UP200S, Germany) was used to mix the nanoclay into the epoxy/hyperbranched polyurethane (HBPU) matrix at 60% of amplitude and a half cycle for 10 min (as described in Chapter 3, section 3.2.2.). The SEM, XRD and TEM were carried out using the same conditions and instrument as mentioned in Chapter 3, section 3.2.2.

The measurements of tensile strength and elongation at break, impact resistance, scratch resistance and gloss characteristics, percent swelling of the cured films were determined as mentioned in Chapter 2, section 2.2.2. and Chapter 3, section 3.2.2.

The vegetable oil based MBPSE has been synthesized as described in Chapter 2, section 2.2.2.1.

4.2.2.1. *Synthesis of Hyperbranched Polyurethane (HBPU)*

The hyperbranched polyurethane was prepared as reported elsewhere.¹⁴ Briefly, 2.5 mol of poly(ϵ -caprolactone) diol, 1.5 mol of monoglyceride of the *Mesua ferrea* L. seed oil, and 6.5 mol of TDI was added drop wise into the reaction mixture at room temperature under nitrogen atmosphere. The reaction was allowed to stir for 3 h at temperature of (70 ± 2) °C to obtain a viscous mass, which was treated as pre-polymer and finally, 2.5 mol of glycerol was added with the help of a dropping funnel. The temperature was then raised again to (110 ± 2) °C and stirred continuously for about 2.5 h and stopped before gelation. The yield of the polymer obtained was 97%.

4.2.2.2. *Modification of Epoxy Resin by HBPU*

The amount of MBPSE and hyperbranched polyurethane is given in Table 4.1 for their different compositions. The MBPSE and the HBPU were mechanically mixed in an oil bath at 80 °C by using a mechanical stirrer. The mixtures were fully stirred for 1 h and then degassed in a vacuum oven to remove any residual gas bubbles or entrapped solvent.

4.2.2.3. *Preparation of Nanocomposites*

The nanocomposites of the HBPU modified MBPSE were prepared, for compositions of 30 wt% HBPU content (EHBPU30) by incorporating OMMT at three different weight percentages (Table 4.1) and the system was heated at 80 °C for 1 h by using a mechanical stirrer. The system was then cooled and sonicated using a single probe sonicator (same as described in Chapter 3, section 3.2.2.) for 30 min. The temperature

of the sample was maintained at (25-30) °C by using a water bath. The dispersed nanoclay/resin system was degassed for 30 min under vacuum before further processing. The prepared nanocomposites were coded as EHPN1, EHPN3 and EHPN5 (Table 4.1).

Table 4.1: Compositions of HBPU modified MBPSE and its nanocomposites

Code*	MBPSE (g)	HBPU (g)	OMMT (g)
EHBPU10	100	10	0
EHBPU20	100	20	0
EHBPU30	100	30	0
EHPN1	100	30	1
EHPN3	100	30	3
EHPN5	100	30	5

*Digits indicate the hyperbranched polyurethane content in the first three codes and for nanocomposites digits indicate OMMT content

4.2.2.4. Curing of the Hyperbranched Polyurethane Modified Epoxy and Nanocomposites

By hand stirring for 20 min a homogenous mixture of the MBPSE, HBPU modified MBPSE and its nanocomposites were cured as described in Chapter 2, section 2.2.2.2.

4.2.2.5. Water Vapor Permeability Measurement

The water permeability of the nanocomposite films were measured in a desiccating chamber containing CaCl₂ as the drying agent under vacuum. Small containers containing weighted amount of distilled water was taken, where middle part of the caps were replaced by experimental nanocomposite film in an airtight manner to avoid any leakage. The containers were then placed in a well equipped desiccating chamber. The weight of the container was again measured after the experiment of 120 h. All the measurements were carried out at (30 ± 1) °C and an average of three samples was taken for each measurement. The reduction in water content in the containers was calculated by using the relationship.

Percent weight loss of water = $[(W_i - W_f)/W_i] \times 100\%$, where, W_i = initial weight and W_f = final weight of the water container.

4.2.2.6. Biodegradation by Broth Culture Technique

A modified broth medium for culture¹⁵ was prepared by dissolving 2.0 g (NH₄)₂SO₄, 2.0 g Na₂HPO₄, 3.61 g KH₂PO₄, 1.75 g MgSO₄·7H₂O, 0.2 g CaCl₂·2H₂O, 50 mg FeSO₄·7H₂O, 1 mg CuSO₄·7H₂O, 1 g MnSO₄·5H₂O, 1 g ZnSO₄·7H₂O, 1 g H₃BO₃·5H₂O and 1 g MoO₃ in 1.0 L of demineralized water. 10 mL of this liquid culture media was poured into 100 mL conical flasks and was sterilized. The media was then allowed to cool down to room temperature and experimental nanocomposites films were applied to the media under sterile condition. Media containing no polymer film were also cultured as negative control.

4.2.2.7. Microbe Selection

P. aeruginosa strain was selected for the study with strain number MTCC 424. A small inoculum of bacteria containing an approximate 1×10^8 /mL microbes (as calculated from McFarland turbidity method) was inoculated into the conical flask containing 10 mL media for each test. The flasks were then incubated under sterile condition at 37 °C for the degradation study. The samples were collected for spectrophotometric observation at 600 nm against blank culture media on weekly basis under sterile condition. Bacterial growth was calculated from the absorbance data using McFarland turbidity as the standard.

4.2.2.8. RBC Haemolysis Protection Assay

The haemolytic activity test was done to see if the nanocomposites have any haemolytic activity on the erythrocytes based on the modified protocol as reported by Nair et al.¹⁶ Briefly, goat blood mixed with the anticoagulant sodium citrate (4%) was centrifuged at 2500 rpm for 10 minutes. The resultant supernatant was discarded and only the erythrocytes were collected. The collected erythrocytes were further washed in PBS (phosphate buffer saline) (pH 7.4) thrice. Now a 10% (v/v) suspension of washed erythrocytes in PBS was prepared in a 50 mL centrifuge tube. 1.9 mL of this erythrocyte solution was taken in a 2 mL centrifuge tube and 100 µL of the extract at two different concentrations (1 mg/mL and 250 µg/mL) were added into it. The extracts were also prepared in PBS. The tubes were then incubated for 2 h respectively at 37 °C. 2% (v/v) Triton X-100 and PBS were taken as positive and negative control. After incubation the tubes with 2 mL medium were centrifuged at 2500 rpm for 10 minutes. 200 µL of the supernatant was taken and 2.8 mL of PBS was added to it and then the absorbance was taken at 415 nm in a UV-VIS spectrophotometer (Thermo, UK).

4.3. Results and Discussion

4.3.1. Modification of Epoxy Resin

Conventional blending or mixing of two or more polymers generally results in a multi-phase morphology due to the thermodynamic incompatibility between the components. This incompatibility is due to small gain in entropy upon mixing the polymers and resulted from contiguity restrictions imposed by their large chain length. However, if mixing was done on a low molecular weight level and crosslinking accomplished simultaneously, phase separation may be kinetically controlled, since than entanglements become permanent by the crosslinking. In other words, phase separation cannot occur without breaking covalent bonds.^{17,18}

For any system, the degree of compatibility between the two components is highly dependent on their chemical and physical nature. *Mesua ferrea* L. seed oil modified epoxy resin has glyceride moiety in its structure, this results in the epoxy resin with structural complexity. These long alkyl chains offer epoxy resin with sufficient amount of flexibility, but lacks adequate strength properties. On the other hand, polyurethane of the same oil has structural in-homogeneity with sufficient amount of toughness. As both the polymers have common component of glyceride moiety of the same oil as well as different types of polar groups in the structure, so the resultant product is expected to possess strong interactions and good homogeneity. Further, this may also result better biodegradability of the epoxy resin.

4.3.2. Nanocomposites Preparation

As discussed in Chapter 3, section 3.3.2. the preparation of suitable nanocomposite of the afore-stated matrix may offer significant improvement of many desirable properties including biodegradation. In this regard, clay plays an effective role in enhancing the rate of biodegradation. Thus octadecylammonium ion modified MMT (i.e. OMMT) based nanocomposites were prepared in the present investigation. Further, it is expected that hyperbranched polyurethane can help in the exfoliation of the clay layers in the epoxy matrix, because of its unique structural features.¹⁴⁻¹⁵ Therefore, the modification of epoxy resin by the organically modified clay and hyperbranched polyurethane altogether may result in the enhancement of the performance characteristics including thermo-stability and biodegradability.

4.3.3. Characterization

4.3.3.1. FTIR Studies of Hyperbranched Polyurethane Modified MBPSE

The FTIR spectra of MBPSE and its modified systems are shown in Fig. 4.3. The FTIR spectrum of MBPSE is well described in Chapter 2, section 2.3.3.2. Some of the characteristic bands (cm^{-1}) observed were: 3423 ($-\text{OH}$ stretching vibrations), 3059 (aromatic C-H stretching vibration), 1729 ($-\text{C}=\text{O}$ stretching vibration of the triglyceride esters), 1605 ($\text{C}=\text{C}$ stretching vibration), 1300 and 1149 (sulfone stretching vibrations), 1246 and 1106 ($\text{C}-\text{O}-\text{C}$ stretching vibrations), and 916 and 832 (oxirane ring stretching vibrations).

The FTIR spectra of the modified systems showed significant shift in the $-\text{OH}$ stretching vibration, before curing (Fig. 4.3). The band position exhibited red shifts of 25 cm^{-1} for EHBPU10, 10 cm^{-1} for EHBPU30 and 3 cm^{-1} for EHBPU20. The band intensity also increased in all the cases, indicating the increase of $-\text{OH}$ species, may be originated from the ring opening of the oxirane ring. Further, the absorption frequency for $-\text{C}=\text{O}$ (carbonyl stretching) shifted to a lower value however, the position of the band in all the cases was found to be similar. The broadening was because of the overlap of the $-\text{NH}$ and $-\text{C}=\text{O}$ absorptions band.¹⁴⁻¹⁵ The shifts however indicates that the $-\text{C}=\text{O}$ group of the HBPU is involved in hydrogen bonding with the $-\text{OH}$ group and $-\text{C}=\text{O}$ group of epoxy resin and vice-versa. The oxirane stretching vibrations showed a decrease in intensity in all cases, this suggests the interaction of the urethane linkage (by $-\text{NH}$ group) with the epoxide group.¹⁸

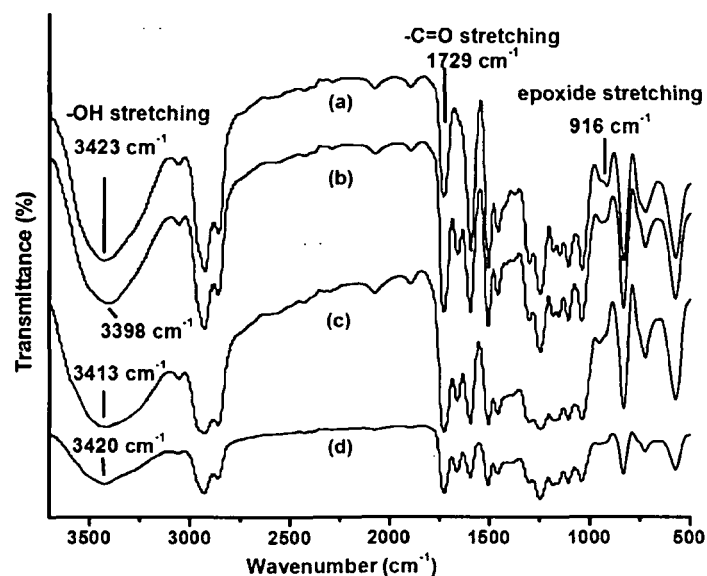


Fig. 4.3: FTIR spectra of (a) MBPSE, (b) EHBPU10, (c) EHBPU20 and (d) EHBPU30 before curing

In the modified system after curing the absorption bands (in all cases) exhibited significant shift and reduction of the band intensity (Fig. 4.4). This indicated the formation of a crosslinked networks. The crosslinking was further supported by observation of diminishing band intensity for epoxide stretching at 916 cm^{-1} in all cases. This suggested extensive amount of interaction to be present in the system. As observed earlier the -OH stretching band for epoxy resin and the -NH band of the hyperbranched polyurethane overlaps and appeared as single broad band around $3154\text{-}3246\text{ cm}^{-1}$. This implies that most of the -NH groups were hydrogen bonded.

The -C=O absorption intensity decreases in all the cases after curing. This is evident of the extensive amount of interaction between the polar functionalities of the epoxy resin and the hyperbranched polyurethane. The number of hydrogen bonds formed largely depends on the amount of hydrocarbon segments present both in epoxy and in polyurethane system. The -CH_2 moiety of monoglyceride of fatty acids does not take part in the hydrogen bonding, but influences the bonding of other groups. Steric shielding of functional groups due to the presence of bulky side groups, steric crowding of hydrogen-bonding groups due to limited spacing between the groups on a polymer chain, and intramolecular screening due to flexible chains bending back upon themselves are some of the important factors that must be considered.

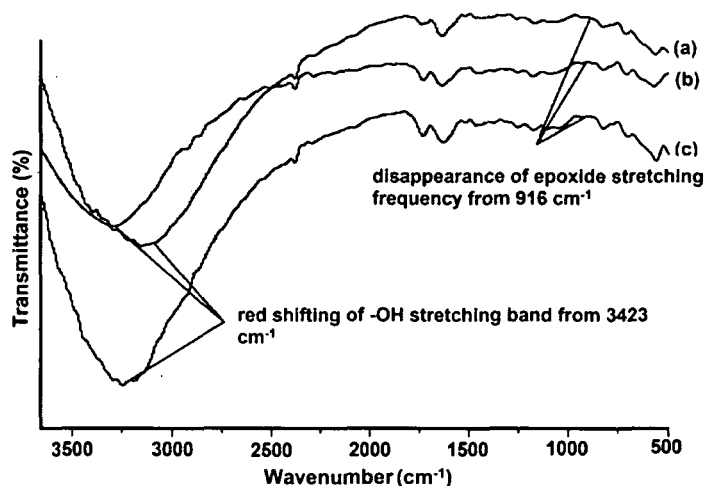


Fig. 4.4: FTIR spectra of (a) EHBPU10, (b) EHBPU20 and (c) EHBPU30 after curing

4.3.3.2. FTIR Studies of Nanocomposites

The structural changes of the nanocomposites from the pristine polymer can also be analyzed through the FTIR spectra (Fig. 4.5 and Fig. 4.6) both before and after curing. The bands observed at about 1034 cm^{-1} and 550 cm^{-1} region in the FTIR spectrum (i.e.

EHBPU30) is due to Si–O and Al–O stretching vibrations of clay¹⁹ and the band at about 3446–3627 cm^{-1} is for the –OH stretching in Si–OH and Al–OH moieties located on the surface of the clay after nanocomposites formation (Fig. 4.5). The interaction of –OH group of clay with the epoxy group and free –OH groups of the intercalated polymer chain was indicated by the broadening of –OH stretching band in the nanocomposites. The sharp band at about 1620 cm^{-1} of OMMT corresponding to the absorbed H–O–H (H_2O) bending vibration (occurring due to hydrophilic nature of the clay) gets minimized in the nanocomposites indicating intercalation by hydrophobic polymer chains.²⁰ The –C=O absorption band prior to curing exhibited a red shift of about $\approx 5\text{--}10 \text{ cm}^{-1}$.

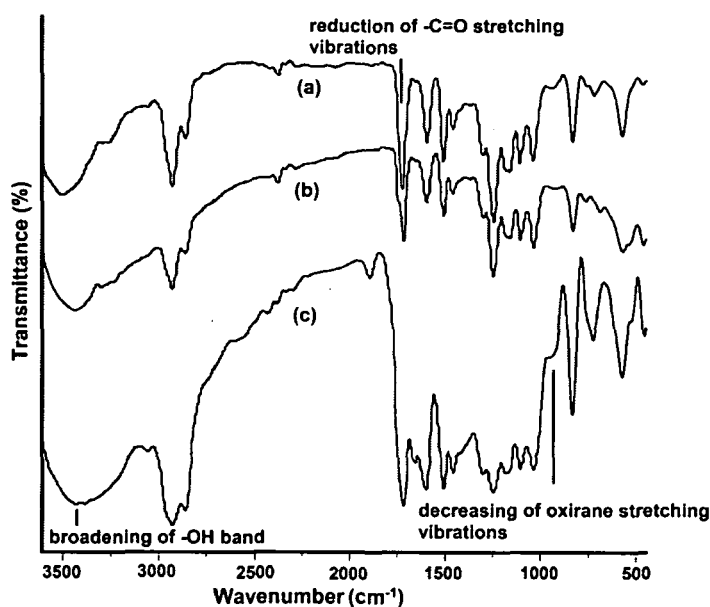


Fig. 4.5: FTIR spectra of (a) EHPN1, (b) EHPN3 and (c) EHPN5 before curing

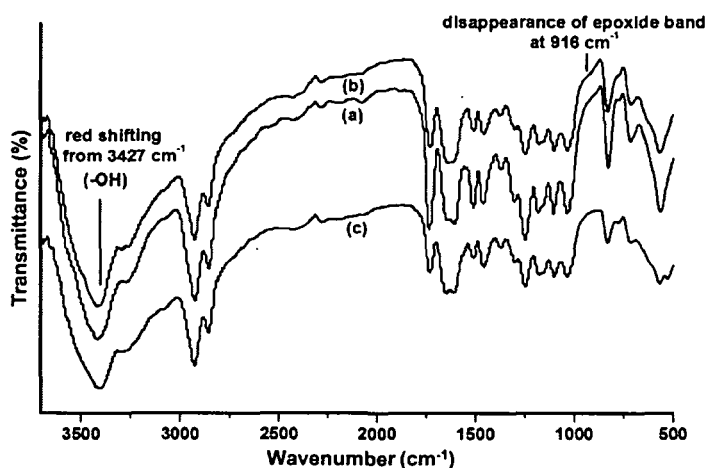


Fig. 4.6: FTIR spectra of (a) EHPN1, (b) EHPN3 and (c) EHPN5 after curing

This red shift indicated lengthening of the -C=O bond thereby decreasing the absorption frequency by hydrogen bonding. However, improper blue shift for -C=O and red shift of -OH absorption band were observed after curing with simultaneous reduction in the absorption band intensity. This is again due to (Fig. 4.6) the significant amount of complex reaction that is occurring during the curing process.

4.3.3.3. XRD Analysis of Hyperbranched Polyurethane Modified MBPSE

The XRD of the modified system revealed the presence of hyperbranched polyurethane in the modified epoxy resin (Fig. 4.7), the appearance of diffraction peaks at $2\theta = 21.2^\circ$ (4.19 \AA) and 23.4° (3.81 \AA) is due to the crystalline nature of PCL moiety in the structure.²¹ The positions of these peaks remained unchanged after modification, though the intensity gradually increases with the increase of HBPU content, which may be due to the increase of the percentage of PCL in the matrix.

4.3.3.4. XRD Analysis of Nanocomposites

The state of distribution of clay in the polymer matrix can be obtained from the diffraction pattern in the XRD spectra (Fig. 4.8). In the case of OMMT strong reflection appeared at $2\theta = 4.15^\circ$ resulting from the $\{001\}$ crystal surface of the layered silicates as discussed in Chapter 3, section 3.3.3.2. The occurrence of reflection at 20° (2θ) corresponds to $\{110\}$ plane. However, in all the nanocomposites, no basal reflection corresponding to $\{001\}$ crystal plane was observed. Thus the XRD diffraction peaks for the nanocomposites indicated the possibility of exfoliated

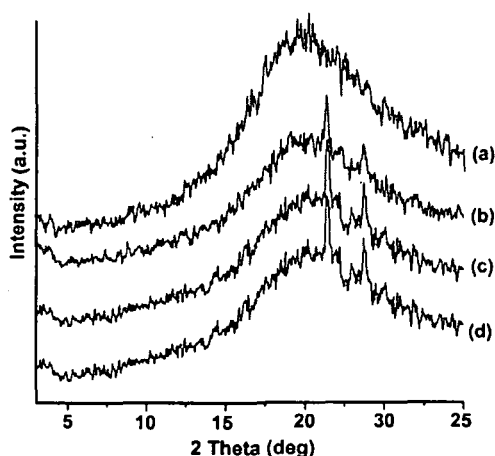


Fig. 4.7: XRD patterns of (a) MBPSE, (b) EHBPU10, (c) HBPU20 and (d) EHBPU30

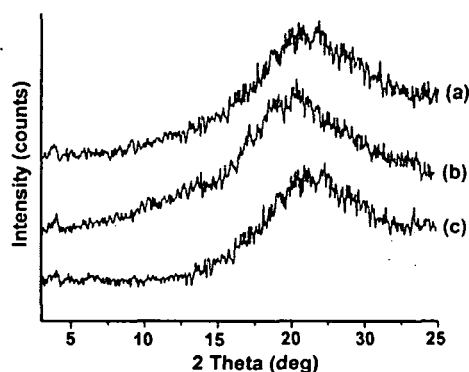


Fig. 4.8: XRD patterns of (a) EHPN1, (b) EHPN3 and (c) EHPN5

nanostructure of clay with different extent of dispersion in the epoxy matrix. In case of epoxy resin the effect of clay modifier on the curing has already been described in Chapter 3, section 3.3.5. The curing rate is much faster inside the galleries than that outside. As a result of these differences more epoxy chains are pulled inside the galleries resulting in expanded d-spacing.

4.3.4. SEM Study

Several factors such as chemical miscibility of the two components, method of mixing, interfacial interaction and crosslinking density, affect the morphology of a two-component system at a given composition.²² Generally, HBPU showed good compatibility with epoxy resin and among the studied system, EHBPU30 showed the best result (Fig. 4.9 a).

However, the size of the domain of the dispersed phase is largely govern by the level of polymer miscibility and is dependent on both the physical and chemical nature of the used components. The good homogenization of epoxy resin with hyperbranched polyurethane (Fig. 4.9 a) may be explained by the polar-polar interaction between the π -bonds of aromatic rings in both resins.¹⁵ In addition to that, the good compatibility may be due to network formation through the reaction of amine groups of hardener with ester groups of epoxy resin along with normal crosslinking of hydroxyl or epoxy groups by amine hardener.

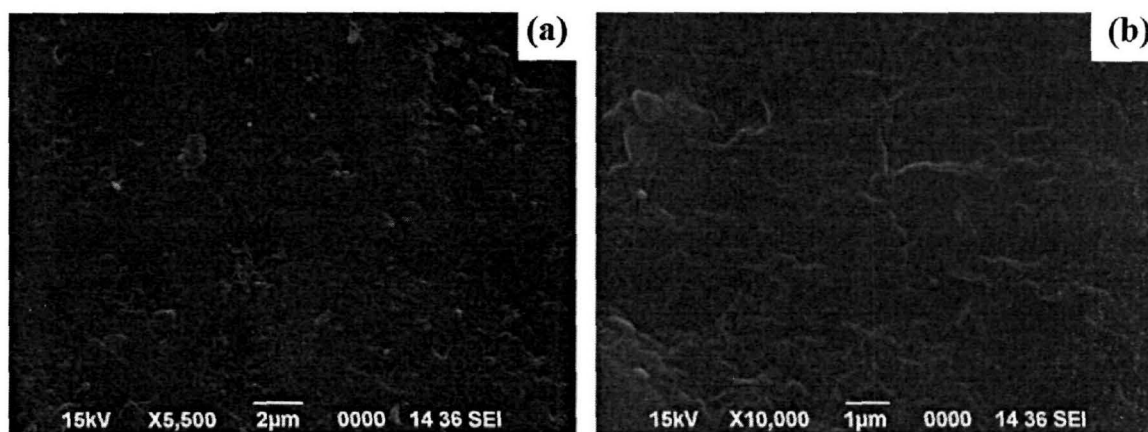


Fig. 4.9: SEM micrographs for (a) EHBPU30 and (c) EHPN3

The possibility of crosslinking reactions by the hydroxyl/urethane groups of polyurethane resin with the hydroxyl/epoxy groups of epoxy resin in the presence of amine hardener (also basic in nature) is also obvious. Along with this, there is the possibility of hydrogen-bonding between $-C=O$ of urethane groups of the polyurethane

resin with the -OH of epoxy resin present in the systems. Thus, the amine hardener also acts as a compatibilizing agent for these systems.

The SEM images of the nanocomposites exhibited uniform distribution of the clay layers in the modified epoxy matrix (Fig. 4.9 b). The SEM image of EHPN3 showed an uneven surface morphology, wherein some protruding white dots or lines can be visualized on the surface. Observation of protruding dots or lines indicate that the embedded clay layers were well adhered to the polymeric surface. As observed for the pristine polymeric system the surface is rather smooth. The thicknesses of the ribbon like lines in the nanocomposites are in the range of a few nanometers.

4.3.5 TEM Study

The TEM micrograph of EHPN3 exhibited a partially delaminated morphology in which partially exfoliated as well as intercalated structure exists (Fig. 4.10). Thus, the TEM micrograph confirmed the fine dispersion of the nanoclay into the modified epoxy matrix.

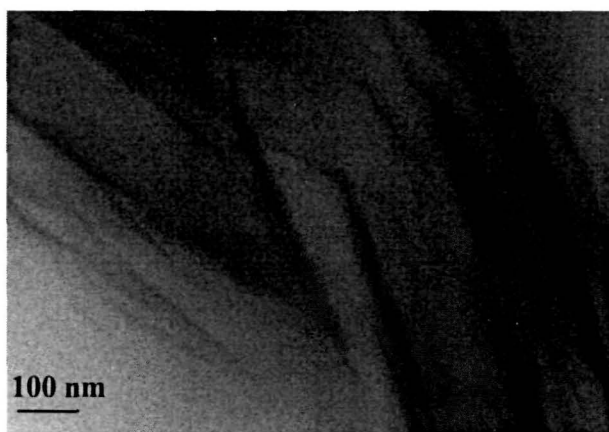


Fig. 4.10: TEM micrograph for EHPN3

4.3.6. Curing Studies

From the curing study, it was found that the curing time (touch free time as well as hard drying time) decreases for the modified systems with the increase of polyurethane content (Table 4.2). This may be due to the increase of the possibility of reaction of epoxy/hydroxyl groups of epoxy resin with hydroxyl/urethane groups of polyurethane resins in the presence of amine hardener as the amount of epoxy and hyperbranched polyurethane is increased.²³ It has been reported²⁴ that the aromatic moiety of polyurethane resin accelerates the crosslinking reaction of epoxy in an epoxy/amine hardener/urethane reaction system by the formation of an active complex of the

hardener with the aromatic moiety of polyurethane with stoichiometric ratio in the curing reaction. The oxirane peak intensity was observed to decrease in the modified system before curing (as discussed in the FTIR section 4.3.3.1.), indicating the interaction of the urethane linkage with the epoxy group. Further, the oxirane absorption band diminishes in the modified epoxy after curing.

Table 4.2: *Drying time of HBPU modified MBPSE and its nanocomposites*

Sample	Touch free time (min)	Hard dry time (min)	Swelling (%)	Water loss (%)
MBPSE	45	65	32	1.45
EHBPU10	43	64	30	1.12
EHBPU20	40	63	29	1.01
EHBPU30	35	57	27	0.95
EHPN1	30	55	25	0.85
EHPN3	27	47	23	0.75
EHPN5	17	40	20	0.68

The hydroxyl group (of clay) plays a catalytic role in enhancing the cure rate, these can also be justified from the decrease in curing time for the nanocomposites. The cure time decreases with the increase in clay loading. The alkylammonium ions present in organoclay are also responsible for the catalytic acceleration of the epoxy curing reaction and thus enhancing the cure rate as has been discussed in Chapter 3, section 3.3.5.

4.3.7. Water Vapor Barrier Study

The enhancement of barrier properties by the formation of true nanocomposite is a well established phenomenon.²⁶ The present study on water vapor permeation also showed no exception (Table 4.2). This can be explained by tortuosity mechanism.

The intercalation/exfoliation of clay platelets in the polymer matrix offers a long tortuous path (mean free path) for the guest molecules to pass through and hence the permeation got retarded.²⁷⁻²⁸ In the present study, it was observed that there was a 2 to 4-fold reduction in the rate of permeability of water vapor with increase in clay loading from 1 to 5 wt% in the nanocomposites. This is understandable from the increase of tortuosity with the increase of clay loading in the matrix.

4.3.8. Performance Characteristics

The performance characteristics like tensile strength, elongation at break, impact resistance, scratch hardness and gloss for HBPU modified MBPSE are shown in Table 4.3, it was observed that the tensile strength of the crosslinked films increases significantly with the HBPU content. This is because, as the crosslink density increases, the bridges among the chain molecules also increase, which in turn demand for more stress value for their rupture. The increase of strength is also due to good compatibility and various intermolecular interactions as discussed earlier. The scratch hardness also increases with the increase of the polyurethane content, which is again caused by the increase of crosslinking density, hydrogen-bond formation, etc. Although the modified epoxy exhibited considerable hardness, still they have enough flexibility as found by the elongation at break values (Table 4.3). The long fatty acid chains of oil, ester and ether linkages of PCL render this high flexibility of the films. The impact resistance of all the films showed excellent result as expected from the tensile strength.

Table 4.3: Performance characteristics of HBPU modified MBPSE and its nanocomposites

Samples	Tensile strength (MPa)	Elongation at break (%)	Impact resistance (cm)	Gloss (60°)	Scratch hardness (kg)
MBPSE	6	95	100	60	3.4
EHBPU10	7.2	97	100	62	4.5
EHBPU20	8.2	105	100	62.7	5.1
EHBPU30	11.23	110	100	65	5.5
EHPN1	12.94	67.45	90	70	6
EHPN3	14.98	55.76	87	75	7
EHPN5	19.78	50.14	80	81	10

The tensile strength and scratch hardness of the prepared nanocomposites were found to increase as compared to that of the pristine polymeric system (Table 4.3). The proliferation of internal inorganic-polymer interface means the majority of polymer chains reside near the inorganic surface. As the polymer chains are confined by the interface, the free energy of the polymer in this region is different from the bulk. In addition, as the domain size of the microphase for the system decreases the

compatibility between the components increases, this in turn enhances the mechanical properties like tensile strength, modulus, etc.²⁵ The mechanical properties gives an idea about the morphological behavior of the nanocomposites better the mechanical properties, the lower is the degree of microphase separation due to more polymer filler interaction.²⁴ The scratch hardness also augmented with the nanoclay loading. The increase in scratch hardness is due to the dissipation of the stress generated at the interface between the moving tip and the film surface throughout the nanocomposite. The stress is than absorbed by the hard clay layers and consequently scratch hardness increase with clay loading in this case.

4.3.9. Thermal Study

Fig. 4.11 shows the thermal profile of the MBPSE and HBPU modified epoxy resin. The initial thermal degradation pattern of the pristine epoxy resin does not exhibit any significant enhancement after modification. MBPSE exhibited initial degradation temperature of 277 °C however after modification there was a slight improvement in the degradation temperature (286 °C). The increase in the thermal stability is due to increase crosslink density thereby bridging the polymer backbone, which results in a tough material.¹⁵ These altogether decreases the segmental mobility and hence improvement in the thermal stability was observed in this case. The weight residue of the hyperbranched polyurethane modified epoxy at 650 °C was 9.54% whereas in case of MBPSE the value was 6.5%. The higher amount of char residue in case of modified system is attributed to the presence of aromatic TDI, bisphenol-S and bisphenol-A moiety. The presence of char provides better heat shielding to the bulk decomposition of the polymer matrix. On incorporation of nanoclay the onset degradation temperature shifted to higher value (Fig. 4.11), i.e. upto 309 °C for EHPN5. The polymer chains exhibiting extensive interaction with the clay layers undergoes restricted segmental motion, which was reflected in higher thermal stability. The hard clay layers thus acts as a barrier from volatilizing the polymer matrix. The weight residue of the nanocomposite (EHPN5) at 650 °C was 10.95%. The higher amount of residue is due to the formation of a thermally stable charred material of reactive degrading species during decompositions. The Hoffman decomposition of the onium modifier of the clay gives protonated montmorillonite that can catalyze the formation of stable carbonaceous residue. However, no significant differences were observed in the onset degradation temperature for the modified systems. Although the difference is not too

large, there was a slight tendency of increase in the initial degradation temperature with nanoclay content.

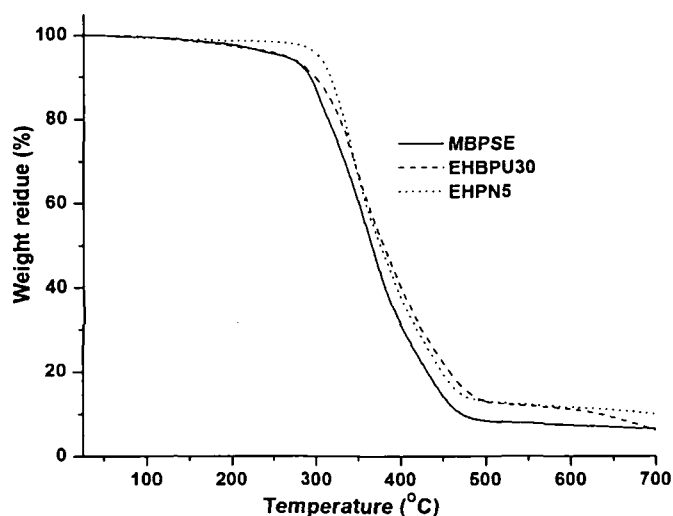


Fig. 4.11: TGA thermograms for MBPSE, EHBPU30 and EHPN5

4.3.10. Biodegradation Study

A striking drawback of the conventional epoxy resin is their non-biodegradability under ambient conditions. *Pseudomonas* sp. being the most prominent organism, as it has high ability to degrade bisphenol-A based epoxy modified vegetable oil based hyperbranched polyurethane¹⁴ so *P. aeruginosa* (MTCC 424) was taken as the microorganism for the present study.

The growth profiling of consortia in the modified broth media lacking dextrose compels the bacteria to use epoxy and modified system as the primary carbon source in each case.²⁹

The biodegradation of both the MBPSE, HBPU modified MBPSE and its nanocomposites were quantitatively tested and confirm by direct exposure to strain of *P. aeruginosa* bacteria by broth culture technique. After keeping the samples in broth culture media for six weeks, the bacterial OD was determined. The difference in the rate of growth initially for two weeks both for the nanocomposites as well pristine system was not significant as can be observe from the curves after two weeks of bacterial exposure (Fig. 4.12).

However, the bacterial growth rate increased significantly after two weeks, as can be realized from the bacterial count. This observation was cleared for the biodegradation of HBPU modified MBPSE and its nanocomposites. The inoculated films were found to be deteriorated to a significant extent especially for the

hyperbranched polyurethane modified epoxy and its nanocomposites. Again, the rate of biodegradation was found to be higher than the corresponding pristine polymers in both the cases. The growth of *P. aeruginosa* bacterial strains, modified epoxy system and various nanocomposites films as well as on the corresponding pristine polymeric films can be realized from Figs. 4.12 and 4.13, respectively.

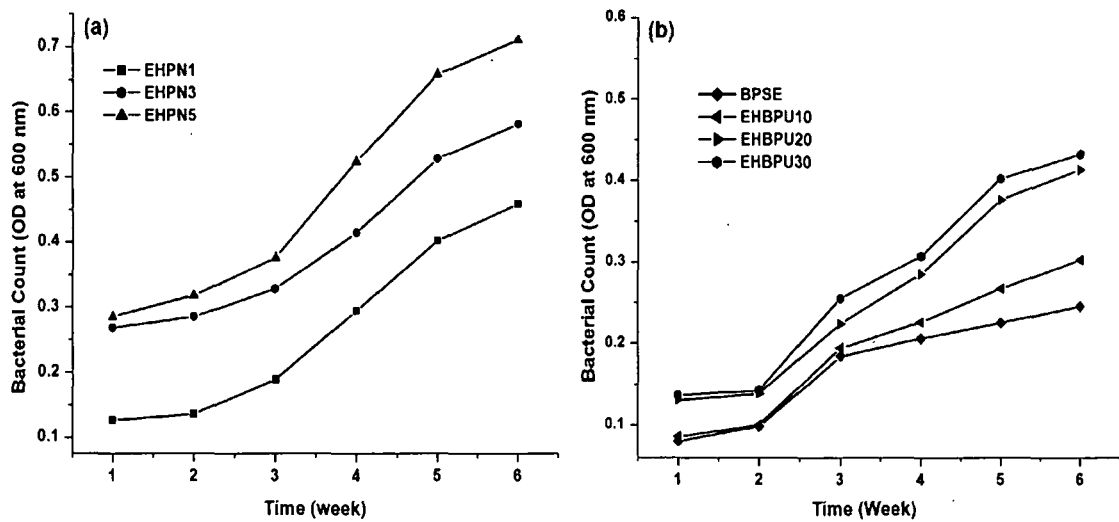


Fig. 4.12: Growth of *P. aeruginosa* bacterial strain, MTCC 424 on (a) HBPU modified epoxy and (b) nanocomposites

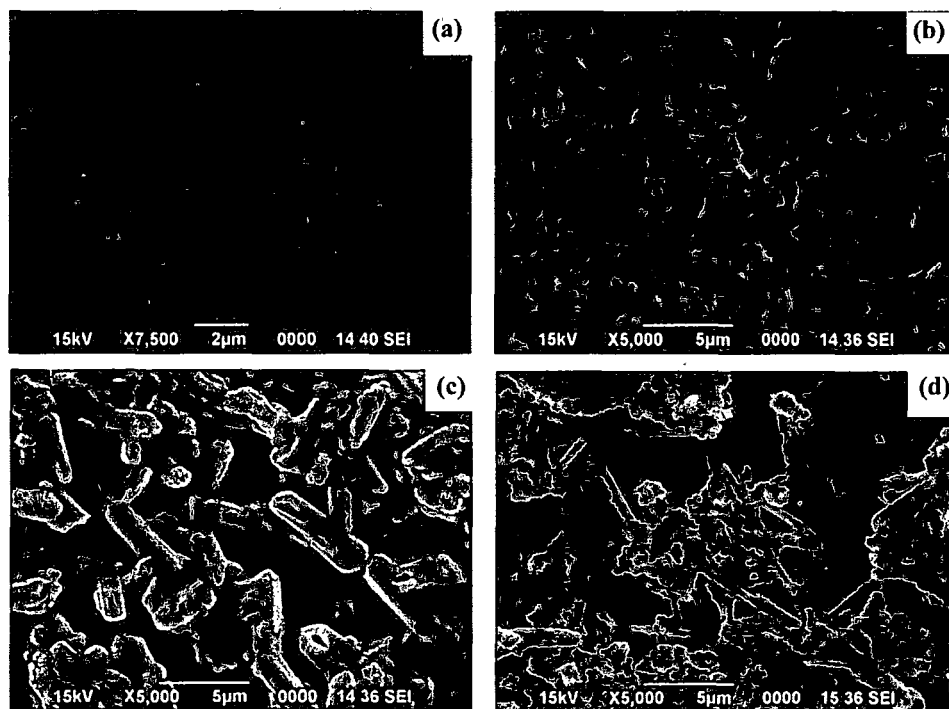


Fig. 4.13: SEM micrographs for films after six weeks of bacterial exposure (a) untreated MBPSE, (b) inoculated MBPSE, (c) EHBPU30 and (d) EHPN5

The polyurethane moiety accelerates the biodegrading process for epoxy resin. The vegetable oil modified polymeric systems are more prone to bacterial attack.³⁰ These facts supported the above observation wherein bacterial degradation increases with the hyperbranched polyurethane content. The SEM micrographs (Fig. 4.13) after six weeks of bacterial exposure exhibit significant topographical changes for polyurethane modified epoxy resin. The bacteria were seen to adhere to the film indicating good biocompatibility of the polymeric system. The acceleration of biodegradation was more prominent for the nanocomposites. Clay can cause heterogeneous hydrolysis of the ester groups in presence of microbes by absorbing water.

The process has an induction time,²⁹ hence tremendous enhancement of biodegradation was observed only after two weeks of bacterial exposure in this case. The progressive degradation changes the microstructure of the composite film resulting, as can be seen from the SEM images (Fig. 4.13).

4.3.11. RBC Haemolysis Protection Assay for Cytocompatibility

To investigate the nanocomposites effect on the mammalian membranes, the haemolysis test was carried out. The nanocomposites exhibited higher inhibition assay as compared to the pristine system (Fig. 4.14). This observation indicates that the presence of clay has a definite role to play in RBC haemolysis prevention. However, compared to Triton X 100, the nanocomposites did not exhibited any significant haemoglobin release and showed almost similar results as that of the negative control PBS. This indicated that it did not cause any lysis of the erythrocyte membranes. The

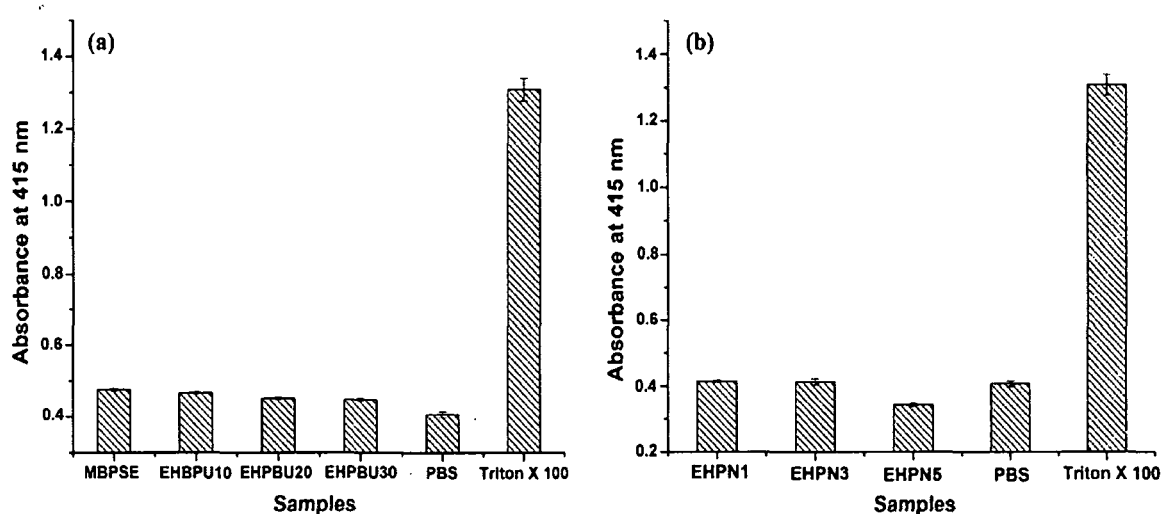


Fig. 4.14: RBC protection assay of (a) HBPU modified MBPSE and (b) nanocomposites

above observation reveals the non-toxic behavior of the nanocomposites to the living cells with concomitant prevention of cell damage against any harmful free radicals.

4.4. Conclusions

The study demonstrated that the performance characteristics of epoxy resin have been enhanced by its modification with vegetable oil based hyperbranched polyurethane and by the formation of nanocomposite with nanoclay. Both the components showed good compatibility as observed by SEM studies. The EHBPU30 showed the best performance characteristics among the studied system. Moreover, the addition of nanoclay in the EHBPU30 matrix further enhances the performance characteristics. The SEM and TEM studies reveal a partially delaminated structure of the nanocomposites. All the systems were found to be biodegradable as studied by broth culture technique. *P. aeruginosa* bacterial strain significantly degrades the system even after 30 days of inoculations. Further, the rate of biodegradation was found to be higher in case of the nanocomposites than the pristine system.

Reference

1. Puglisi, J.S. & Chaudhari, M.A. Epoxies (EP), in *Engineered Materials Handbook*, J.N. Epel et al. eds., OH: ASM International, Metals Park 1988, 240–1.
2. Uyama, H., et al. Green nanocomposites from renewable resources: Plant oil-clay hybrid materials, *Chem. Mater.* **15**, 2492-2494, 2003.
3. David, S.B., et al. Studies on acrylated epoxidized triglyceride resin-co-butyl methacrylate towards the development of biodegradable pressure sensitive adhesives, *J. Mater. Sci. Mater. Med.* **20**, S61-S70, 2009.
4. Ahmed, S., et al. Polyesteramide from pongamia glabra oil for biologically safe anticorrosive coating, *Prog. Org. Coat.* **47**, 95-101, 2002.
5. Meier, M.A.R., et al. Plant oil renewable resources as green alternatives in polymer science, *Chem. Soc. Rev.* **36**, 1788–802, 2007.
6. Mapleston, P. New technologies for a greener industry, *Plastics Eng.* **64**, 10–5, 2008.
7. Athawale, V.D., & Chamankar, A.V. Low cost multipurpose coatings from alkyd-ketonic blends, *Paintindia* **53**, 41-48, 2003.
8. Kaji, M., et al. Synthesis of a bifunctional epoxy monomer containing biphenyl moiety and properties of its cured polymer with phenol novolac, *J. Appl. Polym. Sci.* **74**, 690-698, 1999.
9. Francisa, B., et al. Cure kinetics and morphology of blends of epoxy resin with poly (ether ether ketone) containing pendant tertiary butyl groups, *Polymer* **44**, 3687–3699, 2003.
10. Iijima, T., et al. Toughening of epoxy resin by modification with acrylic elastomers containing pendent epoxy groups, *Eur. Polym. J.* **26**, 145-151, 1990.
11. Frisch, H.L., & Frisch, K.C. Polyurethane-epoxy interpenetrating polymer networks-barrier and surface properties, *Prog. Org. Coat.* **7**, 105-111, 1979.
12. Lamba, N.M.K., Woodhouse, K.A. & Cooper, S.L. et al. *Polyurethanes in Biomedical Applications*, CRC Press, FL, 1998.
13. Huang, S.L., & Lai, J.Y. Structure-tensile properties of polyurethanes, *Eur. Polym. J.* **42**, 1563-7, 1997.
14. Deka, H., & Karak, N. Vegetable oil-based hyperbranched thermosetting polyurethane/clay nanocomposites, *Nanoscale Res. Lett.* **4**, 758–765, 2009.

15. Dutta, S., et al. Biocompatible epoxy modified bio-based polyurethane nanocomposites: Mechanical property, cytotoxicity and biodegradation, *Bioresour. Technol.* **100**, 6391–6397, 2009.
16. Nair, D.G., et al. Antimicrobial activity of omwaprins, a new member of the waprins family of snake venom proteins, *Biochem. J.* **402**, 93–102, 2007.
17. Pospoasiil, J., et al. Degradation and aging of polymer blends I. Thermomechanical and thermal degradation, *Polym. Degrad. Stab.* **65**, 405–414, 1999.
18. Dutta, S., & Karak N. Blends of *Mesua ferrea* L. seed oil based polyurethane with epoxy resin, *Pig. Resin. Technol.* **36**, 74–82, 2007.
19. Wang, J.C., et al. Preparation of thermosetting polyurethane nanocomposites by montmorillonite modified with a novel intercalation agent, *J. Polym. Sci. Part B: Polym. Phys.* **45**, 519–531, 2007.
20. Ding, Q., et al. Synthesis and characterization of polyurethane/montmorillonite nanocomposites by in situ polymerization, *Polym. Int.* **55**, 500–504, 2006.
21. Karak, N., et al. Synthesis and characterization of castor oil modified hyperbranched polyurethanes, *J. Appl. Polym. Sci.* **112**, 736–743, 2009.
22. Jia, Q.M., et al. Synthesis and characterization of polyurethane/epoxy interpenetrating network nanocomposites with organoclays, *Polym. Bull.* **54**, 65–73, 2005.
23. Brydson, J.A. *Plastics Materials*, Butterworths, London, 1982.
24. Jeong, F.H., et al. Effective preparation and characterization of montmorillonite/poly(ϵ -caprolactone)-based polyurethane nanocomposites, *J. Appl. Polym. Sci.* **107**, 803–809, 2008.
25. Zou, H., et al. Study of nanocomposites prepared by melt blending TPU and montmorillonite, *Polym. Compos.* **29**, 385–389, 2008.
26. Ray, S.S., & Okamoto, M. Polymer/layered silicate nanocomposites: A review from preparation to processing, *Prog. Polym. Sci.* **28**, 1539–1641, 2003.
27. Ma, X., et al. Rectorite thermoplastic polyurethane nanocomposites: Preparation, characterization and properties, *J. Appl. Polym. Sci.* **93**, 608–614, 2004.
28. Ni, P., et al. Novel polyether polyurethane/clay nanocomposites synthesized with organically modified montmorillonite as chain extenders, *J. Appl. Polym. Sci.* **99**, 6–13, 2006.

29. Ray, S.S., & Bousmina, M. Biodegradable polymers and their layered silicate nanocomposites: In greening the 21st century materials world, *Prog. Mater. Sci.* **50**, 962-1079, 2005.
30. Riaz, U., et al. Compatibility and biodegradability studies of linseed oil epoxy and PVC, *Biomass Bioenrg.* **34**, 396-401, 2010.

CHAPTER 5

Epoxy/Nanoclay Copper Nanocomposites

5.1. Introduction

In the Chapter 1, section 1.1, Chapter 3, section 3.1 and Chapter 4, section 4.1 the role of nanoclay as nanomaterial is discussed. As the scope of nano-dimensional architecture constrained to academic research has expanded into a full fledged industrial hotbed with newer applications and goals,¹ so other nanomaterials are also very important and needed to be studied. Ensembles of different nanostructures which are able to combine their characteristics and to organize themselves for creating materials owning complex properties have a great potential in optical, electrical, medical, antibacterial etc. applications due to the particular interactions that can be established between nanoscaled architectures and biological interfaces.²⁻⁵ The metallic nanoparticles are most promising as they show good antibacterial properties due to their large surface area to volume ratio, which is coming up as the current research interest due to the growing microbial resistance against metal ions, antibiotics and the development of resistant strains.⁶

Copper and its complexes have been widely utilized as effective materials for sterilizing liquids, textiles and also human tissues for centuries.^{7,8} Some advantages of copper materials including their bactericidal activity were well known even since the time of ancient civilizations, such as ancient Persian. For instance, some copper handicrafts such as cauldron (which need polishing after few usages) have been used at some small towns of Iran for cooking traditional foods. Today copper is utilized as an agent for purification of water and inactivation of some microorganisms and bacteria.^{9,10} In spite of the negligible responsiveness of human tissues to copper,¹¹ microorganisms show high sensitivities to copper.¹² Recently, due to development of some resistant bacteria strains against the antibiotics,¹³ the antibacterial activity of nanomaterials, such as silver¹⁴⁻¹⁶ and copper,^{17,18} with their unique size dependent properties has attracted great attentions.

The use of clay and clay minerals as a support for the synthesis of nanoparticles has been recognized as a promising method. Montmorillonite (MMT) in this regard has been an apt choice due to its chemical and physical nature. MMT has been used for preparation of wide range of nanoparticles like gold, rhodium etc.¹⁹

Advanced coating technology and ability to produce designed materials for implants, adhesives, coatings, packaging, and drug delivery systems are creating a wide variety of important innovations for a number of biotechnological applications. These include the elicited antibacterial coatings for paint applications, biomedical devices or antimicrobial packaging.^{20,21} The rationale for the use of copper lies in the strong toxic action this metal exerts against prokaryotes (i.e., all types of bacteria), while it is much less toxic against eukaryotes (i.e., all other organisms such as humans). Thus copper has been used for decades as an effective antibacterial.

Noteworthy, since the 19th century, dispersions of copper or copper oxide particles into organic matrixes have been employed as antifouling coatings by the paint industry, mainly for marine applications. Such paints (generally addressed as ablative copper) after immersion in seawater undergo dissolution processes at slow rate, eventually provoking the continuous and massive release of toxic species, such as copper, tin, or organometallic compounds, in the marine ecosystem. A worldwide attempt to eliminate or reduce the use of such large-scale coatings is being promoted.²² There are reports for the use of copper/polymer nanocomposites as a bioactive coating against bacteria.²³ Today, the quest for hygienic living conditions prompts new challenges for the development of non-toxic antimicrobial materials which do not permit microorganisms to attach, survive, and proliferate on material surfaces. Such nontoxic antimicrobial protection can reduce the risks of transmitting diseases and prevent the surface biofouling without causing environmental pollution and poisoning. However there is no report of vegetable oil based epoxy/OMMT-Cu (OMMT decorated Cu nanoparticles) nanocomposites system as antimicrobial system.

This chapter reports the synthesis of copper nanoparticles on OMMT nanoclay and nanocomposites formation using MBPSE as the matrix. The antimicrobial properties of the modified nanoclay as well the nanocomposites were studied. Further the cytotoxicity of the nanocomposites were evaluated by RBC haemolysis protection assay. The performance characteristics and thermal properties of the nanocomposites were also studied to view the applicability of the system as advanced antimicrobial coatings.

5. 2. Experimental

5.2.1. Materials

Mesua ferrea L. oil, as described in Chapter 2, section 2.2.1. was used as the vegetable oil. Montmorillonite (OMMT) and *N,N'*-dimethylformamide (DMF) are well described

in Chapter 3, section 3.2.1. and was used as the organonano clay and solvent respectively.

Cupric acetate $[(\text{CH}_3\text{COO})_2\text{Cu} \cdot 2\text{H}_2\text{O}]$ was obtained from SD fine Chemicals, Mumbai, India. Its molecular weight (M_w) is 199.65 g/mol, density 1.88 g/cm³, boiling point (b.p.) 240 °C, melting point (m.p.) 115 °C and minimum assay 98%. The impurities present generally are chloride (0.005%), sulfate (0.03%) and iron (0.02%). It was used as received.

Phenyl hydrazine was obtained from Merck, Germany. Its molecular weight is 108.14 g/mol, density 1.09 g/cm³, boiling point (b.p.) 243 °C, m.p. 19 °C and minimum assay 98%.

Acetone (CH_3COCH_3) was obtained from SD fine Chem, Mumbai. It has molecular weight (M_w) 32.05 g/mol, purity $\geq 99\%$ with water $\leq 0.2\%$, density 0.791-0.892 g/mL at 25 °C and boiling point (b.p.) 64-65 °C. It was used as received.

All the minerals $(\text{NH}_4)_2\text{SO}_4$, Na_2HPO_4 , KH_2PO_4 , $\text{MgSO}_4 \cdot 7\text{H}_2\text{O}$, $\text{CaCl}_2 \cdot 2\text{H}_2\text{O}$, $\text{FeSO}_4 \cdot 7\text{H}_2\text{O}$, $\text{CuSO}_4 \cdot 7\text{H}_2\text{O}$, $\text{MnSO}_4 \cdot 5\text{H}_2\text{O}$, $\text{ZnSO}_4 \cdot 7\text{H}_2\text{O}$, $\text{H}_3\text{BO}_3 \cdot 5\text{H}_2\text{O}$ and MoO_3 used for preparation of bacterial broth culture media during antimicrobial study and PBS (phosphate buffer saline) and Triton X 100 used for RBC haemolysis tests were of same specifications as described in Chapter 4, section 4.2.1. The bacterial strains *Staphylococcus aureus* MTCC 737 and *Klebsiella pneumonia* MTCC 618 used for the antimicrobial study were obtained from the Department of Molecular Biology and Biotechnology (Department of Biotechnology, DBT Centre, Government of India), Tezpur University.

5.2.2. Instruments and Methods

The FTIR and TGA analyses were carried out using the same instruments and conditions as mentioned in Chapter 2, section 2.2.2. and Chapter 3, section 3.2.2. respectively. The XRD, SEM and TEM were carried out using the same instruments and conditions as mentioned in Chapter 3, section 3.2.2. The measurements of tensile strength and elongation at break value, gloss, impact resistance, scratch hardness and chemical resistance were performed according to the standard methods as mentioned earlier (Chapter 2, section 2.2.2.). UV-visible spectra of the OMMT-copper nanocomposites were recorded by UV-visible spectrophotometer, UV-2550 (Shimadzu, Japan) with a 0.001% solution in DMF at room temperature (~ 27 °C). Sonication was done with the same instrument as mentioned in Chapter 3, section 3.2.2. at fixed

amplitude and a half cycle for proper dispersion of the OMMT-Cu in the MBPSE matrix.

Mesua ferrea L. seed oil was extracted from the matured seeds by the same method as described in Chapter 2, section 2.2.1. MBPSE was synthesized as described in Chapter 2, section 2.2.2.1.

5.2.2.1. Preparation of Copper Nanoparticles

The clay suspension was prepared by dispersing 1 g of OMMT in 50 mL DMF. It was then again dispersed by sonication for 20 min. To achieve desired copper loading in the clay/copper system, weight ratio of 1:1, 1:0.5 and 1:0.25 (coded as N1, N0.5 and N0.25, respectively) corresponding to 3.16 g, 1.58 g and 0.792 g of copper acetate, were dissolved in 30 mL, 15 mL and 8 mL DMF respectively. The copper acetate solutions were then added to the clay suspension and stirred for 24 h at 60 °C, followed by sonications for 10 min. The copper precursor was then reduced in the presence of montmorillonite by adding phenyl hydrazine in the mol ratio of 1:3 (copper acetate/phenyl hydrazine). The whole solution was stirred at room temperature for 54 h until reddish brown coloration appears. The whole solution was further sonicated for 15 min. The obtained suspension consisting of copper nanoparticles decorated montmorillonite was centrifuged and washed repeatedly with double distilled water and acetone. The resulting solid phase was dried at 45-50 °C.

5.2.2.2. Fabrication of Nanocomposites

The dried OMMT-Cu system was added into the MBPSE matrix by fixing the percentage of OMMT at 3 wt%. The copper nanoparticles concentrations in the matrix varies viz., 3, 1.5 and 0.75 wt% with respect to 1:1, 1:0.5 and 1:0.25 OMMT-Cu and were coded as ECuN1, ECuN0.5 and ECuN0.25 respectively. The nanocomposites were prepared similarly as described in Chapter 3, section 3.2.2.9. MBPSE and OMMT-Cu were mixed vigorously for 10 min at room temperature followed by sonication for 15 min using a single probe sonicator (UP200S, Hielscher, germany) at half cycle and amplitude of 50%.

5.2.2.3. Curing of the Resin and Nanocomposites

The curing of the resin and the MBPSE/OMMT-Cu nanocomposites were done similarly to method as described in Chapter 2, section 2.2.2.2.

5.2.2.4. Antibacterial Study

The polymer MBPSE, nanoparticles (N1, N0.5 and N0.25) and the nanocomposites were investigated for their antimicrobial activity, separately, using the agar well diffusion study. *Staphylococcus aureus* as Gram positive bacteria and *Klebsiella pneumonia* as Gram negative bacteria were taken for the study. The bacteria were grown overnight in Luria broth media and 50 μL of the broth culture was taken and plated in the agar plates. Agar plates for the antimicrobial test were prepared using Mueller Hinton Agar media for the antibacterial study and as per the manufacturer's instructions. Wells were punched using a well borer with a diameter of 6 mm. 50 μL of the nanocomposite solutions and also the nanoparticles were poured into the wells. Antibiotic solution containing streptomycin sulfate at a concentration of 5 mg/mL was taken as the positive control. The plates were then incubated overnight at 37 °C. The formation of zones of inhibition around the wells indicated the antimicrobial activity of the polymer, nanocomposites and the nanoparticles.

5.2.2.5. RBC Haemolysis Protection Assay

The haemolytic activity²⁴ of the final nanocomposite and polymer films was investigated to find out if the materials possessed any membrane damaging activity. For this study goat blood was collected in a 50 mL centrifuge tube containing an appropriate anticoagulant. The blood was centrifuged at 2000 rpm, the supernatant discarded and the pellet was washed further using PBS (pH 7.4). Finally the pellets were mixed with PBS at a ratio of 1:50 (v/v). From this 2 mL of blood was collected in 2 mL centrifuge tubes and 10 mg of the nanocomposite and polymer films was added to the tubes and incubated for two hours. After the incubation period was over the tubes were centrifuged and then 200 μL of the supernatant was collected and taken separately. To this 2.8 mL of PBS was added and then the final solution was measured in a spectrophotometer (Cecil, UK) at 415 nm. Triton X 100 and PBS were taken as the positive and negative control respectively (as described in Chapter 4, section 4.2.2.8.).

5.3. Results and Discussion

5.3.1. Formation of MBPSE/OMMT-Copper Nanocomposites

The nanoparticles by virtue of their high aspect ratio and surface energy have high tendency to agglomerate. Therefore stabilization of the nanoparticles is a prerequisite for obtaining specific surface chemistry and/or architecture bestow desired surface properties to a given material without significantly altering other desirable properties of

the material.²⁵ Polymers play important roles in dictating nanoparticle size, shape and interparticle spacing. Also it governs the properties of both the interface between the surfaces of the polymer and the nanoparticles. The OMMT was impregnated as the avenue to compensate for the low mechanical and thermal properties of pristine MBPSE by forming nanocomposites. The epoxy/carboxy/hydroxy groups of the MBPSE can easily interact with hydroxyl groups of nanoclay through hydrogen-bonding or other polar-polar interaction to form stable and well dispersed nanocomposites as already mentioned in Chapter 3, section 3.3.2. The use of high shear force and ultrasonication results in the delamination of the nanoclay layers in the polymer matrix. The copper salts were first adsorbed onto the clay surface, and then the copper nanoparticles were prepared in the nanoclay by wet chemical reductive technique employing phenyl hydrazine. OMMT is an expandable 2:1-type clay mineral that has both interlayer sites and ionizable hydroxyl sites on its external surface for metal cation adsorption,²⁶ and the permanent negative layer charge originating from the isomorphous substitution of Mg(II) or Fe(II) for octahedral Al(III) is the origin of the binding of exchangeable cations to the interlayer sites.²⁷ It has a great adsorption capacity, which is attributed to its large specific surface area and high cation exchange capacity (CEC).^{28,29} The nanoclay surface by virtue of its high surface functionality stabilizes the nanoparticles onto its surface. The reduction performed at room temperature may result in nanoparticles with uniform particle size distribution, good antibacterial properties and good dispersion stabilities.

5.3.2. Characterization of the OMMT-Cu Systems and Nanocomposites

5.3.2.1. UV-Visible Spectroscopy

The formation of copper nanoparticles in OMMT was observed by UV-visible absorption studies (Fig. 5.1). Chemical reduction of Cu²⁺-loaded OMMT with excess of phenyl hydrazine resulted in formation of intra-OMMT-Cu nanoparticles. Evidence for this comes from the change in solution color from blue to reddish brown. The absorbance in UV spectra showed broad band from about 588 nm to 612 nm (Fig. 5.1 i).^{29,30} The strong surface-plasmon band may shift depending upon the particle size and shape. The strong surface-plasmon absorption band observed is due to the formation copper nanoparticles. The broadness of the absorption band (Fig. 5.1) probably arises from the wide size distribution of copper nanoparticles.

The incorporation of the nanoparticles in the MBPSE matrix does not affect their surface plasmon significantly as can be observed from the UV-visible spectra. The absorbance band at 589-615 broadens in the nanocomposites (Fig. 5.1 ii).

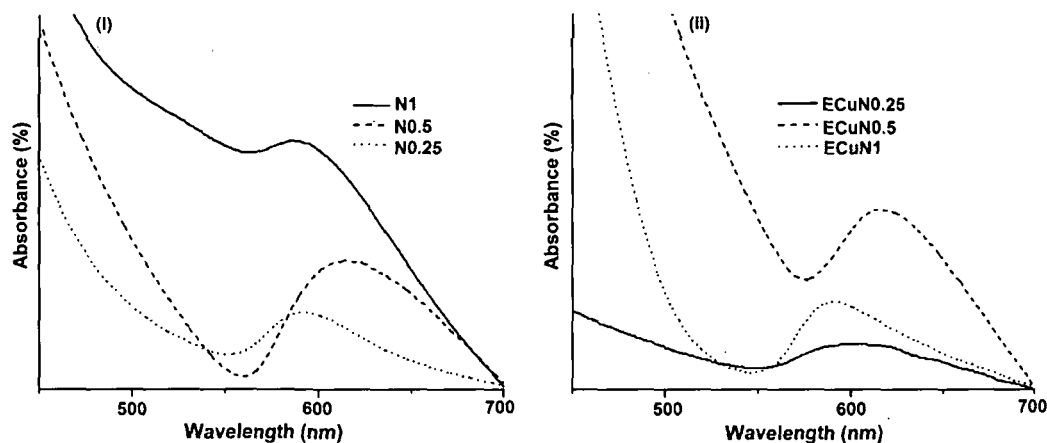


Fig. 5.1: UV-visible spectra of (a) OMMT-Cu systems and (b) nanocomposites

5.3.2.2. XRD Analysis

The X-ray diffractogram (Fig. 5.2) of the powder sample is well agreed with the literature values.^{29,30,31-32} All the reflection peaks at 2θ values of about 43.61° , 50.59° and 74.47° corresponding to $\{111\}$, $\{200\}$ and $\{220\}$ Bragg's reflections of cubic structure of copper were observed in the diffractograms. Besides these, the peaks appearing in the XRD spectra at 35.62° and 61.81° were due to copper oxide (CuO) nanoparticles, though UV-visible is silent about this. The peaks for the layered silicate i.e. OMMT were also observed in all the spectra, the basal reflection corresponding to $\{110\}$ plane for 2θ value of 4.15° for OMMT shifts to 3.64° indicating an increase in the gallery spacing with increase in the copper loading, the other peak observed was at 20.1° corresponding to $\{110\}$ plane. The observation of low-angle peak of OMMT suggests the possible coexistence of stacked nanostructures made up of copper nanoparticles in layered nanoclay. The intensity of the peaks corresponding to copper nanoparticles increases with the increase in the loading of the copper into the layered silicate. As shown by the sharper and more intense band, the degree of crystallinity increases with copper concentrations. The oxidation of the Cu nanoparticles might be responsible for the presence of reflection peak for copper oxide nanoparticles.

However the structure provides sufficient stability and as no structural changes was observed in the spectra taken after two months. This suggested that the clay layer provides sufficient oxidation stability to the copper nanoparticles.

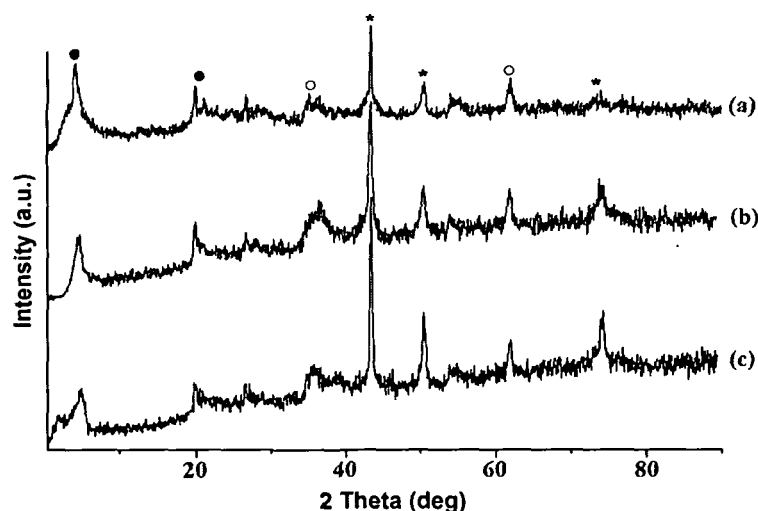


Fig. 5.2: XRD patterns of OMMT-Cu systems, (a) N0.25, (b) N0.5 and (c) N1 (= Cu, o = CuO and • = OMMT)*

The XRD diffractograms of the nanocomposites with 1, 0.5 and 0.25 wt% of copper loading are shown in Fig. 5.3. Diffraction peaks were observed at 43.8° , 50.57° and 74.68° corresponding to $\{111\}$, $\{200\}$ and $\{220\}$ of Bragg's reflection for cubic structure of copper nanoparticles (ICSD 851362). The basal reflections at 30.7° , 65.58° and 83.45° for $\{200\}$, $\{022\}$ and $\{400\}$ planes corresponding to the tetragonal and monoclinic structure of copper oxide nanoparticles (CuO) respectively, were also observed in the spectra of nanocomposites.

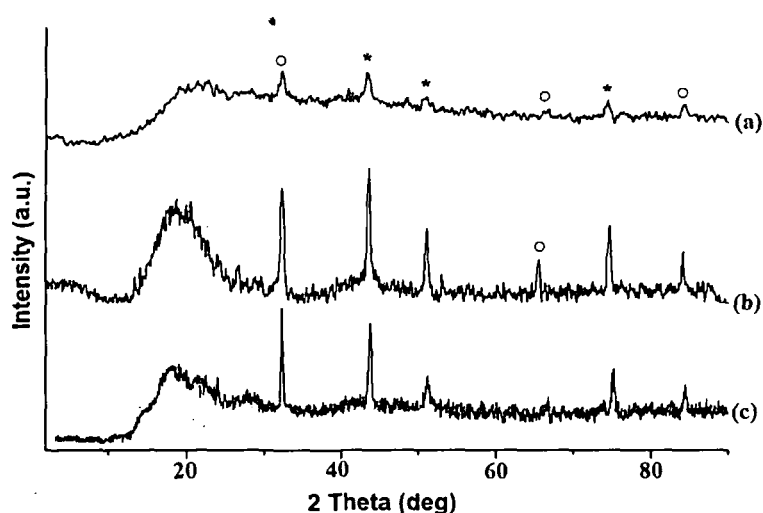


Fig. 5.3: XRD patterns of nanocomposites, (a) ECuN0.25, (b) ECuN0.5 and (c) ECuN1 (= Cu, o = CuO and • = OMMT)*

The basal reflection at $\{110\}$ plane corresponding to peak value of 4.15° was found to be absent in the nanocomposite, which is due to the loss of structural regularity of

the layered silicates in the nanocomposites. A broad peak was observed around 18.9° to 20.13° in the diffractogram of the nanocomposite. This appearance is due to the amorphous nature of the polymer.

5.3.2.3. FTIR Analysis

The Fig. 5.4 shows the FTIR spectrum of copper nanoparticles in OMMT. Obviously the features of the OMMT can also be recognized among the bands of copper nanoparticles in the spectrum. The spectrum of OMMT is discussed in details in Chapter 3, section 3.3.3.1.

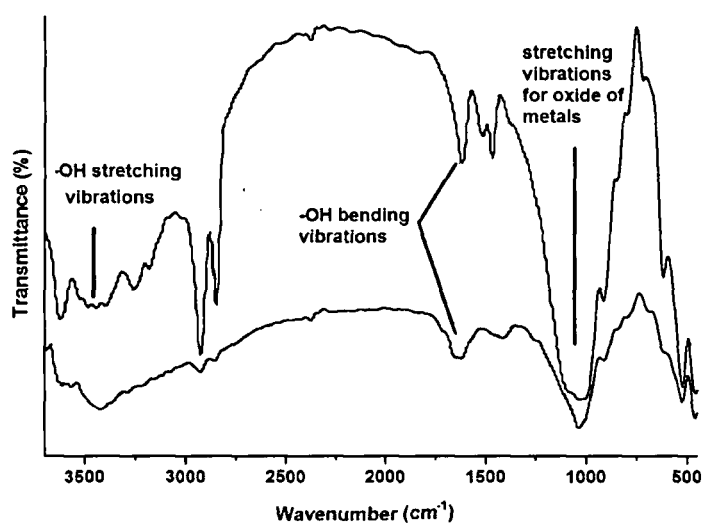


Fig. 5.4: FTIR spectra of (a) OMMT and (b) OMMT-Cu (N0.5)

Multiple broad bands were detected for OMMT in the range $3627\text{--}3403\text{ cm}^{-1}$ that are attributed to the -OH stretching frequencies. These indicate the presence of at least three types of -OH groups that are suggested to be isolated -OH groups. In the high frequency range a well-defined band appeared at 3627 cm^{-1} , associated to the stretching mode of the -OH group coordinated to Al cations.³² This band gets minimized in the OMMT-Cu system (Fig. 5.4), indicating the insertion and stabilization of the Cu nanoparticles. The broad -OH stretching band at about 3446 cm^{-1} due to the Al-OH and Si-OH shifted to 3412 cm^{-1} on the insertion of Cu nanoparticles.

The interaction of the OMMT-Cu with the matrix is shown in Fig. 5.5. The structural features of the nanocomposites and the matrix are not so different although the intensity decreases in all the cases. The -OH stretching band in all the cases exhibited a red shift with the increase of the OMMT-Cu content (Fig. 5.5). The shift (about $4\text{--}13\text{ cm}^{-1}$) primarily occurs due to the hydrogen-bonding between the MBPSE

matrix and the surface $-OH$ group of the nanoclay. The intensity of $-C=O$ stretching vibration band exhibited a decrease with simultaneous blue shifting in all the nanocomposites. The $-C=O$ group can be involved in numerous interactions viz. with the $-NH_2$ group of the hardener or with epoxy group and result chemical bond formation or by hydrogen bonding. This supported the above observation where the intensity decreases nearly half of the original, thus the crosslinking helps in the stabilization of the nanoparticles. Further the formation of $Cu-O-C$ structure cannot be neglected in the nanocomposites, the appearance of a broad band at around $1650-1605\text{ cm}^{-1}$ is indicative of such interactions. The epoxide stretching vibration gets vanished in the nanocomposites indicating the completion of curing via the ring opening of the epoxy group.

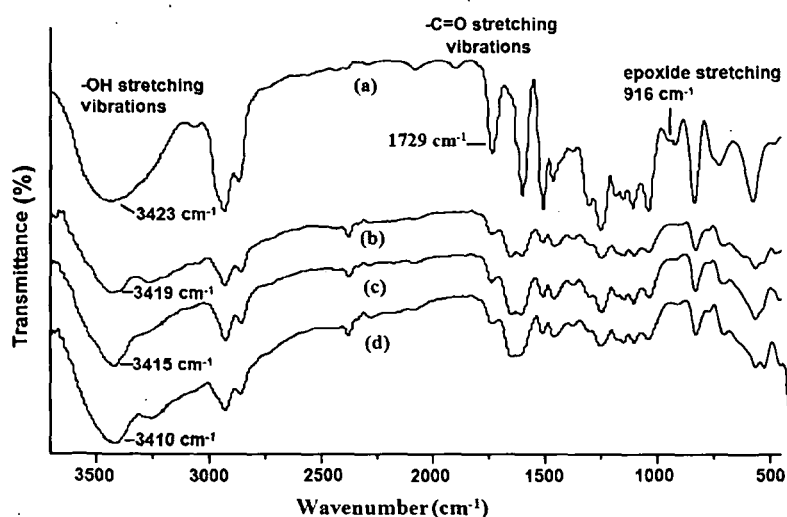


Fig. 5.5: FTIR spectra of (a) MBPSE, (b) ECU0.25, (c) ECU0.5 and (d) ECU1

5.3.2.4. SEM Study

The SEM micrographs of N1 and ECU1 are shown in Fig. 5.6. It was observed that the treated clay contains heterogeneous particles. The white nanoparticles in case of N1 were clearly seen to anchor onto the surface of clay. The particles were seemed to be well dispersed on the clay surface and no agglomerations was observed. The EDX data (Table 5.1) further supports the presence of the copper nanoparticles in the clay, wherein 6.16% of Cu in OMMT and 0.35% in case of ECU1 were observed (Fig. 5.7).

The results indicated that the room temperature reduction was effective in modifying the surface of the OMMT with Cu nanoparticles. The larger interlayer spacing of the 2:1 phyllosilicate (OMMT) provides a greater area of contact for the metal ion to penetrate, however longer time was required for intrinsic sorption because

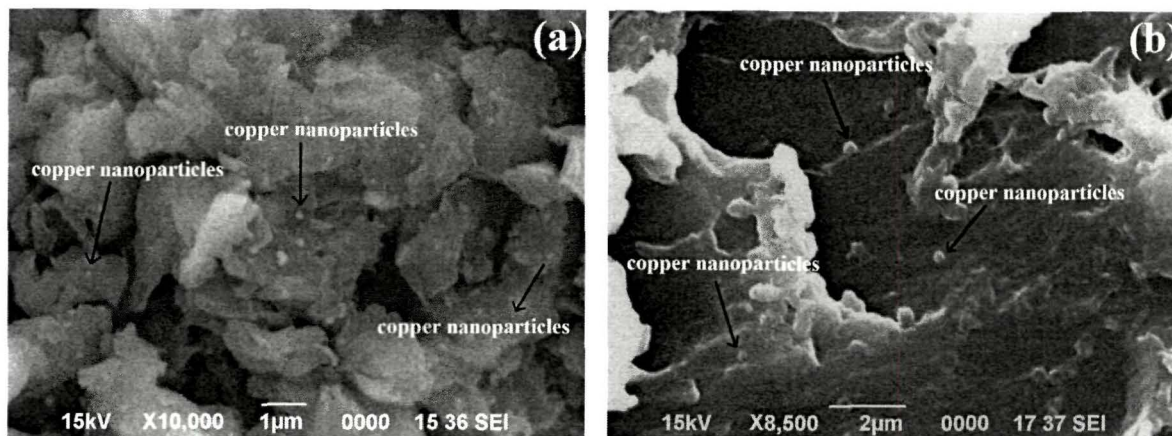


Fig. 5.6: SEM micrographs for (a) NI and (b) ECuNI

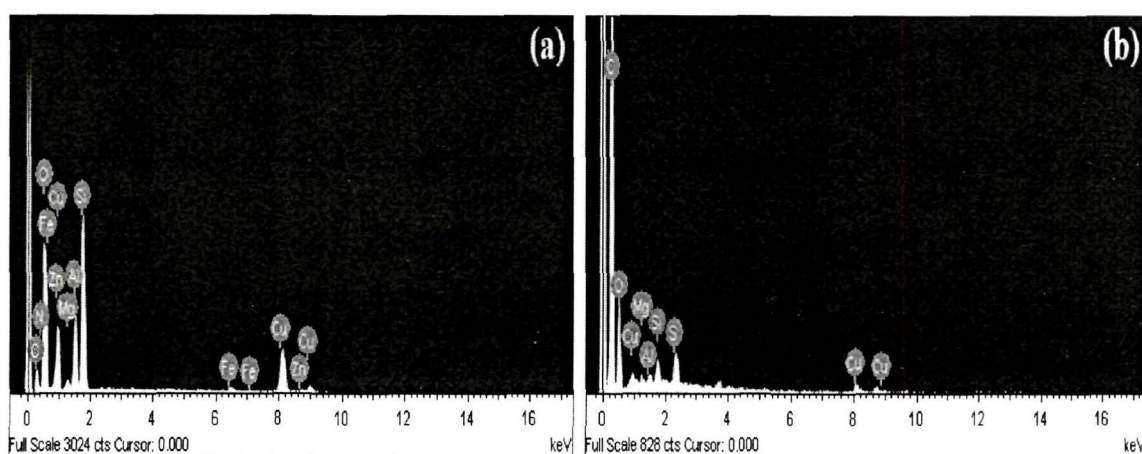


Fig. 5.7: EDX spectra of (a) NI and (b) ECuNI

of the diffusion barrier of the interlayer part. The sorption of the metal ion on the clay layer includes electrostatic adsorption, complex formation and reduction upon exposure to phenyl hydrazine. The crosslinked network of the polymer matrix provides an effective stabilization; the nanoclay with its high surface area extensively interacts with the matrix resulting in the immobilization of the nanoclay.

Table 5.1: EDX data of OMMT-Cu and OMMT-Cu/MBPSE nanocomposites

Samples	Content of element (%)									
	C	O	Mg	Al	Si	S	Fe	Cu	N	Mn
NI	17.71	48.97	0.94	4.36	12.47	-	0.39	6.16	7.77	0.15
ECuNI	75.36	20.39	0.10	0.24	0.36	0.88	0.27	0.35	-	-

5.3.2.5. TEM Study

Fig. 5.8 shows the HRTEM of N1, copper nanoparticles were spotted as dark spherical nanodots of diameters ranging from 10 to 20 nm, which were evenly distributed in size and dispersion across the platelets surface of the nanoclay. The dark spheres anchored onto the clay surface have particles distribution of 10-20 nm in size.

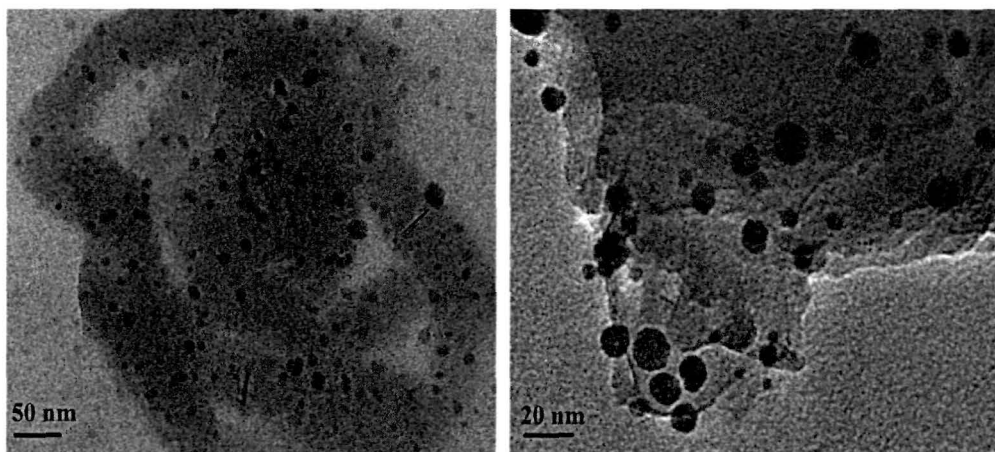


Fig. 5.8: HRTEM micrographs for N1

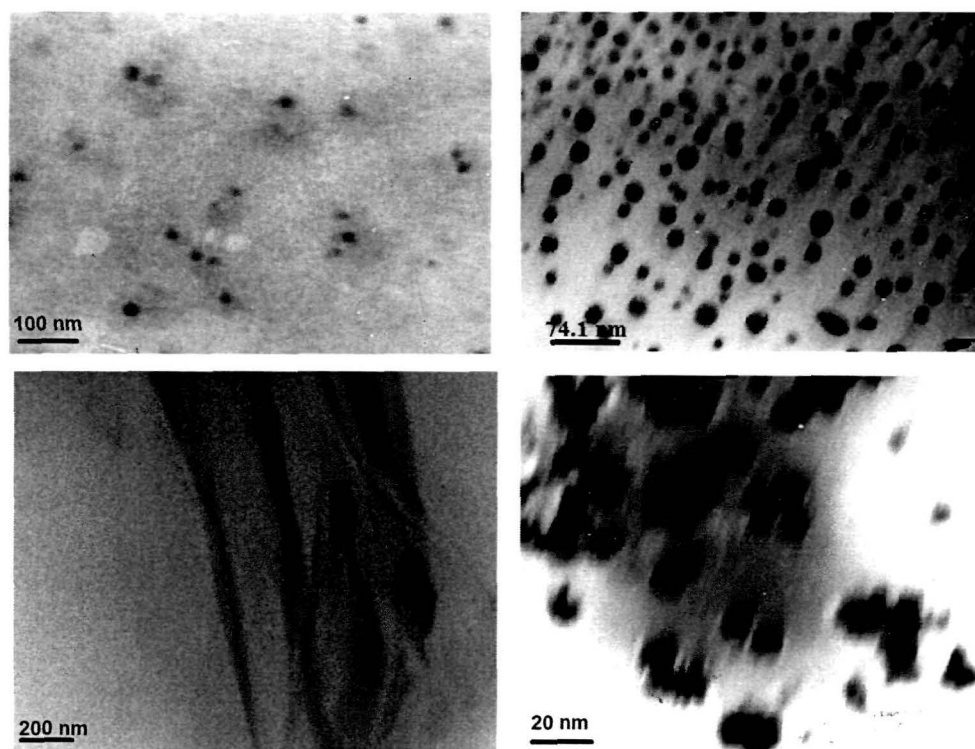


Fig. 5.9: HRTEM micrographs for ECuN1

The polymer proves to be a strong stabilizer for the nanoparticles, as seen in the TEM images (Fig. 5.9) the nanoparticles are uniformly distributed in the matrix. It can be observed from Fig. 5.9 that Cu nanoparticles with an average particle size of less than 20 nm and preponderant distribution were developed and assembled. There was no

agglomeration phenomenon observed in the TEM images of this kind of nanoparticles and Cu particles were well separated into single ones.

The pendant hydroxyl group of the matrix stabilizes the nanoparticles. The hydroxyl groups act as a kind of confined nanoreactors and/or superficial modifiers of Cu nanoparticles, inhibiting their growth and avoiding aggregation.²² The predominately interaction results in the immobilization copper nanoparticles. Inter and intramolecular interactions between the Cu decorated OMMT system and the MBPSE matrix, helps to reduce aggregation and protects from chemical environment resulting in complete stabilization.

5.3.3. Thermal Study

Fig. 5.10 shows the thermal profile of OMMT, N1 and the nanocomposites. OMMT exhibited a three degradation steps pattern, the first step corresponds to the loss externally adsorbed water. The second degradation step at about 290 °C is due to the thermal loss of the organic modifier and the third step corresponds to montmorillonite dehydroxylation at 670 °C. The sharp loss of mass at higher temperature (690 °C) is attributed to desorption of the any organic component, followed by the combustion at higher temperature of the residual modifier trapped in the clay matrix. The initial degradation at about 77 °C was not observed in case of Cu decorated OMMT system.

The presence of Cu nanoparticles has significant effect on the high temperature stability of the OMMT nanoclay. The Cu decorated OMMT exhibited weight residue of 79.6% at 600 °C, whereas for OMMT it was about 67%.

The fact that there are different combustion temperatures for the residual organic modifier in these two types of clay minerals is an indication of different interactions between the copper nanoparticles and the clay surfaces. The thermal stability of the nanocomposites was observed to enhance with the increase in the incorporation of the OMMT-Cu system with respect to the pristine MBPSE. However the difference in the peak temperature among the nanocomposites was not significant. It is well known that the clay plays an effective role in enhancing the thermal stability of the matrix system. The hard aluminum-silicate layer acts a thermal insulator thereby preventing the volatilization of the underlying matrix.

The small size of the copper nanoparticles can enhance the thermal stability of the system by virtue of a barrier. The nanoparticles prevent the escape of volatiles that may generate from the decomposition of the matrix at higher temperature. The weight

residue of the nanocomposites was enhanced after the incorporation of the nanoparticles, ECuN0.25 showed weight residue of about 18%, ECuN0.5 20.41% and ECuN1 showed 24.5%, whereas MBPSE showed a weight residue of only 6.9% at 650 °C (Fig. 5.10). The higher amount of weight residue signifies the noncombustible materials (i.e. char) this char residue forms a shield over the polymer and thus reduces the heat and mass transport from or into the matrix, thereby enhancing the thermo-stability of the system.

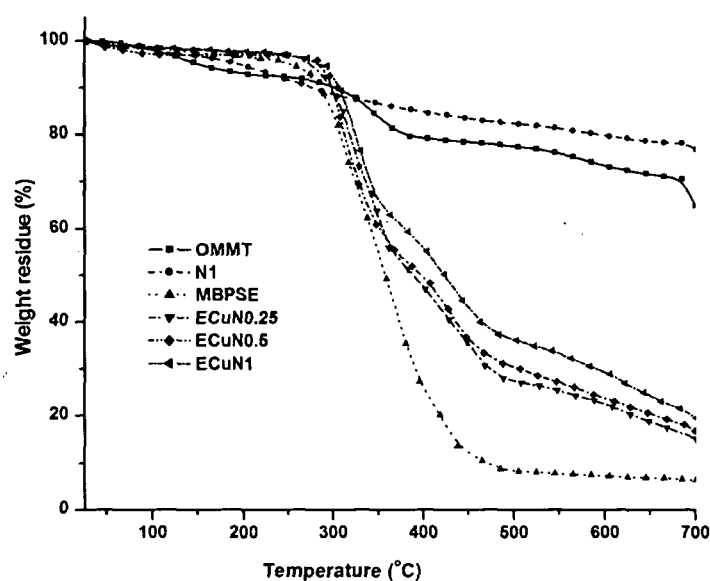


Fig. 5.10: TGA thermograms of OMMT, OMMT-Cu and nanocomposites

5.3.4. Performance Characteristics

The different performance characteristics of the prepared MBPSE/OMMT-Cu nanocomposites like tensile strength, elongation at break, gloss, impact strength and scratch hardness were determined and are given in Table 5.2.

The tensile strength of MBPSE/OMMT-Cu nanocomposites was found to be enhanced to a noticeable degree from 6 to 13.2 MPa with the increase of amount of copper nanoparticles from 0 to 3 wt%. This is attributed to the inclusion of homogeneously dispersed copper nanoparticles into the clay layers that are further delaminated by the polymer chains, thereby strengthening the matrix system. Also maximum surface of the silicate layers are available for strong interaction with the polymer chains and copper nanoparticles after delamination of the aluminosilicate clay layers which leads to increase in tensile strength with the copper contents. The increase of crosslinking density as indicated by swelling results (Table 5.2) due to increase of

copper loading was also responsible for enhancement of strength property of the nanocomposites films.

The gloss value was found to increase with the copper content as large amount of light is reflected from the smooth surface. The scratch hardness value of the films was found to be increased for the nanocomposites with copper loading as compared to the MBPSE. The nanoclay layers along with uniformly disseminated nanosized copper nanoparticles adeptly restrict indentation in the nanocomposites. The impact resistance of the prepared nanocomposites increases as the amount of copper was increase. The evenly distributed nanosize copper particles played a crucial role for this improvement by interacting with the MBPSE segments of the matrix along with the nanoclay platelets. The presence of high interactions by small copper nanoparticles resulted high rigidity. So, they interact with the polymer chains and restrict their mobility which increases the strength of the copper nanocomposite films.

Table 5.2: Performance characteristics of MBPSE and its OMMT-Cu nanocomposites

Sample code	MBPSE	ECuN0.25	ECuN0.5	ECuN1
Tensile strength (MPa)	6	8.2	11.5	13.2
Elongation at break (%)	95	97	105	112
*Impact resistance (cm)	100	100	100	100
Scratch hardness (kg)	3.4	3.8	4.6	8
Gloss (60°)	62	70	74	80
Swelling value (%)	27	25	22	20

*100 cm is the maximum limit of the instrument

5.3.5. Antibacterial Properties

Tables 5.3 and 5.4 show the details of the relative retention of activity (zone of inhibition) of the nanoparticles, MBPSE and its nanocomposites against Gram positive bacteria (*Staphylococcus aureus*) and Gram negative bacteria (*Klebsiella pneumoniae*). After 24 h of incubation, the zones of inhibition of the nanocomposites against Gram negative and Gram positive bacteria ranged from 13 to 16 mm (Table 5.4), whereas pristine MBPSE did not showed any zone of inhibition.

The nanocomposites exhibited significant efficacy against bacteria, especially against *Klebsiella pneumoniae*, and also the efficacy increased with the increase of copper content. These results thus confirmed that the nanocomposites with copper have good antimicrobial efficacy against these bacteria. However, the mechanism of

antimicrobial efficacy against these bacteria. However, the mechanism of bactericidal action of copper nanoparticles is still not well understood. The copper nanoparticles bind strongly to electron donor groups in biological molecules containing oxygen, sulphur or nitrogen.³³ This may result in the formation of defects in the bacterial cell wall so that cell contents are lost. It is reasonable to state that the binding of the particles to the bacteria depends on the surface area available for such interactions. The smaller particles with a larger surface-to-volume ratio provided a more efficient means of antibacterial activity than larger particles. A complex formation with proteins may disturb the metabolism of bacterial cells and their power functions, such as permeability and respiration.³⁴ Both effects lead to death of the bacterial cells.

Table 5.3: Antimicrobial activity of OMMT-Cu systems

Bacteria	Zone of Inhibition (mm)				
	N1	N0.5	N0.25	Streptomycin (positive control) 5mg/mL	Negative Control (DMSO)
<i>Klebsiella pneumoniae</i>	17	16	14	33	Nil
<i>Staphylococcus aureus</i>	15	10	08	28	Nil

Overall comparison of the microbial reduction rates in the present study revealed Gram-negative bacteria to be more susceptible to the antimicrobial effects of copper than Gram positives, presumably due to their thinner murine wall, which may allow more rapid absorption of copper into the cell.³⁵

5.3.6. RBC Haemolysis Protection Assay for Cytocompatibility

To investigate the effect of nanocomposites on the mammalian membranes, the haemolysis test was carried out. The nanocomposites exhibited higher inhibition assay as compared to the pristine system (Fig. 5.11). This observation indicates that the presence of clay has a definite role to play in RBC haemolysis prevention. However, compared to Triton X 100, the nanocomposites did not exhibited any significant haemoglobin release and showed almost similar results as that of the negative control PBS. This indicates that it did not cause any lysis of the erythrocyte membranes. The

above observation reveals the non-toxic behavior of the nanocomposites to the living cells with concomitant prevention of cell damage against any harmful free radicals.

Table 5.4: Antimicrobial activity of MBPSE/OMMT-Cu nanocomposites

Bacteria	Zone of Inhibition (mm)					
	MBPSE	ECuN1	ECuN0.5	ECuN0.25	Streptomycin (positive control) 5mg/mL	Negative Control (DMSO)
<i>Klebsiella pneumoniae</i>	0	16	14	13	33	Nil
<i>Staphylococcus aureus</i>	0	17	13	12	28	Nil

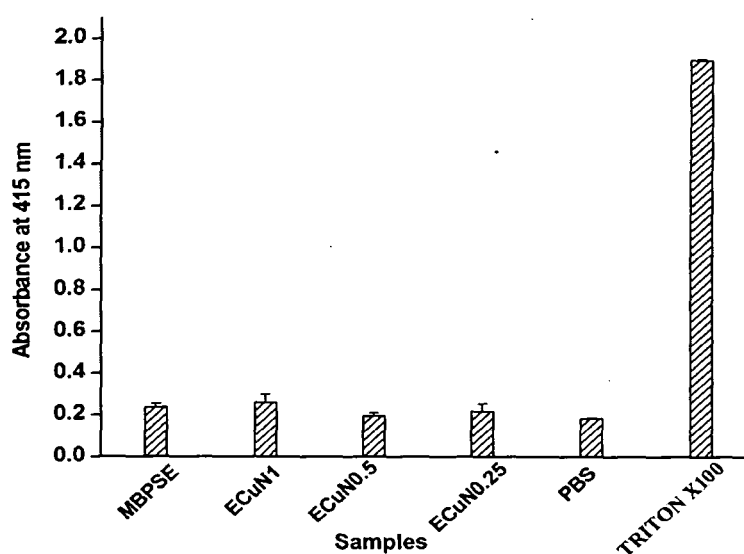


Fig. 5.11: RBC haemolysis protection assay for pristine polymer and OMMT-Cu nanocomposites

5.4. Conclusions

From this chapter it can be concluded that Cu nanoparticles were successfully prepared at room temperature and were sufficiently stable in OMMT. The antibacterial properties showed enhancement after nanocomposite formation. The haemolysis protection assay test reveals the non-toxic behavior of the nanocomposite to mammalian RBC. The thermal and performance characteristics of the nanocomposite

enhances compared to the pristine polymer. The observations vouch for the use of these nanocomposites as advanced antimicrobial surface coating materials.

References

1. Atiyeh, B.S., et al. Effect of silver on burn wound infection control and healing: Review of the literature, *Burns* **33**, 139–148, 2007.
2. Magdassi, S., et al. Copper nanoparticles for printed electronics: Routes towards achieving oxidation stability, *Materials* **3**, 4626-4638, 2010.
3. Huang, H.H., et al. Synthesis, characterization, and nonlinear optical properties of copper nanoparticles; *Langmuir* **13**, 172–175, 1997.
4. Liu, Z., & Bando, Y.A. Novel method for preparing copper nanorods and nanowires, *Adv. Mater.* **15**, 303–305, 2003.
5. Drelich, J., et al. Vermiculite decorated with copper nanoparticles: Novel antibacterial hybrid material, *Appl. Surf. Sci.* **257**, 9435-9443, 2011.
6. Gong, P., et al. Preparation and antibacterial activity of Fe₃O₄@Ag nanoparticles, *Nanotechnology* **18**, 604–611, 2007.
7. Dollwet, H.H.A., & Sorenson, J.R.J. Historic uses of copper compounds in medicine, *Trace Elem. Med.* **2**, 80-87, 1985.
8. Borkow, G., & Gabbay, J. An ancient remedy returning to fight microbial, fungal and viral infections, *Curr. Chem. Bio.* **3**, 272-278, 2009.
9. Dutkiewicz, C., & Fallowfield, H. Assessment of microbial involvement in the elevation of copper levels in drinking water, *J. Appl. Microbiol.* **85**, 597-602, 1998.
10. Pang, Y., et al. The influence of copper concentration and source on ileal microbiota, *Poult. Sci.* **88**, 586-592, 2009.
11. Hostynek, J.J., & Maibach, H.I. Copper hypersensitivity: Dermatologic aspects, *Rev. Environ. Health* **18**, 153-184, 2003.
12. Michels, H.T. Copper alloys for human infectious disease control, Materials Science and Technology Conference, PA Copper for the 21st Century Symposium, September 25-28, Pittsburgh.
13. Kyriacou, S.V., et al. Novel composites of TiO₂ (anatase) and silicate nanoparticles, *Biochemistry* **43**, 140-147, 2004.
14. Akhavan, O., & Ghaderi, E. Enhancement of antibacterial properties of Ag nanorods by electric field, *Sci. Technol. Adv. Mater.* **10**, 015003-015008, 2009.
15. Akhavan, O., & Ghaderi, E. Capping antibacterial Ag nanorods aligned on Ti interlayer by mesoporous TiO₂ layer, *Surf. Coat. Technol.* **203**, 3123-3128, 2009.
16. Kim, B.J., & Park, S.J. Antibacterial behavior of transition-metals-decorated activated carbon fibers, *J. Colloid Inter. Sci.* **325**, 297-299, 2008

17. Kim, Y.H., et al. Preparation and characterization of the antibacterial Cu nanoparticle formed on the surface of SiO₂ nanoparticles, *J. Phys. Chem. B* **110**, 24923-24928, 2006.
18. Gao, F., et al. Copper-based nanostructures: Promising antibacterial agents and photocatalysts, *Chem. Commun.* 3571-3573, 2009.
19. Manikandan, D., et al. Synthesis of platinum nanoparticles in montmorillonite and their catalytic behavior, *Appl. Clay Sci.* **37**, 2007, 193-200.
20. Cioffi, N., et al. Copper nanoparticle/polymer composites with antifungal and bacteriostatic properties, *Chem. Mater.* **17**, 5255-5262, 2005
21. Sunada, K., et al. Copper-deposited TiO₂ thin film under weak UV light illumination, *Environ. Sci. Technol.* **37**, 4785-4789, 2003.
22. Anyaogu, K.C., et al. Synthesis, characterization, and antifouling potential of functionalized copper nanoparticles, *Langmuir* **24**, 4340-4346, 2008.
23. Cubillo, A.E., et al. Antibacterial activity of copper monodispersed nanoparticles into sepiolite, *J. Mater. Sci.* **41**, 5208-5212, 2006.
24. Nair, D.G., et al. Antimicrobial activity of omwaprin, a new member of the waprin family of snake venom proteins, *Biochem. J.* **402**, 93-102, 2007
25. Zhu, H.Y., et al. Novel composites of TiO₂ (anatase) and silicate nanoparticles, *Chem. Mater.* **14**, 5037-5044, 2002.
26. Borchardt, G. Smectites, in *Minerals in Soil Environments*, J.B. Dixon et al. eds., Soil Science of American, Madison (WI), 1989, 675-727.
27. Grim, R.E. *Clay Mineralogy*, McGraw-Hill, New York, 1998, 205-216.
28. Ramos, A.J., & Hernandez, E. In vitro aflatoxin adsorption by means of a montmorillonite silicate, A study of adsorption isotherms, *Anim. Feed Sci. Technol.* **62**, 263-269, 1996.
29. Cao, X., et al. Copper nanorod junctions templated by a novel polymer-surfactant aggregate, *J. Cryst. Growth* **254**, 164-168, 2003.
30. Haas, I., et al. Pulsed sonoelectrochemical synthesis of size-controlled copper nanoparticles stabilized by poly(*N*-vinylpyrrolidone), *J. Phys. Chem. B* **110**, 2006, 16947-16952.
31. Damonte, M., et al. Some aspects of the glyphosate adsorption on montmorillonite and its calcined form, *Appl. Clay Sci.* **36**, 86-94, 2007.
32. Raffi, M., et al. Investigations into the antibacterial behavior of copper nanoparticles against *Escherichia coli*, *Ann. Microbiol.* **60**, 75-80, 2010.

33. Weir, E., et al. The use of nanoparticles in anti-microbial materials and their characterization, *Analyst* **133**, 835-845, 2008.
34. Damm, C., et al. The antimicrobial efficacy of polyamide-6/silver-nano-and microcomposites, *Mater. Chem. Phys.* **108**, 61-66, 2008.
35. Rhim, J.W., et al. Preparation and characterization of chitosan-based nanocomposite films with antimicrobial activity, *J. Agric. Food Chem.* **54**, 5814-5822, 2006.

CHAPTER 6

Epoxy/Multi-Walled Carbon Nanotube Nanocomposites

6.1. Introduction

As already discussed in Chapter 1, section 1.4.1.2 since, the discovery of carbon nanotubes (CNTs) by Iijma,¹ researches related to the nanotubes and their co-related nanocomposite materials has dramatically increased. The arguments for the true mechanical properties of both single-walled (SWCNTs) and multi-walled carbon nanotubes (MWCNTs) never cease. Whether chemical bonding between the nanotubes and their surrounding polymeric matrix in the nanocomposites exists or not, is another disputable topic that researchers have to solve before applying the nanostructural materials to real life applications. The extremely small size makes it suitable to be embedded into any type of light weight and soft materials as reinforcements² to form stable and tough nanocomposites. Consequently, numerous researches have been started focusing on the feasibility of using these nanostructural materials to strengthen polymeric based materials.

Again, the proper selection of an adhesive for biomedical application in contemporary technology is multidisciplinary and challenging to extreme.^{3,4} The type and state of an adhesive, its working principle, the temperature and time required for its curing influence the choice of process for producing good bonded structure. Epoxy resin based on bisphenol-A plays an important role in several technologies such as adhesive tapes, machine part assembly, composite materials etc. because of its excellent thermal, mechanical and adhesive characteristics.⁵⁻⁷ However due to its extensive brittleness and non cytocompatibility the monolithic applications in biomedical field is restricted.⁸ Joint durability is another factor that has been one of the major concerns for application under humid condition (*in-vitro*) as it usually suffers from non uniform distribution of stress over the continuous bonded area and subsequently deterioration of properties.⁹ Therefore, it is necessary to develop high performance epoxy adhesives that can overcome the current problems to meet the requirements of different applications including biomedical.

The adhesive to be useful for biomedical application must be non-toxic, adhere to moist tissue at body temperature and economically satisfactory.⁶ Thus, the development

of biocompatible bonding agents with good structural properties is a relevant aspect of the success of these materials in biomedical field.¹⁰⁻¹³

As discussed in Chapter 1, section 1.1. and Chapter 2, section 2.1. biobased polymers have gained lots of interest in recent times; these evolution has revolutionized the retro thinking about the products obtained from renewable resources. Indeed the current opportunities of biobased polymer nanocomposites in biomedical applications may arise from the potentiality for vast multitude of applications and different functional requirements.^{14,15} In this pursuit biobased epoxy resin has been viewed as a potential substitute to the more conventional epoxy system. However, vegetable oil based epoxies are often attributed with weak mechanical characteristics^{16,17} and hence pose a challenge to the material scientists.

In this regard, the use of CNTs as nanofiller might be one of the best option due to their intrinsic extraordinary thermal and mechanical properties.¹⁸⁻²⁰ The Johnson-Kendall-Roberts theory²¹ suggested that MWCNTs with diameter ranging from 20–30 nm and an aerial density of 10^{10} – 10^{11} tubes/cm², can generate adhesive strength of more than 500 N/cm². However, for efficient reinforcement of CNTs, two main issues are widely recognized as being critical: (i) homogeneous dispersion of the nanofiller within the polymer matrix, and (ii) strong interfacial bonding between the nanofiller and the matrix. Several research works have recently been devoted to reinforcement of epoxy matrices with functionalized carbon nanotubes.²²⁻²⁴ In spite of the aggressive work that has been lately dedicated to this topic, it is recognized that the experimental results are still not convergent and more researches are needed in order to shed light on the development of the nanocomposites with acceptable properties²⁵ in this field.

The advantages of *Mesua ferrea* L. (70% oil content) seed oil and its utilities in different field have already been discussed in Chapter 2, section 2.1.²⁶⁻²⁷ Vegetable oil based sulfone epoxy (MBPSE) has many added advantages as described in Chapter 2, section 2.1 and 2.3.2. The polar functionalities of *Mesua ferrea* L. seed oil based epoxy may increase the physiochemical interaction with the functionalized MWCNTs. Subsequently this may aid to good interfacial bonding between the nanofiller and the matrix.

In this chapter the modification of MWCNTs using mild oxidative technique and preparation of nanocomposites of MBPSE with the modified MWCNTs are described. The mechanical properties, adhesive strength and thermal stability of the nanocomposites were studied at different MWCNTs loadings. The biodegradability test

on epoxy and the nanocomposites were also carried out using *Bacillus subtilis* bacterial strain; further RBC haemolysis assay was studied in order to examine the feasibility of these nanocomposites as biomedical adhesive.

6.2. Experimental

6.2.1. Materials

Mesua ferrea L. oil, as described in Chapter 2, section 2.2.1. was used as the vegetable oil. MWCNTs with diameter and length of about 10–20 nm and 20 μm , respectively, were purchased from Iiljin Nanotech, Korea. The details of the MWCNTs are given in Chapter 1, section 1.4.1.2. Other chemicals used in this chapter such as epichlorohydrin, acetic acid, bisphenol-A, bisphenol-S, HCl, acetone etc. have been already described in Chapter 2, section 2.2.1.

Cetyltrimethylammonium bromide (CTAB, cetrinide) was purchased from Merck, India. Its m.p. is 237–243 $^{\circ}\text{C}$ and M_w 364.45 g/mol. It was used as a surfactant in the modification of MWCNTs.

Potassium dichromate was obtained from Ranbaxy, New Delhi, India. Its M_w is 294.185 g/mol, m.p. 398 $^{\circ}\text{C}$ and density 2.676 g/cm³. It was used as an oxidizing agent to modify the MWCNTs. It is used as an ingredient in cement in which it retards the setting of the mixture and improves its density and texture. It is also used in photography and in photographic screen printing, where it is used as an oxidizing agent together with a strong mineral acid.

All the minerals $(\text{NH}_4)_2\text{SO}_4$, Na_2HPO_4 , KH_2PO_4 , $\text{MgSO}_4 \cdot 7\text{H}_2\text{O}$, $\text{CaCl}_2 \cdot 2\text{H}_2\text{O}$, $\text{FeSO}_4 \cdot 7\text{H}_2\text{O}$, $\text{CuSO}_4 \cdot 7\text{H}_2\text{O}$, $\text{MnSO}_4 \cdot 5\text{H}_2\text{O}$, $\text{ZnSO}_4 \cdot 7\text{H}_2\text{O}$, $\text{H}_3\text{BO}_3 \cdot 5\text{H}_2\text{O}$ and MoO_3 used for preparation of bacterial broth culture media during biodegradation study and PBS (phosphate buffer saline) and Triton X 100 used for RBC haemolysis tests were of same specifications as described in Chapter 4, section 4.2.1. The bacterial strain *bacillus* sp. (AS01A) used for the antimicrobial study was obtained from the Department of Molecular Biology and Biotechnology (Department of Biotechnology, DBT Centre, Government of India), Tezpur University.

6.2.2. Instruments and Methods

The FTIR, TGA and XRD analyses of MBPSE, unmodified MWCNTs, functionalized MWCNTs and nanocomposites were carried out similarly as described in Chapter 3, section 3.2.2. The surface morphology of the samples was studied similarly as

illustrated in Chapter 3, section 3.2.2. The distribution of MWCNTs in the polymer matrix was studied by using JEM-2100, 200 kV (JEOL, Japan) transmission electron microscope (TEM) as mentioned in Chapter 3, section 3.2.2.

The tensile strength and elongation at break (as per the ASTM D 412-51 T), the scratch hardness test and impact strength of the cured resin and the nanocomposites were measured similarly as described in Chapter 2, section 2.2.2. and Chapter 3, section 3.2.3.

The adhesive strength of the cured films was measured by lap-shear test using plywood, aluminum (Al), and polypropylene sheets as the substrates as mentioned in Chapter 2, section 2.2.2. and Chapter 3, section 3.2.2.

6.2.2.1. Modification of Pristine MWCNTs

The modified protocol was adopted as reported by Zhang et al.²⁸ Herein, in this modification a milder oxidizing agent, potassium dichromate was used. Briefly, 0.06 g of pristine MWCNTs was dispersed in 12 mL of dichloromethane by sonication for about 10 min. An amount of 0.5 g phase transfer catalyst (cetrimide) was added to the mixture and sonicated for another 20 min, followed by addition of 2.5 mL of acetic acid and 2.5 g of potassium dichromate in small lots for about 2 h. The reaction mixture was stirred vigorously for 72 h at room temperature. The modified MWCNTs was then obtained by filtering and by washing with concentrated acid, followed by distilled water and acetone. The modified MWCNTs was dried in a vacuum oven at 40-45 °C for 24 h before using. The product was used as functionalized and purified MWCNTs.

6.2.2.2. Preparation of Diglycidyl Ether Bisphenol-S Epoxy Resin (MBPSE)

Mesua ferrea L. seed oil based sulfone epoxy resin (MBPSE) was prepared by the similar method as described in Chapter 2, section 2.2.2.1.

6.2.2.3. Fabrication of Nanocomposites

At first the functionalized MWCNTs was vacuum dried at (40-45) °C for overnight. The nanocomposites were then prepared as described in Chapter 3, section 3.2.2.9. The components were mixed together by hand stirring followed by sonication (pulse cycle 0.5 and amplitude 55-60%) for about 45 min. To avoid the rise of temperature during sonication, water bath was used to maintain the temperature at 25-30 °C. The dispersed MWCNTs/resin system was degassed for 30 min under vacuum before further

processing. The prepared nanocomposites were coded as ECTN1, ECTN2 and ECTN3 for 1, 2 and 3 wt% of MWCNTs loading in the matrix, respectively.

6.2.2.4. Curing of the Resin and Nanocomposites

The curing of the MBPSE and the MWCNTs nanocomposites were carried out as similar to the process described in Chapter 2 and 3, section 2.2.2.2. and 3.2.2.10.

6.2.2.5. Biodegradation by Broth Culture Technique

An inoculum was prepared by growing bacteria in 50 mL Erlenmeyer flasks containing 10 mL of nutrient broth (peptone 5 g/L, beef extract 1.5 g/L, NaCl 5 g/L, yeast extract 1.5 g/L) at 37 °C, pH 7.0, and at an agitation speed of 200 rpm. Then 1 mL of inoculums of bacteria ($\sim 1 \times 10^8$ /mL microbes) was inoculated into the conical flask containing 100 mL nutrient broth (without any carbon source) for each test with experimental nanocomposites films as described in Chapter 4, section 4.2.2.7. Media containing no polymer film were also cultured as negative control. The flasks were then incubated under sterile condition at an agitation speed of 200 rpm and bacterial growth was calculated as described in Chapter 4, section 4.2.2.7. *Bacillus subtilis* strain was selected as the model organism for the study.

6.2.2.6. RBC Haemolysis Protection Assay

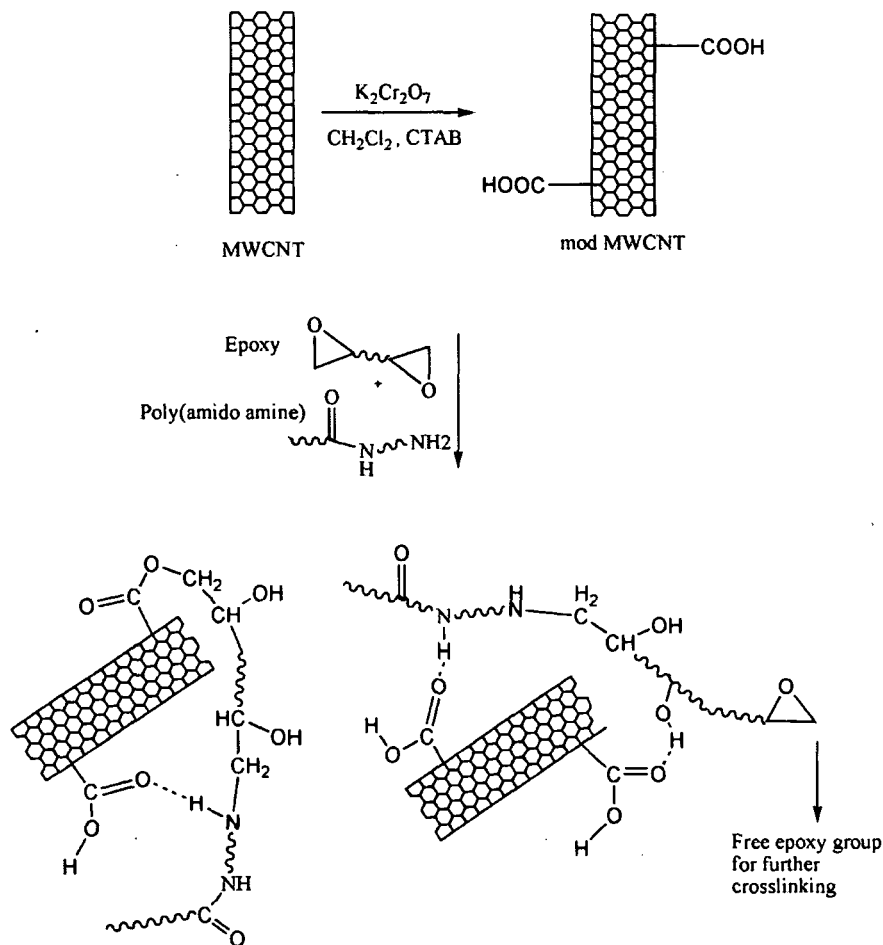
The haemolytic activity test was done to see if the nanocomposites have any haemolytic activity on the erythrocytes based on the modified protocol as reported by Plumel.²⁹ Goat blood was collected and separated as described in Chapter 4, section 4.2.2.8. After centrifugation serum fraction was removed with disposable plastic transfer pipette and precipitate was re-dissolved in 0.9% NaCl solution, it was repeated for 4 to 6 times. After removing NaCl after the last wash step, the whole blood was mixed with 100 mM potassium phosphate buffer (PBS) at pH of 7.4. RBC was then diluted to a ratio of 1:10 with phosphate buffer so as to yields a RBC suspension of $\sim 5 \times 10^8$ RBC/mL.

RBC haemolysis protection assay was carried out according to Zhu et al. with little modification.³⁰ In brief, 10 mg of the nanocomposites was put into 2 mL of RBC suspension and incubated at 37 °C in water bath. About 200 μ L of the suspension was taken out at an interval of 2 h and diluted eight times with PBS and was continued for 6 h. The absorption was measured as described in Chapter 4, section 4.2.2.8.

6.3. Results and Discussion

6.3.1. Functionalization of MWCNTs

Carbon nanotubes has high tendency to agglomerate due to the van der Waal forces, consequently it is very difficult to dispersed and align MWCNTs in the polymer matrix. Thus to develop high performance MWCNTs/epoxy nanocomposites, the challenge is to disperse CNTs uniformly in the polymer matrix so as to achieve high interfacial interactions between the two phases. Nanotube functionalization is the most effective way to achieve good dispersion and interphase control within the matrix polymer, as a result better stress transfer from the polymer to tubes can effectively enhance the mechanical properties of the nanocomposites.³¹ The oxidation of MWCNTs by acidic oxidative methods, oxygen plasma or gas phase treatment has gained lots of attention in an attempt to purify and enhance the chemical reactivity of the graphitic network.³² As already mentioned,^{31,32} acidic oxidative treatment to the MWCNTs material may severely affect its structural properties. Especially, since pristine MWCNTs exhibit



Scheme 6.1: Probable interactions of MWCNTs with MBPSE matrix

significant lack of conjugation and this may lead to an appreciable etching of the carbon material even under moderate oxidation conditions. Thus some precautions should be taken for the purification/surface modification of this materials.³⁰ In order to transfer the optimum properties of MWCNTs to their nanocomposites, the main challenge is the preparation of highly purified material with no appreciable structural damage. Thus MWCNTs was functionalized under mild conditions using $K_2Cr_2O_7$ in the presence of phase transfer catalyst under ambient condition (Scheme 6.1). This causes functionalization (-OH/-COOH) without deterioration of tubes aspect ratio.

6.3.2. Characterization of Modified MWCNTs and Nanocomposites

6.3.2.1. FTIR Analysis

FTIR spectroscopy is an important tool to identify various functional groups present on the graphitic surface of MWCNTs. The modification of the graphitic network of the MWCNTs can be depicted from the FTIR spectra (Fig. 6.1).

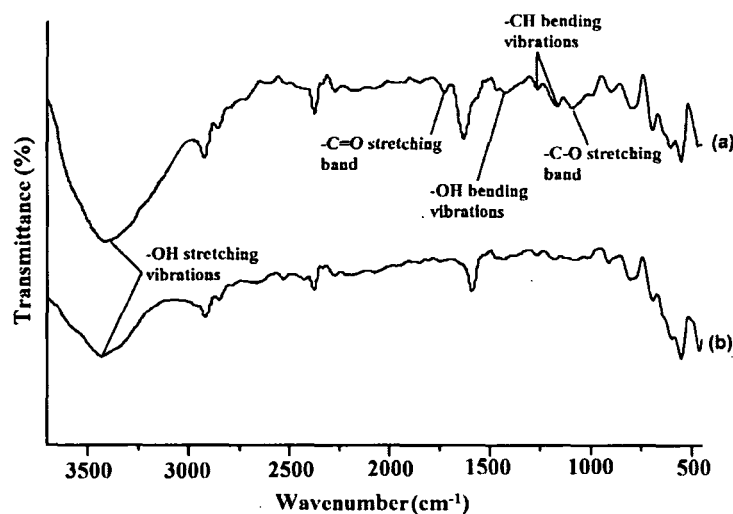


Fig. 6.1: FTIR spectra of (a) unmodified MWCNTs and (b) modified MWCNTs

The pristine MWCNTs exhibited band at 1639 cm^{-1} which is assigned to the -C=O stretching of the quinone groups on the surface.³³ The band observed at around 3433 cm^{-1} is due to the -OH stretching vibrations. After modification broad band for -OH stretching appeared at 3487 cm^{-1} and aliphatic -OH bending appeared at 1447 cm^{-1} . Further, two new bands were observed at around 1719 and 1095 cm^{-1} (Fig. 6.1), which were attributed to -C=O and -C-O stretching vibrations of the carboxylic acid group (-COOH) respectively. Furthermore, new bands were also observed at 2922 , $1262/1165\text{ cm}^{-1}$, mainly attributed to the -CH stretching and bending modes.³⁴ The FTIR study

suggested the carboxyl and hydroxyl functionalization on the MWCNTs surface. These induced carboxyl/hydroxyl functionalities on the MWCNTs surface is expected to enhance the interaction with the MBPSE matrix.

The FTIR spectrum of MBPSE has been already been documented in Chapter 2, section 2.3.3.2. Some of the characteristic bands (cm^{-1}) observed were: 3423 ($-\text{OH}$ stretching vibrations), 3059 (aromatic C-H stretching vibration), 1729 (C=O stretching vibration of the triglyceride esters), 1605 (C=C stretching vibration), 1300 and 1149 (sulfone stretching vibrations), 1246 and 1106 (C-O-C stretching vibrations), and 916 and 832 (oxirane ring stretching vibrations).

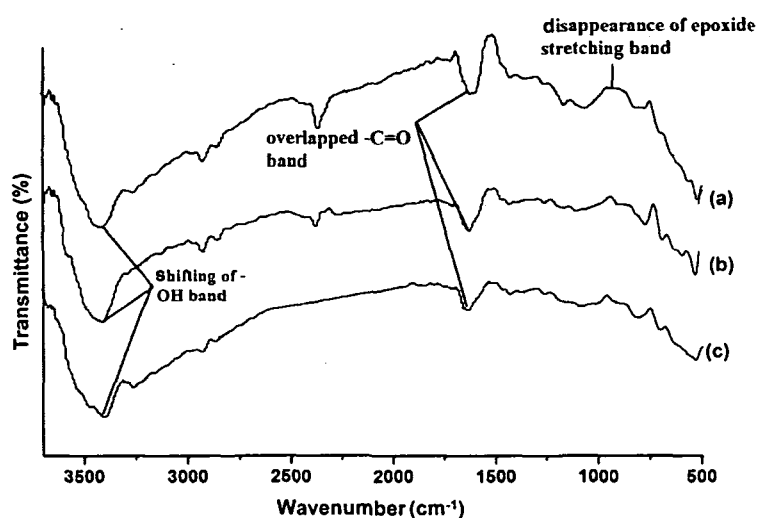


Fig. 6.2: FTIR spectra of MWCNTs/MBPSE nanocomposites viz., (a) ECTN1, (b) ECTN2 and (c) ECTN3

The FTIR spectra of the nanocomposites are shown in Fig. 6.2. With the increase of the MWCNTs loading the $-\text{OH}$ absorption band of MBPSE exhibited a red shift with simultaneous reduction in the band intensity. The $-\text{C=O}$ stretching band however, appeared as a single broad band with reduced intensity in the region of $1619\text{--}1647\text{ cm}^{-1}$, which may be due to the overlapping of the $-\text{C=O}$ stretching band of the quinone group of MWCNTs with that of the MBPSE. The crosslinking of the epoxy resin with amine hardener in presence of MWCNTs suggested extensive amount of interactions present in the system. The $-\text{C=O}$ group of the modified MWCNTs and epoxy group of the matrix are interacted with $-\text{NH}_2$ group of the hardener through hydrogen-bonding. Moreover, the $-\text{OH}$ group of MBPSE is involved in hydrogen-bonding with the $-\text{C=O}$ group of the MWCNTs (Scheme 6.1). Thus, the poly(amido amine) hardener also served as a compatibilizer between the epoxy and the MWCNTs. The oxirane

stretching vibration (916 cm^{-1}) in all the nanocomposites diminished after curing. This indicated the completion of curing of the epoxy resin via ring opening of the oxirane group. These interactions altogether facilitates the stable and uniform distribution of the MWCNTs in the epoxy matrix.

6.3.2.2. Dispersion of MWCNTs

It is well known³² that MWCNTs have a strong tendency to agglomerate due to their nanosize and their respective high surface energy. Dispersion of MWCNTs in polar aprotic solvent is shown in Fig. 6.3.

Pristine MWCNTs were quickly precipitated in DMF solution even after sonication for 30 min. However, the MWCNTs exhibited good dispersion in DMF even after 72 h. The MWCNTs were also dispersed in DMAc, the stability of each of the dispersion was found to be enhanced after modifications. This phenomenon of uniform nanotube dispersion in solvents is one of the properties of functionalized nanotubes. It has been reported that due to the nanoscale size, the high surface energy of nanotubes gives them a strong tendency to agglomerate. Even with the help of ultrasonic vibration, the untreated nanotubes may not remain in any solvent in quiescent suspension. However, appropriate functionalization of the nanotubes can dramatically raise the stability of suspensions.²⁸

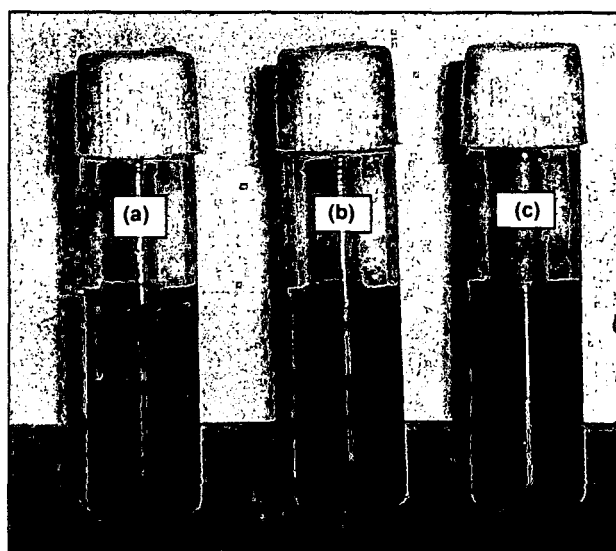


Fig. 6.3: Dispersion stability of (a) unmodified MWCNTs, (b) modified MWCNTs in DMF and (c) modified MWCNTs in DMAc

The functionalization process induces a negatively charged surface, particularly

through the ionization of acidic surface groups. The resulting electrostatic repulsion leads to the stable uniform colloidal dispersion.

6.3.2.3. XRD Analysis

The X-ray diffraction results for the nanocomposites are shown in Fig. 6.4. The X-ray diffraction pattern of the functionalized MWCNTs revealed the presence of two crystalline peaks at $2\theta = 25.8^\circ$ and 42.8° , corresponding to the interlayer spacing of 0.34 nm and 0.21 nm, respectively.

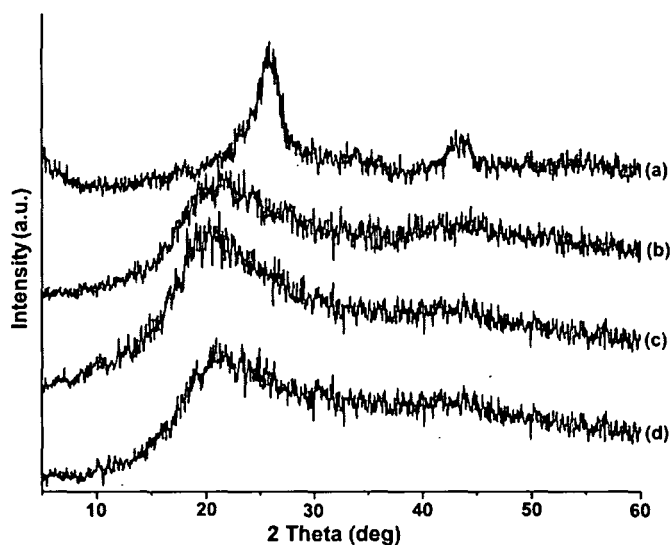


Fig. 6.4: XRD patterns of (a) modified MWCNTs, (b) ECTN1, (b) ECTN2 and (c) ECTN3

These are due to $\{002\}$ and $\{100\}$ planes of the carbon atoms, respectively.³⁵ The spectra of the nanocomposites revealed no peaks for the MWCNTs, however a broad peak was found around 19.9° in the spectra, which is due to the amorphous nature of MBPSE matrix. The XRD indicated uniform dispersion of the nanotubes in the matrix. However since small amount of nanotubes (3 wt%) was used in the nanocomposites formation, so this may also be one of the reason for the absence of X-ray diffraction peak in the nanocomposites.

6.3.2.4. SEM & TEM Studies

The morphology and spatial distribution of the MWCNTs in the epoxy matrix were examined with the help of SEM and TEM analyses (Figs. 6.5 and 6.6). The platinum coated surface of the sample was observed in SEM. The random distribution of the nanotubes in the epoxy matrix can be distinctly viewed from Fig. 6.5. The polymer

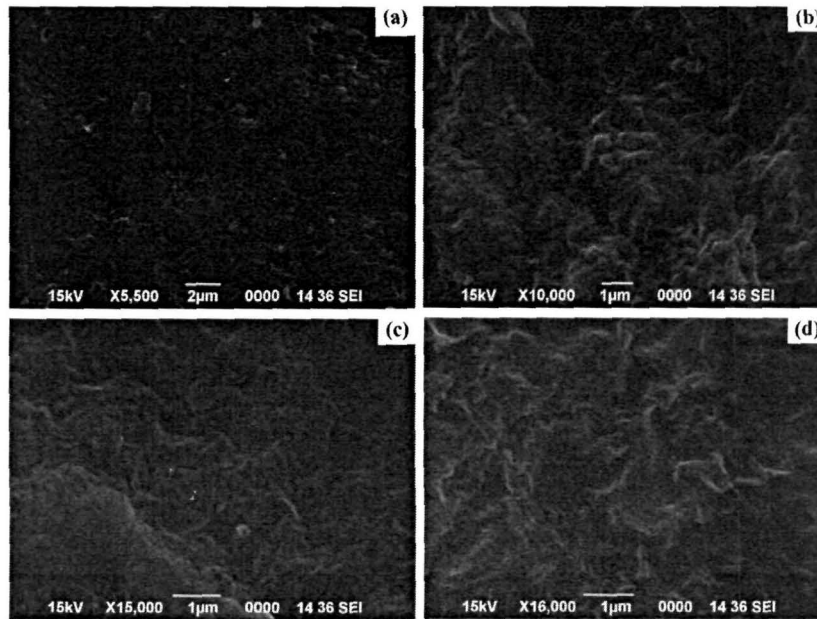


Fig. 6.5: SEM micrographs for (a) MBPSE, (b) ECTN1, (c) ECTN2 and (d) ECTN3

embedded MWCNTs appeared as tiny bright thread like lines in the micrographs. The bright lines increased with the increase of MWCNTs loading. Interestingly, no aggregate or agglomerate was observed in the nanocomposite with different MWCNTs concentrations. This is the effect of chemical modification of the MWCNTs that facilitates wetting by the MBPSE and phase adhesion between the two systems.³⁶

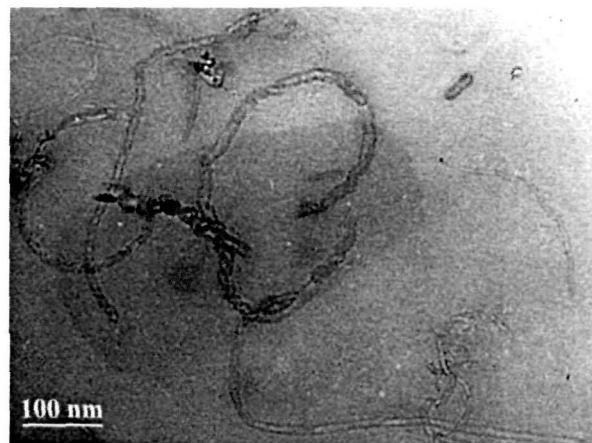


Fig. 6.6: TEM micrograph for ECTN3

This homogeneous dispersion of the MWCNTs in the matrix will definitely enhance the properties. Thus, the MWCNTs were successfully dispersed in the vegetable oil based matrix.

The TEM micrograph gives further evidence of the fine dispersion of the MWCNTs in the epoxy matrix. The representative TEM micrograph of ECTN3

is shown in Fig. 6.6, the presence of individual tubes proved the debundling of the MWCNTs. The visibly dark line in the micrograph represents the nanotubes, the uniform dispersion of the tubes revealed good interaction between the matrix and the tubes.

6.3.3. Curing Study

The influence of MWCNTs loading on the curing reaction of MBPSE is depicted in Table 6.1. The initial curing was found to accelerate with MWCNTs loading as indicated by the touch free time (Table 6.1). ECTN3 exhibited the lowest curing time among the studied system. In the early stage, the reaction is initiated by any hydrogen-bond donor molecules which can be solvent molecules or any other impurities. The reaction is then accelerated by these molecules and the hydroxyl groups formed during the reaction (as revealed by FTIR spectra). In the final stage, the viscosity of the mixture increase significantly and the reaction is diffusion-controlled.³⁷

Table 6.1: *Drying time of MBPSE and its MWCNTs nanocomposites*

Sample code	Touch free time (min)	Hard dry time (min)
MBPSE	45	65
ECTN1	37	63
ECTN2	30	64
ECTN3	22	65

Consequently, the hard dry time does not show any significant variation on MWCNTs loading. The high cure rate obtained in the initial phase could be counter balanced by the rapid decrease of the cure in the diffusion-controlled stage. Lower or comparable cure time of the nanocomposites compared to the pristine resin was observed.

6.3.4. Thermal Study

The thermogravimetric profiles of the MBPSE and the nanocomposites are shown in Fig. 6.7. MWCNTs are known to exhibit superior thermal stability.³⁶ The incorporation of MWCNTs in the polymer matrix has a significant effect on the thermal stability of the nanocomposite as evident from Fig. 6.7. The thermal stability was found to increase with the increase of MWCNTs loading. MBPSE showed onset degradation temperature of 277 °C, whereas the onset degradation temperature shifted to 293 °C for ECTN1, 302

°C for ECTN2 and to 318 °C for ECTN3. Addition of 1 wt% of nanoclay resulted in about 16 °C enhancement in the onset temperature. MWCNTs act as a thermal insulator, which has strong interfacial interaction between the epoxy chains thus retarding the segmental mobility of the chains. The higher weight residue of the nanocomposites as compared to MBPSE, further justified the above statement. As evident from Fig. 6.7, for ECTN3 the weight residue at 650 °C was about 16.97%, 14.9% for ECTN2 and 8.37% for ECTN1, whereas for MBPSE it was only 6.65%. The char acts as a thermal insulator, thereby preventing the underlying matrix from volatilization and consequently enhancing the degradation temperature. Also, the strong interaction between MWCNT and epoxy matrix reduces the diffusion of volatiles through the matrix³⁸ at high temperature, thereby increasing the thermal stability of the matrix.

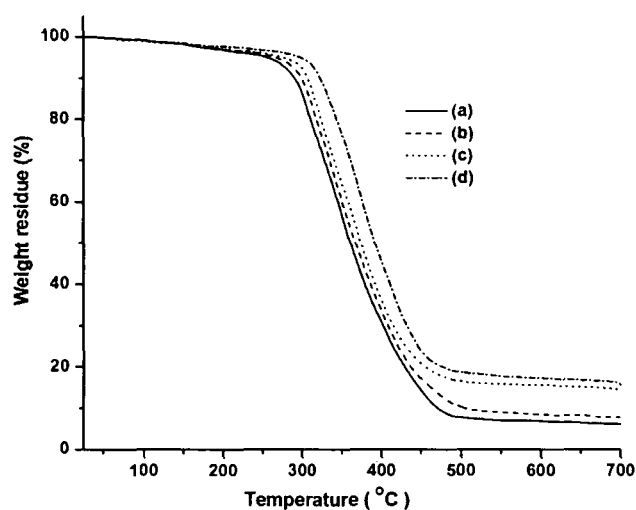


Fig. 6.7: TGA thermograms of (a) MBPSE, (b) ECTN1, (c) ECTN2 and (d) ECTN3

6.3.5. Performance Characteristics

The mechanical properties of nanocomposites depend on various factors such as state of distribution of the filler, aspect ratio, shape and size of the different domains and of course their orientations. The interfacial interaction between MWCNTs and the matrix is the measurement of the increment in the strength properties of the nanocomposites.³⁶ The mechanical properties of the pristine polymer and the nanocomposites are shown in Table 6.2.

The inclusion of 3 wt% of MWCNTs significantly increased the tensile strength from 6 to 15.4 MPa (Table 6.2). The nanoscale dispersion of the CNTs into individual layer plays a multifold role in enhancing the tensile strength of the nanocomposites.

Table 6.2: Performance characteristics of MBPSE and its MWCNTs nanocomposites

Sample code	MBPSE	ECTN1	ECTN2	ECTN3
Tensile strength (MPa)	5.7	8.4	12.3	15.4
Elongation at break (%)	95	103.4	110.4	126.3
*Impact resistance (cm)	100	100	100	100
Scratch hardness (kg)	3.4	4.7	6.2	7

* 100 cm is the maximum limit of the instrument

The homogeneously dispersed tubes provide a greater degree of interfacial bonding between the polymer chains and the tube surface.³⁹ A good interface is eminent for a material to withstand the applied stress. A strong bond reflects efficient stress transfer in the interface between the two phases, which increases with MWCNTs loading. Thus, the room temperature modification of the MWCNTs was found to be efficient in reinforcing the matrix. The elongation at break value for the nanocomposites was found to increase as compared to the pristine polymer. The increase in the elongation at break depends on the state of dispersion of the nanotubes in the matrix polymer. The surface functionalization induces chemical bonding (covalent bonding, van der Waals forces, π -stacking etc.) of the carbon structure of the CNTs with the molecular structure of the thermosetting matrix, this resulted in efficient load transfer. Also the elongation at break depends more seriously on the internal bond strength rather than crosslinking density and the phenomenon is guided by chain breakage rather than chain slippage.

The scratch hardness also augmented with the MWCNTs loadings. The increase in scratch hardness is due to the dissipation of the stress generated at the interface between the moving tip and the film surface throughout the nanocomposite. The stress is then absorbed by the nanotubes and consequently scratch hardness was observed to increase in this case.

6.3.6. Adhesive Strength

To determine the influence of the surfaces on the adhesive strength of MBPSE and its nanocomposites different substrates such as plywood, aluminium and plastic were taken. The average lap shear strength values of the specimens with different MWCNTs loadings are shown in Fig. 6.8. The shear stress of each MWCNTs weight fractions was repeated three times and the result were repeatable within deviations of $\pm 3.5\%$. The adhesive strength was found to be the highest for the wood substrate and it increases with the increase in the MWCNTs content (8.4 MPa in case of ECTN3). Uniformly

dispersed MWCNTs have certain effects on the physical and chemical properties of the adhesion for epoxy adhesive. They provide stronger anchoring and hence increased adhesive strength by virtue of their positioning in the surface asperities of the wood surfaces.⁴⁰ Adhesive or cohesive forces may be attributed to either short or long range interactions. The increment of adhesive strength is due to the strong interactions of polar hydroxyl, epoxy, ether and other polar groups of the MBPSE/MWCNTs nanocomposite with the hydroxyl groups of the substrate. The interactions are through hydrogen-bonding, polar-polar and polar-induced-polar interactions, or/and chemical bond formation. MBPSE also showed good adhesion on metal substrate. The lap shear strength exhibited a continuous increase with MWCNTs loading. ECTN3 displayed 145 percent increase in lap shear strength for Al substrate. Virtually all common metal surfaces exist as hydrated oxides. Thus the adhesive used for these materials must firmly interact with the metal oxide layer. The plausible explanation for good adhesion on to the steel substrate to better interlocking and formations of secondary bonds

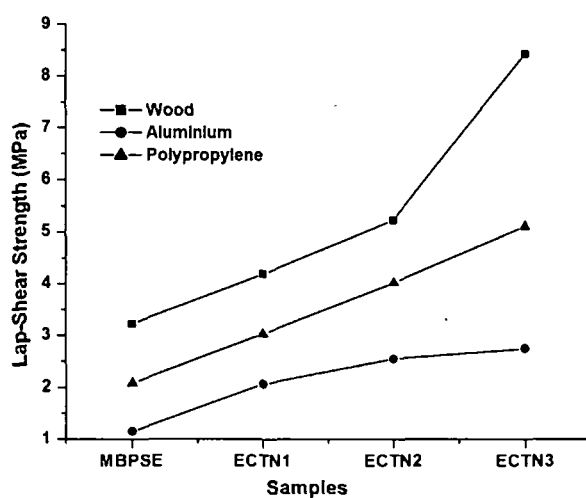


Fig. 6.8: Lap shear adhesive strength of MBPSE and MWCNTs nanocomposites on different substrates (wood/aluminium/polypropylene)

with the rough surface of metal, aided by the induced functionality (hydroxyl/carboxyl, etc) on the MWCNTs after modification.⁴¹ Poor adhesive strength was observed in case of polypropylene substrate, compare to wood and aluminium substrates. This result suggest that the surface treatment of the polypropylene with HNO_3 may generate active sites for interaction with the matrix, but that are still not enough compared to wood or aluminium substrate.

6.3.7. Biodegradation Study

As seen from Chapter 4, section 4.3.10. MBPSE exhibits biodegradability by *Pseudomonas aeruginosa* bacteria. In this chapter the biodegradability of MBPSE and its MWCNTs nanocomposites by *bacillus subtilis* (AS01A) bacterial strain was studied. Same as in Chapter 4, broth culture technique was used to study biodegradability in this case.

The biodegradation of MBPSE and its nanocomposites were quantitatively tested and confirmed by direct exposure to strain of *bacillus* sp. bacteria by broth culture technique. The growth of *bacillus* sp. bacterial strain on epoxy system and various nanocomposites films can be realized from Figs. 6.9 and 6.10, respectively. After keeping the samples in broth culture media for six weeks, the bacterial OD was determined.

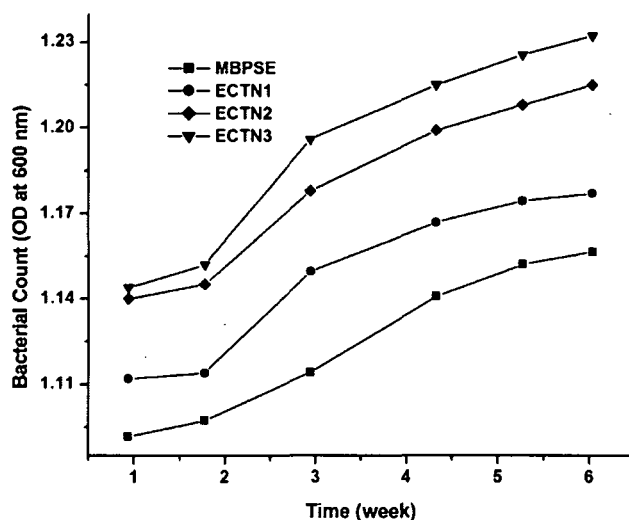


Fig. 6.9: Statistics of growth of *bacillus subtilis* in MBPSE and nanocomposites post 6 weeks of inoculations

The difference in the rate of growth initially for two weeks both for the nanocomposites as well pristine system was not significant as can be observe from the curves after two weeks of bacterial exposure (Fig. 6.9). However, the bacterial growth rate increases significantly after two weeks, as can be realized from the bacterial count. The inoculated films were found to deteriorate significantly after two weeks (Fig. 6.10). Again, the rate of biodegradation was found to be higher than the corresponding pristine polymer in both the cases (Fig. 6.9). The growth profiling of consortia in the modified broth media deficient of carbon source forces the bacteria to use MBPSE and its nanocomposites as the chief carbon source in each case.⁴² The presence of the vegetable oil moiety in the epoxy structure plays an important role in assisting the

microbial degradation of the systems. The surface topography as visualized by SEM in the case of treated samples exhibited deteriorations of structure integrity. The presence of MWCNTs was found to accelerate the rate of degradations.⁴³ The functionalized MWCNTs accelerates the biodegradation by absorbing water, which helps the hydrolysis of the MBPSE matrix in presence of the microbes, thus initializing the degradation of the matrix.

6.3.8. RBC Haemolysis Protection Assay for Cytocompatibility

The emergence of nanotechnology also raises the question of safety from any possible toxic effect of nano structures.³⁶ Thus it is imperative to investigate the adverse effect of MWCNTs based biomaterials before they may be forwarded for widespread acceptance and uses. Here, the cytocompatibility for the MBPSE and its nanocomposites

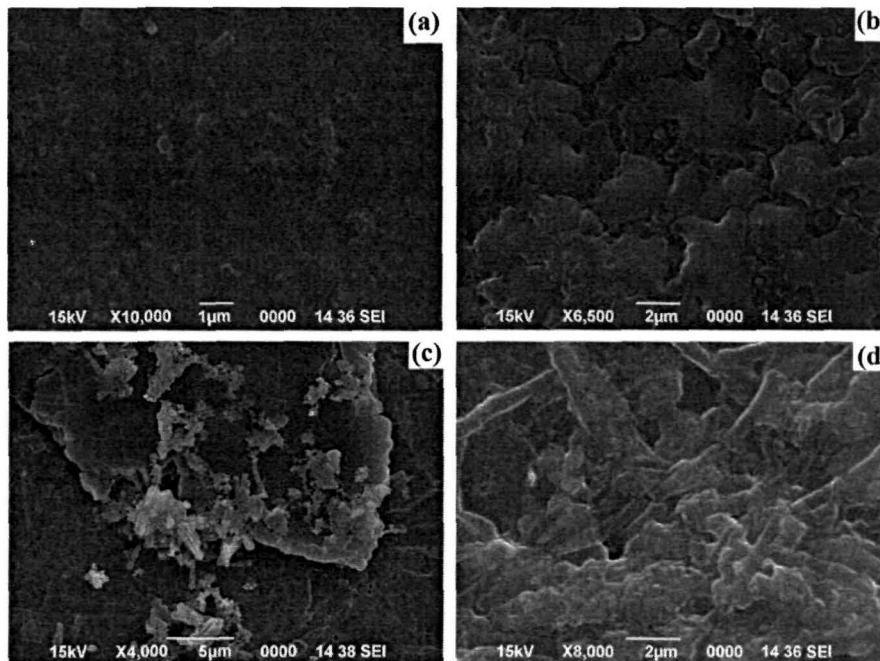


Fig. 6.10: SEM micrographs for (a) untreated MBPSE and MWCNTs/MBPSE nanocomposites post 6 weeks of inoculations: (b) ECTN1, (c) ECTN2 and (d) ECTN3

was investigated by RBC haemolysis protection assay (as discussed in Chapter 4, section 4.3.11.) and the results are shown in Fig. 6.11. In the study water was taken as the positive control and PBS as the negative control. Examining the plots revealed the haemolysis prevention of the nanocomposites to be similar to that of the negative control. The test was carried out for 6 h and it was observed that after 3 h the inhibition capability started to decline. The increasing saturation of MWCNTs may be the reason for the decline.^{29,36} However up to six hours the nanocomposites retained sufficient

inhibition capability. The nanocomposites showed dose dependent inhibition behaviour, and is a direct effect of the MWCNTs. The films are non-cytotoxic as implied by the assessment. The nanocomposites prominently prevented the damage to the cell by the free radicals. This is due to the high free radical scavenging property of MBPSE/MWCNTs nanocomposites that react with free radicals, by two mechanisms viz., electron transfer process and adduct formation.³⁶ The virgin polymer showed less RBC haemolysis prevention capacity. This indicates that the MWCNTs plays a crucial role in the RBC haemolysis prevention. Thus the study revealed that the nanocomposites are not only non-toxic but are also capable of preventing the cell from the attack of harmful radicals.

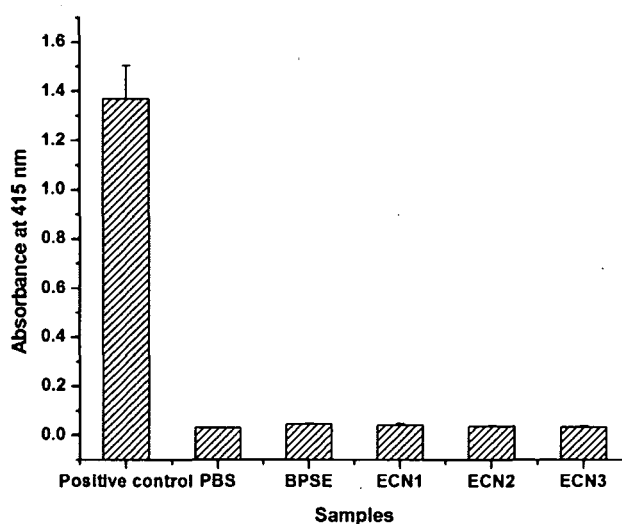


Fig. 6.11: RBC protection assay of MBPSE and nanocomposites

6.4. Conclusions

From this study this can be concluded that the mild oxidative technique with phase transfer catalyst introduces sufficient functionality which aids in the good dispersion of the MWCNTs in the *Mesua ferrea* L. seed oil modified epoxy resin. The homogeneous dispersion of the MWCNTs was revealed by XRD, SEM, TEM and FTIR techniques. The nanocomposites showed enhancement in the mechanical properties and thermal properties with the increase of MWCNTs loading. The adhesive strength of MWCNTs/MBPSE nanocomposites tested on different substrates (wood/aluminium/polypropylene) by lap shear test method and result shows sufficient strength of the bonded joint. The nanocomposite material has also displayed biocompatibility in terms of non-toxicity at the cellular level and biodegradability.

In view of these features, the MWCNTs/MBPSE nanocomposites may be viewed as a potential candidate for further exploration for determining their sustainability in biomedical applications such as in dentistry, tissue adhesive etc.

Reference

1. Iijima, S. Helical microtubes of graphitic carbon, *Nature* **354**, 56–8, 1991.
2. Lu, J.P. Elastic properties of single and multilayered nanotubes, *J. Phys. Chem. Solids* **58**, 1649–1652, 1997.
3. Suarez, J.C. et al. Case studies in adhesives selection, *J. Mater. Process. Technol.* **143-144**, 219-244, 2003.
4. Yu, S., et al. Use of carbon nanotubes reinforced epoxy as adhesives to join aluminium plates, *Mater. Design* **31**, S126-S129, 2010.
5. Yoon, N., et al. Modification of hydrogenated bisphenol-A epoxy adhesives using nanomaterials, *Int. J. Adhes. Adhes.* **31**, 119-125, 2011.
6. Katz, D., Brandeis, E. and Klein, J. *Biomedical adhesive compositions*, **US Patent No. 5266608**, November 30, 1999.
7. Sekulic, A., & Curnier, A. Experimentation on adhesion of epoxy, *Int. J. Adhes. Adhes.* **30**, 89-104, 2010.
8. Harmand, M.F., et al. In vitro evaluation of an epoxy resin's cytocompatibility using cell lines and human differentiated cells, *J. Biomater. Sci. Polym. Edn.* **2**, 67-79, 1991.
9. Mubashar, A., et al. Moisture absorption–desorption effects in adhesive joints, *Int. J. Adhes. Adhes.* **29**, 751-760, 2009.
10. Packham, D.E. Adhesive technology and sustainability, *Int. J. Adhes. Adhes.* **29**, 248-252, 2009.
11. Metzger, H.O., & Eissen, M. Concepts on the contribution of chemistry to a sustainable development, Renewable raw materials, *Comptes. Rendus. Chimie.* **7**, 569-581, 2004.
12. Finch, C.A. *Handbook of adhesion*, Wiley, Chichester, 2009.
13. Gruber, E. Limitations of efficient usage of renewable materials, *Wochenbl. fur Papierfabrik.* **128**, 594-598, 2000.
14. Kinloch, A.J. *Adhesion and Adhesives: Science and Technology*, Chapman and Hall, London, 1987.
15. Janota, R.B. *High-Performance Adhesive Bonding*, Society of Manufacturing Engineers, Michigan, 1983.
16. Mohanty, A.K., et al. Sustainable bio-composites from renewable resources: Opportunities and challenges in the green materials world, *J. Polym. Environ.* **10**, 19-26, 2002.

17. Miyagawa, H., et al. Biobased epoxy/clay nanocomposites as a new matrix for CFRP, *Compos. Part A* **37**, 54-62, 2006.
18. Moniruzzaman, M., & Winey, K.I. Polymer nanocomposites containing carbon nanotubes, *Macromolecules* **39**, 5194–205, 2006.
19. Xie, X., et al. Dispersion and alignment of carbon nanotubes in polymer matrix: A review, *Mater. Sci. Eng. R: Rep.* **49**, 89–112, 2005.
20. Belin, T., & Epron, F. Characterization methods of carbon nanotubes: A review, *Mater. Sci. Eng: B* **119**, 105–18, 2005.
21. Zhao, Y., et al. Interfacial energy and strength of multiwalled-carbon-nanotube-based dry adhesive, *J. Vac. Sci. Technol. B.* **24**, 331-335, 2006.
22. Gojny, F.H., et al. Carbon nanotube-reinforced epoxy-composites: Enhanced stiffness and fracture toughness at low nanotube content, *Compos. Sci. Technol.* **64**, 2363–2371, 2004.
23. Miyagawa, H., et al. Nanocomposites from biobased epoxy and single-wall carbon nanotubes: Synthesis, and mechanical and thermophysical properties evaluation, *Nanotechnology* **1**, 118 (pp. 7), 2005.
24. Wang, S., et al. Effective amino-functionalization of carbon nanotubes for reinforcing epoxy polymer composites, *Nanotechnology* **17**, 1551 (pp. 7), 2006.
25. Perez, H.A., et al. Effective properties of multiwalled carbon nanotube/epoxy composites using two different tubes, *Compos. Sci. Technol.* **68**, 1422-1431, 2008.
26. Dutta, S., et al. Biocompatible epoxy modified bio-based polyurethane nanocomposites: Mechanical property, cytotoxicity and biodegradation, *Bioresour. Technol.* **100**, 6391-6397, 2009.
27. Mahapatra, S.S., & Karak, N. Synthesis and characterization and of polyesteramide resins from Nahar seed oil for surface coating applications, *Prog. Org. Coat.* **51**, 103-108, 2004.
28. Zhang, N., et al. Functionalization of carbon nanotubes by potassium permanganate assisted with phase transfer catalyst, *Smart Mater. Struct.* **11**, 962-965, 2002.
29. Zhu, Q.Y., et al. Inhibitory effects of cocoa flavanols and procyanidin oligomers on free radical-induced erythrocyte hemolysis, *Exp. Biol. Med.* **227**, 321-329, 2002.
30. Plumel, M. Hoffman Group–Standard procedure for hemolysis assay, *Bull. Soc. Chim. Biol.* **30**, 129-131, 1949.
31. Sahoo, N.G., et al. Polymer nanocomposites based on functionalized carbon nanotubes, *Prog. Polym. Sci.* **35**, 837-867, 2010.

32. Datsyuk, V., et al. Chemical oxidation of multiwalled carbon nanotubes, *Carbon* **46**, 833-840, 2008.
33. Ma, P.C., Dispersion, interfacial interaction and re-agglomeration of functionalized carbon nanotubes in epoxy composites, *Carbon* **48**, 1824-1834, 2010.
34. Chen, X., et al. Mechanical and thermal properties of epoxy nanocomposites reinforced with amino-functionalized multi-walled carbon nanotubes, *Mater. Sci. Eng: A* **492**, 236-242, 2008.
35. Rana, S., et al. Enhanced dispersion of carbon nanotubes in hyperbranched polyurethane and properties of nanocomposites, *Nanotechnology* **19**, 495707 (pp. 10), 2008.
36. Deka, H., et al. Biocompatible hyperbranched polyurethane/multi-walled carbon nanotube composites as shape memory materials, *Carbon* **48**, 2013-2022, 2010.
37. Allaoui, A., & Bounia, N.E. How carbon nanotubes affect the cure kinetics and glass transition temperature of their epoxy composites?- A review, *eXPress Polym. Lett.* **3**, 588-594, 2009.
38. Hu, Y., et al. Comparison of the thermal properties between composites reinforced by raw and amino-functionalized carbon materials, *Compos. Sci. Technol.* **70**, 2176-2182, 2010.
39. Kim, J.A., et al. Effects of surface modification on rheological and mechanical properties of CNT/epoxy composites, *Carbon* **44**, 1898-1905, 2006.
40. Deka, H., & Karak, N. Bio-based hyperbranched polyurethane/clay nanocomposites: Adhesive, mechanical, and thermal properties, *Polym. Adv. Technol.* **26**, 973-980, 2009.
41. Petrie, E.M. *Handbook of Adhesive and Sealants*, McGraw-Hill, New York, 2000.
42. Sinha, R.S., & Okamoto, M. Polymer/layered silicate nanocomposites: A review from preparation to processing, *Prog. Polym. Sci.* **28**, 1539-1641, 2003.
43. Rafeeqi, T., & Kaul, G. Elucidation of interaction between multi-walled carbon nanotubes and cell culture medium by spectroscopy supports biocompatibility of these nanotubes, *Adv. Sci. Lett.* **4**, 536-540, 2011.

CHAPTER 7

Biodegradation of Epoxidized oil/Poly(vinyl chloride)/Clay Nanocomposites

7.1. Introduction

PVC is a well known material which has been used commercially for decades. However, due to its inherent limitations, such as low thermal stability, difficulties in conventional melt processing and inadequate flexibility, PVC has found limited use in many advanced applications.¹ Strategies to develop new PVC products with desirable properties could open new applications for PVC. Plasticizers are often used to enhance the softness, elongation and low temperature flexibility.² Likewise plasticizers also modify thermal and mechanical properties of PVC. The esters of phthalic acid, particularly bis(2-ethylhexyl phthalate) (DEHP)³ commonly known as dioctyl phthalate (DOP), and dibutyl phthalate⁴ are the most widely used plasticizers for PVC.

Plasticized PVC has numerous applications such as in medical, pharmaceutical, packaging and consumer sectors.⁵ However, the debate on the environmental issues of the traditional plasticizers has led to a rapid change in PVC industry. Strict regulations of human exposure to traditional phthalates plasticizers along with raising societal concerns and environmental consciousness have triggered the exploration for other alternatives. It has been found that the low molecular weight plasticizers are lost easily from the plasticized PVC matrix.⁶ Consequently, the loss of plasticizer may result in deterioration of the physio-chemical properties of PVC products. Alternatives to these are polymeric plasticizers, such as polyadipates, their high molar mass limits them from leaching or migration from the matrix to the surroundings. However, these plasticizers have two main disadvantages, (i) their direct chromatographic quantitative detection is difficult and (ii) they provide highly viscous plastisols often leading to difficulty in processing.⁷

Epoxidized oil is one of the most commercially used alternatives to the traditional plasticizers.¹ The long-chain macromolecules with low to medium molecular weights are often used as plasticizers in polymers due to their good compatibility and stability.⁸

Parts of this work are published in: (i) J. Vinyl. Addit. Technol. (2011) (online) and (ii) J. Hazard. Mater. (2011) (under review)

Fats and oils are renewable resources that can be chemically or enzymatically treated to obtain materials that often act as a substitute for materials derived from petroleum.⁹⁻¹⁴ The use of epoxidized oil as plasticizer can provide a platform for the creation of environmentally benign materials.¹⁵ The main problem with this system, however, is the inferior physical and mechanical properties under the used service conditions.¹⁶

Again, for the enhancement of thermal stability of pristine PVC the main classes of thermal stabilizers used are lead salts, metal soaps and organotin compounds. The lead salts have an excellent stabilization effect on PVC, but have disadvantages in terms of toxicity and environmental pollution. The metal soaps and organotin stabilizers are safer than lead salts, but their stabilization effects are usually lower than those of lead salts. Currently attention is being focused on thermal stabilizers that are non-toxic and environmentally benign. In this regard the use of clay and clay like materials are increasing day by day. The use clay can significantly improve the thermal stability of the PVC matrix as well as it can also act as effective reinforcing filler.^{17,18}

However, the commercial feasibility of PVC is often confronted by the issues of non-biodegradability and eco-toxicity associated with the disposal of the single-time-use products. This calls for devising novel strategies to endow inherent biodegradability of PVC based materials, standing as an answer to the growing concerns of landfill and incineration.¹⁹⁻²⁴

However, the plethora of literature describes a very few work on biodegradation of epoxidized oil plasticized PVC and its nanocomposites. The limited reports on biodegradation of plasticized PVC by *Pseudomonas aeruginosa* and fungi^{25,26} highlighted more on the microbial degradation rather than providing a mechanistic explanation on the alterations in the structural aspects and its consequences on the performance characteristics.

A critical aspect of biodegradation is that the films need to be resistant to degradation both prior to and during use, yet should undergo degradation if discarded into either terrestrial or aquatic environments.²⁶ These conflicting demands of resistance to microbial colonization during use and degradability when discarded can sometimes be resolved by the inclusion of suitable additives to the polymer. These additives enhance the rate of degradation of some highly resistant polymers, e.g., starch in polythene.²⁴ Materials of organic origin, including the natural polymers, have an inherent tendency to decompose.^{27,28} Consequently, the bioresource based polymers

play a significant role when modified or used in mixtures of synthetic polymers for their degradability.

The use of epoxidized *Mesua ferrea* L. as a plasticizer for commercially available unplasticized PVC is described in this chapter. The nanocomposites of epoxidized *Mesua ferrea* L. seed oil plasticized PVC with organically modified nanoclay (OMMT) was investigated. The biodegradation of these nanocomposites was studied for a period of 180 days by using *Pseudomonas aeruginosa* and *Achromobacter* sp. isolated from soil samples of Assam (North-eastern state of India). Further the effect of biodegradation on the performance characteristics including thermal properties of the nanocomposites was also evaluated.

7.2. Experimental

7.2.1. Materials

Mesua ferrea L. seed oil was collected and used as described in Chapter 2, section 2.2.1.

Hydrogen peroxide (50%), acetic acid (99%) and sulfuric acid (98.9%) and organo montmorillonite (OMMT) are well described in Chapter 2, section 2.2.1 and Chapter 3, section 3.2.1. respectively.

Poly(vinyl chloride) (PVC) (weight-average molecular weight, M_w) = 1.5×10^3 g/mol, density = 1.4 g/cc) was obtained from Kumud Enterprise, India and has been used as the base polymer. Other solvents and chemicals used in this chapter such as THF, NaOH, HCl etc. are described well in Chapter 2, section 2.2.1.

The minerals $(\text{NH}_4)_2\text{SO}_4$, Na_2HPO_4 , KH_2PO_4 , $\text{MgSO}_4 \cdot 7\text{H}_2\text{O}$, $\text{CaCl}_2 \cdot 2\text{H}_2\text{O}$, $\text{FeSO}_4 \cdot 7\text{H}_2\text{O}$, $\text{CuSO}_4 \cdot 7\text{H}_2\text{O}$, $\text{MnSO}_4 \cdot 5\text{H}_2\text{O}$, $\text{ZnSO}_4 \cdot 7\text{H}_2\text{O}$, $\text{H}_3\text{BO}_3 \cdot 5\text{H}_2\text{O}$ and MoO_3 used for the preparation of M9 medium for the biodegradation study were same as described in Chapter 4, section 4.2.1. The bacterial strains used in this chapter *P. aeruginosa* (NBTU01) and *Achromobacter* sp. (NBTU02) were obtained from the Department of Molecular Biology and Biotechnology (Department of Biotechnology, DBT Centre, Government of India), Tezpur University.

The epoxidized oil was prepared as reported in the Chapter 2, section 2.2.2.1.

7.2.2. Instruments and Methods

FTIR, XRD, SEM and TEM analyses for the pristine PVC, ENO, plasticized PVC and nanocomposites were carried same as described in Chapter 3, section 3.2.2.

The solution viscosity was measured by Brookfield viscometer (Model LVT, Middleboro, USA) using spindle number 2 at 30 rpm ($K = 10$). The melt flow rate (MFR) value was measured as the amount in gram of the material extruded by the action of a specified piston under a load of 2.16 kg/cm^2 through the standard orifice of diameter 0.1 mm using the standard plastometer (S.C. Dey, Kolkata) at $170 \text{ }^\circ\text{C}$ for the samples over a specified period of time (10 min).

The tensile strength, elongation at break, gloss and impact strength were measured as described in Chapter 2, section 2.2.2 and Chapter 3, section 3.2.2. The hardness of the films was measured by the help of a Shore-A hardness tester. The instrument is a Durameter of shore A and shore D, made by S.C. Dey's & Co. and the instrument is as per the standard ASTM D 676-59.

Thermogravimetric (TG) analysis, the flame retardancy test of all the samples were done as described in Chapter 2, section 2.2.2.

Chemical resistance tests for all the samples were carried out by immersing the sample for 21 days in water and for 7 days in aqueous solution of 0.5% NaOH (w/v) and 2% HCl (v/v) at room temperature. The heat aging test was carried out at $70 \text{ }^\circ\text{C}$ for 7 days in an electrically heated air-circulating oven as per the standard ASTM D 573 procedure.

7.2.2.1. Plasticization of PVC by ENO and Nanocomposites Formation

The pristine PVC was mixed with ENO at different weight ratio of PVC/ENO (100/0, 75/25, 50/50 and 25/75) using THF as the solvent. Further OMMT (5 wt% with respect to the system) swelled in the same solvent (5-6% w/v) was also added to the mixture

Table 7.1: Compositions of pristine as well plasticized PVC nanocomposites

Code	ENO (g)	PVC (g)	MMT (g)
PVC	0	100	0
PVCNC	0	100	5
PVCENC25	25	75	5
PVCENC50	50	50	5
PVCENC75	75	25	5
PVCENO50	50	50	0

(Table 7.1). The mixture was thoroughly mixed by a mechanical stirrer for 2 h followed by sonication for 10 min (30% amplitude, half cycle of UP200S, as described in Chapter 3, section 3.2.2.). The samples were then cast on glass plates and dried at

room temperature for 4 to 5 days to remove the traces of residual solvent to get the thin films. The PVC/ENO weight ratio of 50/50 (PVCENO50) and pristine PVC without OMMT were also investigated for comparison.

7.2.2.2. Microbial Growth in Presence of Pristine PVC and PVC/ENO Nanocomposites

Bacterial strains used in this study viz., *P. aeruginosa* (NBTU01) and *Achromobacter* sp. (NBTU02) were isolated from crude petroleum-oil contaminated soil samples of North East India. Pure cultures of bacteria were screened for their ability to grow on M9 medium²⁹ supplemented with 1% (w/w) of 0, 25, 50 and 75% (w/w) PVC/ENO systems as a sole source of carbon and energy. All culture flasks were maintained in a rotary shaker incubator at 37 °C, pH 6.8 and 200 rpm. The pH of culture medium and temperature of incubation were adjusted as per the optimum growth conditions of the individual isolate. Kinetics of bacterial growth on pristine PVC and PVC/ENO system was assessed by measuring the bacterial cell population (viable count), protein concentration and dry biomass with respect to time.²⁹ The flasks which have only PVC/ENO nanocomposites and no bacteria served as positive control and the flasks with only inoculums served as negative control system.

7.2.2.3. Biodegradation of PVCENC75 in Culture Medium

Percent (%) of biodegradation of PVCENC75 by individual bacterium was determined by quantifying the residual that remained in the flasks post inoculation at different time intervals.³⁰ The rate of biodegradation and abiotic loss of PVCENC75 were evaluated by comparing the residual weight with the control sample as well as with initial weight of the same. The un-inoculated flasks served as control system. Residual of the samples in the culture medium at the onset and after the end of the experiment was determined by the standard gravimetric method.

7.3. Results and Discussion

7.3.1. Plasticization and Biodegradation of PVC

Epoxidized *Mesua ferrea* L. seed oil was used for the first time as a sole plasticizer for PVC. In this study a low cost material has been used to develop a value added industrial product. The epoxidized oil with functional groups like epoxide, ester and hydroxyl may exhibit good interaction with the PVC matrix and thereby minimizing plasticizer loss. The presence of the epoxidized oil may enhance the low temperature flexibility, flowability and the biodegradability of the pristine PVC. In this present

study a new strategy was investigated for the preparation of nanocomposite wherein organically modified nanoclay was added into epoxidized *Mesua ferrea* L. seed oil plasticized PVC matrix by mechanical shearing and ultrasonication.

Biodegradation of PVC is one of the most challenging tasks in terms of its use in industrial scale. PVC finds application as mulch film in agricultural field, biodegradable biomaterial such as urine and colostomy bags etc. It also commands a large share in commodities application, food packaging etc. Material from natural resources has inherent biodegradability.^{28,31} The use of epoxidized oil with PVC is an industrially well accepted process; however, the effect and optimization of different bacteria on biodegradation have not been fully probed into. ENO with its sufficient polarity displays good homogenizations with the PVC matrix. Further, it can provide an anchorage for microbes and may support their growth. The degree of crystallinity is a crucial factor affecting biodegradability, since microbes mainly attack the amorphous domains of a polymer. The molecules in the amorphous region are loosely packed, and thus made it more susceptible to degradation. The crystalline part of the polymers is more resistant than the amorphous region. Moreover, clay can substantially accelerate the biodegradation by facilitating microbial anchorage onto its surfaces. Therefore, the presence of clay and epoxidized oil in the matrix resulted in degradation of PVC.³²

7.3.2. Bacterial Culture in the Presence of Pristine PVC and PVC/ENO Nanocomposites Utilizing Bacteria

The bacterial strains utilized for biodegradation of pristine PVC and PVC/ENO nanocomposites were isolated from crude petroleum-oil contaminated soil samples collected from petroleum oil fields of North-East India. The bacteria were able to utilize PVC/ENO nanocomposites as the sole source of carbon and energy (Table 7.2).

This was vouched by the increase in bacterial dry biomass, protein content of culture supernatant and cell density post 96 h of incubation in different percentages of PVC/ENO nanocomposites containing medium (Table 7.2). Bacterial cell density in presence of different percentages of PVC/ENO nanocomposites ranged from 1.1×10^6 – 2.3×10^6 mL⁻¹ post 96 h of incubation. In sharp contrast, the growth of bacteria in absence of PVC/ENO nanocomposites (negative control) was negligible (Table 7.2).

7.3.3. Biodegradation of PVC/ENO Nanocomposites in Culture

Biodegradation of PVC/ENO nanocomposite in the culture medium by bacterium of interest is an important criterion for successful bioremediation and waste management.

Table 7.2: Yield of bacterial dry biomass and protein content after 96 h of culture

Bacterial species	PVC/ENO	Cells mL ⁻¹	Dry biomass (g L ⁻¹)	Protein content (mg mL ⁻¹)
Negative Control	-	*ND	ND	ND
	0	0.5 ± 0.01 x 10 ⁶	0.22 ± 0.01	0.30 ± 0.01
	25	0.8 ± 0.02 x 10 ⁶	0.36 ± 0.01	0.53 ± 0.02
<i>P. aeruginosa</i>	50	1.6 ± 0.01 x 10 ⁶	2.17 ± 0.005	0.85 ± 0.008
	75	2.3 ± 0.007 x 10 ⁶	2.24 ± 0.008	1.50 ± 0.01
<i>Achromobacter</i> sp.	0	0.5 ± 0.02 x 10 ⁶	0.10 ± 0.005	0.25 ± 0.04
	25	0.7 ± 0.01 x 10 ⁶	0.17 ± 0.04	0.35 ± 0.01
	50	0.9 ± 0.01 x 10 ⁶	0.80 ± 0.01	0.68 ± 0.05
	75	1.1 ± 0.005 x 10 ⁶	1.33 ± 0.01	0.93 ± 0.02

*ND = Not Determined

The higher percent of degradation of PVC/ENO nanocomposites by individual bacterial isolates was evident from the time course dependent decrease in PVC/ENO contents from culture medium (Fig. 7.1 a,b).

The percent (%) biodegradation of PVCENC75 is shown in Fig. 7.1 b. It was observed that *Pseudomonas aeruginosa* and *Achromobacter* sp. could degrade 35.65% and 34.62% PVCENC75 respectively, post 180 days of inoculation (Fig. 7.1 b). In contrast, the degradation of PVCENC75 in positive control flasks was only 2.28% under the identical conditions (Fig. 7.1 b). In the beginning of biodegradation, the rate of weight loss appeared very slow, owing to the fact that during this initial phase of biodegradation, microorganisms moved and adhered onto the surface of the PVCENC75, followed by further propagation. In the second phase of degradation, the weight of PVCENC75 decreased significantly, which was primarily due to the biodegradation of ENO. For PVC/ENO inoculated with *P. aeruginosa*, this stage continued for 60 days, indicating higher amount of biodegradation. In the third stage, weight loss rate became slow, which suggested biodegradation of the PVC component of the system. This was due to the catalyzing action of both the ENO component and organoclay.

The biodegradability of any system relies on its constituents. Since the presence of ester in the matrix may make it more susceptible to microbial attack;^{33,34} therefore the presence of epoxidized oil in the PVC matrix renders biodegradability. PVC was degraded by the hydrolytic cleavage of the ester groups of ENO and was affected by

the chemical structure and molecular arrangement of the polymer chain as well as the state of the polymer surface, since contact with microorganisms represents the first step in biodegradation process. The action of enzymes secreted by bacteria acted on

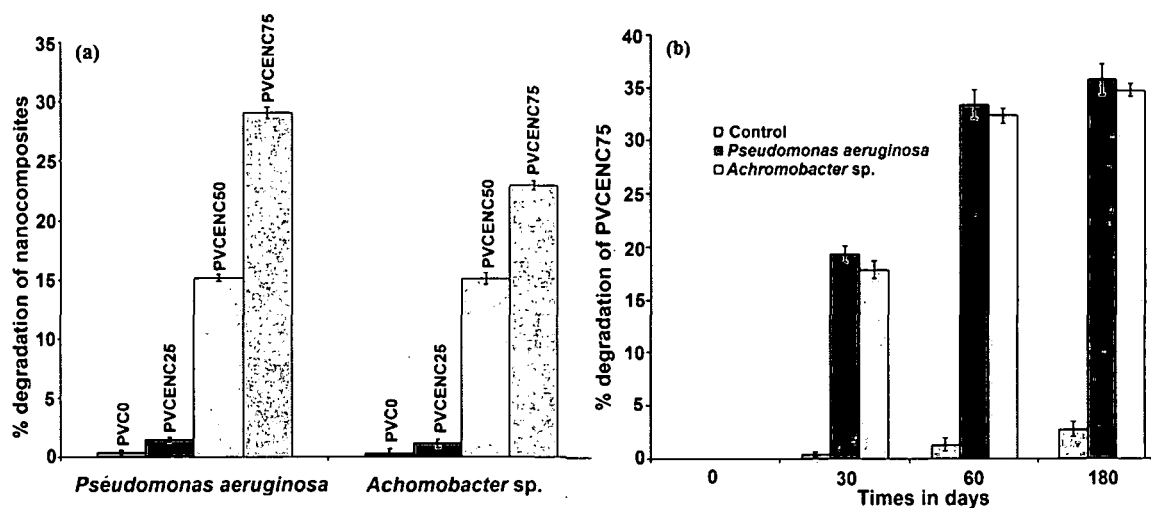


Fig. 7.1: (a) Biodegradation of PVC/ENO systems in culture medium by individual bacterial isolates post 90 days of incubation and (b) Biodegradation of PVCENC75 by individual bacterial isolates post 180 days of incubation

ENO resulting in the fragmentation of PVC and consequently a greater area of contact with the enzyme made it easier to degrade the system.³⁵ The biodegradation phenomenon of PVC/linseed oil blend by enzymatic hydrolysis was studied by Riaz et al.²⁶ They observed that the degradability of the system increases with the increase in the epoxidized oil in the PVC matrix. They inferred that hydrolysis was responsible for the initial degradation process followed by microbial degradation in the blend films. However, the presence of clay and its role in biodegradation cannot be neglected. As reported clay plays a catalytic role in the biodegradation of biodegradable material. Herein clay helps in adsorption of more moisture and also provide an affective support or template for more proximal contact with the functional groups like the ester, hydroxyl etc. and consequently helps in hydrolysis of the ester groups of ENO in the PVC matrix.³⁶ It may be presumed that after adsorbing water, the terminal hydroxyl groups of clay in the presence of microbes caused heterogeneous hydrolysis of the ester groups. The dilute solution viscosities in THF (0.1% w/v) of PVC, PVCENC75 and PVCENC75 post 180 days inoculations were determined. The viscosities of PVC was 1.8 dl/g, for PVCENC75 1.10 dl/g and for samples after biodegradation of 180 days by *Pseudomonas sp.* was 0.65 dl/g and for *Achromobacter*

sp. it was found to be 0.86 dl/g respectively. These decreased indicated and chain scission of the PVC main chains by the studied bacteria.

7.3.4. FTIR Analysis

7.3.4.1. FTIR Analysis of ENO and ENO Plasticized PVC/OMMT Nanocomposites

The characteristic absorption bands for the epoxidized oil (ENO) were well described in Chapter 2, section 2.3.3.2. The spectrum of OMMT has also been discussed in detail in Chapter 3, section 3.3.3.1. For PVC, aliphatic C-H stretching vibrations was observed around 2977-2860 cm^{-1} . The bands in the region of 600-700 cm^{-1} indicate the C-Cl stretching vibrations.³⁷

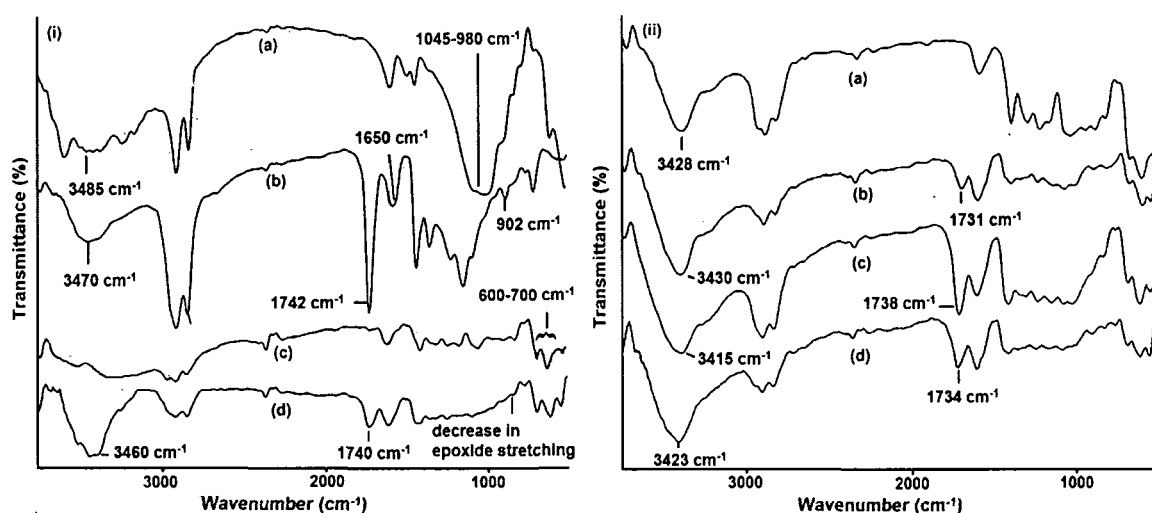


Fig. 7.2: (i) FTIR spectra of (a) OMMT, (b) ENO, (c) PVC and (d) PVCENO50 and (ii) FTIR spectra of (a) PVCNC, (b) PVCENC25, (c) PVCENC50 and (d) PVCENC75

The interactions of PVC with ENO can be observed from the spectrum of PVCENO50 (Fig. 7.2 i). In this spectrum, a new band at around 1740 cm^{-1} was observed which is due to the -C=O stretching vibration of the fatty acid. A shift in -OH stretching vibrations from 3470 cm^{-1} (ENO) to 3460 cm^{-1} was observed in the spectrum of PVCENO50. Besides the above, the absorption band for the epoxy group at 902 cm^{-1} also showed a red shift with decrease in intensity, which suggests the involvement of epoxy group in hydrogen-bonding with the polar C-Cl group of the PVC. At the same time the C-Cl stretching vibration also followed a similar trend. This observation clearly indicates the involvement of the different functional groups of ENO in hydrogen-bonding with the PVC matrix. So the above facts clearly supported the interaction of ENO with the PVC matrix.

The FTIR spectra for PVCNC, PVCENC25, PVCENC50 and PVCENC75 are also shown in Fig. 7.2 ii. The interactions of clay with the ENO/PVC matrix can be clearly understood from the FTIR spectra. For ENO, the -OH stretching vibration at 3466 cm^{-1} showed a red shift after nanocomposites formation. This hydroxyl stretching band was shifted to 3428 cm^{-1} for PVCNC, to 3430 cm^{-1} for PVCENC25, whereas to 3415 cm^{-1} and 3423 cm^{-1} for PVCENC50 and PVCENC75 respectively. Further, the absorption band for carbonyl and epoxy group also followed a similar trend. As seen from the spectrum for PVCENC25, the -C=O and the epoxy group stretching vibrations shifted to 1731 cm^{-1} and 917 cm^{-1} with decrease in intensity. Similarly, for PVCENC50 and PVCENC75, C=O stretching vibrations shifted to 1738 cm^{-1} and to 1734 cm^{-1} respectively. Thus these observations clearly confirmed the presence of extensive interactions of nanoclay with the PVC/ENO matrix.³⁸

7.3.4.2. FTIR Analysis of PVCENC75 post Biodegradation

Fig. 7.3 shows the FTIR spectra of pure PVCENC75 and treated samples with *P. aeruginosa* for 30, 60 and 180 days respectively. Transmittance data, on a common scale, showed that all bands in FTIR spectra of PVCENC75 (Fig. 7.3) decreased in size

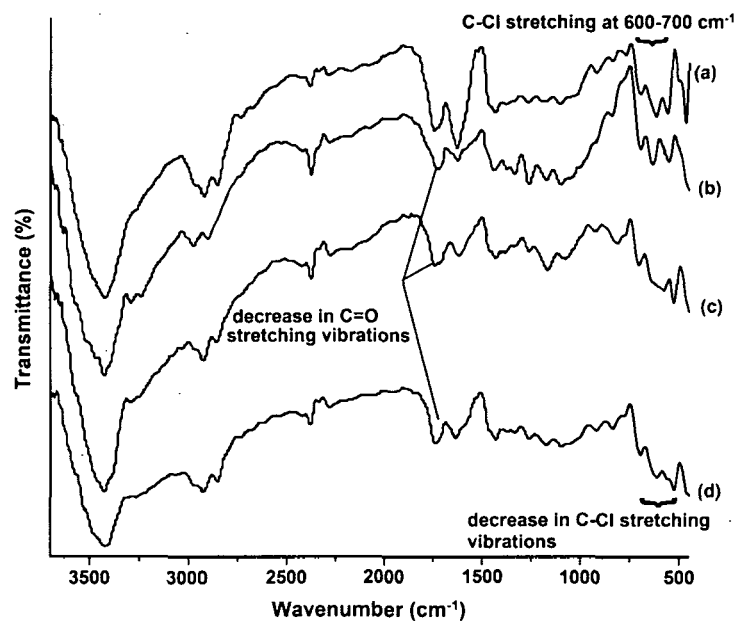


Fig. 7.3: FTIR spectra of PVCENC75 (a) control, (b) 30 days of post inoculation, (c) 60 days post treatment and (d) 180 days post treatment by *Pseudomonas aeruginosa* respectively

after biodegradation for 60 and 180 days. Reduction of band related to carbonyl (1743 cm^{-1}) and ether (1102 cm^{-1}) suggested chain scission.³⁹ The intensity of the C-Cl

stretching frequency ($600\text{-}700\text{ cm}^{-1}$) post biodegradation also exhibited a decrease.

However the of decrease of intensity after 180 days was more visible, the decrease can be related to the reduction in the VC-VC (vinyl chloride) units in the PVC main chain. The decrease in the viscosity post biodegradation of PVCENC75 inoculated with *P. aeruginosa* further supported the above observation. In all the above cases the relative absorbance of the carbonyl peaks decreased over the time course investigated. These changes are due to the hydrolysis of the ester bonds⁴⁰ and hence the bacterial species grown in the media without any source of nutrients except for the PVCENC75 was utilized as a source of energy. The FTIR study of *Archomobacter* sp. treated PVCENC75 also showed the similar result.

7.3.5. XRD Analysis of PVC and ENO Plasticized PVC/OMMT Nanocomposites

The X-ray diffraction pattern for the nanoclay in the polymer matrix is shown in Fig. 7.4. OMMT exhibited a sharp peak at around 4.15° , this peak corresponds to $\{001\}$ basal reflection of the organoclay (as discussed in Chapter 3, section 3.3.3.2.). However, the characteristic diffraction peak of OMMT was absent in the all the nanocomposites, indicating that silicate layers of organoclay may be exfoliated as they do not have any regular repeating distance. The molecular interactions between the clay layers and the PVC chains facilitate further migration of the macromolecular chains in between the clay galleries. These resulted in the separation of the clay layers, hence the interlayer spacing becomes large and consequently OMMT layers were delaminated (as discussed in Chapter 3, section 3.3.4.2.).⁴¹

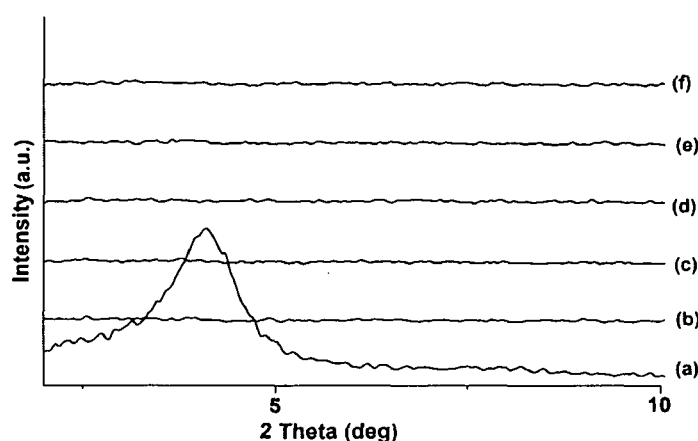


Fig. 7.4: XRD patterns for (a) OMMT, (b) PVC, (c) PVCNC, (d) PVCENC25, (e) PVCENC50 and (f) PVCENC75

In the case of PVC/ENO nanocomposites excellent compatibility between PVC and

ENO perhaps was more favourable for achieving good dispersion of OMMT in the matrix.

7.3.6. Morphological Characterization

7.3.6.1. SEM Study of PVC and ENO Plasticized PVC/OMMT Nanocomposites

The morphology as observed by SEM micrographs for PVC, PVCENO50, PVCNC and PVCENC50 revealed a homogenous distribution of ENO as well nanoclay in the base polymer matrix (Fig. 7.5). The above observation indicated that ENO has good compatibility with PVC (as studied by FTIR in the section 7.3.4.1.). The uniform homogenizations of such systems may be attributed to specific interactions such as hydrogen-bonding and dipole-dipole interactions between molecules of the constituent polymers. The interaction of α -hydrogen of vinyl chloride (PVC matrix) moiety with the carboxyl group or epoxy group (hydrogen-bond acceptor of the ENO) is a key factor in achieving good compatibility by the formation of hydrogen bonding.^{42,43}

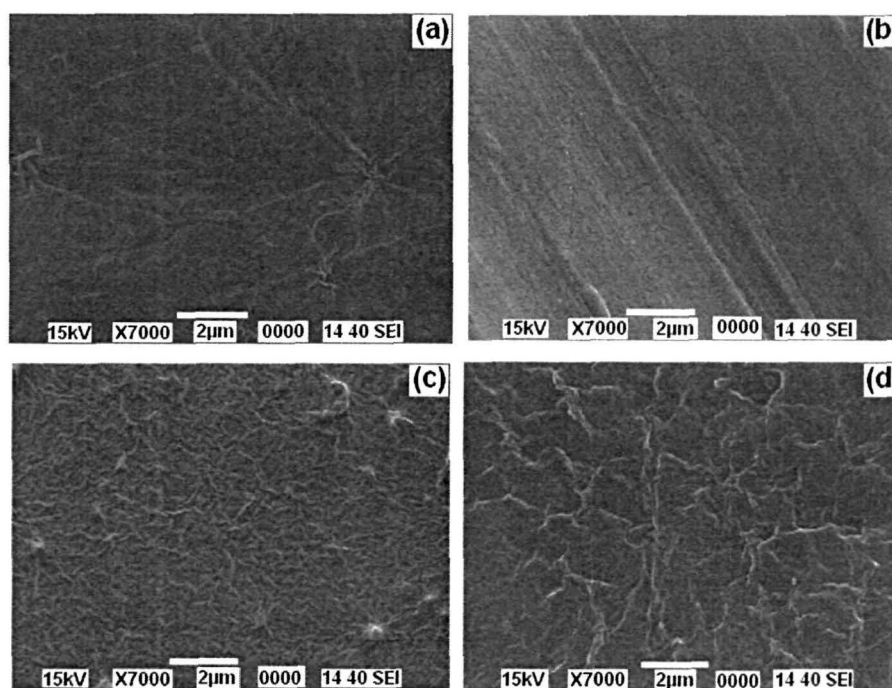


Fig. 7.5: Representative SEM micrographs for (a) PVC, (b) PVCENO50, (c) PVCNC and (d) PVCENC50

The compatibility between these systems also depends upon the energy and entropy of interactions between the polymer and the plasticizer. Any strong interaction between the polymer and the plasticizer may result in negative entropy of mixing, which does not favour miscibility. For this reason, it is necessary to increase the

combinatorial entropy of mixing which can only be done when the plasticizer molecules are sufficiently flexible. When other conditions are equal, the plasticizer molecules which possess sufficient internal mobility are always more compatible with the substrate polymer (the internal mobility here refers to the ability of the molecules to undergo conformational changes easily).^{43,44} Thus ENO with moderate molecular weight and sufficient flexibility exhibited good compatibility with the rigid PVC matrix.

7.3.6.2. TEM Study of Nanocomposites

TEM micrograph of PVCENC50 exhibited a good distribution of the clay layers in the PVC matrix (Fig. 7.6).

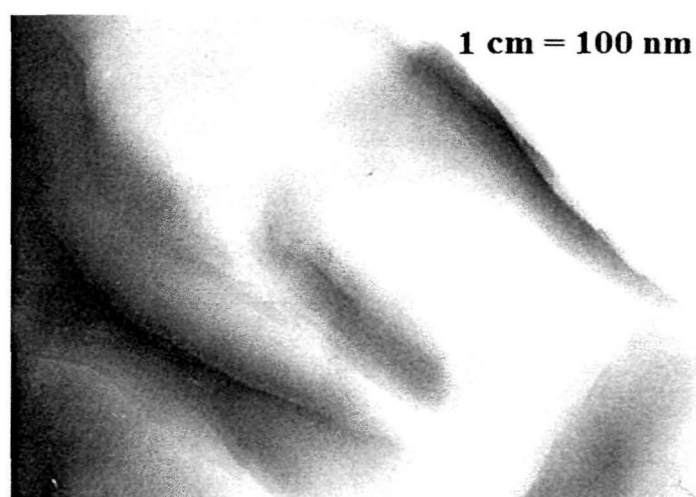


Fig. 7.6: TEM micrograph for PVCENC50

In the representative TEM micrograph the visibly dark lines correspond to the silicate nanolayers. Layer spacing of clay in the matrix increases, thus it can be concluded that the clay layers were uniformly distributed in the nanometer scale in the matrix (Fig. 7.6). This uniform dispersion of the clay resulted in toughening of the matrix. The good dispersion of the clay was due to the sufficient polarity (epoxy, ester groups) of ENO, which helps to achieve uniform dispersion.

7.3.6.3. SEM Study of PVCENC75 post Biodegradation

The SEM images of the film prior to and post biodegradation showed significant changes in the topographical morphology as can be visualized from Figs. 7.7-7.9. For polymer prior to biodegradation and in buffer (positive control) the surfaces were rather smooth. In contrast, the surface erosion due to bacterial degradation becomes more and more prominent with increase in the test period.

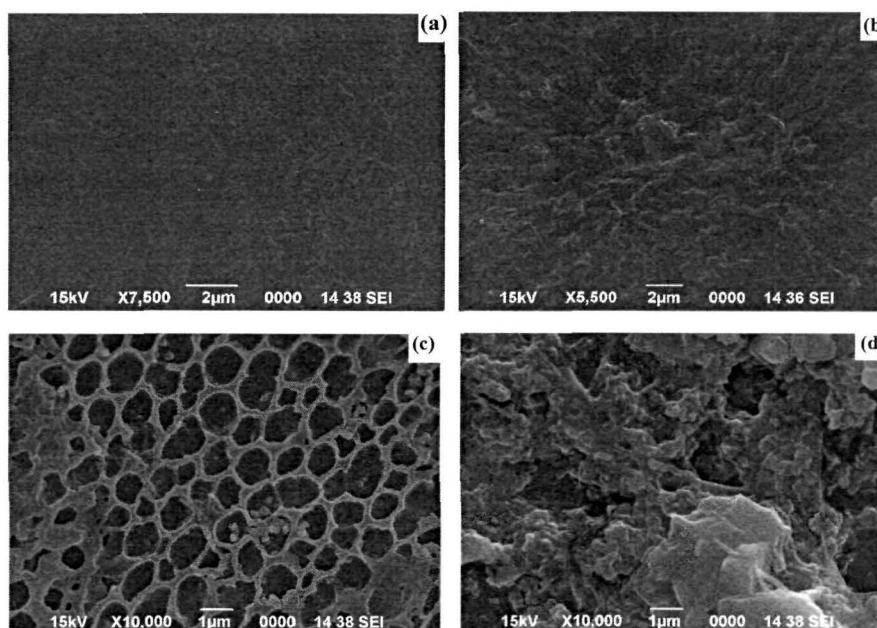


Fig. 7.7: SEM micrographs for PVCENC75 after 30 days of inoculations with (a) untreated PVCENC75, (b) control, (c) *Pseudomonas* sp. and (d) *Achromobacter* sp.

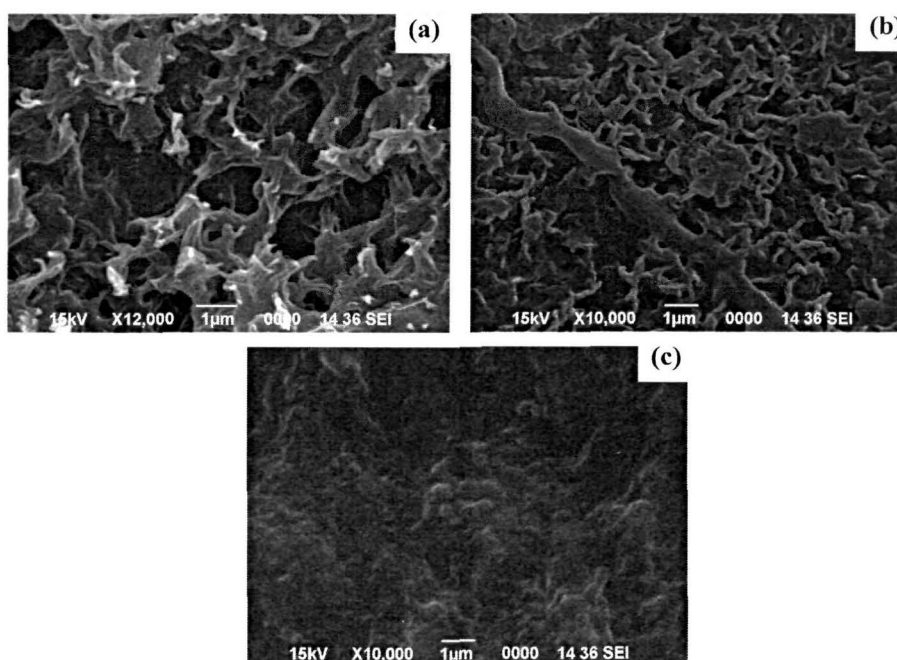


Fig. 7.8: SEM micrographs for PVCENC75 after 60 days of inoculations with (a) *Pseudomonas* sp., (b) *Achromobacter* sp. and (c) control

The samples after 60 days showed higher surface erosion with significant morphological changes (Fig. 7.8). After 180 days of inoculation (Fig. 7.9) the bacterial penetrations to the inner surface can be observed.⁴⁵ The surface erosion property was more prominent for samples inoculated in *P. aeruginosa* strain. Ester groups (O-CO)

are known to be more easily hydrolyzable than carbon–carbon bonds because of the oxygen adjacent to the carbon which provide a good nucleophilic centre of attack for molecules like water in the presence of clay. Hence it can be hypothesized that clay accelerates the degradation of the matrix.

As discussed above ENO helps in the degradation process of the matrix as a whole, the hydrolytic breakdown of the matrix by the bacterial enzyme instigated the degradation process. For samples taken out after 30 days of inoculation network of crater types structure was seen to form on the surface of the films with *P. aeruginosa* inoculation (Fig. 7.7). However, for *Achromobacter* sp. the surface of treated material becomes rough with no surface penetration.

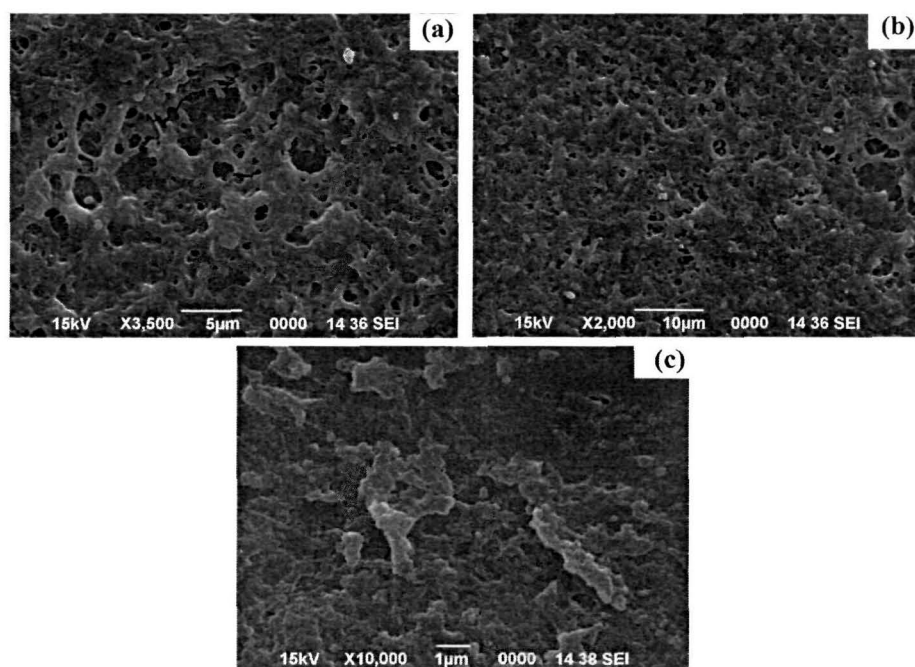


Fig. 7.9: SEM micrographs for PVC/ENOC75 after 180 days of inoculations with (a) *Pseudomonas* sp., (b) *Achromobacter* sp. and (c) control

7.3.7. Brookfield Viscosity and Melt Flow Rate (MFR) of PVC and ENO Plasticized PVC/OMMT Nanocomposites

As indicated from Table 7.3, the viscosity showed a gradual decrease in trend with the increase of amount of ENO. The viscosity decreases nearly 7 times for PVC/ENO50 with respect to the original value (PVC); this indicated that by increasing the amount of ENO in the system plasticization of PVC can be increased. The decrease in viscosity in all cases of PVC/ENO systems may be due to the presence of long hydrocarbon chain of the oil (mixture of oleic, linoleic, stearic and palmitic acid of the fatty acid) which by its plasticizing action prevents sufficient interaction between the polymer chains of

PVC and thereby helping the sliding of chains more easily. This plasticizing effect was observed to enhance with the increase of ENO amount in the PVC matrix. These results indicated that there is no chemical reaction occurring between the two polymers, as the viscosity of the system is lower than that of neat PVC. The MFR results also indicated good processing characteristics of the systems, obtained by the incorporation of ENO, thus adhering to the theory of plasticization.⁴⁴ PVC exhibited MFR of 1.8, whereas PVCNC showed MFR of 1.7. The value of MFR in case of PVCNC did not varied significantly with the incorporation of nanoclay. However, the MFR value for epoxidized oil plasticized PVC systems increased with the increase of ENO amount (Table 7.3).

Table 7.3: Viscosity and MFR value for PVC, PVCNC and PVC/ENO nanocomposites

Samples	Viscosity @ 30 °C (cps)*	MFR (g/min)
PVC	530	1.81
PVCNC	500	1.70
PVCENC25	115	2.1
PVCENC50	80	3.0
PVCENC75	30	3.4
PVCENO50	70	3.1

*Solution viscosity in THF (10% w/v) measured by Brookfield viscometer

The highly electronegative nature of chlorine atom in PVC leads to generation of dipole along the polymer chains. Thus this results in high concentration of secondary forces, which in turn reduce the flexibility of individual molecule, and consequently, increases the rigidity of unplasticized PVC.⁴⁴ With the incorporation of ENO, reduction in the dipole bonding occurs, which in turn decreases the restrictions on deformation of the polymer chain. The non-polar segments of ENO act as shields between the polymer dipoles, thus resulting in overall less cohesion, with consequent increase in freedom of molecular movement. As a result, the chain flexibility increases and thus flow properties are enhanced.⁴⁶

7.3.8. Performance Characteristics

7.3.8.1. Performance Characteristics of PVC, ENO Plasticized PVC/OMMT Nanocomposites

The tensile measurement was carried out for all samples and the data are given in Table 7.4. PVCNC showed the highest tensile strength, though it exhibited the characteristic feature of a brittle material. The incorporation of nanoclay significantly enhances the tensile strength of PVC. The well dispersed nanoclay with a high aspect ratio results in strong interactions with the polymer chains and thus providing a high stress-bearing capability. This behaviour resulted in good tensile properties for PVCNC. However, a little increase in elongation at break value for PVCNC was observed compared to pure PVC, though PVCNC undergoes a small deformation under stress and the failure occurred at 9% elongation only. On the contrary a gradual decrease in the tensile strength with the increase of ENO content was observed for all PVC/ENO systems. However, PVCENO50 showed significant increase in the tensile strength with the incorporation of nanoclay (PVCENC50). This signifies the reinforcing ability of the nanoclay as discussed above.

Hence clay prevented significant deterioration of strength for PVC/ENO system. However, at the same time an increase in the elongation at break value was observed in all cases. These may result from the uniform distribution of the plasticizer between the polymer chains which interacts with different functional groups, thereby reducing the interactions between PVC chains, consequently increasing the elongation at break value. However, it has been observed that the strength properties are affected by the amount of ENO in the PVC matrix (Table 7.4).

Thus, ENO enhanced the segmental mobility which modified the material properties. PVCENC25 showed good tensile strength value and low elongation at break compared to the other PVC/ENO compositions. The hardness also followed a similar trend, as the amount of ENO in the matrix increases; the surface becomes soft and hence easier for making indentation. The incorporation of nanoclay resulted in enhanced hardness for PVCENO50. The high hardness value for PVCENC50 resulted from the good interfacial adhesion between clay and the polymer matrix. Thus the uniformly distributed clay layers (as seen from SEM images) in the matrix with large surface areas would alter the local stress of the surrounding matrix. Since, hardness can be related to rigidity and strength so it is the combination of these two factors that governs the observed results.

The impact strength was found to increase with the increase in the amount of ENO (Table 7.4). Since ENO contains long flexible hydrocarbon part of the fatty acid the applied energy gets evenly distributed within the matrix and consequently impact

resistance increases. Moreover the interaction between the PVC/ENO matrix and polar hydroxyl groups of OMMT also contributed to the increase of impact resistance. This is evident from Table 7.4, where PVCENC50 exhibited higher impact strength compared to PVCENO50. It can also be seen that PVC/ENO nanocomposites showed higher impact strength than PVCNC, this is attributed to the excellent compatibility and plasticization of ENO with the PVC matrix.⁴¹

Table 7.4: Performance characteristics for PVC, PVCNC, PVCENO50 and PVC/ENO nanocomposites

Sample	Tensile strength (MPa)	Elongation at break (%)	Impact resistance (cm)	Hardness (Shore-A)
PVC	20 ± 0.12	5.78 ± 3.21	19 ± 0.45	85 ± 0.45
PVCNC	37 ± 0.021	9.76 ± 4.56	20 ± 0.01	97 ± 0.23
PVCENC25	18.86 ± 0.012	10 ± 2.14	25 ± 0.015	94 ± 0.47
PVCENC50	15.95 ± 0.21	69.96 ± 5.67	55 ± 0.03	92 ± 0.31
PVCENC75	11.07 ± 0.054	94.09 ± 3.56	75 ± 0.021	89 ± 0.40
PVCENO50	8.23 ± 0.073	60.12 ± 5.3	49 ± 0.3	77 ± 0.21

7.3.8.2. Performance Characteristics of PVCENC75 post Biodegradation

The tensile measurements were carried out for all samples and the data are presented in Table 7.5. For the sake of comparison, the tensile strength value of pristine PVCENC75 is also shown in this table. After 30 days of inoculation the variation of tensile strength is quite visible. *P. aeruginosa* degraded samples showed higher rate of decrease in the tensile strength properties for the stipulated period of observation. After 30 days, a decrease of about 14.63% in tensile strength was observed, whereas samples treated for 60 and 180 days showed 32.70% and 53.83% decrease in tensile strength, respectively. It is noteworthy to mention that PVCENC75 inoculated with *Achromobacter* sp. displayed lower decrease in the tensile strength compared to *P. aeruginosa* (Fig. 7.10).

The two faces of PVCENC75 were strongly eroded to leave sponge like structures for samples inoculated with *P. aeruginosa* for 30 and 60 days. The boundaries between these zones were very well defined because the boundaries were mainly composed of crystallite defects or amorphous material which could be preferentially degraded. The presence of both networks like structures and craters might reflect different degrees of degradation; the later reflected a more advanced degradation. The decrease of the

tensile strength is practically inferred to the change of this surface morphology which leaves the PVC/ENO matrix with a great deal of voids.

Table 7.5: Performance characteristics for PVCENC75 after biodegradations

Samples	Durations (Days)	Tensile strength (MPa)	Elongation at break (%)	Impact resistance (cm)	Hardness (Shore-A)
PVCENC75	0	11.07 ± 0.51	94.09 ± 0.23	75 ± 0.20	89 ± 0.25
PVCENC75	30	9.45 ± 0.11	90.12 ± 0.21	70 ± 0.32	82 ± 0.23
inoculated with <i>P. aeruginosa</i>	60	7.54 ± 0.34	86.13 ± 0.24	66 ± 0.12	78 ± 0.21
	180	5.11 ± 0.21	56.90 ± 0.32	52 ± 0.36	73 ± 0.29
PVCENC75	30	10.34 ± 0.52	89.50 ± 0.38	73 ± 0.15	85 ± 0.48
inoculated with <i>Achromobacter sp.</i>	60	8.75 ± 0.31	87.21 ± 0.55	69 ± 0.71	80 ± 0.57
	180	6.21 ± 0.22	68.23 ± 0.17	63 ± 0.45	75 ± 0.67

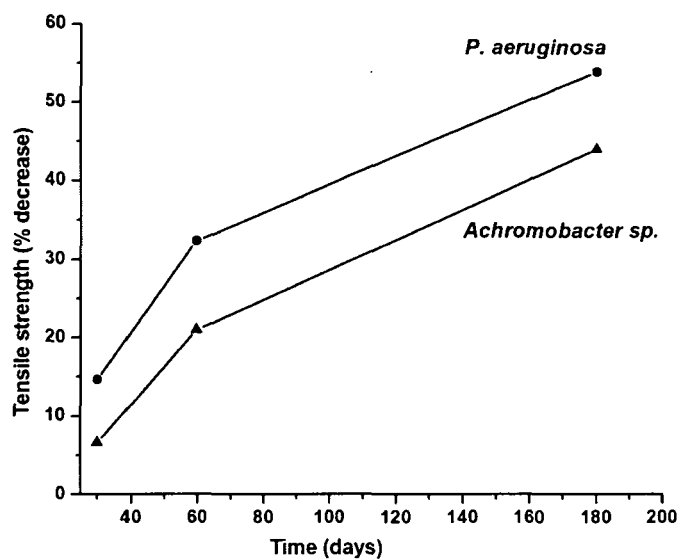


Fig. 7.10: Decrease in tensile strength with time of PVCENC75 post biodegradation with *Pseudomonas sp.* and *Achromobacter sp.*

Tensile strength measured after 180 days of inoculation exhibited more than 50% decrease for *P. aeruginosa* inoculated strain. The bacterial degradation seriously affected the structural integrity of the matrix and the chains were broken down into smaller fragments. The elongation at break also decreased for all the samples post biodegradations as has been confer to the substantial loss of the ENO moiety. The degradation results in structural inhomogeneity, consequently affecting the plasticizer distribution in the matrix. Consequently the presence of voids (as discussed earlier)

results chain breakage even at low stress. As shown in Table 7.5 the impact resistance also suffered a significant loss post biodegradation.

7.3.9. Thermal Study

7.3.9.1. Thermal Study of PVC and ENO Plasticized PVC/OMMT Nanocomposites

The TGA curves for the pristine and nanocomposites (PVC, PVCNC, PVCENO50, PVCENC25, PVCENC50 and PVCENC75) systems are shown in Fig. 7.11 and the data were used to assess the effect of ENO and OMMT on the degradation pattern of PVC (Table 7.6). A three-stage degradation pattern in the case of neat PVC and two stage patterns for PVC/ENO system were observed. In case of PVC the initial stage started at (T_{01}) 105 °C and ends at 170 °C (T_{f1}) with a peak temperature of 134 °C (T_{max1}). The second stage of degradation for PVC was observed with T_{02} at 272 °C, T_{max2} 289 °C and end temperature of 308 °C (T_{f2}). For the third stage T_{03} was observed at 439 °C, T_{max3} at 455 °C and T_{f3} at 468 °C (Fig. 7.11 i). For PVC the initial 10% weight loss is attributed to the elimination of HCl from the system. In the second degradation step the HCl gas that was eliminated further catalyzes the elimination of HCl from the next repeating unit, resulting in rapid unzipping of more acid leaving behind long polyene sequence, and this corresponds to a weight loss of about 60%. In the third stage ($T_{max1} = 455$ °C) thermal degradation of the polyene sequences occurs yielding aromatic and aliphatic compounds by the intramolecular cyclization of the conjugated products. However, in the PVCNC an increase in the stability for the first thermal degradation temperature was observed (Table 7.6) i.e. $T_{max1} = 154$ °C in PVCNC compared to $T_{max1} = 134$ °C for PVC. There are two probable ways that might govern the thermal stability of PVCNC. In the first mechanism the dispersed clay layers decreases the amount of mass transportation of degraded products and limits diffusion of oxygen from the gas phase into the bulk of the nanomaterial.⁴⁷⁻⁴⁹ On the other hand, enhancement of thermal stability of PVC on addition of OMMT can be related to the suppression of the molecular mobility of the polymer chains. As molecular mobility is the major factor that contributes to the transportations of reactive species within the polymer chains the formation of nanocomposite is likely to lower the reactivity and therefore, greater chemical and thermal stability than the virgin polymer was obtained in the case of PVCNC.⁵⁰

However in the second stage of degradation, it can be observed from the TG curve that for PVC T_{max2} is 289 °C but 254 °C for PVCNC. This is due to the existence of

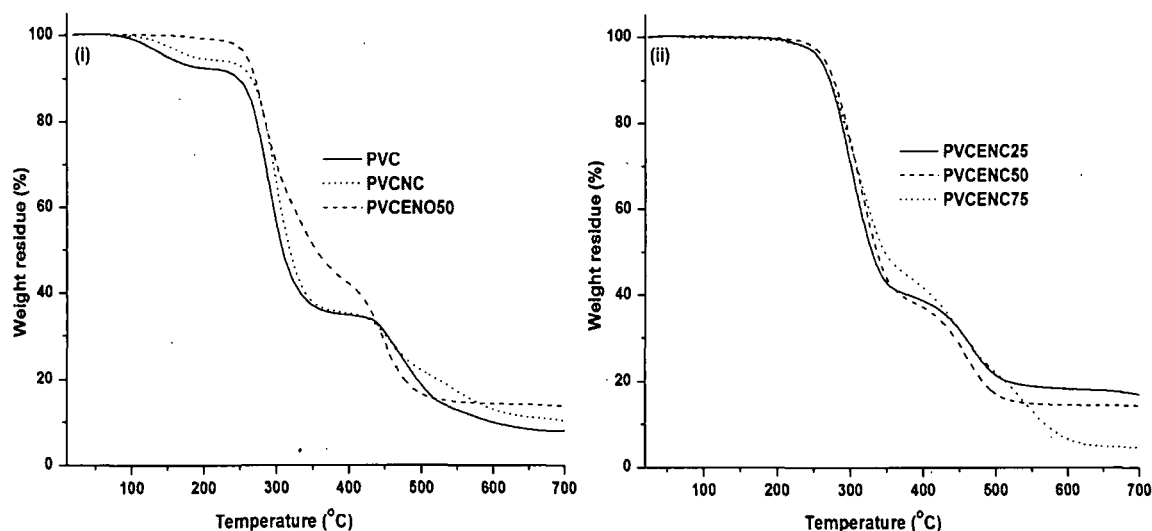


Fig. 7.11: (i) TGA thermograms of (a) PVC, (b) PVCNC and (c) PVCENO50 and (ii) TGA thermograms of (a) PVCENC25, (b) PVCENC50 and (c) PVCENC75

organic ammonium salt contained in the OMMT. It is known that the thermal decomposition of the quaternary ammonium salt could take place following the Hofmann degradation mechanism. During the Hofmann degradation of the ammonium salts, an amount of H^+ and HCl are produced, which may further accelerate the dehydrochlorination of the PVC chains. Therefore, OMMT in nanocomposites may assist in the secondary dehydrochlorination of PVC.^{51,52} For PVCENC25, the first stage occurred at (T_{01}) 268 °C and ends at 330 °C (T_{f1}) with a peak temperature of 299 °C (T_{max1}) (Fig. 5 (ii)). This corresponds to a weight loss of about 40%, which is attributed to the elimination of HCl molecules leaving behind polyene chains. However, the second stage of degradation was observed at 431 °C (T_{02}) and ends at 494 °C with a peak temperature of 451 °C (T_{max2}). Similar patterns were also observed for PVCENC50 with $T_{01} = 273$ °C and degradation ends at 340 °C with a peak temperature of 306 °C (Table 7.6).

The significant increase in the initial degradation temperature is attributed to the presence of ENO and stability increases with the increases of ENO amount. The stabilizing action of the epoxy fatty acid is attributed to the presence of the epoxy group in the plasticizer's chains. The oxirane ring is a well known acid acceptor in PVC. HCl from initial degradation is scavenged by the epoxide, converting the epoxy group to a chlorohydrin, thus ENO acted as a polyene blocker.⁵³ Further, improvement in the thermal stability of PVCENC50 (Fig. 7.11 ii) by 26 °C over PVCENO50 was observed with the incorporation of clay. The improvement in the thermal stability of the system can be attributed to the presence of clay which acts as a heat barrier and thereby

preventing degradation. Thus the well dispersed clay layers resulted in the enhancement of thermal properties of the polymer matrix. Moreover, the clay layers assist in the formation of char after thermal decomposition that could also enhance the overall thermal stability of the system (as discussed in Chapter 3, section 3.3.10.). Thus compared to PVC, PVCNC and PVCENO50, the overall thermal stability in PVC/ENO nanocomposites was due to the combined action of both clay and ENO.⁵⁴

Table 7.6: Thermal degradation parameters for PVC, PVCNC, PVCENO50 and PVC/ENO nanocomposites

Samples	Initial degradation temperature (T_0), °C			Peak temperature (T_{max}), °C			End temperature (T_f), °C		
	T_{01}	T_{02}	T_{03}	T_{max1}	T_{max2}	T_{max3}	T_{f1}	T_{f2}	T_{f3}
PVC	105	272	439	134	289	455	170	308	468
PVCNC	125	254	425	154	245	454	190	353	472
PVCENC25	268	431	-	299	457	-	330	494	-
PVCENC50	273	426	-	306	453	-	340	491	-
PVCENC75	276	410	-	303	471	-	343	591	-
PVCENO50	247	416	-	295	448	-	372	492	-

7.3.9.2. Thermal Study of PVCENC75 post Biodegradation

The thermal stability of PVCENC75 post biodegradation is shown in Fig. 7.12. The thermal degradation pattern varied for the test period as well as for the bacterial species tested (Table 7.7). The decrease in the thermal stability of PVCENC75 was more in case of *P. aeruginosa* treatment compared to *Achromobacter sp.* treatment. After 180 days of biodegradation there was a substantial decrease in the thermal stability of PVCENC75.

These results advocated the above observation of polymer biodegradation by the inoculated strains. The structural integrity of the plasticized PVC was greatly affected by the biodegradation, resulting in generation of low molecular weight species more prone to thermal degradation at low temperature.

The thermal spectra revealed more weight loss in case of *P. aeruginosa* treated samples as compared to PVCENC75 post 180 days of inoculation (Fig. 7.12). However, in case of *Achromobacter sp.* treated PVCENC75 decrease in the thermal stability was less significant compared to *P. aeruginosa* treated PVCENC75.

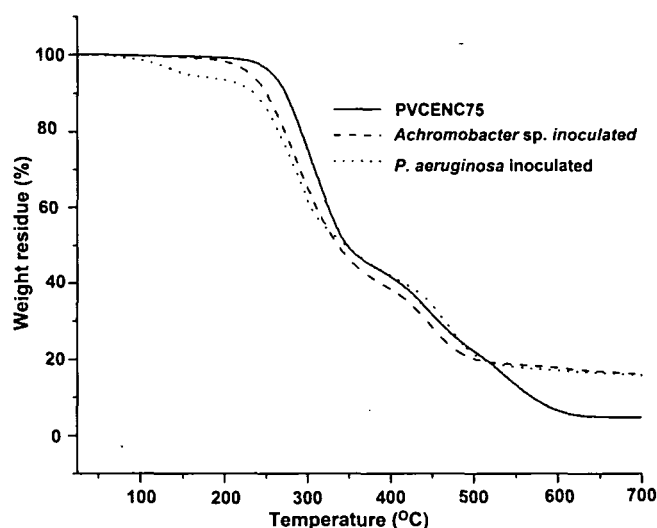


Fig. 7.12: TGA thermograms of PVCENC75 (a) control, (b) after 180 days, inoculated with *Pseudomonas* sp. and (c) after 180 days inoculated with *Achromobacter* sp.

Table 7.7: Thermal degradation parameters for PVCENC75 post biodegradation for 180 days

Samples	Initial degradation temperature (T_0), °C			Peak temperature (T_{max}), °C			End temperature (T_f), °C		
	T_{01}	T_{02}	T_{03}	T_{max1}	T_{max2}	T_{max3}	T_{f1}	T_{f2}	T_{f3}
PVCENC75	-	276	410	-	303	471	-	343	591
PVCENC75 inoculated with <i>P. aeruginosa</i>	128	218	427	139	274	467	151	313	502
PVCENC75 inoculated with <i>Achromobacter</i> sp.	-	222	405	-	292	446	-	351	476

7.3.10. Isothermal Gravimetric Tests

The isothermal gravimetric tests for the nanocomposites were carried out at three different temperatures and their weight losses were calculated. The FTIR spectra of all the heat treated samples were taken to analyze structural changes that had occurred by these isothermal heating (Fig. 7.13). As evident from Table 7.8, the maximum weight loss was observed for PVCNC in all the temperature ranges. These correspond to the loss of HCl from the matrix as evident from the decrease in intensity of C-Cl stretching vibrations band at around 600-700 cm^{-1} in the spectra for the PVCNC (Fig. 7.13 i-iii).

This factor becomes even more severe with the increase of temperature as was observed from their weight losses given in Table 7.8. Furthermore, an increase in the intensity for the C=C stretching vibration band was observed in all the spectra for the nanocomposites suggesting the formation of polyene sequences due to the elimination of HCl molecules (Fig. 7.13 i-iii).

The weight loss is greatly reduced for PVC/ENO nanocomposites system in comparison to PVCNC (Table 7.8). PVCENC50 exhibited the highest stability to loss of weight at the measured temperature range (Table 7.8). This is due to greater interaction of ENO with PVC. From the FTIR spectra it was seen that the intensity for the -C=O absorption peak increases in all the cases (Fig. 7.13 i-iii). One reason for these may be the thermal oxidative degradation of the polymer in the presence of oxygen from air which results in the formation of α -chlorocarboxylic groups. Thus the presence of oxygen accelerated the thermal degradation, oxygen will react with the polyenes, forming peroxides which may react with the polyenes in a chain reaction or attack the polymer chain leading to secondary initiation of HCl loss.⁵⁵

At 200 °C, however, there was a dramatic increase in the absorption band for the Si-O and Al-O (Fig. 7.13 iii) compared to C-Cl stretching vibrations for the nanocomposites. This indicated that the surface of the nanocomposite exhibits plentiful carbonaceous OMMT char, which takes an important role in protection of the degradation of PVC chains. Thus PVC/ENO nanocomposites system exhibited higher resistance to degradation than PVC alone as measured by their weight losses. In this

Table 7.8: *Weight losses of the systems as measured by isothermal test at three different temperatures*

Samples	% weight changes after heating for 5 h		
	100 °C	150 °C	200 °C
PVCNC	10	12	40
PVCENC25	4.5	1.6	15.9
PVCENC50	1.5	0.4	21.5
PVCENC75	3.1	0.3	22.5

regard ENO and clay play important roles and due to the synergism of their actions, higher thermal stability was observed in these cases compared to PVCNC. The high stability (as measured by weight loss) is due to low amount of initial release of chlorine as HCl. This means that ENO and clay play multipurpose roles during thermal-

oxidative stabilization of PVC. These included replacement of unstable chlorines, scavenging of evolved HCl to block the growing polyenes, and destroying of peroxides or peroxy radicals.⁵⁵

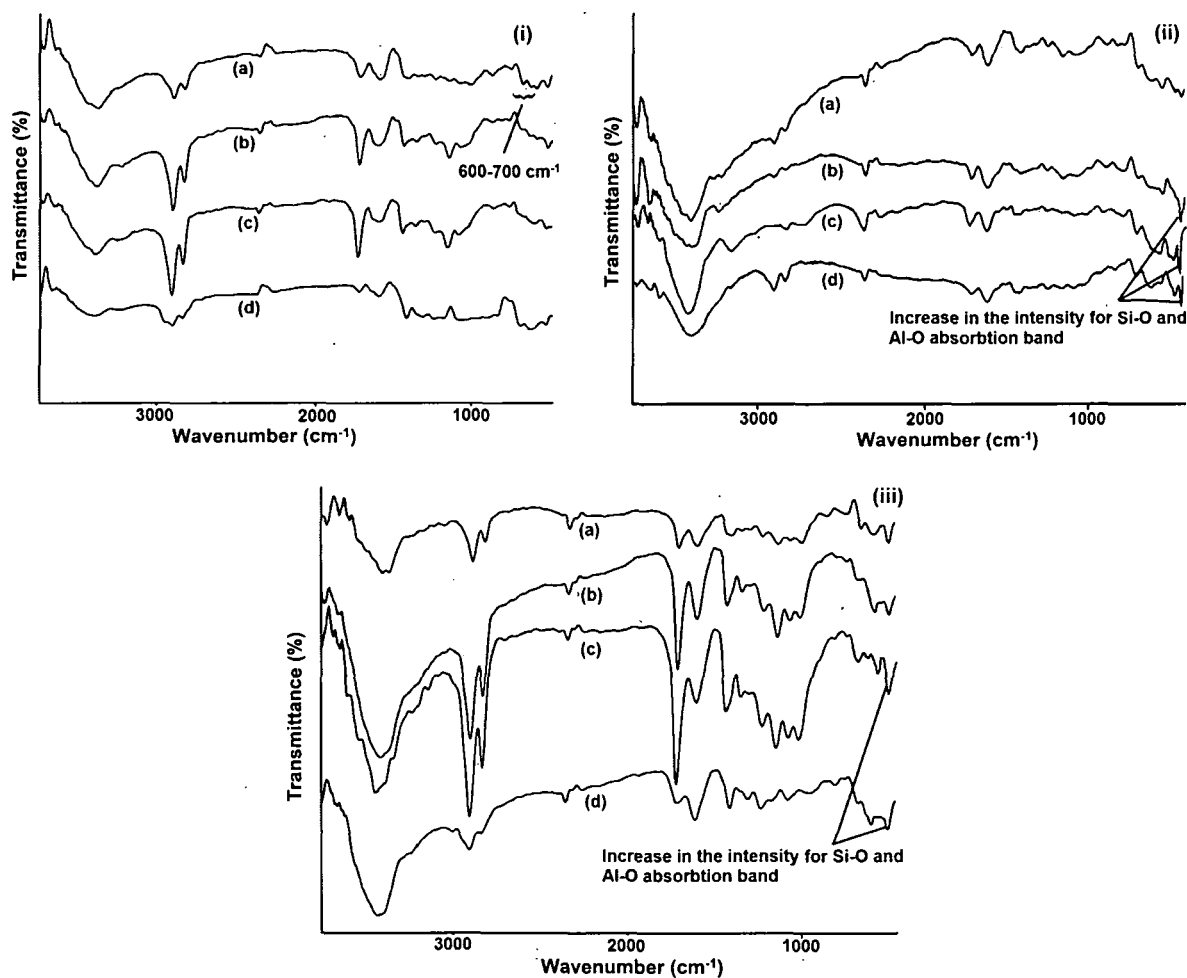


Fig. 7.13: (i) FTIR spectra of isothermally heated samples at 100 °C, (ii) FTIR spectra of isothermally heated samples at 150 °C and (iii) FTIR spectra of isothermally heated samples at 200 °C for (a) PVCENC25, (b) PVCENC50, (c) PVCENC75 and (d) PVCNC, respectively

7.3.11. Flame Retardancy

Improvement in flame retardancy for PVCNC (V0) was found compared to PVC. However, there was a gradual decrease in the flame retardancy for the PVC/ENO nanocomposites as measured by UL 94 test and LOI value (Table 7.9). PVC is considered to be an inherently flame retardant material due to the presence of the high amount of chlorine in its structure. The cleavage of a C–Cl bond leads to the formation of HCl, which serves as the flame retardant through vapor phase mechanism.⁵⁴ The incorporation of ENO decreases the flame retardancy for PVCENO50 as was observed

by the UL 94 and LOI values (Table 7.9). The presences of large amount of hydrocarbon resulted in decrease of flame retardancy for PVCENO50 and PVCENC75.

However, a slight improvement in the LOI value was observed for PVCENC50 with addition of clay. Clay played an effective role in sustaining the flame retardancy of the system. The stable char residue formed (as discussed in Chapter 3, section 3.3.11.) acts as an insulator and slows down heat transfer and thereby retards the movement of gases to feed the flame. Furthermore, the formation of gas bubbles also enhances the flame retardancy as has been discussed in Chapter 3, section 3.3.11. In case of the nanocomposites, the LOI values and V0 ratings with respect to the pristine polymer (Table 7.9) were almost comparable.⁵⁵

Table 7.9: Limiting Oxygen Index (LOI) and UL 94 ratings for PVC, PVCNC, PVCENO50 and PVC/ENO nanocomposites

Samples	Limiting Oxygen Index (%)	UL 94 ratings
PVC	34.5 ± 0.23	V0
PVCNC	36.5 ± 0.03	V0
PVCENO50	27.1 ± 0.21	V1
PVCENC25	33.1 ± 0.07	V0
PVCENC50	29.2 ± 0.19	V0
PVCENC75	28.7 ± 0.054	V1

7.3.12. Heat Aging and Chemical Aging

Leaching behaviour was characterized by measuring the retention of properties (Table 7.10) of the specimens under four different test conditions designed to simulate the environments where flexible PVC products may be used. The test methods were designed to replicate each representative environment for plasticizer migration into different contacting media. For example, the heat aging test simulates the migration of plasticizer from the flexible PVC product to the open atmosphere. The chemical leaching test simulates the variety of environments where migration may occur to a liquid medium in contact.

From Table 7.10, it can be seen that PVC/ENO nanocomposites exhibited good retention of properties over pristine PVC. The effect of heat aging and chemical leaching on the properties of PVC is very critical and showed severe deterioration of

properties. PVC/ENO nanocomposites demonstrated considerable resistance to leaching and consequently retention of properties is the maximum. The effect of heat

Table 7.10: Retention of properties after leaching and heat aging on the performance of PVC/ENO systems

Samples	Sample treatment	% retention of properties after treatment		
		Tensile strength (MPa)	Elongation at break (%)	Hardness (Shore-A)
PVC	HL	85 ± 0.19	80 ± 0.02	83 ± 0.23
	AL	87 ± 0.21	90 ± 0.21	84 ± 0.54
	BL	83 ± 0.09	89 ± 0.029	82 ± 0.23
	WL	94 ± 0.32	92 ± 0.055	97 ± 0.12
PVCNC	HL	87 ± 0.12	91 ± 0.12	85 ± 0.49
	AL	91 ± 0.049	88 ± 0.095	86 ± 0.31
	BL	90 ± 0.55	82 ± 0.21	85 ± 0.09
	WL	90 ± 0.019	89 ± 0.45	97 ± 0.01
PVCENC25	HL	92 ± 0.69	95 ± 0.29	95 ± 0.78
	AL	94 ± 0.66	82 ± 0.45	92 ± 0.28
	BL	90 ± 0.15	97 ± 0.21	95 ± 0.65
	WL	93 ± 0.09	96 ± 0.39	98 ± 0.23
PVCENC50	HL	93 ± 0.22	90 ± 0.77	94 ± 0.15
	AL	96 ± 0.27	95 ± 0.85	95 ± 0.18
	BL	93 ± 0.087	90 ± 0.20	91 ± 0.81
	WL	97 ± 0.01	98 ± 0.05	96 ± 0.46
PVCENC75	HL	59 ± 0.26	56 ± 0.20	67 ± 0.35
	AL	61 ± 0.23	42 ± 0.01	50 ± 0.05
	BL	67 ± 0.56	96 ± 0.055	80 ± 0.11
	WL	71 ± 0.12	68 ± 0.88	73 ± 0.41
PVCENO50	HL	94 ± 0.27	92 ± 0.69	89 ± 0.35
	AL	95 ± 0.45	92 ± 0.13	98 ± 0.77
	BL	87 ± 0.02	82 ± 0.01	90 ± 0.36
	WL	90 ± 0.01	91 0.051	92 ± 0.07

* HL= Heat leaching, AL= Acid leaching, BL= alkali leaching and WL= water leaching

leaching on the PVC property loss can be related to the loss of HCl from the moiety which consequently affects the structural integrity. The presence of plasticizer retards the physical and chemical changes of PVC and consequently prevents significant deterioration of the properties. In addition to the above, the incorporation of nanoclay in ENO may prevent hydrolytic breakdown of PVC/ENO matrix and consequently retention of properties is more for PVC/ENO nanocomposites than PVC/ENO50 as observed by aging test in different test media (Table 7.10). However, in the plasticized PVC a little decrease in flexibility was observed and all samples were found to be slightly stiffened after aging. The loss of flexibility is due to network formation, loss of ENO etc.

7.4. Conclusions

Epoxidized *Mesua ferrea* L. seed oil was successfully incorporated as a plasticizer in the PVC matrix with 5 wt% nanoclay loading. The system exhibited improved thermal properties over the pristine PVC. Thus the study demonstrated improvement in the processing behaviour without deterioration of the other properties. SEM indicated that the PVC/ENO systems were miscible with uniform distribution of components in the matrix. The flame retardancy of the system was not affected significantly by the incorporation of the ENO and all the systems exhibited good flame retardancy. The good retention of properties of the studied systems indicates leaching and volatilization of plasticizer was minimal.

The study also demonstrated that epoxidized *Mesua ferrea* L. seed oil assisted the biodegradation of PVC. PVC with varying content of ENO was subjected to microbial degradation under laboratory conditions. The degradation mechanism can be described as a three-stage process. The first stage involved colonization of microorganisms. The second stage was the degradation of ENO, whereas the final stage was achieved by degrading the PVC component. The biodegradability tests revealed that the composite with ENO content 75 wt% has the best biodegradability; the tensile loss at post 180 days of biodegradation exceeded 50%. The study also demonstrated that both *P. aeruginosa* and *Achromobacter* sp. strains were effective in degrading the system.

References

1. Krauskopf, L.G. *Encyclopedia of PVC*, Dekker, New York, 1988.
2. James, S.F., & Armando, G.M. Physical morphology and quantitative characterization of chemical changes of weathered PVC/pine composites, *J. Polym. Environ.* **18**, 57-64, 2010.
3. Matuana, L.M., et al. The effect of low levels of plasticizer on the rheological and mechanical properties of poly(vinyl chloride)/newsprint-fiber composites, *J. Vinyl Addit. Technol.* **3**, 265–273, 2004.
4. Murphy, J. *Additives for Plastics Handbook*, Elsevier Science, New York, 2001.
5. Athalye, A.S. & Trivedi, P. *PVC Technology: Compounding, Processing and Application*, Springer-Verlag, Bombay, 1994.
6. Castle, L., et al. Migration from plasticized films into foods. 4. Use of polymeric plasticizers and lower levels of di-(2-ethylhexyladipate) plasticizer in PVC films to reduce migration into foods, *Addit. Contam: Part A.* **5**, 277-282, 1988.
7. Ferrer, C.B., et al. Characterization and thermal stability of poly(vinyl chloride) plasticized with epoxidized soybean oil for food packaging, *Polym. Degrad. Stab.* **95**, 2207-2212, 2010.
8. Yan, L., et al. Application of the long-chain linear polyester in plastification of PVC, *J. Wuhan. Univer. Technol. Mater. Sci. Ed.* **23**, 100-104, 2008.
9. Ikhuoria, E.U., et al. Preparation and characterization of water-reducible alkyds with fumarized rubber seed oil, *Prog. Org. Coat.* **52**, 238-240, 2005.
10. Ahmed, S., et al. Polyesteramide from pongamia glabra oil for biologically safe anticorrosive coating, *Prog. Org. Coat.* **47**, 95-101, 2002.
11. Mahapatra, S.S., & Karak, N. Synthesis and characterization and of polyesteramide resins from Nahar seed oil for surface coating applications, *Prog. Org. Coat.* **51**, 103-108, 2004.
12. Dutta, S., & Karak, N. Synthesis and characterization of poly(urethane amide) resins from Nahar seed oil for surface coating applications, *Prog. Org. Coat.* **53**, 147-152, 2005.
13. Piazza, G.J., & Foglia, T.A. One-pot synthesis of fatty acid epoxides from triacylglycerols using enzymes present in oat seeds, *J. Am. Oil Chem. Soc.* **83**, 1021-1025, 2006.
14. Vlcek, T., & Petrovic, Z.S. Optimization of the chemoenzymatic epoxidation of soybean oil, *J. Am. Oil Chem. Soc.* **83**, 247-252, 2006.

15. Karmalm, P., et al. Thermal stability of poly(vinyl chloride) with epoxidized soybean oil as primary plasticizer, *Polym. Degrad. Stab.* **94**, 2275-2281, 2009.
16. Ramesan, M.T., et al. Investigations on the addition of styrene butadiene rubber in natural rubber and dichlorocarbene modified styrene butadiene rubber blends, *J. Mater. Sci.* **37**, 109-116, 2003.
17. Sterky, K., et al. Effect of montmorillonite treatment on the thermal stability of poly(vinyl chloride) nanocomposite, *Polym. Degrad. Stab.* **94**, 1564-1570, 2009.
18. Wang, D., et al. PVC-clay nanocomposites: Preparation, thermal and mechanical properties, *J. Vinyl Addit. Technol.* **7**, 203-213, 2001.
19. Wilkes, C.C. & Summers, J.W. *PVC Handbook*, Carl Hanser Verlag, Germany, 2005.
20. Wiles, D.M., & Scott, G. Poly(vinyl chloride) film filled with microcrystalline cellulose prepared from cotton fabric waste: Properties and biodegradability study, *Polym. Degrad. Stab.* **91**, 1581-1592, 2006.
21. Bilck, A.P., et al. Biodegradable mulch films for strawberry production, *Polym. Test.* **29**, 471-476, 2010.
22. Kohn, J., et al. A new approach to the rationale discovery of polymeric biomaterials, *Biomaterials* **28**, 4171-4177, 2007.
23. Andricic, B., et al. Polymer blends based on poly(vinyl chloride) and biodegradable aliphatic-aromatic copolyester, *J. Appl. Polym. Sci.* **109**, 1002-1008, 2008.
24. Shah, A.A., et al. Biological degradation of plastics: A comprehensive review, *Biotechnol. Adv.* **26**, 246-265, 2008.
25. Kaczmarek, H., & Krzysztof, B. Biodegradation of plasticized poly(vinyl chloride) containing cellulose, *J. Polym. Sci. Part B: Polym. Phys.* **45**, 903-919, 2007.
26. Riaz, U., et al. Compatibility and biodegradability studies of linseed oil epoxy and PVC blends, *Biomass Bioenerg.* **34**, 396-401, 2010.
27. Ratajska, M., & Boryniec, S. Physical and chemical aspects of biodegradation of natural polymers, *React. Funct. Polym.* **38**, 35-49, 1998.
28. Shogren, R.L., et al. Biodegradation behavior of some vegetable oil-based polymers, *J. Polym. Environ.* **12**, 173-178, 2004.
29. Das, K., & Mukherjee, A.K. Characterization of biochemical properties and biological activities of biosurfactants produced by *Pseudomonas aeruginosa* mucoid and non-mucoid strains, *J. Appl. Microbiol. Biotechnol.* **69**, 192-195, 2005.

30. Das, K., & Mukherjee, A.K. Crude petroleum-oil biodegradation efficiency of *Bacillus subtilis* and *Pseudomonas aeruginosa* strains isolated from petroleum oil contaminated soil from North-East India, *Bioresour. Technol.* **98**, 1339-1345, 2007.
31. Lamba, N.M.K., et al. In vitro investigation of the blood response to medical grade PVC and the effect of heparin on the blood response, *Biomaterials* **21**, 89-96, 2000.
32. Frohberga, P., et al. Effect of crystalline substances in biodegradable films, *Chem. Eng. Res. Des.* **88**, 1148–1152, 2010.
33. Jang, B.N., et al. The relationship between thermal degradation behavior of polymer and the fire retardancy of polymer/clay nanocomposites, *Polymer* **46**, 10678-10687, 2005.
34. Deka, H., et al., Biocompatible hyperbranched polyurethane/multi-walled carbon nanotube composites as shape memory materials, *Carbon* **48**, 2013-2022, 2010.
35. Lakshmi, S.N., & Cato, T.L. Biodegradable polymers as biomaterials, *Prog. Polym. Sci.* **32** 762–798, 2007.
36. Lilichenko, N., et al. A biodegradable polymer nanocomposite: Mechanical and barrier properties, *Mech. Compos. Mater.* **44**, 45-56, 2008.
37. Shabbir, S., et al. Miscibility studies of PVC/Aramid blends, *Col. Polym. Sci.* **286**, 673–681, 2008.
38. Gong, F., et al. Thermal properties of poly(vinyl chloride)/montmorillonite nanocomposites, *Polym. Degrad. Stab.* **84**, 289-294, 2004.
39. Pamula, E. FTIR study of degradation products of aliphatic polyesters–carbon fibers composites, *J. Mol. Struct.* **596**, 69-75, 2001.
40. Kay, M.J., et al. Chemical and physical changes occurring in polyesters urethane during biodegradation, *Int. Biodeterior. Biodegrad.* **31**, 209-225, 1993.
41. Ren, T., et al. Preparation, characterization and properties of poly(vinyl chloride)/organophilic-montmorillonite nanocomposites, *Polym. Compost.* **27**, 55-64, 2006.
42. Demertzis, P.G., et al. Study of compatibility of PVC and polyester-type plasticizer blends by inverse gas chromatography, *Eur. Polym. J.* **26**, 137-140, 1990.
43. Castro, R.E.N. Crystallisation and miscibility of poly(ethylene oxide)/poly(vinyl chloride) blends, *J. Mater. Sci.* **38**, 699-703, 2003.
44. Titow, W.V. *PVC Plastics: Properties, Processing, and Applications*, Elsevier Applied Science, New York, 1990.

45. Umare, S.S., & Chandure, A.S. Synthesis, characterization and biodegradation studies of poly(ester urethane)s, *Chem. Eng. J.* **142**, 65–77, 2008.
46. Santra, R.N., et al. Thermogravimetric studies on miscible blends of ethylene-methyl acrylate copolymer (EMA) and polydimethylsiloxane rubber (PDMS), *Thermochim. Acta.* **219**, 283-292, 1993.
47. Leszczynska, A., et al. Polymer/montmorillonite nanocomposites with improved thermal properties: Part I. Factors influencing thermal stability and mechanisms of thermal stability improvement, *Thermochim. Acta.* **453**, 75-96, 2007.
48. Beyer, G. Organoclays as flame retardants for PVC, *Polym. Adv. Technol.* **19**, 485-488, 2008.
49. Davis, R.D., et al. Improved thermal stability of organically modified layered silicates, *Clays Clay Miner.* **52**, 171-179, 2004.
50. Xie, W., et al. Thermal degradation chemistry of alkyl quaternary ammonium montmorillonite, *Chem. Mater.* **13**, 2979-2990, 2001.
51. Benanibaa, M.T., et al. Stabilizing effect of epoxidized sunflower oil on the thermal degradation of poly(vinyl chloride), *Polym. Degrad. Stab.* **74**, 501–505, 2001.
52. Song, R., et al. Influences of catalysis and dispersion of organically modified montmorillonite on flame retardancy of polypropylene nanocomposites, *J. Appl. Polym. Sci.* **106**, 3488-3494, 2007.
53. Zheng, X.G., et al. Dehydrochlorination of PVC materials at high temperature, *Energy Fuels* **17**, 896-900, 2003.
54. Basfar, A.A. Flame retardancy of radiation cross-linked poly(vinyl chloride) (PVC) used as an insulating material for wire and cable, *Polym. Degrad. Stab.* **77**, 221–226, 2002.
55. Liang, Z.M., et al. PVC/montmorillonite nanocomposites based on a thermally stable, rigid-rod aromatic amine modifier, *J. Appl. Polym. Sci.* **92**, 567–575, 2004.

CHAPTER 8

Conclusions and Future Directions

8.1. Conclusions

Epoxy resin is one of the most industrially important polymeric materials in the contemporary technology. Much of the work lately has been diverted to development of biobased epoxy products. The biobased epoxy may be an apt choice for industrial application since it exhibits the combination of properties such as strength, flexibility and at the same time it is ecofriendly.

So in this pursuit this thesis highlights the synthesis, characterization, properties evaluation and application of *Mesua ferrea* L. seed oil based epoxidized oil, epoxy resins and their various nanocomposites with different types of nanofillers. The thesis also deals with the modification of nanomaterials like nanoclay and MWCNTs.

Thus, from the present investigation the following conclusions are drawn.

- (i) A low cost non-edible vegetable oil, *Mesua ferrea* L. seed oil was successfully utilized for the first time to prepare industrially important epoxidized oil and epoxy resins.
- (ii) The synthesized epoxidized oil and epoxy resins were successfully characterized by the conventional analytical and spectroscopic techniques.
- (iii) The modification of the epoxy resin by hyperbranched polyurethane and subsequent nanocomposites formation significantly improved the properties especially mechanical properties, thermal stability and biodegradation.
- (iv) The nanocomposites of ENO (epoxidized *Mesua ferrea* L. seed oil)/Araldite LY 250 with OMMT, *Mesua ferrea* L. seed oil based epoxy resins viz. TBP AE (tetrabromobisphenol-A based epoxy) with OMMT, BPSE (bisphenol-S based epoxy) with OMMT, and MBPSE (modified BPSE) with OMMT, OMMT modified by fatty amido-amine of the oil, OMMT modified by hyperbranched polyurea, bentonite modified by fatty amido-amine of the oil (mMMT) and bentonite (MMT) were successfully prepared by solution technique. The prepared nanocomposites exhibited noticeable improvement in overall performance characteristics of the epoxy thermosets.
- (v) The MBPSE (modified BPSE) is a good matrix for the dispersion and stabilization of copper nanoparticles decorated OMMT. The well dispersed

copper nanoparticles decorated OMMT clay based nanocomposites showed better properties than the pristine system. The nanocomposites also exhibited acceptable antimicrobial property.

- (vi) The MBPSE/MWCNTs nanocomposites showed excellent improvements in the properties like mechanical and thermal. They also showed higher biodegradation and more cytocompatibility compared to the pristine system.
- (vii) The studied nanocomposites have the high potential to be used as advanced surface coating materials, adhesive materials, highly thermo-stable materials, flame retardant materials, biodegradable biomaterials.
- (viii) The epoxidized oil modified PVC/OMMT nanocomposite showed high potentiality to be used as biodegradable plasticized PVC for various applications. Thus in a nut shell, the prime achievement of the present investigation is the successful exploitation of a less significant renewable raw material to industrially important products with great social impact.

8.2. Future Directions

Although a systematic and comprehensive study was made in the present investigation but still there are a few future scopes of *Mesua ferrea* L. seed oil based epoxy and its nanocomposites to be worth mentioned for further studies.

- (i) Epoxidation of *Mesua ferrea* L. seed oil can be carried by chemo-enzymatic approach or by using different ion exchange resins.
- (ii) More detail study of the biodegradation pattern and the mechanism of biodegradation of the epoxidized oil plasticized PVC or epoxy resin clay/MWCNTs nanocomposites can be carried out.
- (iii) *Mesua ferrea* L. seed oil based epoxy nanocomposites could be evaluated by *in-vitro* and *in-vivo* tests for different biomedical applications.
- (iv) To develop different metal nanoparticles immobilized nanoclays for application in catalysis or antimicrobial coatings.

List of Publications

In Journals

1. Das, G., & Karak, N. Epoxidized *Mesua ferrea* L. seed oil-based reactive diluent for BPA epoxy resin and their green nanocomposites, *Prog. Org. Coat.* **66**, 59–64, 2009.
2. Das, G., & Karak, N. Vegetable oil-based flame retardant epoxy/clay nanocomposites, *Polym. Degrad. Stab.* **94**, 1948-1954, 2009.
3. Mahapatra, S.S., & Das, G., & Karak, N. Hyperbranched polyamines as potential agents for epoxy resin, *Paintindia LXI* **6**, 55-60, 2009.
4. Das, G., & Karak, N. Thermostable and flame retardant *Mesua ferrea* L. seed oil based non-halogenated epoxy resin/clay nanocomposites, *Prog. Org. Coat.* **69**, 495-503, 2010.
5. Das, G., & Karak, N. *Mesua ferrea* L. seed oil based epoxy resin, *J. Appl. Polym. Sci.* **118**, 128–134, 2010.
6. Konwar, U., Das, G., & Karak, N. *Mesua ferrea* L. seed oil based highly branched polyester and epoxy blends and their nanocomposites, *J. Appl. Polym. Sci.* **121**, 1076-1085, 2011.
7. Das, G., & Karak, N. Epoxidized *Mesua ferrea* L. seed oil plasticized thermostable PVC and clay nanocomposites, *J. Vinyl Addit. Technol.* 2011 (*proof corrected*).
8. Das, G., & Karak, N. *Mesua ferrea* L. seed oil based amido-amine modified nanoclay/epoxy nanocomposites. *J. Appl. Polym. Sci.* 2011 (*online*), DOI/10.1002/app.35304.
9. Das, G., Roy, J.K., Mukherjee, A.K., & Karak, N. *Mesua ferrea* L. seed oil modified sulfone epoxy resin and multi-walled carbon nanotube nanocomposites and their biomedical and mechanical properties, *Adv. Sci. Lett.* 2011 (*online*).
10. Das, G., Bordoloi, N.K., Rai, S.K., Mukherjee A.K., & Karak, N. Biodegradable and biocompatible epoxidized vegetable oil modified thermostable poly(vinyl chloride): Thermal and Performance characteristics post biodegradation with *Pseudomonas aeruginosa* and *Achromobacter sp.*, *J. Hazard. Mater.* 2011 (*online*).
11. Das, G., Kalita, R.D., Deka, H., Buragohain, A.K., & Karak, N. Biodegradation, cytotoxicity and performance studies of vegetable oil based hyperbranched polyurethane modified biocompatible sulfonated epoxy resin/clay nanocomposites, *Biomass Bioenerg.* 2011 (*under review*).

12. **Das, G.,** Deka, M., Deka, H., Kumar, A., & Karak, N. Bio-based sulfonated epoxy/hyperbranched polyurea-modified OMMT nanocomposites as advanced polymeric materials, *Int. J. Polym. Mater.* 2011 (*accepted*).
13. Gogoi, A., **Das, G.,** Karak, N., Choudhury, A.J., & Ahmed, G.A. Measurement of the light scattering properties of Bentonite clay particles embedded in transparent cylindrical polymer matrix, *Atti Accad. Pelorit. Pericol. Cl. Sci. Fis. Mat. Nat.* **89**, C1V89S1P039, 1-5, 2011.
14. **Das, G.,** Kalita, R.D., Deka, H., Buragohain, A.K., & Karak, N. Antibacterial properties of copper nanoparticles decorated nanoclay and epoxy nanocomposites, *J. Nanopart. Res.* 2011 (*communicated*).

Conference Presentation (Published as Proceeding)

1. Mahapatra, S.S. **Das, G.,** & Karak, N. Hyperbranched polyamine amine as potential agents for epoxy resin, COMME, NMRI Thane, India, 2008.
2. **Das, G.,** & Karak, N. Prospects and challenges of vegetable oil based epoxy/clay nanocomposites, National Seminar on Photonics and Quantum structures, Tezpur University, Assam, 2009.
3. **Das, G.,** & Karak, N. Hyperbranched polyether polyamine modified clay and its nanocomposites, ICANN, IIT Guwahati, India, 2009.
4. Karak, N., Mahapatra, S.S., Dutta, S., Deka, H., Konwar, U., **Das, G.,** & Konwarh, R. Polymer nanocomposites-multifaceted advanced materials for today's society National Seminar on Photonics and Quantum Structures (NSPQS), Tezpur University, Assam, 2009.
5. **Das, G.,** & Karak, N. Biodegradation, cytotoxicity and performance studies of vegetable oil based hyperbranched polyurethane modified biocompatible sulfonated epoxy resin/clay nanocomposites, National Conference on Smart Nanostructures (NCSN), Tezpur University, Assam, 2011.
6. Gogoi, A., **Das, G.,** Karak, N., Choudhury, A.J., & Ahmed, G.A. Measurement of the light scattering properties of Bentonite clay particles embedded in transparent cylindrical polymer matrix, AAPP-Electromagnetic and Light Scattering XIII, Taormina, Italy, 2011.
7. **Das, G.,** Kalita, R.D., Deka, H., Buragohain, A.K., & Karak, N. Antibacterial properties of copper nanoparticles decorated nanoclay epoxy nanocomposites,

National Conference on Chemistry and Chemical Technology and Society
(NCCCTS), Tezpur University, Assam, 2011.